UCLA

Title

Protein Arginine Methyltransferases: The Breakfast Club of Enzymes

Permalink

https://escholarship.org/uc/item/40s2z8p2

Author

Lowe, Troy Lucas

Publication Date

2024

Peer reviewed|Thesis/dissertation

UNIVERSITY OF CALIFORNIA

Los Angeles

Protein Arginine Methyltransferases: The Breakfast Club of Enzymes

A dissertation submitted in partial satisfaction of the requirements for the degree of Doctor of

Philosophy in Biochemistry, Molecular and Structural Biology

by

Troy Lucas Lowe

2024

ABSTRACT OF THE DISSERTATION

Protein Arginine Methyltransferases: The Breakfast Club of Enzymes

by

Troy Lucas Lowe

Doctor of Philosophy in Biochemistry, Molecular and Structural Biology

University of California, Los Angeles, 2024

Professor Steven G. Clarke, Chair

Post translational modifications of proteins alter the biological landscape creating functional diversity. One modification, arginine methylation, was first identified in 1968 from calf thymus hydrolysates producing guanidino-methylated arginine derivatives. However, the enzymes that produce these modifications were poorly characterized until 1996 when the genes of the first protein arginine methyltransferases were cloned from yeast and mammalian cells. At this time, a family of nine mammalian genes has been identified that encode protein arginine methyltransferases (PRMTs). In vitro experiments identified three distinct types. Type I PRMTs catalyze asymmetric dimethylarginine (ADMA) (PRMTs 1-4, 6 and 8), Type II PRMTs catalyze symmetric dimethylarginine (SDMA) (PRMT5 and 9), and the only type III PRMT that catalyzes monomethylarginine (MMA) (PRMT7). The active sites of each of the major enzymes that form ADMA, SDMA and MMA have distinct structural architectures allowing for their specificity.

In this dissertation I have focused my work on the major type I enzyme, PRMT1, the major type II enzyme, PRMT5, and the type III enzyme, PRMT7. I showed that each of these human enzymes behave differently under physiological stress conditions associated with temperature,

pH, and ionic strength thus potentially leading to alterations in the proteomic arginine methylation landscape. In particular, PRMT7 is maximally active at sub-physiological temperatures and at nonphysiological pH and ionic strength, suggesting regulatory roles. I then characterized the unusual substrate specificity of the PRMT7 enzyme with peptide substrates to demonstrate the exquisite dependence upon variations of the Arg-X-Arg motif.

With the identification of a PRMT7 motif in the human Fhod1 and Fhod3 actin binding proteins, I characterized methylation reactions that were dependent upon the phosphorylation state of an adjacent serine residue. These results pointed to the cross-talk that can occur between phosphorylation and methylation reactions. Interestingly, I found little or no effect of methylation on ROCK1 protein kinase activity.

PRMT enzymes have been identified to be oncogenic and closely associated with cancer progression. Surprisingly, it was found that methionine-dependent malignant cancer cells had no detectable alteration of protein arginine methylation than methionine-independent less malignant cells, suggesting that the methionine effect maybe be regulated through alternative pathways.

The dissertation of Troy Lucas Lowe is approved.

Catherine F. Clarke

Joseph A. Loo

Megan M. McEvoy

Steven G. Clarke, Committee Chair

University of California, Los Angeles

2024

DEDICATION

I would like to dedicate this work to my family.

To my dad, Les Lowe, and my mom, Josephine Lucas, thank you for everything and the support

you have given me throughout my life. Allowing me to be whatever I want and whatever gives

me joy and happiness.

To my sisters, Cassie and Christie, we're hella old.

TABLE OF CONTENTS

LIST OF FIGURES

LIST OF TABLES

ACKNOWLEDGEMENTS

I would like to thank Dr. Steven Clarke for his amazing mentorship and guidance that he has constantly provided throughout my graduate career at UCLA. I would also like to thank my previous PI from San Francisco State University, Dr. Raymond Esquerra for initially accepting me into his laboratory and giving me the confidence to pursue a PhD. I would have not been able to be where I am at today without both.

I would also like to thank previous lab members, Dr. Jonathan Lowenson for the thoughtful and critical questions during group meetings and journal clubs. Dr. Andrea Hadjikyriacou, for first showing me around the lab when I needed help in my first year. Dr. Kanishk Jain for the guidance and mentorship when I initially rotated in the Clarke lab, and Dr. Jonelle White for the amazing pep talks about graduate school.

I would also like to thank the current graduate students, Eric Pang and Cindy Wang, for their own individual expertise: Structural biology and computational chemistry. As well as their thoughtful questions and ideas during group meetings and journal clubs.

I would also like to say a special thank you to the three undergraduate students who have made me proud to be a mentor. Cyrus Safaeipour for his work and contributions to the PRMT7 and PRMT9 inhibitor paper, Tim Bondoc for his work on the exquisite specificity of PRMT7, and Ashley Holtz for her work on PRMTs in osteosarcoma cells.

I would also like to give a special thank you to my committee members for all the help and support throughout the years – Dr. Catherine Clarke, Dr. Joseph Loo, and Dr. Megan McEvoy.

Chapter 3 of this dissertation is a publication titled "Protein arginine methyltransferases can be optimally active at nonphysiological conditions" in the Journal of Biological Chemistry. I

VITA

2007-2015   Bachelors of Science in Biochemistry

San Francisco State University, San Francisco, CA

2017-2024   Doctorate of Philosophy in Biochemistry and Molecular Biology

(Expected)   University of California, Los Angeles, Los Angeles, CA

2018-2024   Teaching Assistant, Department of Chemistry and Biochemistry

University of California, Los Angeles, Los Angeles, CA

2018-2020   Cellular and Molecular Biology Predoctoral Fellow, Trainee

University of California, Los Angeles, Los Angeles, CA

2019   Candidate in Philosophy in Biochemistry and Molecular Biology

University of California, Los Angeles, Los Angeles, CA

2022-2023   Audree Fowler Fellowship in Protein Science

University of California, Los Angeles, Los Angeles, CA

2022   Taylor M. Brown Memorial Award

University of California, Los Angeles, Los Angeles, CA

2024   Daniel E. Atkinson and Charles A. West Dissertation Award

University of California, Los Angeles, Los Angeles, CA

PUBLICATIONS

Lowe, T.L., Valencia, D.A., Velasquez, V. E., Quinlan, M. E., and Clarke, S.G. "Arginine methylation of the family of formin homology domain containing proteins (FHOD) by protein arginine methyltransferase 7 (PRMT7) is inhibited by serine phosphorylation." *Journal of Biological Chemistry* 300.3 (2024). 10.1016/j.jbc.2024.106829

Holtz, A.G., **Lowe, T.L.**, Aoki, Y., Kubota, Y., Hoffman, R.M. and Clarke, S.G., 2023. Asymmetric and symmetric protein arginine methylation in methionine-addicted human cancer cells. *Plos one*, *18*(12), p.e0296291. DOI: 10.1371/journal.pone.0296291

Feoli, A., Iannelli, G., Cipriano, A., Milite, C., Shen, L., Wang, Z., Hadjikyriacou, A., **Lowe, T.L.**, Safaeipour, C., Viviano, M. and Sarno, G., 2023. Identification of a Protein Arginine Methyltransferase 7 (PRMT7)/Protein Arginine Methyltransferase 9 (PRMT9) Inhibitor. *Journal of Medicinal Chemistry*, *66*(19), pp.13665-13683. DOI: 10.1021/acs.jmedchem.3c01030

Bondoc, T.J., **Lowe, T.L.** and Clarke, S.G., 2023. The exquisite specificity of human protein arginine methyltransferase 7 (PRMT7) toward Arg-X-Arg sites. *Plos one*, *18*(5), p.e0285812. DOI: 10.1371/journal.pone.0285812

Lowe, T.L. and Clarke, S.G., 2022. Human protein arginine methyltransferases (PRMTs) can be optimally active under nonphysiological conditions. *Journal of Biological Chemistry*, *298*(9). DOI: 10.1016/j.jbc.2022.102290

Chapter 1

Plan of Dissertation

In Chapter 2 I introduce protein arginine methyltransferases (PRMTs) including the common techniques to test their activity. In particular I briefly explain the history of arginine methylation, as well as introduce the major type I enzyme, PRMT1, the major type II enzyme, PRMT5, and only type III enzyme, PRMT7. As part of the common techniques to test PRMT activity, I highlight personal experience of the pitfalls of the techniques used.

Chapter 3 will demonstrate the idea that PRMTs can be most optimal at nonphysiological conditions. While the goal of this chapter was to initially establish parameters that govern PRMT activity, it was ultimately discovered that the major enzymes of the individual subcategories are all quite unique to some degree. Utilizing recombinant purified enzymes from *E. coli* and purchased purified enzymes from HEK293 cells, in vitro characterization of temperature, pH and ionic strength were performed. This chapter was sparked from an idea that was previously established in the Clarke lab prior to me joining. Evidence was provided that PRMT7 activity was most active at temperatures lower than the human body temperature, thus leading to the idea that other intracellular conditions may have a profound effect on enzyme activity.

Chapter 4 examines why histone H2B is presently the best *in vitro* substrate known for PRMT7. Previously established research in the Clarke Lab identified histone H2B as an excellent substrate for PRMT7, with monomethylation detected *in vitro* at arginine residues 29, 31, and 33, and defined RXR motifs as substrate recognition elements. However, other groups have found that H2B was not methylated by PRMT7 in higher oligomeric chromatin structures. This chapter

examines both *H. sapiens* and *X. laevis* histone H2B as substrates for PRMT7 while also identifying how adjacent amino acid residues might affect PRMT7 activity utilizing some of the conditions established in chapter 3.

In Chapter 5 we utilize findings from chapter 4 and further identify new potential substrates for PRMT7 as well as to elaborate on how modifications of adjacent amino acids affect PRMT7 activity. Here we take advantage of a collaboration with the Margot Quinlan laboratory at UCLA to study the interaction of methylation and phosphorylation on the actin binding Fhod1 and Fhod3 proteins. In this chapter I examine how serine phosphorylation affects arginine methylation.

Chapter 6 investigates how arginine methylation might be involved in cancer. While protein arginine methyltransferases have been identified to be overexpressed in cancer, little is still known of the possible mechanisms linking arginine methylation to uncontrolled cellular growth. In this chapter we explored the Hoffman effect where malignant cancer cells demonstrate enhanced methionine usage and potential increases in protein arginine methylation. However, in this chapter we found no evidence for this. We concluded that any linear relationship between cancer, methionine, *S*-adenosylmethionine, and protein arginine methyltransferases is not straightforward.

Chapter 7 highlights my contributions to a collaboration with the Sbardella Lab at the University of Salerno in Italy that identified a novel dual inhibitor for PRMT7 and PRMT9.

The final chapter of this thesis, Chapter 8, contains unpublished data from key experiments performed throughout my graduate career. The purpose of this chapter is to present the preliminary data collected and to aid future researchers of protein arginine methyltransferases.

Chapter 2

Introduction to Protein Arginine methyltransferases (PRMTs)

In this chapter, I give a brief introduction to the three members of the mammalian PRMT family that I have studied in this dissertation – PRMT1, PRMT5, and PRMT7. I also introduce the major experimental methods that were used in these studies.

Introduction

The enzymatic post translational methylation of arginine residues was initially identified in late 1960s by Sangduk Kim and Woon Ki Paik from Fels Research Institute at the Temple University School of Medicine (Paik 2007). This modification results from a basic SN2 reaction between *S*-adenosylmethionine and the nitrogens of the guanidino sidechain of arginine (Fulton 2018). While arginine methylation is considered as one of the most abundant post translational modifications, with nearly 2% of all arginines to be methylated (Lee 2009), full knowledge of its biological relevance is still lacking (Paik 2007). To date nine mammalian genes encoding distinct protein arginine methyltransferase (PRMTs) have been identified (Bedford 2009). Isozymes have been identified but are less studied (Bedford 2007). Additionally, PRMTs are often overexpressed in cancer (Hwang 2021) and changes in arginine methylation have been identified in other disease states (Aletta 2008). Type I PRMTs catalyze asymmetric dimethylarginine (ADMA) (PRMTs 1-4, 6 and 8), Type II PRMTs catalyze symmetric dimethylarginine (SDMA) (PRMT5 and 9), and the only type III PRMT that catalyzes monomethylarginine (MMA) (PRMT7) (Holtz 2023).

PRMT1 the major Type I protein arginine methyltransferase

Protein arginine methyltransferase 1 (PRMT1) is the major type I enzyme of the family of arginine methyltransferases and accounts for approximately 85% of all arginine methylation (Zhang 2003). PRMT1 catalyzes asymmetric dimethylarginine ubiquitously throughout the human body, with the highest mRNA expression for its gene found in Epstein-Barr virus transformed lymphocytes (GTEx Portal website, see reference 10). While PRMT1 is known to methylate many protein substrates, a specific amino acid motif has not been identified for enzyme recognition. However, proteins containing sequences rich in glycine and arginine residues are generally good PRMT1 substrates (Wang 2023). Asymmetric dimethylarginine formation of these proteins are associated with transcriptional regulation, RNA processing, DNA damage repair, and signal transduction (Thiebaut 2021). Knockouts of the PRMT1 gene are known to lead to embryonic lethality in mice (Yu 2009). Additionally, PRMT1 knockout in HEK293T cells leads to growth arrest in the G2/M phase, and promotion of apoptosis (Zhou 2022). Studies have also identified that PRMT1 is not required for embryogenesis in *Xenopus tropicalis* but is important for growth and development. (Shibata 2020). While it is unknown how PRMT1 activity is regulated in the body, structural and enzymological approaches have discovered the minimal requirements for activity including oligomerization into either a heterodimer with other PRMTs, or homodimers (Morales 2015)(Pak 2011), low ionic strength, and homeostatic body temperature and pH (Lowe 2022).

PRMT5 the major Type II protein arginine methyltransferase

Protein arginine methyltransferase 5 (PRMT5) is one of two type II enzymes that catalyze symmetric dimethylarginine, accounting for the bulk of SDMA formation in mammalian cells (Bedford and Clarke 2009). PRMT5 is an important target for cancer therapeutics due to its

overexpression in cancer (Lattouf 2019). Because PRMT5 is so heavily researched, many inhibitors have been identified for PRMT5 that are highly selective (Gao 2023). The methyltransferase activity of PRMT5 is enhanced when it is complexed with the MEP50 protein (Antonysamy 2017), and knockouts of the PRMT5 gene lead to embryonic lethality (Stopa, 2015). It has been noted PRMT5 binds to antibodies recognizing FLAG tags, leading to the potential misidentification of other binding partners (Nishioka 2003).

PRMT7 the major Type III protein arginine methyltransferase

Protein arginine methyltransferase 7 (PRMT7) is the only type III PRMT to catalyze monomethylarginine as a final product (Zurita 2012) and methylates proteins containing RXR motifs (Feng 2013). PRMT7 has been studied much less intensively than PRMT1 and PRMT5. To date there have been 141 published papers on PubMed that mention PRMT7, with the first paper attempting to characterize *D. melanogaster* homologs, DARTs (Boulanger 2004). While this initial study was the groundbreaking work to first characterize the PRMT7 gene, northern blot analysis of the mRNA from varying stages and organs of Drosophila males and females resulted in little to no PRMT7 mRNA (Boulanger 2004). Additionally, it wasn't until 2006 when the first binding partner, the testis specific factor CTCFL, of PRMT7 was reported (Jelinic 2006). Unfortunately, there has been no reported evidence of CTCFL as a direct substrate for PRMT7 methylation. However, CTCFL does contain a sequence in its C-terminal region that may be recognized by PRMT7, RTRKR. To date there are 51 reported human individuals containing PRMT7 gene mutations, leading to loss of activity and neurodevelopmental disorders, skeletal abnormalities, and endocrine abnormalities (Cali 2023). While mutations of PRMT7 cause such issues, it is unknown if the cause of such phenotypes pertains to lack of function or alterations in structure.

Techniques for identification of PRMT activity

2D chromatography followed by amino acid hydrolysis.

Prior to the isolation of the PRMT genes, methylated amino acids were identified after protein hydrolysis. This approach led to the discovery of methylated lysine residues, using two-dimensional chromatography to separate individual amino acids (Ambler 1959). It wasn't until 1970 when methylated arginine residues were identified in hydrolysates of rat liver nuclei (Paik 1970). While this approach is powerful and still used today, the initial characterization of cell lysates resulted only in the identification of the modified amino acid without any knowledge of biological relevance or knowing which enzyme(s) was associated with each modification. To better understand the specific modification in a biologically relevant context, purified proteins identified from pulldowns are used with amino acid hydrolysis and methylarginine standards. Results from these experiments have identified that methylarginine peptides could be subcategorized into asymmetric dimethylarginine, symmetric dimethylarginine, and monomethylarginine (Lin 1996)(Branscombe 2001)(Zurita-Lopez 2012).

Direct methylation assays using radioactive S-adenosylmethionine

While much of today's research involves the identification of post translational modifications with the use of high-throughput techniques like mass-spectrometry of cell lysates, low-throughput techniques like direct modification of a substrate provides clearer evidence. Through the use of oriented peptide array libraries (OPALs) and direct methylation assays coupled with mass spectrometry, it was discovered that specific PRMTs recognize distinct amino acid sequences. PRMT1 recognizes arginine and glycine rich motifs (GARs) with preference over

strings of RGG (Herrmann 2005), PRMT5 also methylates GAR motifs but can also methylate PGM motifs (Bedford 2009), and PRMT7 has preference for RXR motifs (Feng 2013).

Two distinct assays were performed in this thesis. While both use a direct methylation with a [*methyl*-^{3}H]-AdoMet molecule, each have their own pros and cons and will be outlined. The first direct methylation assay involves a radioactive gel assay. PRMT, substrate, and [*methyl*-^{3}H]-AdoMet are mixed together and allowed to incubate. Post termination, the polypeptides are separated using SDS-PAGE. The signal of the [*methyl*-^{3}H]-AdoMet is enhanced by then soaking the gel in a liquid autoradiography enhancer and then exposure to a silver halide autoradiograph film where the radioactive source will exposure the film. Some pros with this technique include not having to separate excess nonreacted [*methyl*-^{3}H]-AdoMet prior to exposure. Additionally, the separation of individual polypeptides helps to identify which proteins are methylated with the subsequent step of mass spectrometry identification. Some cons involved with this technique include the length of gel exposure to the autoradiograph film. The time needed to obtain a result can vary with results being obtained between 1 day to 60 days. Another con involves the identification of methylated peptides (Thomas 2014). I found that small peptides are not able to stay within the polyacrylamide matrix in gel separation, leading to a loss of sample. The other direct methylation assay involves a P81 phosphocellulose binding assay. Similar to the previous assay, PRMT, substrate, and [*methyl*-^{3}H]-AdoMet are mixed together and allowed to incubate. Post termination, the samples are blotted onto a phosphocellulose paper, the proteins and methylated proteins are bound to the paper while the excess [*methyl*-^{3}H]-AdoMet can be washed away. While this assay is quicker than a gel assay with results being obtained within a day, I found that it was not without problems. These problems include the inconsistent commercial availability and quality of the P81 phosphocellulose paper. Additionally, I found that the backgrounds for each assay can vary heavily where you can get a range of 50-3000 counts per minute differences. I postulate that the proteins that are blotted onto the paper can trap excess [*methyl*-^{3}H]-AdoMet and that is not readily washed away from the paper.

7

References

1) Paik, Woon Ki, David C. Paik, and Sangduk Kim. "Historical review: the field of protein methylation." *Trends in biochemical sciences* 32.3 (2007): 146-152.

2) Fulton, Melody D., Tyler Brown, and Y. George Zheng. "Mechanisms and inhibitors of histone arginine methylation." *The Chemical Record* 18.12 (2018): 1792-1807.

3) Lee, Young-Ho, and Michael R. Stallcup. "Minireview: protein arginine methylation of nonhistone proteins in transcriptional regulation." *Molecular endocrinology* 23.4 (2009): 425-433.

4) Bedford, Mark T., and Steven G. Clarke. "Protein arginine methylation in mammals: who, what, and why." *Molecular cell* 33.1 (2009): 1-13.

5) Hwang, Jee Won, et al. "Protein arginine methyltransferases: promising targets for cancer therapy." *Experimental & molecular medicine* 53.5 (2021): 788-808.

6) Aletta, John M., and John C. Hu. "Protein arginine methylation in health and disease." *Biotechnology annual review* 14 (2008): 203-224.

7) Holtz, Ashley G., et al. "Asymmetric and symmetric protein arginine methylation in methionine-addicted human cancer cells." *Plos one* 18.12 (2023): e0296291.

8) Bedford, Mark T. "Arginine methylation at a glance." *Journal of cell science* 120.24 (2007): 4243-4246.

9) Zhang, Xing, and Xiaodong Cheng. "Structure of the predominant protein arginine methyltransferase PRMT1 and analysis of its binding to substrate peptides." *Structure* 11.5 (2003): 509-520.

10) The GTEx Portal on 05/05/24 and/or dbGaP accession number phs000424.v8.p2 on 05/05/24.

11) Wang, Yi-Chun, et al. "Identification and characterization of glycine-and arginine-rich motifs in proteins by a novel GAR motif finder program." *Genes* 14.2 (2023): 330.

12) Thiebaut, Charlène, et al. "Structure, activity, and function of PRMT1." *Life* 11.11 (2021): 1147.

13) Yu, Zhenbao, et al. "A mouse PRMT1 null allele defines an essential role for arginine methylation in genome maintenance and cell proliferation." *Molecular and cellular biology* (2009).

14) Zhou, Mei-Lin, Jin-Ni Ma, and Lu Xue. "Effect of Protein Arginine Methyltransferase 1 Gene Knockout on the Proliferation of Human Embryonic Kidney 293T Cells." *Biology Bulletin* 49.Suppl 2 (2022): S1-S11.

15) Shibata, Yuki, et al. "Knocking out histone methyltransferase PRMT1 leads to stalled tadpole development and lethality in Xenopus tropicalis." *Biochimica et Biophysica Acta (BBA)-General Subjects* 1864.3 (2020): 129482.

16) Morales, Yalemi, et al. "Redox control of protein arginine methyltransferase 1 (PRMT1) activity." *Journal of Biological Chemistry* 290.24 (2015): 14915-14926.

17) Pak, Magnolia L., et al. "A protein arginine N-methyltransferase 1 (PRMT1) and 2 heteromeric interaction increases PRMT1 enzymatic activity." *Biochemistry* 50.38 (2011): 8226-8240.

18) Lowe, Troy L., and Steven G. Clarke. "Human protein arginine methyltransferases (PRMTs) can be optimally active under nonphysiological conditions." *Journal of Biological Chemistry* 298.9 (2022).

19) Lattouf, Hanine, Coralie Poulard, and Muriel Le Romancer. "PRMT5 prognostic value in cancer." *Oncotarget* 10.34 (2019): 3151.

20) Gao, Jing, et al. "A patent review of PRMT5 inhibitors to treat cancer (2018-present)." *Expert Opinion on Therapeutic Patents* 33.4 (2023): 265-292.

21) Antonysamy, Stephen. "The structure and function of the PRMT5: MEP50 complex." *Macromolecular Protein Complexes: Structure and Function* (2017): 185-194.

22) Stopa, Nicole, Jocelyn E. Krebs, and David Shechter. "The PRMT5 arginine methyltransferase: many roles in development, cancer and beyond." *Cellular and molecular life sciences* 72 (2015): 2041-2059.

23) Nishioka, Kenichi, and Danny Reinberg. "Methods and tips for the purification of human histone methyltransferases." *Methods* 31.1 (2003): 49-58.

24) Zurita-Lopez, Cecilia I., et al. "Human protein arginine methyltransferase 7 (PRMT7) is a type III enzyme forming ω-NG-monomethylated arginine residues." *Journal of Biological Chemistry* 287.11 (2012): 7859-7870.

25) Feng, You, et al. "Mammalian protein arginine methyltransferase 7 (PRMT7) specifically targets RXR sites in lysine-and arginine-rich regions." *Journal of Biological Chemistry* 288.52 (2013): 37010-37025.

26) Thomas, Dylan, et al. "Protein Arginine N-Methyltransferase Substrate Preferences for Different Nη-Substituted Arginyl Peptides." *ChemBioChem* 15.11 (2014): 1607-1613.

27) Boulanger, Marie-Chloé, et al. "Characterization of the Drosophila protein arginine methyltransferases DART1 and DART4." *Biochemical journal* 379.2 (2004): 283-289.

28) Jelinic, Petar, Jean-Christophe Stehle, and Phillip Shaw. "The testis-specific factor CTCFL cooperates with the protein methyltransferase PRMT7 in H19 imprinting control region methylation." *PLoS biology* 4.11 (2006): e355.

29) Cali, Elisa, et al. "Biallelic PRMT7 pathogenic variants are associated with a recognizable syndromic neurodevelopmental disorder with short stature, obesity, and craniofacial and digital abnormalities." *Genetics in Medicine* 25.1 (2023): 135-142.

30) Ambler, R. P., and M. W. Rees. "ε-N-methyl-lysine in bacterial flagellar protein." *Nature* 184.4679 (1959): 56-57.

31) Paik, Woon Ki, and Sangduk Kim. "ω-N-Methylarginine in Protein." *Journal of Biological Chemistry* 245.1 (1970): 88-92.

32) Lin, Wey-Jinq, et al. "The mammalian immediate-early TIS21 protein and the leukemia-associated BTG1 protein interact with a protein-arginine N-methyltransferase." *Journal of Biological Chemistry* 271.25 (1996): 15034-15044.

33) Branscombe, Tina L., et al. "PRMT5 (Janus kinase-binding protein 1) catalyzes the formation of symmetric dimethylarginine residues in proteins." *Journal of Biological Chemistry* 276.35 (2001): 32971-32976.

34) Herrmann, Frank, et al. "Dynamics of human protein arginine methyltransferase 1 (PRMT1) in vivo." *Journal of Biological Chemistry* 280.45 (2005): 38005-38010.

35) Zeng, Hao, and Wei Xu. "Enzymatic assays of histone methyltransferase enzymes." *Epigenetic technological applications.* Academic Press, 2015. 333-361.

Chapter 3

Human Protein Arginine Methyltransferases (PRMTs) Can Be Optimally Active Under Non-Physiological Conditions

The work described in this chapter has been reproduced from:

Significance Statement

Understanding the relationship between an enzyme and its substrate can give insights to an enzyme's biological relevance. However, in some instances this is not the case. Protein arginine methyltransferases catalyze methylarginine on a multitude of substrates that have been identified using high throughput approaches. Because many of these high throughput approaches have not been verified, correlation of these enzymes to a specific biological process has remained difficult. Depending on these specific variables and circumstances, methylarginine marks have been identified as a ubiquitous modification in cancer, epigenetic regulation, disease states, as well as development.

Enzyme families usually contain highly conserved structural motifs leading to similar enzymatic catalysis. While the family of protein arginine methyltransferases are no different, the final modification that each can produce differs to some degree. The major three enzymes that catalyze the three types of methylated arginines include: PRMT1 catalyzing asymmetric dimethylarginine, PRMT5 catalyzing symmetric dimethylarginine, and PRMT7 catalyzing monomethylarginine (PRMT7). While all three of these enzymes have been identified to be overexpressed in a variety of cancers, the importance and involvement of each enzyme remains indistinguishable. Because the microenvironment of a cell is altered in a cancerous state, I was curious as to how these three enzymes behave under non-physiological conditions. It was determined that the conditions for PRMT1 and PRMT5 optimal activity are very similar but differ with pH. Additionally, the conditions that make PRMT7 most active are completely non-physiological, allowing PRMT7 to be more discernible in activity compared to PRMT1 and PRMT5.

The work provided in this study highlights that small differences in a cellular environment can alter PRMT activity. While important to know, it is still unknown whether these small differences translate to an in vivo system or are relevant due to the ever-changing landscape of a cell.

Human protein arginine methyltransferases (PRMTs) can be optimally active under nonphysiological conditions

Troy L. Lowe[1,2] **and Steven G. Clarke**[1,2,*]

From the [1]Department of Chemistry and Biochemistry, and [2]Molecular Biology Institute, University of California Los Angeles, Los Angeles, California, USA

Edited by Brian Strahl

Protein arginine methylation is involved in many biological processes and can be enhanced in cancer. In mammals, these reactions are catalyzed on multiple substrates by a family of nine protein arginine methyltransferases (PRMTs). However, conditions that may regulate the activity of each enzyme and that may help us understand the physiological role of PRMTs have not been fully established. Previous studies had suggested unexpected effects of temperature and ionic strength on PRMT7 activity. Here we examine in detail the effects of temperature, pH, and ionic strength on recombinant human PRMT1, PRMT5, and PRMT7. We confirmed the unusual temperature dependence of PRMT7, where optimal activity was observed at 15 °C. On the other hand, we found that PRMT1 and PRMT5 are most active near physiological temperatures of 37 °C. However, we showed all three enzymes still have significant activity at 0 °C. Furthermore, we determined that PRMT1 is most active at a pH of about 7.7, while PRMT5 activity is not dependent on pH in the range of 6.5 to 8.5. Significantly, PRMT7 is most active at an alkaline pH of 8.5 but shows little activity at the physiological intracellular pH of about 7.2. We also detected decreased activity at physiological salt conditions for PRMT1, PRMT5, and PRMT7. We demonstrate that the loss of activity is due to the increasing ionic strength. Taken together, these results open the possibility that PRMTs respond in cells undergoing temperature, salt, or pH stress and demonstrate the potential for *in vivo* regulation of protein arginine methylation.

Protein diversity heavily relies on many enzymes that modify amino acid residues. A major site of protein posttranslational modification is methylation at the guanidino group of arginine residues. These modifications create distinct interactions between proteins and play a significant role in biology including transcription of DNA, activation of enzyme activity, and protein degradation (1–4). In mammals, nine specific enzymes (protein arginine methyltransferases [PRMTs]) have been characterized and are classified based on the specific reaction they catalyze (5–7). While all PRMTs can initially catalyze monomethylarginine formation, type I PRMTs (PRMT1, 2, 3, 4, 6, and 8) catalyze asymmetric dimethylarginine formation and type II PRMTs

(PRMT 5 and 9) catalyze symmetric dimethylarginine formation, while type III PRMTs (PRMT7) only catalyzes monomethylarginine formation. Determination of the *in vitro* activity of these purified PRMT enzymes can give important clues to their substrate specificity and their possible regulation (8–12).

For intracellular cytosolic mammalian enzymes, the assumption is usually made that activity will be at or near optimum levels at the physiological pH of about 7.2 (13), an ionic strength of about 120 mM (14), and a temperature of 37 °C (15). However, we were surprised to find that PRMT7 had little activity at 37 °C and maximum activity was noted at colder temperatures (16, 17). Additionally, little activity was found at the physiological salt concentrations that occur within a cell (16). However, these measurements were generally not taken under initial velocity conditions and we were thus interested in a more detailed picture of PRMT7 catalysis, especially under nonphysiological conditions. We were also interested in comparing the catalysis shown by PRMT7 with that of PRMT1, the major type I enzyme, creating asymmetric dimethylarginine, and PRMT5, the major type II enzyme, creating symmetric dimethylarginine residues.

Here we show that human PRMT1, PRMT5, and PRMT7 activity is optimal under varying conditions. Specifically, PRMT7 activity is optimal at subphysiological temperatures in an alkaline environment containing low salt concentrations. We have also shown that PRMT1 and PRMT5 activities are most optimal closer to physiological temperature and pH, but where reaction mixtures contain little salt.

Results

GST-HsPRMT7 is active at physiological temperatures but has optimal activity at subphysiological temperatures

Recent findings have demonstrated that human histone H2B (HsH2B) is an excellent substrate for PRMT7, with methylation sites detected at arginine residues 29, 31, and 33 (10). A synthetic peptide containing residues 23 to 37 (HsH2B (23–37)) was also an excellent substrate (10). Significantly, optimal PRMT7 activity was found at about 20 °C with very little activity at 37 °C (16). Similar effects were found with the bacterially expressed GST human enzyme fusion protein and the insect-expressed untagged mouse enzyme (10). However, because these activities were measured at long incubation times, we wanted to determine the temperature dependence

under initial rate conditions. We first determined that GST-HsPRMT7 activity is linear with time up to 1 h at both 20 °C and 37 °C with the HsH2B (23–37) peptide (Fig. 1). At 37 °C, we found only about 25% of the activity as found at 20 °C. We also showed no significant increase of activity when the peptide concentration was raised from 10 µM to 50 µM, indicating that enzyme was saturated with the peptide substrate at the lower concentration. These results now clearly show that PRMT7 activity is not optimal at the physiological temperature.

Similar results to those shown in Figure 1 with the HsH2B (23–37) peptide substrate were found when we used the GST-GAR protein substrate (Fig. 2). At the 60-min and 120-min timepoints, only about 20 to 30% of the activity at 20 °C was found at 37 °C. Using an alternate assay where the ^{3}H-methylated GST-GAR polypeptides formed in a 2-h assay were fractionated by SDS-PAGE and analyzed by densitometry following fluorimetry, we found 9.2% of the activity at 37 °C as found at 20 °C (data not shown). We also used this latter assay with a recombinant full-length human HsH2B protein and found less than 11% of the activity at 37 °C as found at 20 °C (data not shown).

In Figure 3, we measured GST-HsPRMT7 activity at temperature values between 0 °C and 45 °C with the HsH2B (23–37) peptide using the P81 phosphocellulose assay. We found the peak of activity at 15 °C with half activity at 0 °C and at 20 to 25 °C. At the physiological temperature of 37 °C, only about 20% of the activity was found compared to that of 15 °C. These data clearly show that PRMT7 is most active in the cold.

Decreased human PRMT7 activity at 37 °C is not due to enzyme instability

To determine if incubation at 37 °C irreversibly denatured PRMT7, we performed the experiment in Figure 4. Here, we preincubated the enzyme at 4 °C, 20 °C, and 37 °C for 2 h and
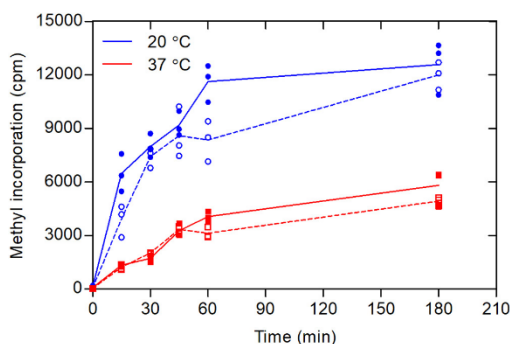
Figure 1. Human PRMT7 is more active at subphysiological temperatures with histone H2B peptide as a substrate. P81 phosphocellulose assay of GST-HsPRMT7 and HsH2B (23–37) was performed at 20 °C and 37 °C as described in the Experimental procedures section. Five micrograms of GST-HsPRMT7 was incubated with peptide and 0.14 µM [^{3}H]AdoMet. *Blue lines* represent reaction mixtures at 20 °C using 10 µM peptide (*closed circles*) or 50 µM peptide (*open circles*). The *red line* represents reaction mixtures at 37 °C using 10 µM peptide (*closed squares*) or 50 µM peptide (*open squares*). HsH2B, histone H2B; PRMT, protein arginine methyltransferase.

then assayed activity at each of these temperatures. We found little or no loss of activity when assayed at 4 °C, suggesting that PRMT7 was not denatured at 37 °C. In all cases, similar activities were found when each of the incubated samples was assayed at the indicated temperature. Additionally, previous work had shown that the circular dichroism spectrum of PRMT7 was identical at 4 °C, 17 °C, and 37 °C, suggesting that the enzyme is stable at these temperature ranges (18). Additionally, it was shown that the molecular weight of PRMT7 by sedimentation equilibrium analysis was also identical at these three temperatures (18).

His-HsPRMT1 and HsPRMT5/MEP50 are most active near physiological temperatures

We then wanted to establish the generality of the methyltransferase activity at subphysiological temperatures with the major type I enzyme PRMT1 and the major type II enzyme PRMT5. We thus tested His-HsPRMT1 and HsPRMT5/MEP50 under similar conditions to those used above for GST-HsPRMT7 (Fig. 5). For PRMT1, we found a broad optimal peak between 20 °C and 37 °C with half optimal activities at about 15 °C and 45 °C. For PRMT5, the temperature optimum was found at 37 °C with half optimal activity of 25 °C and over 45 °C. Taken together, these results show that PRMT1 and PRMT5 have temperature optimums near physiological body temperature and show distinct patterns from PRMT7. However, we did detect the activity of both enzymes throughout this temperature range.

PRMT1, PRMT5, and PRMT7 are all active at 0 °C

We found that PRMT1, PRMT5, and PRMT7 all displayed activity at 0 °C. To confirm this surprising result, we performed additional time course experiments in assays done entirely on ice (Fig. 6). All of these enzymes were found to have significant activity at 0 °C. GST-HsPRMT7 activity was almost 6-fold higher at 0 °C than at 37 °C. His-HsPRMT1 activity was 6-fold lower in activity at 0 °C than in reaction mixtures that were performed at 37 °C, and HsPRMT5/MEP50 activity was about 3-fold lower at 0 °C than at 37 °C.

PRMT7 is active at alkaline pH

Our finding that PRMT7 is most active at nonphysiological temperatures lead us to examine its activity as a function of pH. As shown in Figure 7A, we were surprised to find little to no activity at the physiological pH of 7.2. This enzyme was found to be more active at alkaline pH values with a pH optimum of 8.4. We performed a control experiment showing that changes in pH did not affect the P81 phosphocellulose assay (Fig. S1). These results suggest that PRMT7 might respond to changes in cellular pH that lead to alkalization.

We also performed pH studies using a substrate of GST-GAR and an SDS-PAGE assay as described in the Experimental procedures (Fig. S2). The results shown here are very similar to those found in Figure 7A with the HsH2B (23–37) peptide and the P81 phosphocellulose assay.

15
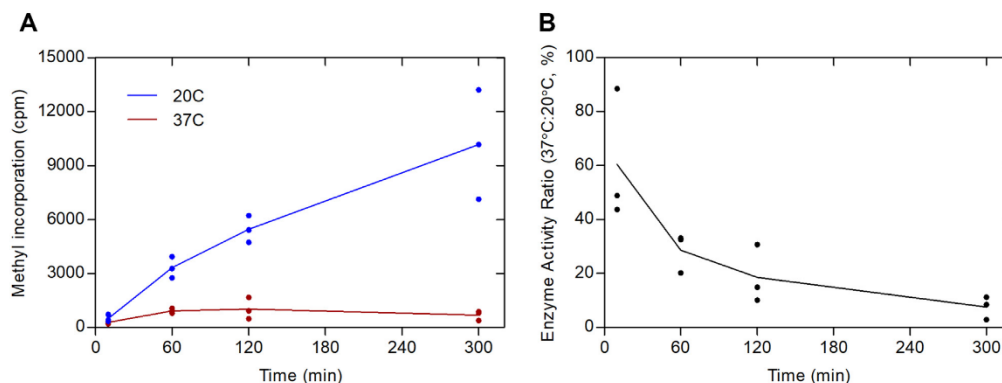
Figure 2. Human PRMT7 is more active at subphysiological temperatures with GST-GAR as a substrate. *A*, P81 phosphocellulose assay of GST-HsPRMT7 activity. GST-HsPRMT7, 6.2 μg GST-GAR, and 0.7 μM [³H]AdoMet was incubated at either 20 °C or 37 °C as described in Experimental procedures. The *blue line* represents the averages of individual reactions at 20 °C (*blue dots*). The *red line* represents individual replicates of reaction mixtures tested at 37 °C (*red dots*). *B*, ratios of reactions performed at 37 °C to 20 °C. The *black line* represents the averages of the individual ratios calculated from *A*. PRMT, protein arginine methyltransferase.

PRMT1 and PRMT5 have distinct pH activity profiles from PRMT7

To compare the activity of the major PRMT1 type I enzyme and the major PRMT5 type II enzyme with PRMT7 as a function of pH, we performed the assays shown in Figure 7, *B* and *C*. We found that His-PRMT1 has a pH optimum of about 7.7 with good activity at the physiological pH of 7.2. Additionally, we found that PRMT5/MEP50 is equally active across a wide range of pH values between 6.6 and 8.5. Here, PRMT1 and PRMT5 appeared to differ from PRMT7 in showing activity at the physiological pH.

PRMT7 is inhibited by the addition of salts

Previous studies have shown that GST-HsPRMT7 activity decreases with increasing NaCl concentrations with little activity seen at physiological salt concentrations, particularly for the HsH2B (23–37) peptide (16). Additionally, a loss of approximately 50% activity was found in 2 mM magnesium and calcium salts (16). Given our results above that PRMT7 has optimal activity outside of the normal physiological range of pH and temperature, we wanted to expand upon these findings. In Figure 8, we show that GST-HsPRMT7 activity decreases not only with NaCl but also with KCl. To ask if this effect is due to ionic strength, we also assayed the enzyme in Na_2SO_4. We found that the activity is dependent on the ionic strength with half activity at about 50 mM and almost no activity at 150 mM. Since typical intracellular ionic strength values range from about 130 to 270 mM (14), these results

Figure 3. Human PRMT7 is more active at lower temperatures under steady-state kinetics. P81-based assay of GST-HsPRMT7, 10 μM HsH2B (23–37), and 0.14 μM [³H]AdoMet was carried out as described in Experimental procedures. Reaction mixtures were incubated for 30 min, spotted on P81 phosphocellulose paper, and further assayed as described in Experimental procedures. The data shown are from a single experiment: similar results were seen in three additional replicated experiments. HsH2B, histone H2B; PRMT, protein arginine methyltransferase.

Figure 4. Human PRMT7 activity is stable from 4 °C to 37 °C. GST-HsPRMT7 was preincubated for 2 h at 4 °C, 20 °C, and 37 °C in the presence of the HsH2B (23–37) substrate and 50 mM K-Hepes, 1 mM DTT at a final pH of 8.5. The enzymatic reaction was then initiated by addition of a final concentration of 0.7 μM [³H]AdoMet and was then incubated for 2 h at the indicated temperature followed by the P81 phosphocellulose assay as described in Experimental procedures. Data are shown for triplicate of samples with standard deviation shown as error bars. HsH2B, histone H2B; PRMT, protein arginine methyltransferase.

ASBMB

J. Biol. Chem. (2022) 298(9) 102290 **3**

16
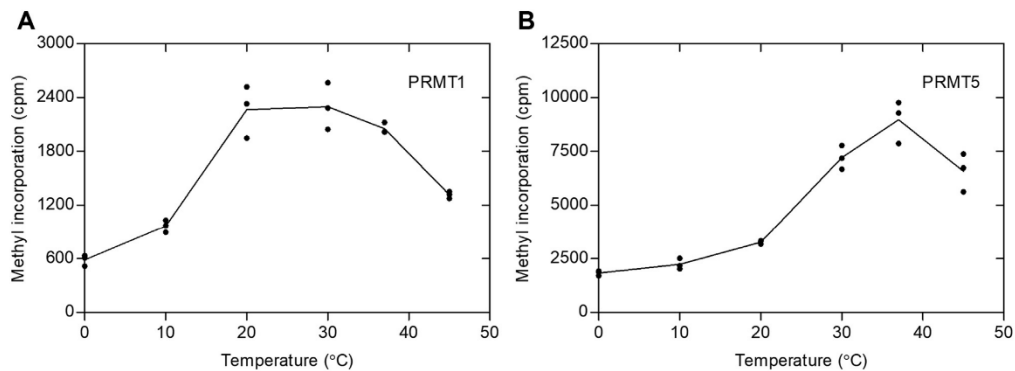
Figure 5. Human PRMT1 and PRMT5/MEP50 are more active near physiological temperatures. *In vitro* reaction mixtures were incubated at the specified temperatures and assayed using a P81 phosphocellulose assay. Reaction mixtures contained 50 mM K-HEPES, 1 mM DTT and had a final pH of 8.0. Reactions were allowed to incubate for 30 min. *A*, 80 nM of His-HsPRMT1 was incubated with 10 µM HsH4 (1–21) and 0.14 µM [^{3}H]AdoMet. *B*, 5.6 nM of HsPRMT5/MEP50 was incubated with 10 µM of HsH4 (1–21), and 0.14 µM [^{3}H]AdoMet. HsH4, histone H4; PRMT, protein arginine methyltransferase.
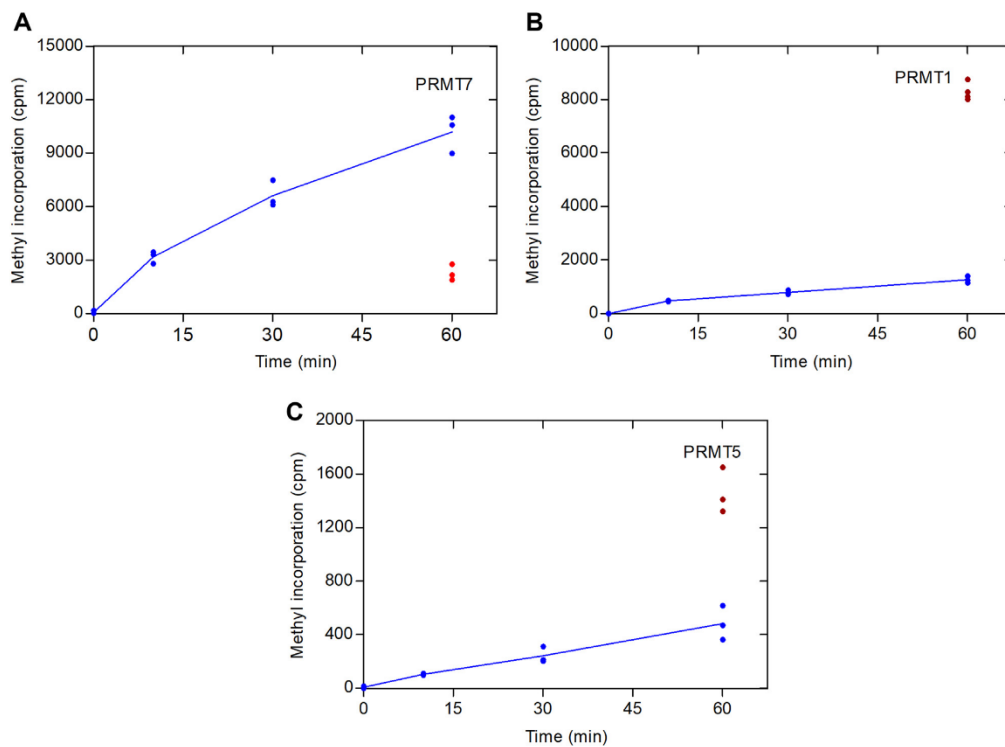
Figure 6. Human PRMT7, PRMT1, and PRMT5/MEP50 are active at 0 °C. P81 phosphocellulose assays of reactions containing GST-HsPRMT7 with HsH2B (23–37), His-HsPRMT1 with HsH4 (1–21), or HsPRMT5/MEP50 with HsH4(1–21) was carried out as described in Experimental procedures. *A*, Five micrograms of GST-HsPRMT7 was mixed with 10 µM HsH2B (23–37) and 0.14 µM of [^{3}H]AdoMet. Reaction mixtures contained 50 mM K-Hepes, 1 mM DTT, at a final reaction pH of 8.5. *B*, 40 nM of His-HsPRMT1 was mixed with 10 µM HsH4 (1–21) and 0.14 µM of [^{3}H]AdoMet. Reaction mixtures contained 50 mM K-Hepes, 1 mM DTT, at a final reaction pH of 7.0. *C*, 5.6 nM of HsPRMT5/MEP50 was mixed with 10 µM HsH4 (1–21) and 0.14 µM [^{3}H]AdoMet. Reaction mixtures contained 50 mM K-Hepes, 1 mM DTT, at a final reaction pH of 7.0. All reaction mixtures were equilibrated to 0 °C for 2 min prior to initiation with [^{3}H] AdoMet. The *blue line* represents averages of replicates at 0 °C. *Red dots* represent reactions incubated at 37 °C. HsH2B, histone H2B; HsH4, histone H4; PRMT, protein arginine methyltransferase.

17
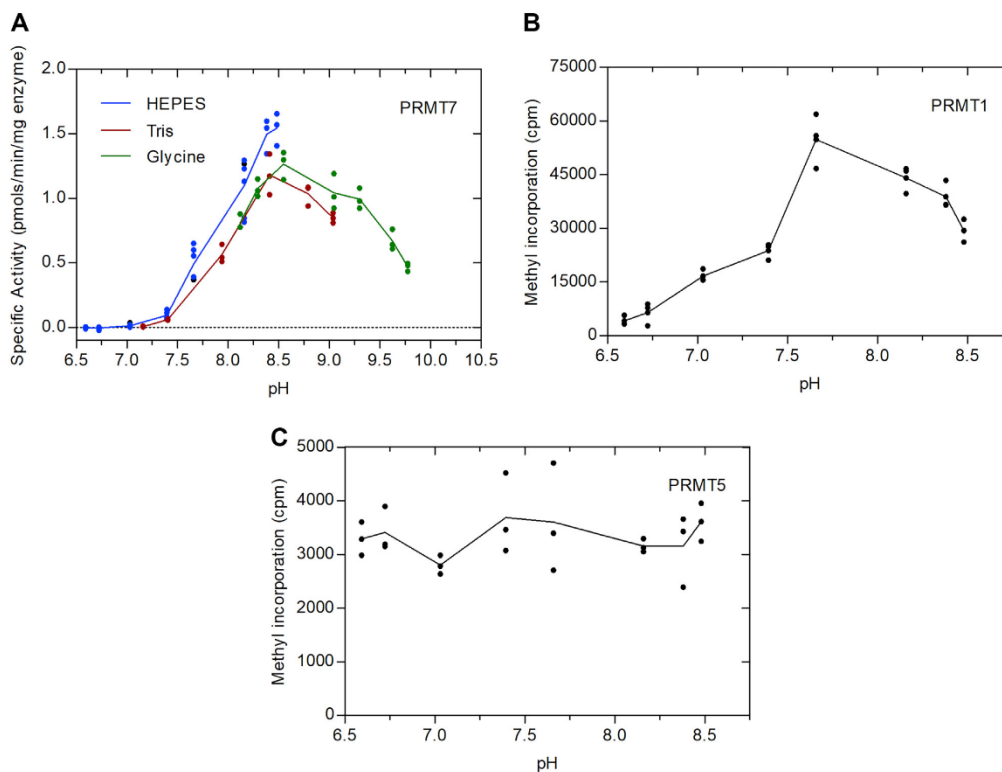
Figure 7. pH dependence of human PRMT7, PRMT1, and PRMT5/MEP50. P81 phosphocellulose assay with either GST-HsPRMT7 and HsH2B (23–37), His-HsPRMT1 and HsH4 (1–21) or HsPRMT5/MEP50 and HsH4 (1–21) was carried out as described in Experimental procedures. *A,* five micrograms of of GST-HsPRMT7, 10 µM of HsH2B (23–37), and 0.14 µM [^{3}H]AdoMet. The *red line* represents averages of replicates where reaction mixtures contain 50 mM K-Hepes, 1 mM DTT. The *green line* represents averages of replicates reaction mixtures containing 50 mM glycine and 1 mM DTT. The *blue line* represents averages of replicates where reaction mixtures contain 50 mM Tris and 1 mM DTT. Reaction mixtures were incubated at 20 °C for 60 min. *B,* 40 nM of His-HsPRMT1, 10 µM HsH4 (1–21), and 0.14 µM [^{3}H]AdoMet were mixed with 50 mM K-Hepes and 1 mM DTT and incubated at 37 °C for 30 min. *C,* 5.6 nM of HsPRMT5/MEP50, 10 µM of HsH4 (1–21) and 0.14 µM [^{3}H]AdoMet were mixed with 50 mM K-Hepes and 1 mM DTT and incubated at 37 °C for 30 min. The *black line* represents the averages of *black dot* replicates for His-HsPRMT1 and HsPRMT5/MEP50. In all cases, the final pH was determined from mock mixtures of buffer components, the buffer used in the enzyme preparation, and the solvent for the [^{3}H]AdoMet. HsH2B, histone H2B; HsH4, human histone H4; PRMT, protein arginine methyltransferase.

suggest that PRMT7 activity is generally repressed under physiological conditions. Control experiments showed that changes in the ionic strength of the incubation mixture did not affect the efficiency of the P81 phosphocellulose assay (Fig. S3). We also performed assays on the effect of ionic strength using GST-GAR as a substrate and the SDS-PAGE assay (Fig. S4). We note that the loss of activity with ionic strength is less with the GST-GAR substrate than with the HsH2B (23–37) peptide, confirming the results of Feng *et al.* (16).

We then examined the effect of calcium and magnesium ions on the activity of PRMT7. Here we found inhibition greater than expected from the ionic strength. With calcium ions, we found half inhibition at approximately 0.7 mM, and with magnesium ions, we found half inhibition at about 1.6 mM (Fig. 8). Since intracellular calcium ion concentrations are submicromolar, we might expect little effect on PRMT activity except perhaps when cells undergo intracellular

calcium release. Intracellular free magnesium concentration has been estimated in the cytosol of mammalian cells at about 0.5 mM (19), suggesting little inhibition of PRMT7 with changes in magnesium ion concentration. Taking all of these results together, it appears that PRMT7 may only be active under conditions where intracellular temperature, pH, and ionic conditions are disrupted.

PRMT1 and PRMT5 are also inhibited by the addition of salts

Finally, we sought to determine whether PRMT1 and PRMT5 activity was also affected by ionic strength or calcium and magnesium ions (Fig. 9). For His-HsPRMT1 with the human histone H4 (1–21) peptide, we found half maximal inhibition by ionic strength at about 100 mM and half maximal inhibition by calcium and magnesium ions at about 2 mM. For HsPRMT5/MEP50 under similar conditions, we found half

ASBMB

J. Biol. Chem. (2022) 298(9) 102290 **5**

18
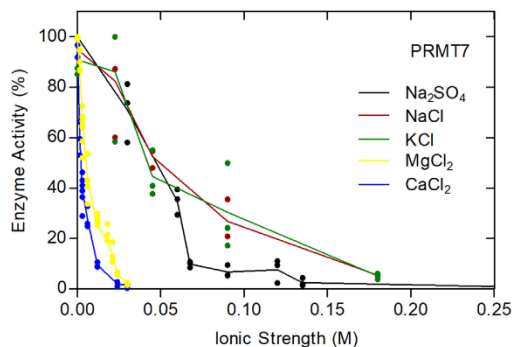
Figure 8. Human PRMT7 activity decreases with ionic strength. Five micrograms of GST-HsPRMT7 was mixed with 10 μM HsH2B (23–37) and 0.7 μM [³H]AdoMet. All reaction mixtures contained 50 mM K-Hepes and 1 mM DTT with a final pH of 8.5. Thee *black line* represents averages when Na₂SO₄ was added to reaction mixtures. The *red line* represents averages when NaCl was added to reaction mixtures. The *green line* represents averages when KCl was added to reaction mixtures. The *yellow line* represents averages when MgCl₂ was added to reaction mixtures. The *blue line* represents the averages when CaCl2 was added to the reaction mixtures. All reactions were incubated for 10 min at 20 °C. HsH2B, histone H2B; PRMT, protein arginine methyltransferase.

maximal inhibition by ionic strength at about 120 mM, half maximal inhibition of calcium ions at about 5 mM, and half maximal inhibition of magnesium ions at about 8 mM. Interestingly, these enzymes are also inhibited in the physiological ionic strength range, although the inhibition by calcium and magnesium ions is less than that seen with PRMT7. It appears that PRMT1 and PRMT5 would not be significantly inhibited by physiological levels of calcium and magnesium.

Discussion

In this study, we were surprised to find that human PRMT1, PRMT5, and PRMT7 had optimal catalytic activities *in vitro*

under nonphysiological conditions. For example, all three enzymes displayed markedly reduced activity at ionic strengths comparable to the cytosol of mammalian cells. While PRMT1 and PRMT5 were active at a range of pH values, PRMT7 had little activity at the expected intracellular pH of 7.2 and was only fully active at alkaline pH values. Finally, all of the three enzymes displayed a significant catalytic activity at low temperatures, including 0 °C. Significantly, human PRMT7 had markedly reduced activity at the physiological temperature of 37 °C, while PRMT1, PRMT5, and PRMT9 (17) had near-optimal activity at 37 °C. We note that the PRMT7 from the soil nematode worm *Caenorhabditis elegans* has a distinct temperature profile with optimal activity at about 20 °C near that of its environment in nature (17).

We wanted to know if the optimal activity of PRMTs under these nonphysiological conditions would mean that PRMTs are responding to environmental stresses. We wanted to ask under what conditions would PRMTs be exposed to temperatures lower than 37 °C, under what conditions would PRMTs be exposed to pH values above 7.2, and under what conditions would PRMTs be exposed to ionic strengths lower than what is generally found in mammalian cells.

Humans generally maintain their temperature at 37 °C even when exposed to environmental cold. However, skin cells and cells lining the lungs can be significantly affected (20, 21). We note that mammalian cells have "cold shock" proteins that are induced by a cold shock response (22-24). One example of cold response is that optimal human sperm production is maintained when the testis is 2 to 7 °C below body temperature (25). It has been suggested that the TRPM8 sensor protein is important for the cold shock response in testes (21). Moderately reduced temperatures have also been found to suppress apoptosis of neural stem cells although it is not clear when such cells would be exposed to lower temperatures (26).

Interestingly, a comparison of genes has associated PRMT7, along with a small group of other genes, to the adaptation of
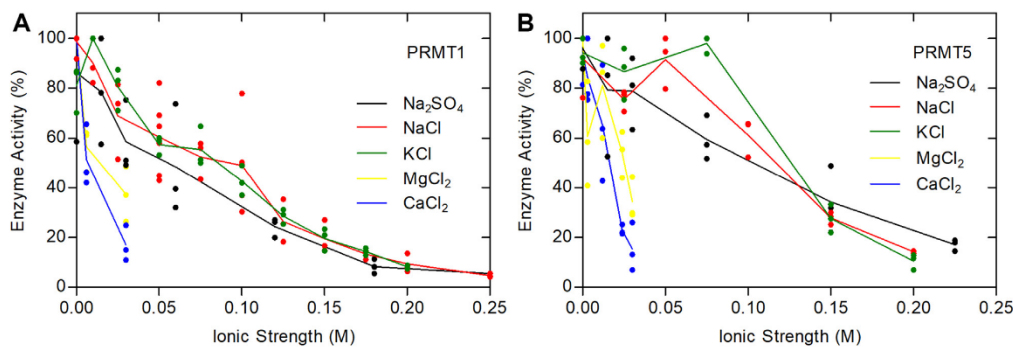
Figure 9. Human PRMT1 and PRMT5/MEP50 activities are reduced with increasing ionic strength. P81 phosphocellulose of His-HsPRMT1 or HsPRMT5/ MEP50 with HsH4 (1–21) was carried out as described in Experimental procedures. *A*, 40 nM of His-HsPRMT1, 10 μM HsH4 (1–21), and 0.7 μM [³H]AdoMet were incubated with 50 mM K-Hepes and 1 mM DTT at a final pH of 7.5. Reaction mixtures were incubated at 37 °C for 15 min. *B*, 5.6 nM of HsPRMT5/MEP50, 10 μM HsH4 (1–21), and 0.7 μM [³H]AdoMet were incubated with 50 mM K-Hepes and 1 mM DTT at a final pH of 7.5. Reaction mixtures were incubated at 37 °C for 30 min. The *black line* represents averages when Na₂SO₄ was added to reaction mixtures. The *red line* represents averages when NaCl was added to reaction mixtures. The *green line* represents averages when KCl was added to reaction mixtures. The *yellow line* represents averages when MgCl₂ was added to reaction mixtures. The *blue line* represents the averages when CaCl₂ was added to the reaction mixtures. HsH4, human histone H4; PRMT, protein arginine methyltransferase.

elephantid species to cold environments, particularly of mammoths to the arctic (27).

Many mammalian proteins have been shown to be denatured at subphysiological temperatures (28). However, it is not uncommon for enzymes to adapt to low temperatures, especially those in fish and in bacteria exposed to cold environments (29).

To determine how common is cold activation of enzymes, we searched the literature for publications reporting on the temperature dependence of human or mammalian S-adenosylmethionine methyltransferases. While many of these enzymes show optimal activities around 37 °C as expected, we were interested to find an example of an enzyme that displayed cold activation similar to what we report here for PRMT7. This enzyme is the NS5 RNA methyltransferase from the Dengue virus 4. Optimal activity was found between 22 °C and 30 °C, with less than 20% of this activity found at 37 °C (30). It is presently unclear what the biological advantage is for PRMT7 or the RNA methyltransferase to be cold activated. Additionally, it is unknown why PRMT1, PRMT5, and PRMT7 have significant enzymatic activity at 0 °C.

PRMT7 was shown here to have very little activity at the expected cytosolic pH of about 7.2 in mammalian cells (13, 31). The activity of PRMT7 at pH 7.2 was found to be less than 5% of its optimal activity at pH 8.4. In comparison to pH 7.2, human PRMT1 has about 30% of its optimal activity at pH 7.6, while PRMT5 has a broad optimal range between 6.5 and 8.5. Interestingly, the Dengue virus 4 NS5 RNA methyltransferase also shows enhanced activity at alkaline pH. Its activity at 7.2 is only about 20% of its optimal activity at pH 9.0 (30). A similar situation occurs with the PRDM9 histone H3 lysine 36 methyltransferase where the activity at pH 7.2 is only about 15% of the optimal activity at pH 8.5 (32). All of these results suggest that PRMT7, the NS5 RNA methyltransferase, the histone lysine methyltransferase, and possibly PRMT1 may be regulated by conditions resulting in the alkalization of cells.

PRMT1, PRMT5, and PRMT7 all show inhibition with increasing ionic strength. For PRMT7, this inhibition was much more pronounced with the HsH2B (23–37) peptide than for the GST-GAR substrate. We were intrigued to find that Dengue virus-4 RNA methyltransferase and the PRDM9 histone lysine methyltransferase also showed sensitivity to ionic strength (30, 32). The physiological relevance of such sensitivity is not clear although it has been suggested that cells can respond to changes in ionic strength (14). Normal intracellular ionic strength has been estimated at about 110 to 130 mM in the human embryonic kidney cell line HEK293 reflecting the known intracellular sodium ion and potassium ion levels (14). At this ionic strength, PRMT7 (at least with the HsH2B (23–37) peptide substrate) and the histone lysine methyltransferase PRDM9 have less than 10% activity, while PRMT1, PRMT5, and the Dengue-4 RNA methyltransferase have less than 50% activity.

Finally, PRMT1, PRMT5, and PRMT7 are all inhibited by increasing concentrations of magnesium ions. PRMT7 was found to be inhibited by magnesium ion concentration with half activity found at 1.6 mM, while PRMT1 was half inhibited at 2 mM and PRMT5 was half inhibited at 8 mM. Since the intracellular free magnesium ion concentration has been estimated at about 0.5 mM (19), it appears that the inhibition seen here would not be physiologically relevant. These methyltransferases are also inhibited by calcium ions at levels much greater than the levels found intracellularly.

At present, we do not understand the importance of the subphysiological activities of PRMT1, PRMT5, and PRMT7 and the RNA and protein lysine methyltransferases as described earlier in the study. The similarities in the responses to temperature, pH, and ionic strength are, however, remarkable.

Evidence has been presented that physiological levels of hydrogen peroxide can inhibit human PRMT1 and that this inhibition can be reversed by reducing agents, suggesting a possible regulation of PRMT1 by redox reactions (33). It is clear that PRMT7 activity is dependent upon a reducing environment as well (17, 34). In all of our experiments, we performed incubations in 1 mM DTT (17).

It remains to be shown whether or not PRMTs, especially PRMT7, are regulated *in vivo* by intracellular temperature, pH, or ionic strength. Unfortunately, it has been challenging to measure the individual activities of the nine family members of mammalian PRMTs in cells cultured under normal or low temperature conditions, or under conditions that would affect their intracellular ionic strength or pH. This is particularly a problem for PRMT7, whose activity appears to be generally low in comparison with the major type I PRMT1 enzyme or the major type II PRMT5 enzyme (5, 35). Although evidence has been presented for a number of *in vivo* sites of PRMT7 methylation (7, 10, 36-38), it is not clear so far that these are specifically modified by PRMT7 alone and are not also sites for methylation by other PRMTs (39). Additionally, PRMT7 methylation of Arg-17 of a histone H4 peptide has been shown to allosterically activate PRMT5 methylation at the distinct Arg-3 site (9). Such cross talk between PRMTs can complicate the analysis of specific PRMT activity in cells. Finally, it is now clear that reductions in the activity of one PRMT can result in the methylation of its sites by other members of the PRMT family (40, 41). The identification of specific substrates and the generation of specific antibodies raised against their monomethylation site(s) will be important steps in quantitating PRMT7 activity in cells and testing how this activity may respond to changes in their intracellular environment.

Experimental procedures

Preparation of enzymes and protein substrates

Recombinant *H. sapiens* PRMT7 DNA was cloned into a pGEX-2T plasmid and expressed in BL21 DE3 *E. coli*. This plasmid encodes the full sequence (residues 1–218) of glutathione S-transferase from *Schistosoma japonicum* followed by the linker SDLVPRGSST and the full sequence (residues 1–692) of human PRMT7 and was designated as GST-HsPRMT7. This plasmid is available from Addgene.org #34693. Cells were grown in 2L of LB media at 37 °C to an A_{600} nm of 0.6 to 0.8 in the presence of 100 μg/ml ampicillin.

Isopropyl-beta-D-thiogalactoside (CAS # 367–93–1, GoldBio) was then added to a final concentration of 1 mM, and the culture was incubated for an additional 16 to 20 h at 20 °C. Cells were harvested by centrifugation, and 0.5 g of cells was resuspended in 40 ml of 140 mM NaCl, 2.7 mM KCl, 10 mM Na_2HPO_4, and 1.8 mM KH_2PO_4, pH = 7.5, supplemented with an EDTA-free protease inhibitor tablet (Catalog No. PIA32965, Thermo Scientific). The cell suspension was lysed using a Fisher Scientific 550 Sonic Dismembrator with a microtip attachment in four cycles on ice for 1 min, 0.5 s on pulse, and 0.5 s off pulse at 25% amplitude. The lysate was then centrifuged at 27000g for 1 h, and the supernatant was loaded onto a manually packed column (ID 1.5 cm × 15 cm, 4 ml bed volume) containing glutathione Sepharose 4B resin (Catalog No. 17075601, GE Healthcare Life Sciences) equilibrated in the aforementioned buffer at 22 °C. Enzyme was eluted with 10 mM glutathione and 50 mM Tris-HCl, pH 8.0. Purified GST-*Hs*PRMT7 was then dialyzed overnight in 50 mM K-Hepes, 1 mM DTT, pH 8.0, at 4 °C. GST-*Hs*PRMT7 was then mixed with glycerol to a final concentration of 20% and stored at −80 °C. The total GST-HsPRMT7 concentration was determined using a NanoDrop 2000c spectrophotometer by the absorption at 280 nm, assuming that 1 mg/ml would give 1 A.

An N-terminal His-tagged construct of human PRMT1 (designated His-HsPRMT1) was prepared as described previously and purified using a HisTrap Fast Flow (Cytiva 17–5255–01) as per the manufacturer's protocol (42).

Human PRMT5/MEP50 (HsPRMT5/MEP50) FLAG-tag His-tag complex protein was purchased from BioSciences as recombinantly coexpressed and purified proteins in HEK293T cells (0.64 mg/ml, Catalog No. 51045, Lot 170407A; BPS Biosciences), formulated in 40 mM Tris-HCl, pH 8.0, 110 mM NaCl, 2.2 mM KCl, 80 µg/ml FLAG peptide, 20% glycerol, and 3 mM DTT.

A fusion protein of glutathione S-transferase followed by the linker SDLVPRGS and human fibrillarin residues 1 to 145 with substitutions K2E and A145V (GST-GAR) was prepared by expression of plasmid #34697 of Addgene.org. (17). The protein was purified as described for GST-HsPRMT7 above.

Human HsH2B was purchased from NEB, Cat. No. M2505S, as a recombinant protein expressed in *E. coli*, stored in 300 mM NaCl, 1 mM EDTA, and 20 mM sodium phosphate at pH 7.

Peptides

Synthetic peptides HsH2B (23–37) (Ac-KKDGKKRKR SRKESY, 98.6% purity, MW: 1936.23, Lot No. P17171304) and human histone H4 (1–21) (Ac-SGRGKGGKGLGKGGAKR HRKV, 96.2% purity, MW: 2133.47, Lot No. 89488400001/ PE1586) were purchased from Genescript.

In vitro *methylation reactions using P81 phosphocellulose*

GST-*Hs*PRMT7, His-HsPRMT1, or PRMT5/MEP50 was mixed with a peptide derived from residues 23 to 37 of HsH2B, GST-GAR, or a peptide derived from the acetylated N-

terminus of histone H4 (residues 1–21). Reactions were initiated with S-adenosyl-L-[*methyl*-³H]methionine ([³H]AdoMet) (81.9 Ci/mmol, 7 µM in 9:1 10 mM H_2SO_4:ethanol; Catalog No. NET155H001MC, PerkinElmer) in a final volume of 30 µl. The reaction mixtures were equilibrated to the desired temperature for 2 min prior to the addition of [³H]AdoMet and incubation in a temperature-regulated water bath. Post incubation, the reaction mixtures were terminated with 0.5 µl of 100% trifluoracetic acid and spun down for 10 s at 10,600g in an Eppendorf microcentrifuge (Model 5415C). All reaction mixtures contained 1 mM DTT and unless otherwise described a final concentration of 50 mM K-HEPES at a final pH of 8.5. To determine the final pH of reaction mixtures, mock mixtures were created containing the appropriate volumes of the enzyme buffer (50 mM K-Hepes, 1 mM DTT, pH 8.0), the [³H]AdoMet solvent (18 mM HCl), and the reaction buffer containing 1 mM DTT and 50 mM K-Hepes, 50 mM glycine, or 50 mM Tris-HCl.

The extent of methylation was determined by a P81 phosphocellulose assay. Twenty-five microliters of reaction mixture was spotted on to a 1 × 1-cm² of phosphocellulose P81 paper (Catalog No. 05–717-2A, Lab Alley). Papers were dried for 90 min at room temperature and were then washed 3 times with 300 ml of 50 mM sodium bicarbonate, pH = 9.0. The papers were dried again for 90 min in 20-ml scintillation vials (Catalog No. 66021-704, VWR), and 5 ml of scintillation fluid (111177-CS, RPI) was added. Vials were counted in a Beckman LS 6500 Liquid Scintillation Counter for four cycles at 5 min per cycle. The sum of enzyme-only and substrate-only controls was subtracted from individual replicates.

In vitro *methylation gel assay*

Recombinant GST-*Hs*PRMT7 was incubated with either GST-GAR as described earlier in the study or recombinant human HsH2B expressed in *E. coli* (Catalog No. M2505S, New England BioLabs) in a total volume of 30 µl. Post incubation, the reaction mixtures were spun down for 10 s at 10,600g. The reactions were then terminated with 5 µl of 5× sample buffer: 250 mM Tris-HCl, 10% SDS, 30% glycerol, 500 mM DTT, and 0.05% bromophenol blue and heated for 1 min in a 95 °C sand bath. The reaction mixtures were allowed to cool to room temperature before loading either onto a 4 to 12% 15-well ExpressPlus PAGE gel (Catalog No. NC1486979, Fisher Scientific Co) or 4 to 20% 10-well Express PAGE gel (Catalog No. NC0613877, Fisher Scientific Co). The gel was allowed to run for 1 h at 140 V, 400 mA using a BioRad PowerPac 300 electrophoresis Power supply. The gels were stained for 1 h in Coomassie stain: 50% methanol and 10% acetic acid, followed by an overnight destain consisting of 15% methanol and 10% acetic acid. The gels were then soaked in water for minimum 3 h prior to enhancing with En³Hance (Catalog No. 6NE9701, PerkinElmer) for 30 min. The gels were then put into water for 1 h post enhancement, wrapped in gel-drying film (Catalog No. PR-V713, Promega), and dried in a Model 583 Gel Dryer, Biorad for 2 h at 80 °C. The dried gel was placed in an autoradiography cassette, and an HyBlot CL autoradiography film

(Catalog No. NC9556985, Thermo Scientific) was placed on top of the gel. The film was exposed for 3 to 30 days at −80 °C before development

Data availability

All data described in the manuscript are contained within the manuscript. Additional data are available upon request.

Abbreviations—The abbreviations used are: HsH2B, human histone H2B; PRMT, protein arginine methyltransferase.

References

1. Jarrold, J., and Davies, C. C. (2019) PRMTs and arginine methylation: cancer's best-kept secret? *Trends Mol. Med.* **25**, 993–1009
2. Wu, Q., Schapira, M., Arrowsmith, C. H., and Barsyte-Lovejoy, D. (2021) Protein arginine methylation: from enigmatic functions to therapeutic targeting. *Nat. Rev. Drug Discov.* **20**, 509–530
3. Xu, J., and Richard, S. (2021) Cellular pathways influenced by protein arginine methylation: implications for cancer. *Mol. Cell* **81**, 4357–4368
4. Yang, Y., and Bedford, M. T. (2013) Protein arginine methyltransferases and cancer. *Nat. Rev. Cancer* **13**, 37–50
5. Bedford, M. T., and Clarke, S. G. (2009) Protein arginine methylation in mammals: who, what, and why. *Mol. Cell* **33**, 1–13
6. Tewary, S. K., Zheng, Y. G., and Ho, M.-C. (2019) Protein arginine methyltransferases: insights into the enzyme structure and mechanism at the atomic level. *Cell. Mol. Life Sci.* **76**, 2917–2932
7. Halabelian, L., and Barsyte-Lovejoy, D. (2021) Structure and function of protein arginine methyltransferase PRMT7. *Life (Basel)* **11**, 768
8. Frankel, A., and Brown, J. I. (2019) Evaluation of kinetic data: what the numbers tell us about PRMTs. *Biochim. Biophys. Acta - Proteins Proteomics* **1867**, 306–316
9. Jain, K., Jin, C. Y., and Clarke, S. G. (2017) Epigenetic control *via* allosteric regulation of mammalian protein arginine methyltransferases. *Proc. Nat. Acad. Sci. U. S. A.* **114**, 10101–10106
10. Feng, Y., Maity, R., Whitelegge, J. P., Hadjikyriacou, A., Li, Z., Zurita-Lopez, C., *et al.* (2013) Mammalian protein arginine methyltransferase 7 (PRMT7) specifically targets RXR sites in lysine- and arginine-rich regions. *J. Biol. Chem.* **288**, 37010–37025
11. Fulton, M. D., Brown, T., and Zheng, Y. G. (2018) Mechanisms and inhibitors of histone arginine methylation. *Chem. Rec.* **18**, 1792–1807
12. Li, A. S. M., Li, F., Eram, M. S., Bolotokova, A., dela Seña, C. C., and Vedadi, M. (2020) Chemical probes for protein arginine methyltransferases. *Methods* **175**, 30–43
13. Casey, J. R., Grinstein, S., and Orlowski, J. (2010) Sensors and regulators of intracellular pH. *Nat. Rev. Mol. Cell Biol.* **11**, 50–61
14. Liu, B., Poolman, B., and Boersma, A. J. (2017) Ionic strength sensing in living cells. *ACS Chem. Biol.* **12**, 2510–2514
15. Bisswanger, H. (2014) Enzyme assays. *Perspect. Sci.* **1**, 41–55
16. Feng, Y., Hadjikyriacou, A., and Clarke, S. G. (2014) Substrate specificity of human protein arginine methyltransferase 7 (PRMT7): the importance of acidic residues in the double E loop. *J. Biol. Chem.* **289**, 32604–32616
17. Hadjikyriacou, A., and Clarke, S. G. (2017) *Caenorhabditis elegans* PRMT-7 and PRMT-9 are evolutionarily conserved protein arginine methyltransferases with distinct substrate specificities. *Biochemistry* **56**, 2612–2626
18. Jain, K. (2018) *Protein Arginine Methyltransferases: Catalytic Mechanisms and Crosstalk in Epigenetics.* PhD Thesis, University of California, Los Angeles
19. Vormann, J. (2003) Magnesium: nutrition and metabolism. *Mol. Aspects Med.* **24**, 27–37
20. Juan, Y., Haiqiao, W., Xie, W., Huaping, H., Zhong, H., Xiangdong, Z., *et al.* (2016) Cold-inducible RNA-binding protein mediates airway inflammation and mucus hypersecretion through a post-transcriptional regulatory mechanism under cold stress. *Intl J. Biochem. Cell Biol.* **78**, 335–348
21. Borowiec, A.-S., Sion, B., Chalmel, F., Rolland, A. D., Lemonnier, L., De Clerck, T., *et al.* (2016) Cold/menthol TRPM8 receptors initiate the cold-shock response and protect germ cells from cold-shock–induced oxidation. *FASEB J.* **30**, 3155–3170
22. LLeonart, M. E. (2010) A new generation of proto-oncogenes: Cold-inducible RNA binding proteins. *Biochim. Biophys. Acta - Rev. Cancer* **1805**, 43–52
23. De Leeuw, F., Zhang, T., Wauquier, C., Huez, G., Kruys, V., and Gueydan, C. (2007) The cold-inducible RNA-binding protein migrates from the nucleus to cytoplasmic stress granules by a methylation-dependent mechanism and acts as a translational repressor. *Exp. Cell Res.* **313**, 4130–4144
24. Phadtare, S., Alsina, J., and Inouye, M. (1999) Cold-shock response and cold-shock proteins. *Curr. Opin. Microbiol.* **2**, 175–180
25. Aldahhan, R. A., and Stanton, P. G. (2021) Heat stress response of somatic cells in the testis. *Mol. Cell Endocrinol.* **527**, 111216
26. Saito, K., Fukuda, N., Matsumoto, T., Iribe, Y., Tsunemi, A., Kazama, T., *et al.* (2010) Moderate low temperature preserves the stemness of neural stem cells and suppresses apoptosis of the cells *via* activation of the cold-inducible RNA binding protein. *Brain Res.* **1358**, 20–29
27. Lynch, V. J., Bedoya-Reina, O. C., Ratan, A., Sulak, M., Drautz-Moses, D. I., Perry, G. H., *et al.* (2015) Elephantid genomes reveal the molecular bases of woolly mammoth adaptations to the arctic. *Cell Rep.* **12**, 217–228
28. Privalov, P. L. (1990) Cold denaturation of protein. *Crit. Rev. Biochem. Mol. Biol.* **25**, 281–306
29. Marshall, C. J. (1997) Cold-adapted enzymes. *Trends Biotech.* **15**, 359–364
30. Dong, H., Chang, D. C., Hua, M. H. C., Lim, S. P., Chionh, Y. H., Hia, F., *et al.* (2012) 2'-O methylation of internal adenosine by flavivirus NS5 methyltransferase. *PLoS Pathog.* **8**, e1002642
31. Roos, A., and Baron, W. F. (1981) Intracellular pH. *Physiol. Rev.* **61**, 296–434
32. Eram, M. S., Bustos, S. P., Lima-Fernandes, E., Siarheyeva, A., Senisterra, G., Hajian, T., *et al.* (2014) Trimethylation of histone H3 lysine 36 by human methyltransferase PRDM9 protein. *J. Biol. Chem.* **289**, 12177–12188
33. Morales, Y., Cáceres, T., May, K., and Hevel, J. M. (2016) Biochemistry and regulation of the protein arginine methyltransferases (PRMTs). *Arch. Biochem. Biophys.* **590**, 138–152
34. Zurita-Lopez, C. I., Sandberg, T., Kelly, R., and Clarke, S. G. (2012) Human protein arginine methyltransferase 7 (PRMT7) is a type III enzyme forming ω-N^G-monomethylated arginine residues. *J. Biol. Chem.* **287**, 7859–7870

ASBMB

J. Biol. Chem. (2022) 298(9) 102290 **9**

35. Blanc, R. S., and Richard, S. (2017) Arginine methylation: the coming of age. *Mol. Cell* **65**, 8–24

36. Jain, K., and Clarke, S. (2019) PRMT7 as a unique member of the protein arginine methyltransferase family: a review. *Arch. Biochem. Biophys.* **665**, 36–45

37. Haghandish, N., Baldwin, R. M., Morettin, A., Dawit, H. T., Adhikary, H., Masson, J. Y., *et al.* (2019) PRMT7 methylates eukaryotic translation initiation factor 2α and regulates its role in stress granule formation. *Mol. Biol. Cell* **30**, 778–793

38. Szewczyk, M. M., Ishikawa, Y., Organ, S., Sakai, N., Li, F., Halabelian, L., *et al.* (2020) Pharmacological inhibition of PRMT7 links arginine mon-omethylation to the cellular stress response. *Nat. Commun.* **11**, 2396

39. Gao, W.-W., Xiao, R. Q., Peng, B.-L., Xu, H.-T., Shen, H.-F., Huang, M.-F., *et al.* (2015) Arginine methylation of HSP70 regulates retinoid

acid-mediated RARβ2 gene activation. *Proc. Natl. Acad. Sci. U. S. A.* **112**, E3327–E3336

40. Dhar, S., Vemulapalli, V., Patananan, A. N., Huang, G. L., Di Lorenzo, A., Richard, S., *et al.* (2013) Loss of the major Type I arginine methyl-transferase PRMT1 causes substrate scavenging by other PRMTs. *Sci. Rep.* **3**, 1311

41. Wang, Y., Person, M. D., and Bedford, M. T. (2022) Pan-methylarginine antibody generation using PEG linked GAR motifs as antigens. *Methods* **200**, 80–86

42. Debler, E. W., Jain, K., Warmack, R. A., Feng, Y., Clarke, S. G., Blobel, G., *et al.* (2016) A glutamate/aspartate switch controls product specificity in a protein arginine methyltransferase. *Proc. Nat. Acad. Sci. U. S. A.* **113**, 2068–2073

23

Chapter 3: Supporting information

Human Protein Arginine Methyltransferases (PRMTs) Can Be Optimally Active Under

Non-Physiological Conditions

Troy L. Lowe and Steven G. Clarke

List of material included:

Figure 1S: pH Does not affect the P81 methylation assay efficiency.

Figure 2S: pH dependence of human PRMT7 with a protein substrate.

Figure 3S: Salts do not affect the P81 methylation assay efficiency.

Figure 4S: Human PRMT7 activity decreases with ionic strength with a GST-GAR substrate.
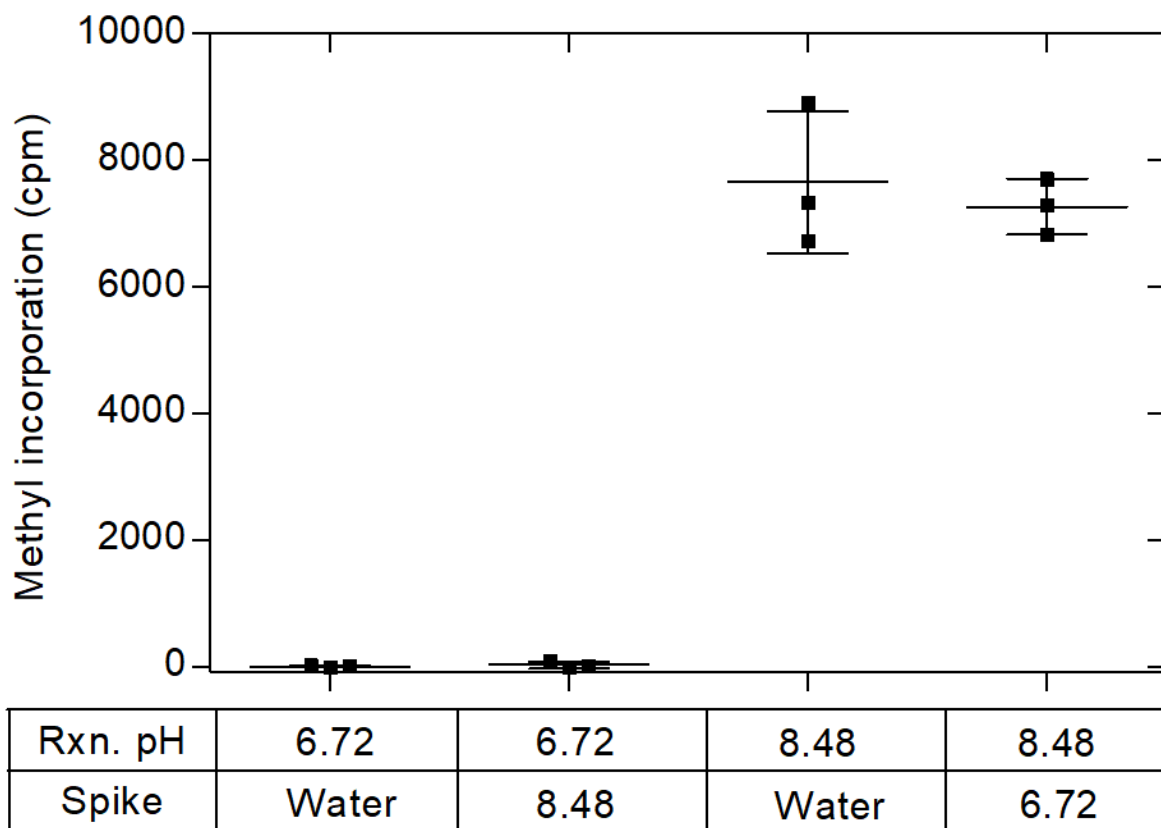
Rxn. pH	6.72	6.72	8.48	8.48
Spike	Water	8.48	Water	6.72

Figure 1S: pH does not affect the P81 methylation assay efficiency. Replica reaction mixtures in a final volume of 30 µL were prepared containing 5 µg GST-HsPRMT7, 10 µM HsH2B (23-37), 50 mM K-HEPES, 1 mM DTT, and 0.7 µM [^{3}H]AdoMet at a final pH of 8.48, or a final pH of 6.72. These reaction mixtures were incubated for 1 hr at 20 °C and were then terminated by the addition of 0.5 µL of 100% TFA. At this point, either 3 µL of water or 3 µL of 500 mM K-HEPES, pH 8.48 or 6.72 were added and the assay performed as described in the "Experimental Procedures" section. ANOVA analysis showed no significant difference between the activity with the addition of water or buffer with a pH of 8.48 or 6.72.
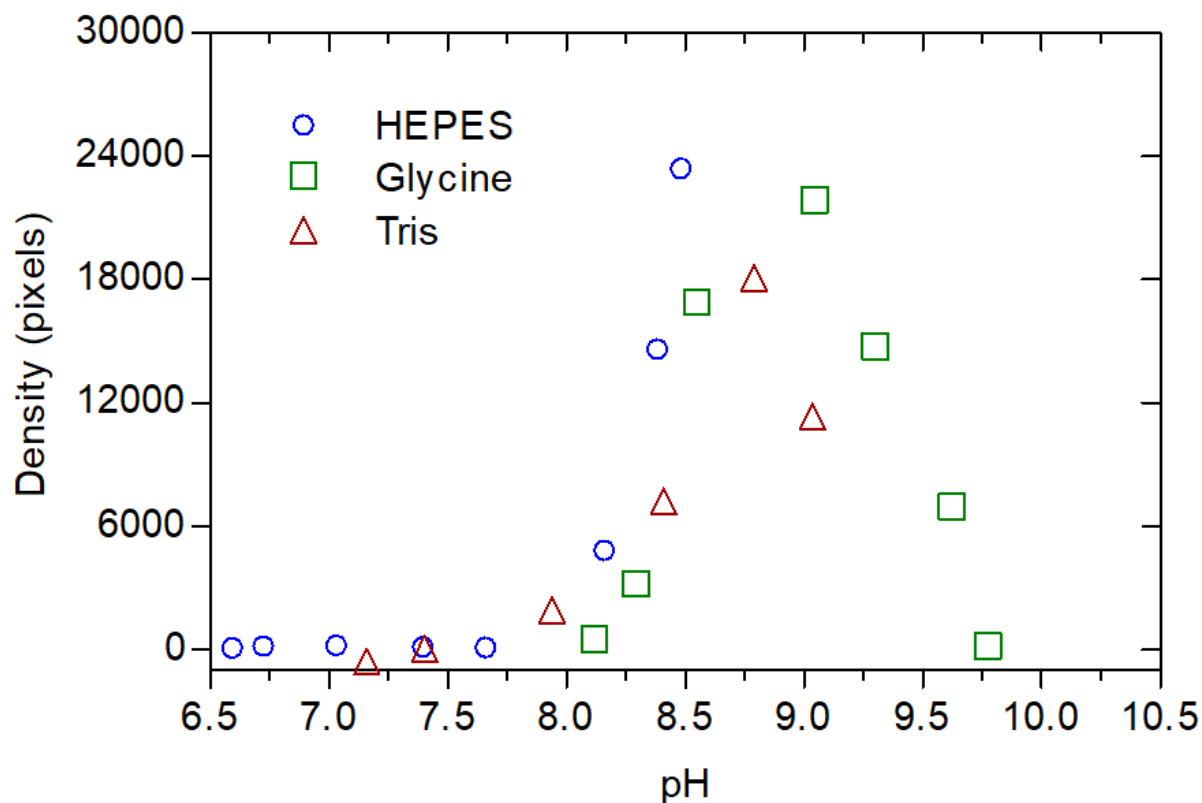
Figure 2S: pH dependence of human PRMT7 with a protein substrate. GST-HsPRMT7 5 µg was incubated with 6.2 µg GST-GAR, 1 mM DTT, 50 mM of the indicated buffer, and 0.14 µM [³H]AdoMet in a final volume of 30 µL. The reaction was performed for 1 h at 20 °C. The reaction was than quenched by the addition of SDS sample buffer and the mixtures were fractionated by SDS-PAGE as described in "Experimental Procedures." Films were analyzed by densitometry using ImageJ software after scanning. Blue open circles represent samples incubated in K-HEPES at the indicated final pH values, while red open triangles represent samples incubated in Tris-HCl, and green open squares represents samples incubated in a glycine buffer.
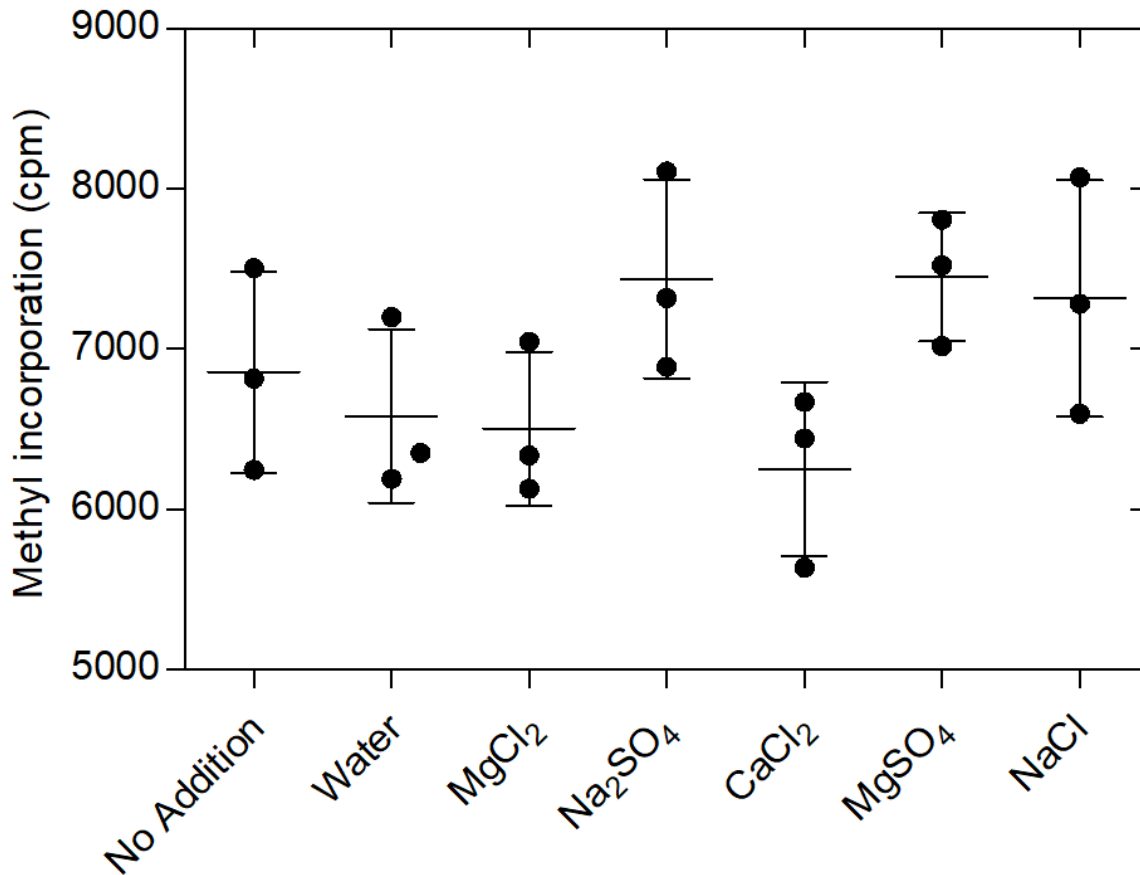
Figure 3S: Salts do not affect the P81 methylation assay efficiency. Replica reaction mixtures in a final volume of 30 µL were prepared containing 5 µg GST-HsPRMT7, 10 µM HsH2B (23-37), 50 mM K-HEPES, 1 mM DTT, and 0.7 µM [^{3}H]AdoMet at a final pH of 8.5. These reaction mixtures were incubated for 1 hr at 25 °C and were then terminated by the addition of 0.5 µL of 100% TFA. At this point, either no addition was made or 3 µL of water, 3 µL of 300 mM $MgCl_2$, Na_2SO_4, or $CaCl_2$, or 3 µL of 900 mM NaCl, or 3 µL of 225 mM $MgSO_4$ were added and the assay performed as described in the "Experimental Procedures" section. ANOVA analysis showed no significant difference between the activity with no addition or with the water or salt additions.
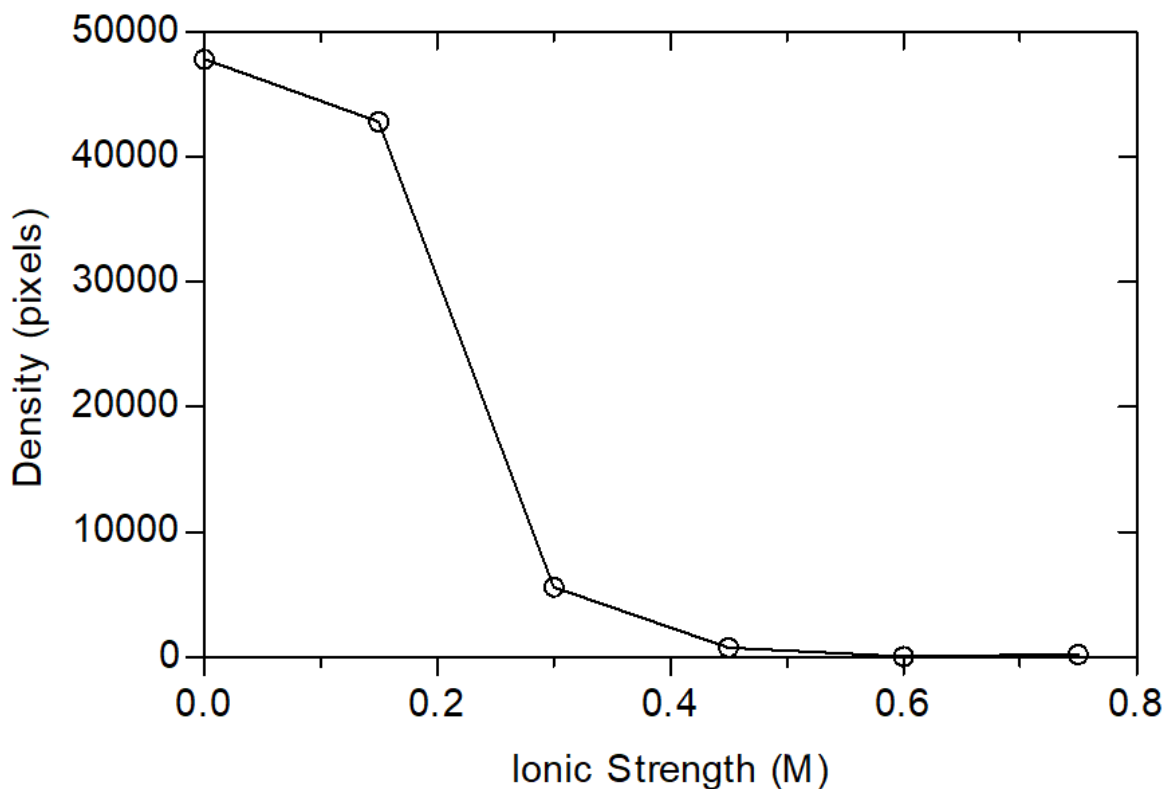
Figure 4S: Human PRMT7 activity decreases with ionic strength with a GST-GAR substrate.

5 µg GST-HsPRMT7 was incubated with 6.2 µg GST-GAR, 1 mM DTT, 50 mM K-HEPES, and 0.14 µM [^{3}H]AdoMet in a final volume of 30 µL and a final pH of 8.5. The ionic strength was adjusted with sodium sulfate to the indicated level. The reaction was performed for 1 h at 20 °C. The reaction was quenched by the addition of SDS sample buffer and the mixtures were fractionated by SDS-PAGE as described in "Experimental Procedures." Films were analyzed by densitometry of the GST-GAR using ImageJ software after scanning.

Chapter 4

The exquisite specificity of human protein arginine methyltransferase 7 (PRMT7) toward Arg-X-Arg sites

The work described in this chapter has been reproduced from:

Significance Statement

PRMT7 is the only enzyme in the family of nine that solely catalyzes monomethylarginine. While all other PRMTs are able to catalyze monomethylarginine, the specificity of a monomethylated substrate seems to remain exclusive to this particular enzyme. PRMT7 catalyzes monomethylation of RXR specific substrates, while PRMT1 and PRMT5 are known to catalyze monomethylation of RGG specific substrates.

Histone H2B arginine residues 29, 31, and 33 were identified to be methylated by PRMT7. The N-terminal region of histone H2B is highly conserved across higher order species from humans to mice. However, the sequence from 29-33 alters to some degree in lower order species like frogs and fruit flies. In particular the histone H2B (29-33) sequence of *X. laevis* contains a

switch of the arginine and lysine residues at positions 30 and 31, resulting in an RRKSR instead of an RKRSR. Ideally in theory, this switch in amino acids should completely abolish PRMT7 activity since no RXR motif is present.

Findings demonstrate that the histone H2B of *X. laevis* is in fact not a substrate for PRMT7, however additional data suggests that the residues surrounding the arginines that can be methylated by PRMT7 play a large role in substrate specificity. In particular if a lysine is present, we observe an increase in affinity of the substrate binding to enzyme. However, this can be reversed with increasing ionic strength.

This work provides evidence that PRMT7 can in fact methylate substrates containing a single arginine as long as a positively charged residue is in close proximity. Additionally, these results confirm those of the previous chapter, demonstrating how increased ionic strength alters PRMT7 activity.

PLOS ONE

The exquisite specificity of human protein arginine methyltransferase 7 (PRMT7) toward Arg-X-Arg sites

Timothy J. Bondoc⬤, Troy L. Lowe⬤, Steven G. Clarke⬤*

Department of Chemistry and Biochemistry and the Molecular Biology Institute, University of California Los Angeles, Los Angeles, California, United States of America

* clarke@chem.ucla.edu

Abstract

Mammalian protein arginine methyltransferase 7 (PRMT7) has been shown to target substrates with motifs containing two arginine residues separated by one other residue (RXR motifs). In particular, the repression domain of human histone H2B (29-RKRSR-33) has been a key substrate in determining PRMT7 activity. We show that incubating human PRMT7 and [^{3}H]-AdoMet with full-length *Xenopus laevis* histone H2B, containing the substitutions K30R and R31K (RKRSR to RRKSR), results in greatly reduced methylation activity. Using synthetic peptides, we have now focused on the enzymology behind this specificity. We show for the human and Xenopus peptide sequences 23–37 the difference in activity results from changes in the V_{max} rather than the apparent binding affinity of the enzyme for the substrates. We then characterized six additional peptides containing a single arginine or a pair of arginine residues flanked by glycine and lysine residues. We have corroborated previous findings that peptides with an RXR motif have much higher activity than peptides that contain only one Arg residue. We show that these peptides have similar apparent k_m values but significant differences in their V_{max} values. Finally, we have examined the effect of ionic strength on these peptides. We found the inclusion of salt had little effect on the V_{max} value but a considerable increase in the apparent k_m value, suggesting that the inhibitory effect of ionic strength on PRMT7 activity occurs largely by decreasing apparent substrate-enzyme binding affinity. In summary, we find that even subtle substitutions in the RXR recognition motif can dramatically affect PRMT7 catalysis.

Introduction

Post-translational modifications (PTMs) of proteins are chemical modifications ranging from single methyl groups to entire proteins (i.e., ubiquitin) that occur after a protein is translated from messenger RNA [1]. These modifications expand the chemical properties of the twenty canonical amino acids encoded by the DNA, further diversifying the structure and function of the proteome [1]. Protein arginine methylation, for example, is a widespread post-translational

31

modification in mammalian cells with suggested regulatory roles in cellular functions such as transcription, translation, cell signaling, DNA repair and protein stability [2].

Protein arginine methyltransferases (PRMTs) modify peptidyl arginine residues by transferring methyl groups from S-adenosyl-L-methionine onto the ω-nitrogen atoms of the guanidino group of the arginine side chain [3, 4]. To date, nine PRMTs have been identified in mammals [5]. The PRMTs are classified as type I (PRMTs 1–4, 6, 8), type II (PRMTs 5 and 9), or type III (PRMT7) based on whether they form asymmetric dimethylarginine (ADMA), symmetric dimethylarginine (SDMA), or ω-monomethylarginine (MMA), respectively [6]. Protein arginine methylation proceeds through MMA as an intermediate, after which a second methylation reaction occurs to form either ADMA or SDMA [7]. As a unique member of the PRMT family, PRMT7 is the only known type III PRMT and forms only MMA as product [8].

Recent work has demonstrated that PRMT7 is optimally active under non-physiological temperature, pH, and ionic strength conditions [9–11]. However, more insight is needed to understand PRMT7's broader biological role. PRMT7 has been implicated in cancer metastasis and in particular with certain forms of breast cancer [12–15]. More recently, one group reported that PRMT7 is likely involved in maintaining leukemia stem cells in chronic myeloid leukemia [16]. Finally, evidence has been presented that PRMT7 activity can prime the activity of PRMT5 [17].

Recently, there has been much interest in identifying the physiological substrates of PRMT7. For instance, studies of PRMT7 activity in human cell lines including MCF7, HEK293T, and HeLa proposed that the cytosolic proteins eIF2α and HSP70 are probable *in vivo* substrates, suggesting that PRMT7 occupies some regulatory role in cellular stress response [18, 19]. However, multiple *in vitro* studies also suggest that core histones are good substrates of PRMT7, of which histones H2B and H4 are particularly good methyl acceptors [8, 10, 20]. Feng and coworkers further identified the sites in histone H2B that PRMT7 recognizes as the lysine- and arginine-rich regions containing an Arg-X-Arg motif (RXR), consisting of two Arg residues separated by any other amino acid, which exists near the N-terminal tail of histone H2B with the sequence 29-RKRSR-33 [8, 11]. Thus, understanding the specificity of PRMT7 toward basic RXR-containing regions could be helpful in identifying additional *in vivo* substrates.

This report has four aims: first, we explore how minor sequence substitutions in the 29-RKRSR-33 target sequence in human H2B affect PRMT7 methylation activity. Second, we aim to identify key residues and motifs that promote methylation of histone H2B (23–37) by GST-*Hs*PRMT7. Third, we measure the contributions of specific residues and motifs in the 29-RKRSR-33 target sequence with Michaelis-Menten kinetic experiments. Fourth, we use the Michaelis-Menten kinetic model to explore the inhibitory effect of ionic strength on PRMT7 methylation activity. We confirm that even subtle substitutions in the RXR recognition motif in substrate peptides dramatically affect PRMT7 methylation activity. Additionally, we show that the presence of an Arg-X-Arg (RXR) motif is a key substrate feature promoting methylation by PRMT7. Further, we suggest that changes to the 29-RKRSR-33 target sequence lead to lower PRMT7 methylation activity *via* decreased catalytic turnover. Lastly, we show that increased ionic strength can inhibit PRMT7 methylation activity primarily by decreasing apparent enzyme-substrate binding affinity.

Materials and methods

Preparation of proteins, peptide substrates, and full-length histone substrates

Human PRMT7 used in this study was expressed in BL21 DE3 *E. coli* as a fusion protein of full-length (residues 1–218) glutathione S-transferase from *Schistosoma japonicum* (GST) and

32

Table 1. Summary of protein and peptide substrates.

Protein or Peptide Name	Sequence	Theoretical[c,d] m.w. (Da)	Experimental[d] m.w. (Da)	HPLC Purity[e]
H. sapiens H2B	_ [a]	13,906 [a,c]	—	—
X. laevis H2B	_ [b]	13,934 [b,c]	—	—
H. sapiens H2B (23–37)	Ac-KKDGKKRKRSRKESY-amide	1935.25	1935.6	87.8%
X. laevis H2B (23–37)	KKDGKKRRKSRKESY	1894.20	1894.0	88.8%
Mono R	Ac-KKGGRGGGGKKY-amide	1234.39	1233.0	95.5%
RGR	Ac-KKGGRGRGGKKY-amide	1332.56	1332.3	92.0%
KRGR	Ac-KKGKRGRGGKKY-amide	1403.69	1403.2	96.0%
RKR	Ac-KKGGRKRGGKKY-amide	1403.69	1403.2	97.9%
RGRK	Ac-KKGGRGRKGKKY-amide	1403.69	1403.2	98.1%
RER	Ac-KKGGRERGGKKY-amide	1404.63	1404.4	97.0%

[a] Obtained from UNIPROT accession number P62807.

[b] Obtained from UNIPROT accession number P02281.

[c] Theoretical molecular weight using Expasy Compute pI/Mw tool.

[d] Theoretical/experimental molecular weight determined by GenScript.

[e] Experimentally determined HPLC purity reported on GenScript peptide analysis certificate.

https://doi.org/10.1371/journal.pone.0285812.t001

full-length human PRMT7 (residues 1–692) linked by the sequence SDLVPRGSST (Addgene. org plasmid no. 34693) [21]. We designated this GST-human PRMT7 fusion protein as GST-*Hs*PRMT7. Transformed cells were lysed, followed by purification of GST-*Hs*PRMT7 *via* column chromatography with glutathione-Sepharose beads as described previously [9]. Recombinant full-length human histone H2B was purchased from New England Biolabs (NEB catalog no. M2505S). Full-length *Xenopus laevis* histone H2B was received as a generous gift from Maria Vogelauer and Siavash Kurdistani at the Department of Biological Chemistry at UCLA [22]. Synthetic peptides used in this study included human histone H2B (23–37), *X. laevis* H2B (23–37), "Mono R," "RGR," "KRGR," "RKR," "RGRK," and "RER" which were purchased from GenScript. At least 85% HPLC purity and TFA salt removal was guaranteed by GenScript. All peptides arrived in lyophilized form and were dissolved in distilled water to form 10 mM stock solutions and were further diluted in water to form 100 μM and 500 μM stock solutions to be used in methylation assays described in this study. A summary table of all protein and peptide sequences is included in Table 1.

In vitro methylation assay of GST-*Hs*PRMT7 with protein and peptide substrates

In vitro methylation assays were performed with GST-*Hs*PRMT7, the indicated substrate protein or peptide, and 1.4 μM S-adenosyl-L-[*methyl*-^{3}H]methionine ([^{3}H]-AdoMet; PerkinElmer cat no. NET155V), prepared from diluting a stock of 7.0 μM [^{3}H]-AdoMet (81.9 Ci/mmol, 1 mCi/mL in 9:1 10 mM H_2SO_4:EtOH, v/v) in 10 mM HCl. All reactions were performed using distilled water buffered with 50 mM potassium HEPES, pH 9.5 and 1 mM DTT, reaching a final reaction volume of 30 μL. The reactions were initiated by adding [^{3}H]-AdoMet to a final concentration of 0.14 μM. Control reactions (enzyme-only, substrate-only) contained distilled water instead of substrate or GST-*Hs*PRMT7, respectively. After initiation with [^{3}H]-AdoMet, all reactions analyzed *via* P81 phosphocellulose filter paper assay were incubated in a water bath at 25°C unless otherwise indicated for the specified time periods and were terminated with 0.5 μL 100% (w/v) trifluoroacetic acid (TFA). P81 assays performed at t = 0 were

33

individually terminated immediately following initiation. Samples analyzed *via* SDS-PAGE were incubated at 4°C for 24 hours and were quenched by adding 5x SDS sample loading buffer (250 mM Tris-HCl, pH 6.8; 10% SDS, 30% glycerol, 10% β-mercaptoethanol, 0.2% bromophenol blue), followed by heating at 97°C for 3 min.

SDS-PAGE and fluorography of methylated full-length histones

In vitro methylation assays with GST-*Hs*PRMT7, full-length histone H2B substrates, and [^{3}H]-AdoMet were set up as described previously [9]. Reaction samples with human and *X. laevis* histone H2B contained 1 μg and 3 μg, respectively. After quenching, samples were immediately loaded onto a 4–20% Bis-tris 10-well ExpressPlus PAGE gel (GenScript catalog no. M42010). Gel electrophoresis was performed for approximately 60 min at 140 V and 400 mA (BioRad PowerPac 300). The gel was stained with Coomassie Blue for one hour followed by overnight destain in 15% methanol and 10% acetic acid. After soaking the destained gel overnight in water, the gel was treated with EN3HANCE autoradiography fluid as per the manufacturer's recommendations (PerkinElmer catalog no. 6NE9701) and dried under vacuum. To visualize species methylated with [^{3}H]-methyl groups, the gel was exposed to autoradiography film at -80°C for 1 and 74 days, and then [^{3}H] fluorographs were developed and digitally scanned.

P81 phosphocellulose filter paper methylation assay

In vitro methylation assays with GST-*Hs*PRMT7, selected methyl-accepting substrates, and [^{3}H]-AdoMet were set up as described previously [9] and performed in triplicate. Following incubation at 25°C unless otherwise indicated for the time periods specified, all samples were quenched with 0.5 μL 100% TFA and centrifuged at 9,300 *g* for 10 seconds in an Eppendorf centrifuge (Model 5417C). 1 cm^2 pieces of P81 phosphocellulose filter paper (LabAlley catalog no. 05-717-2A) were spotted with 25 μL from each reaction mixture and set to dry overnight. The following day, all filter paper pieces were washed three times with 50 mM sodium bicarbonate solution, pH 9.0, and dried again in liquid scintillation vials. After 5 mL of Safety Solve fluor (RPI industries) was added to each vial, [^{3}H] radioactivity in each sample was quantified *via* liquid scintillation counter (Beckman LS6500) for four total cycles at 5 minutes per sample. All data presented are expressed as averages of the cpm from cycles 2–4.

Statistical methods

Statistical analyses were performed using the "Analyze Data" function on GraphPad Prism v.8.0.1. To determine statistical significance, unpaired homoscedastic two-tailed Student's *t* tests were performed with significance level $\alpha = 0.05$ with the relevant data. To obtain apparent k_m and V_{max} values, kinetic data were analyzed by non-linear regression using the Michaelis-Menten equation.

Results

GST-*Hs*PRMT7 methylates full-length *Homo sapiens* histone H2B but not full-length *Xenopus laevis* histone H2B

Previous studies have showed that human histone H2B is specifically methylated by PRMT7 at arginine residues 29, 31, and 33 [8]. This region includes Arg-X-Arg (RXR) sequences shown to be specific for PRMT7 methylation [8, 9, 11]. To study the importance of the RXR target sequence for PRMT7 catalysis, we first compared PRMT7 *in vitro* methylation activity with human histone H2B, containing the sequence 29-RKRSR-33, to that with histone H2B from *X. laevis*, which contains instead the sequence 29-RRKSR-33. The sequences adjacent to this

```
H.sapiens    MPDPAKSAPAPKKGSKKAVTKAQKKDGKKRKRSRKESYSVYVYKVLKQVHPDTGISSKAM    60
X.laevis     MPEPAKSAPAPKKGSKKAVTKTQKKDGKKRRKSRKESYAIYVYKVLKQVHPDTGISSKAM    60
             **:******************:*******::*****::*******************
```

```
H.sapiens    GIMNSFVNDIFERIAGEASRLAHYNKRSTITSREIQTAVRLLLPGELAKHAVSEGTKAVT   120
X.laevis     SIMNSFVNDVFERIAGEASRLAHYNKRSTITSREIQTAVRLLLPGELAKHAVSEGTKAVT   120
             .********:***************************************************
```

```
H.sapiens    KYTSSK    126
X.laevis     KYTSAK    126
             ****:*
```

Fig 1. *H. sapiens* histone H2B and *X. laevis* histone H2B are highly similar. The amino acid sequences of *H. sapiens* histone H2B (UniProt accession **Q93079**) and *X. laevis* histone H2B (UniProt accession **P02281**) were aligned using Clustal Omega. Highlighted is the region spanning amino acids 23–37 which contains the target sequence 29-RKRSR-33 present in human histone H2B that is methylated by PRMT7. Other than the substitutions at Lys-30 and Arg-31, the sequences of *H. sapiens* and *X. laevis* histone H2B differ at only seven locations.

https://doi.org/10.1371/journal.pone.0285812.g001

region are nearly identical in the human and Xenopus proteins (Fig 1). Methylation assays were conducted by incubating bacterially expressed human GST-PRMT7 fusion protein, [³H]-AdoMet, and purified recombinant histone H2B from human and *X. laevis*, respectively, for 24 h as described in **Materials and Methods**. Reaction samples were analyzed by SDS-PAGE. After Coomassie Blue staining, we observed major bands at ~15, 26, and 100 kDa, which corresponded to the expected sizes for human and *X. laevis* H2B, GST, and GST-*Hs*PRMT7, respectively (Fig 2). As controls, we analyzed reaction mixtures containing only PRMT7, human H2B, or *X. laevis* H2B in parallel.

To visualize methylation of H2B substrates by PRMT7, we obtained 1-day and 74-day [³H]-fluorograph exposures of all samples (Fig 2). Only human histone H2B appeared to be methylated after a 1-day exposure. In either the 1-day or the 74-day exposure, no methylation of *X. laevis* H2B was detectable, suggesting that even the minor substitution of Arg-31 and Lys-30 in the 29-RKRSR-33 human H2B sequence leads to loss of RXR sites and elimination of methyl accepting activity for PRMT7.

The 29-RKRSR-33 sequence in human H2B is critical for GST-*Hs* PRMT7 methylation activity

As a next step, we wanted to investigate whether changes to the 29-RKRSR-33 sequence could explain the loss of human PRMT7 methylation activity with Xenopus H2B. To isolate any possible effect from this target sequence, we designed two synthetic peptides consisting of amino acids 23–37 of histone H2B from human and Xenopus whose sequences are identical except at amino acids positions 30 and 31. Whereas 29-RKRSR-33 is present in human H2B (23–37), Xenopus H2B (23–37) instead contains 29-RRKSR-33, with all other residues being identical. In Fig 3, we assayed Xenopus histone H2B (23–37) peptide with GST-*Hs*PRMT7 for 40 min at 25°C alongside the human histone H2B (23–37) peptide. We show that GST-*Hs*PRMT7 activity is highest with human histone H2B (23–37), whereas no significant methylation activity over background was detected for Xenopus histone H2B (23–37). These results clearly show that even minor substitutions to the 29-RKRSR-33 human H2B sequence can lead to a near total reduction in GST-*Hs*PRMT7 activity, supporting previous findings that this region is a critical target sequence for human PRMT7 [8]. This result confirms that the amino acid changes in this region and not elsewhere is responsible for the loss of PRMT7 activity.

To explore whether reduced human PRMT7 methylation activity with Xenopus histone H2B (23–37) can be explained by decreased enzyme-substrate binding affinity, we raised the

35
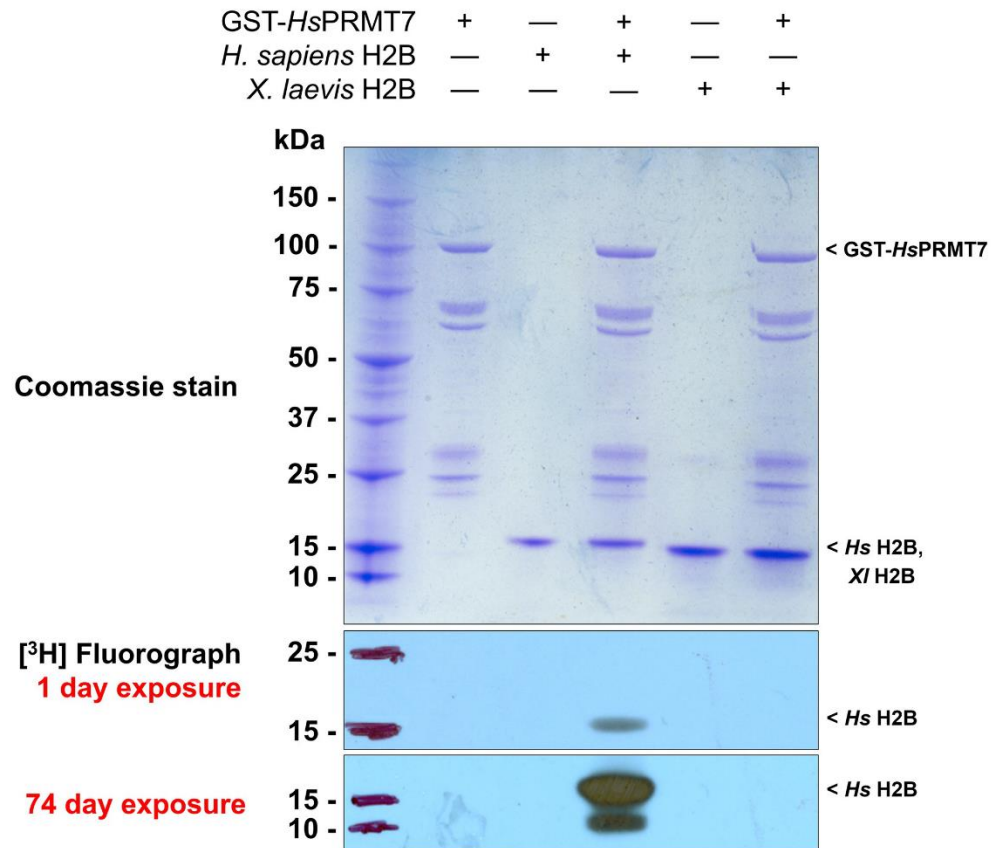
Fig 2. Xenopus histone H2B is not methylated by human PRMT7. After incubation for 24 h at 4°C, reaction samples were terminated and then separated by SDS-PAGE and visualized by Coomassie blue staining (top) and [³H]-fluorography (bottom) as described in Materials and Methods. Samples were exposed for 1 and 74 days. Lane 1 contains protein MW standards. Lanes 2, 3, and 5 are used as negative control and contain GST-*Hs*PRMT7 only, human histone H2B only, and *X. laevis* H2B only, respectively. Lane 4 contains GST *Hs*PRMT7 and human histone H2B and is used as positive control. Lane 6 contains GST-*Hs*PRMT7 and *X. laevis* histone H2B. Key species present are annotated at their expected MW.

https://doi.org/10.1371/journal.pone.0285812.g002

peptide concentration from 10 µM to 50 µM in the experiment performed in Fig 4. Over a time course spanning 0, 1, 2, and 3 hours, we now detected significant PRMT7 methylation activity over background for all peptide substrates that increased linearly over 0–1 hour. Unlike the results shown in Fig 3, these data suggest that Xenopus histone H2B (23–37) is indeed methylated by human PRMT7, albeit at low levels. We also observed that increasing the concentration of *X. laevis* histone H2B (23–37) did not lead to a significant increase in methylation activity under the same conditions, suggesting that PRMT7 was already saturated at the 10 µM peptide concentration. We observed that the measured methylation activity within reaction assays containing 50 µM *X. laevis* histone H2B (23–37) was consistently less

36

than those containing 10 µM *X. laevis* histone H2B (23–37) at each of the 1, 2, and 3-hour time points (Fig 4), suggesting some substrate inhibition. Conversely, the positive control assays containing enzyme and human histone H2B (23–37) reached approximately 6,000 cpm after just 1 hour, with maximum activity occurring at t = 3 hours at approximately 8,000 cpm (Fig 4). Taken together, the data suggest that the K30R/R31K substitutions in the 29-RKRSR-33 target sequence affects PRMT7 methylation activity by affecting the turnover rate more so than the apparent substrate binding affinity.

The RXR motif is necessary for PRMT7 methylation activity

After observing the significant change in PRMT7 activity with just a minor sequence substitution in the methyl-accepting substrate from 29-RKRSR-33 to 29-RRKSR-33, we aimed to identify the residues and sequence motifs that were necessary for PRMT7 catalysis. Previous studies indicated that one crucial motif for PRMT7 catalysis is Arg-X-Arg (RXR), consisting of two arginine residues separated by any other amino acid [8, 11]. Thus, we designed two simple peptides that contain only Arg and Gly in the target sequence and Lys and Gly in the surrounding contextual region: Ac-KKGG**R**GGGGKKY-amide ("mono R") and Ac-KKGG**R**G**R**GGKKY-amide ("RGR"). A single tyrosine residue was added to the C-terminus to quantify peptide concentration by A_{280} absorption. Since Tyr also exists on the C-terminus of human H2B (23–37), we did not expect any major effects from this inclusion. The sequence, predicted molecular weight, and experimentally determined molecular weight of these peptides are summarized in Table 1.

Initially, we compared the PRMT7 methylation activity with human H2B (23–37), mono R, and RGR peptide substrates at t = 20 hours in Fig 5, similar to the experiments performed in Fig 3. As expected, we observed the highest PRMT7 methylation activity with the human H2B (23–37) peptide substrate (Fig 5). Comparatively, PRMT7 activity with the RGR peptide decreased about 4 to 5-fold, whereas methylation of the mono R peptide was barely detectable over the PRMT7-only control.

As a next step, we sought to model the GST-*Hs*PRMT7 methylation with Michaelis-Menten kinetics in order to determine whether the activity differences with each peptide substrate can be explained by changes in apparent binding affinity (k_m) or catalytic turnover (V_{max}). We designed a time-course methylation experiment similar to Fig 4 to identify the linear initial rate region and investigate the contribution of the arginine residue(s) within the mono R and RGR peptides toward PRMT7 methylation activity. Fig 6 illustrates the change in methylation activity over time from 0, 15, 30, 60, and 120 minutes for reaction mixtures containing GST-*Hs*PRMT7 and either 10 µM mono R peptide or 10 µM RGR peptide. For comparison, we also included reaction assays containing enzyme and 10 µM Xenopus histone H2B (23–37) (Fig 6). As positive control, we compared all assays to reactions containing enzyme and 10 µM human histone H2B (23–37). As negative control, we included reaction assays containing enzyme only. As expected, reactions containing enzyme and human histone H2B (23–37) peptide showed high methylation activity as early as t = 15 min, reaching a maximum value of about 4,000 cpm at t = 120 min. By comparison, the RGR peptide showed a roughly linear increase in cpm from t = 0 to t = 120 min, reaching a maximum value of about 800 cpm at t = 120 min. *X. laevis* histone H2B (23–37) showed low methylation activity but was significantly above control. Methylation activity with samples containing mono R peptide was not significantly greater than control. These data demonstrate that the presence of the RXR motif in the substrate sequence is important for methylation by human PRMT7. However, the substantial difference in activity between the RGR and human H2B (23–37) peptides suggest that other

37
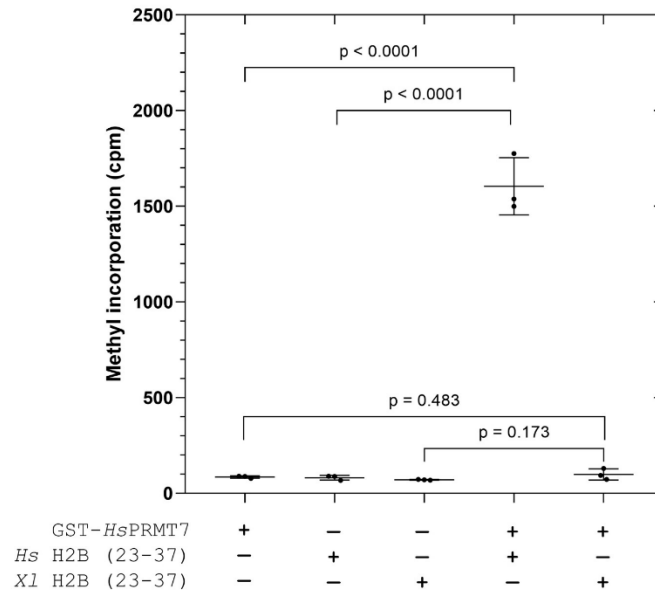
Fig 3. Methylation of Xenopus histone H2B (23–37) peptide by human PRMT7 is undetectable. The methylation activity of GST-HsPRMT7 with H. sapiens histone H2B (23–37) and X. laevis histone H2B (23–37) substrates was assessed using the P81 phosphocellulose paper assay as described in **Materials and Methods**. 5 μg of GST-HsPRMT7 was incubated with 10 μM of the indicated substrate and 0.14 μM [^{3}H]-AdoMet for 40 min at 25°C. Statistical significance was determined via Student's t-test. All reactions indicated were run in triplicate. Hs H2B (23–37), H. sapiens histone H2B (23–37) peptide; Xl H2B (23–37), X. laevis histone H2B (23–37) peptide.

https://doi.org/10.1371/journal.pone.0285812.g003

residues within the 29-RKRSR-33 sequence also have a role in optimizing enzyme-substrate binding or catalysis.

Differences in methylation of substrates appears to result from changes in the rate of catalysis and not in the binding affinity

The results in Fig 6 demonstrated a large difference in GST-HsPRMT7 methylation activity between the RGR peptide and the human H2B (23–37) peptide used as positive control despite the presence of the RXR motif in both peptides. As such, we sought to explore whether the presence of charged residues in the target sequence in conjunction with the RXR motif could lead to higher methylation activity. To do this, we first designed four additional synthetic peptides (KRGR, RKR, RGRK, and RER) with nearly identical sequences to the mono R and RGR peptides shown previously, save for an additional lysine or glutamate residue within the target sequence (Table 1). To determine the effect of the RXR motif and charged residues on GST-HsPRMT7 binding and catalysis, we modeled the methylation activity with each peptide substrate with Michaelis-Menten kinetic experiments and compared each peptide's calculated apparent k_m and V_{max} values (Fig 7).

From the experiments shown in Fig 7, we show that the RGR, KRGR, RKR, and RGRK peptides have very similar binding affinities ranging from 0.57 to 0.85 μM whereas the

38
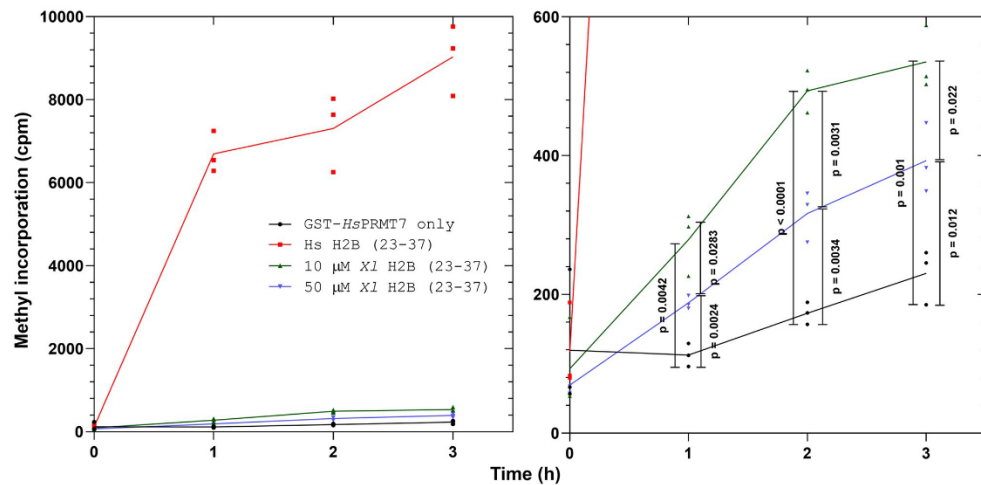
Fig 4. Comparison of human PRMT7-mediated methylation of human and Xenopus H2B (23–37) peptide substrates over time. The methylation activity of GST-*Hs*PRMT7 with human histone H2B (23–37) and Xenopus histone H2B (23–37) substrates was assessed using the P81 phosphocellulose paper assay as described in **Materials and Methods**. *Left-hand side*: radioactive counts per minute of reactions containing 5 μg of GST-*Hs*PRMT7 incubated with 10 μM *Hs* H2B (23–37), 10 μM *Xl* H2B (23–37), 50 μM *Xl* H2B (23–37), and 0.14 μM [^{3}H]-AdoMet for 0, 1, 2, and 3 h at 25°C. *Right-hand side*: statistical significance was determined for GST-*Hs*PRMT7 only, 10 μM *Xl* H2B (23–37), and 50 μM *Xl* H2B (23–37) at each time point *via* Student's t-test. All reactions indicated were run in triplicate. *Hs* H2B (23–37), *H. sapiens* histone H2B (23–37) peptide; *Xl* H2B (23–37), *X. laevis* histone H2B (23–37) peptide.

https://doi.org/10.1371/journal.pone.0285812.g004

corresponding V_{max} values varied significantly from 200 to 1400 μM s^{-1}. Comparatively, the mono R and RER peptides showed slightly increased apparent k_m values of 1.4 μM and 2.8 μM, respectively, as well as strongly decreased V_{max} values. Conversely, the calculated V_{max} values varied substantially depending on the presence of the RXR motif and charged residues within the peptide target sequence (Fig 7). We observed the highest V_{max} values with RKR, followed by KRGR, RGR and RGRK. In contrast, the V_{max} values calculated for Mono R and RER were 5–6 times lower than RKR. Taken together, these data suggest that PRMT7 activity could be enhanced by the presence of a positively charged Lys residue within the targeted RXR motif.

Increases in salt concentration inhibits PRMT7 by decreasing enzyme-substrate binding affinity

Previous studies indicate that GST-*Hs*PRMT7 activity with human H2B (23–37) peptide substrate decreases by half with the addition of 50 mM NaCl or KCl [9]. Comparatively, a previous study of ionic strength in human HEK293 cells estimates the intracellular concentration of potassium ions to be about 120–140 mM in human cells [23, 24]. As such, our results in Fig 7 led us to question whether this dramatic decrease in activity may be associated with a loss of either substrate-enzyme binding affinity or catalytic activity.

To explore this question, we compared the PRMT7 methylation activity of the human histone H2B (23–37), mono R, RGR, KRGR, RKR, RGRK, and RER peptides *via* P81 methylation assay with and without addition of 130 mM KCl (Fig 8). Apparent k_m and V_{max} values

39
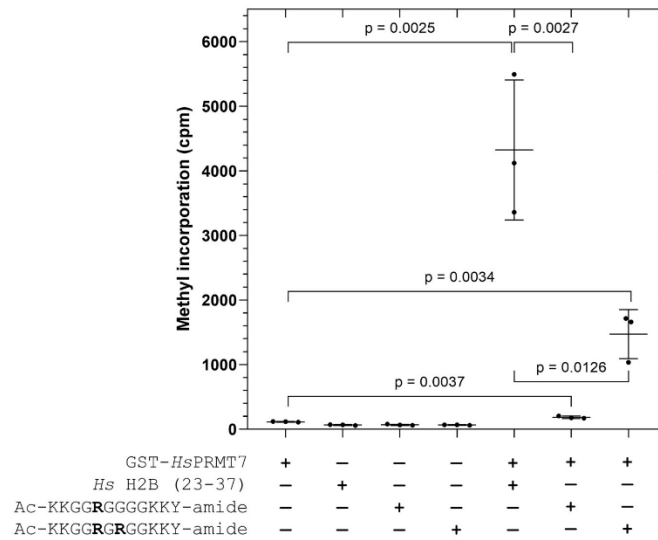
Fig 5. The effect of the RXR motif on substrate methylation by human PRMT7. The methylation activity of GST-*Hs*PRMT7 with *Hs* H2B (23–37), mono R, and RGR peptide substrates was assessed using the P81 phosphocellulose paper assay as described in **Materials and Methods**. 5 μg of GST-*Hs*PRMT7 was incubated with 10 μM of the indicated substrate and 0.14 μM [³H]-AdoMet for 20 h at 4°C. Statistical significance was determined *via* Student's t-test. All reactions indicated were run in triplicate. *Hs* H2B (23–37), *H. sapiens* histone H2B (23–37) peptide; mono R, Ac-KKGG**R**GGGGKKY-amide; RGR, Ac-KKGG**R**G**R**GGKKY-amide.

calculated for each peptide under these conditions are summarized in Table 2. As shown in Fig 8, adding 130 mM KCl to reaction assays showed significantly increased apparent k_m values for all indicated peptide substrates. This apparent k_m increase was up to 30-fold, in the case of the human histone H2B (23–37) control peptide. Moreover, the mono R, KRGR, RKR, RGRK, and RER peptides showed roughly linear initial PRMT7 methylation activity in the chosen concentration range with 130 mM KCl present, further suggesting that the decrease in methylation activity occurs *via* decreases in enzyme-substrate binding affinity. However, it is unclear whether the inhibitory effect of ionic strength in these experiments is purely competitive. For instance, whereas the V_{max} values with and without added salt remained relatively unchanged for human histone H2B (23–37), this was not the case with the RGR, KRGR, RKR, and RGRK peptides, which showed up to an approximately three-fold decrease in V_{max} after adding 130 mM KCl. Taken together, these data suggest that ionic strength primarily affects human PRMT7 substrate binding.

Discussion

We confirm that human PRMT7 activity is quite sensitive to changes in the RXR target sequence in the substrate protein. The observed loss of PRMT7 methylation activity with the K30R/R31K substitutions in the human histone H2B sequence complements previous findings, where either R29K or R33K substitutions in human histone H2B (23–37) peptides led to at least a two-thirds reduction of PRMT7 activity and an R31K-substituted human H2B (23–

40
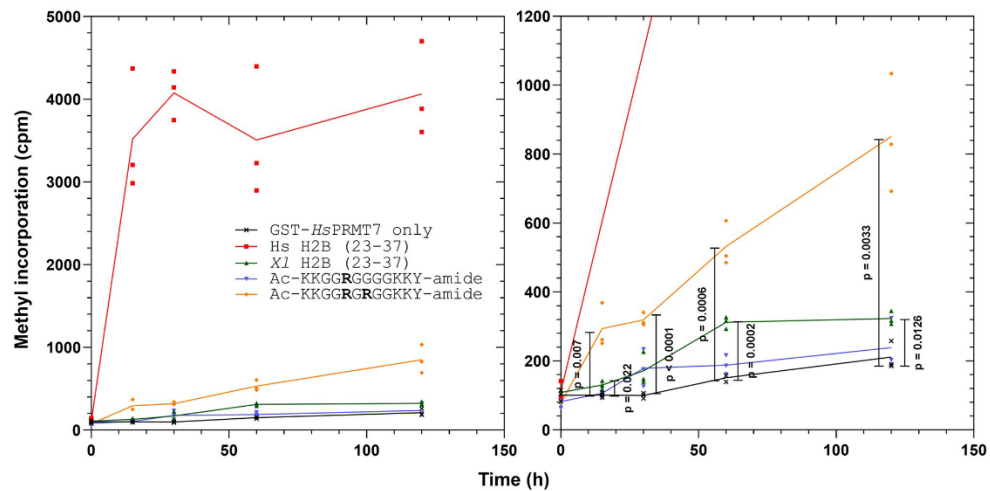
Fig 6. Comparison of human PRMT7-mediated methylation of human H2B (23–37), Xenopus H2B (23–37), and synthetic peptide substrates over time. The methylation activity over time of GST-*Hs*PRMT7 with human histone H2B (23–37), Xenopus histone H2B (23–37), mono R and RGR peptide substrates was compared using the P81 phosphocellulose paper assay as described in **Materials and Methods**. *Left-hand side*: radioactive counts-per-minute of reactions containing 5 μg of GST-*Hs*PRMT7 incubated with 10 μM *Hs* H2B, *Xl* H2B (23–37), mono R, or RGR peptide and 0.14 μM [^{3}H]-AdoMet for 0, 15, 30, 60, and 120 min at 25°C. *Right-hand side*: statistical significance was determined for GST-*Hs*PRMT7 only, *Xl* H2B (23–37), mono R, and RGR at each time point *via* Student's t-test. All reactions indicated were run in triplicate. *Hs* H2B (23–37), *H. sapiens* histone H2B (23–37) peptide; *Xl* H2B (23–37), *X. laevis* histone H2B (23–37) peptide; mono R, Ac-KKGG**R**GGGGKKY-amide; RGR, Ac-KKGG**R**G**R**GGKKY-amide.

https://doi.org/10.1371/journal.pone.0285812.g006

37) peptide showed no methyl-accepting activity [11]. The exquisite specificity of PRMT7 toward the basic RXR motif can be contrasted to the much broader specificity of the major type I protein arginine methyltransferase (PRMT1) and the major type II enzyme (PRMT5). These latter enzymes have been shown to methylate multiple amino acid sequences [11, 25]. PRMT1, the major type I PRMT and the enzyme responsible for ~85% of protein arginine methylation, was initially thought to target specific glycine-arginine rich (RGG) motifs such as GG**R**G**R**GG in human fibrillarin and G/FGG**R**GGG/F in heterogenous nuclear ribonuclear proteins [26–28]. However, later work showed that PRMT1 can methylate a much wider range of substrates than that predicted by the RGG consensus sequence, including histone H2AR11 (8-GKA**R**AK-13) and histone H4R3 (1-SG**R**GK-5) [29–33]. PRMT5, the major type II arginine methyltransferase, has also been shown to target a wide range of substrates containing an RG/GRG sequence, although the involvement of substrate-binding adaptor proteins such as pIC1n, RIOK1, and COPR5 in PRMT5-mediated methylation is distinct from the other PRMTs [34]. Methylation studies performed *in vitro* with *Trypanosoma brucei* PRMT7 (*Tb*PRMT7) and peptides based on amino acids 1–21 of histone H4 (1-SG**R**GK-5) showed that *Tb*PRMT7 also targeted GRG substrate motifs, in a distinct specificity than the mammalian isoforms [3, 35, 36]. PRMT9, a minor type II methyltransferase, also appears to be very specific, as to date it has only been shown to methylate the splicing factor SF3B2 at Arg508 (505-CFK**R**KYL-511) with reported k_m value of 0.08 μM [7, 37, 38]. Unlike the other PRMTs, PRMT9 does not appear to methylate either core histones or RGG-containing sequences [7].

41
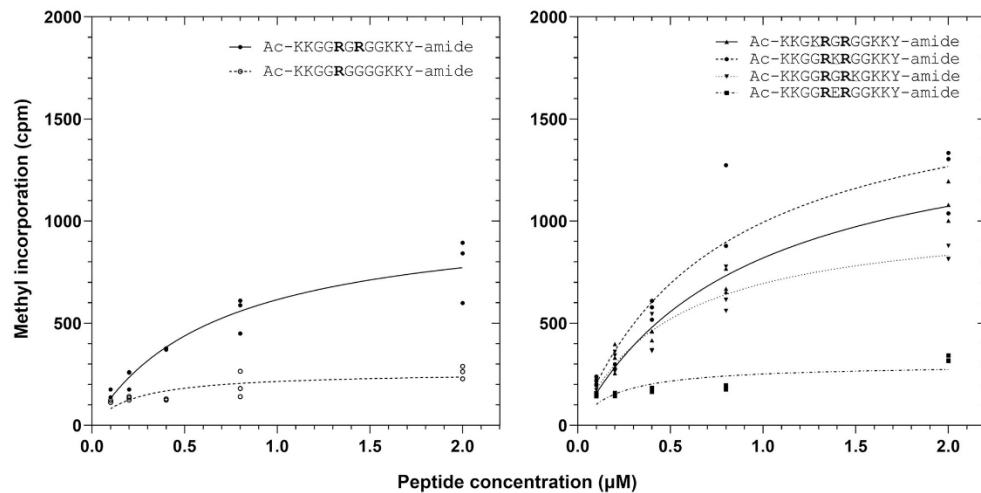
Fig 7. The effect of the RXR motif and charged residues on PRMT7-substrate enzyme kinetics. The apparent binding affinity k_m and maximum initial activity V_{max} of GST-HsPRMT7 with synthetic peptide substrates was modeled with Michaelis-Menten kinetics using data gathered by P81 phosphocellulose paper assay as described in **Materials and Methods**. *Left*, methylation of mono R compared to RGR substrates. *Right*, comparison of methylation of KRGR, RKR, RGRK, and RER substrates. 5 μg of GST-HsPRMT7 was incubated with various concentrations of the indicated peptide and 0.14 μM [³H]-AdoMet for 60 min at 25˚C. All reactions indicated were run in triplicate. Human histone H2B (23–37) peptide was used as a positive control (not shown). Mono R, Ac-KKGG**R**GGGGKKY-amide; RGR, Ac-KKGG**R**G**R**GGKKY-amide; KRGR, Ac-KKG**KR**G**R**GGKKY-amide; RKR, Ac-KKGG**R**K**R**GGKKY-amide; RGRK, Ac-KKGG**R**G**R**KGKKY-amide; RER, Ac-KKGG**R**E**R**GGKKY-amide.

Interestingly, a recent study presented *in vitro* and *in silico* evidence that human PRMT7 methylates R548 (544-SPC**R**DSV-551) and R753 (750-FCG**R**KQF-756) on the C-terminus of proliferator-activated receptor gamma coactivator-1 alpha [39]. These results could importantly imply the existence of PRMT7 substrates that do not conform to the RXR consensus sequence illustrated here. In a recent review Halabelian and Barsyte-Lovejoy summarized in their Table 1 reports of PRMT7 modification of different proteins [40]. We note that many of these suggested arginine methylation sites have sequences distinct from the Arg-X-Arg motif sequences studied here. Further work will be needed to confirm these distinct sites and to evaluate whether PRMT7 can target distinct types of methyl-accepting sites. We do note that the proposed methylation sites of histone H4 at Arg3, determined indirectly, may in fact reflect methylation by PRMT5 [17]. Additionally, we recognize that there may be significant differences in the recognition of Arg residues by PRMT7 in structured proteins as opposed to unstructured peptides.

At present, it is generally understood that PRMT-substrate recognition and methylation depend on both specific sequence motifs as described above as well as the surrounding primary amino acid context [25]. Previous work suggested that suitable substrates for PRMT7 can contain an RXR motif surrounded by basic residues, as in the lysine- and arginine-rich amino acid 23–37 region of human histone H2B (23-KKDGKK**R**K**R**S**R**KESY-37) [4, 8, 11]. As such, we were interested in isolating critical residues within the 29-RKRSR-33 sequence in human H2B while also minimizing the effect of contextual amino acids. To approach this goal, our synthetic peptide design prioritized the 29-RKRSR-33 target sequence, including only

42
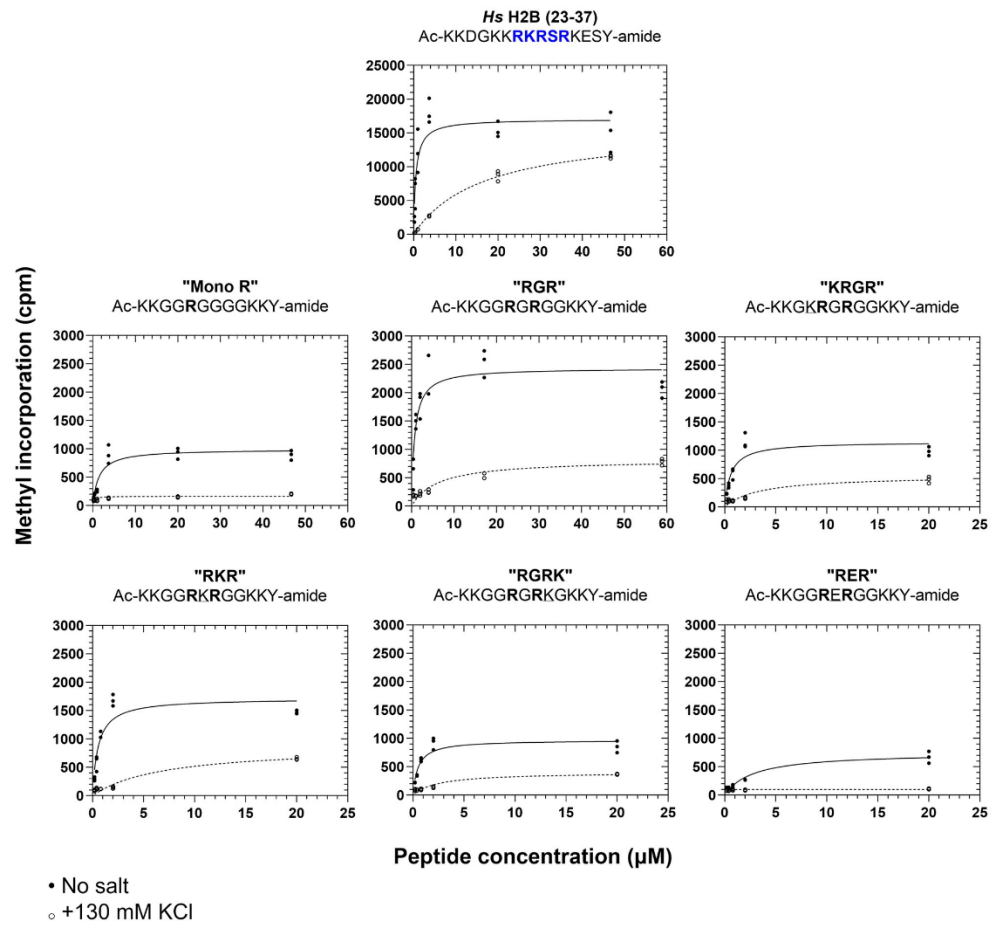
Fig 8. Increases in ionic strength affects PRMT7-substrate binding affinity and maximum initial reaction velocity. The apparent binding affinity k_m and maximum initial activity V_{max} of GST-HsPRMT7 with synthetic peptide substrates was modeled with Michaelis-Menten kinetics using data gathered by P81 phosphocellulose paper assay as described in **Materials and Methods**. For all reactions, 5 µg of GST-HsPRMT7 was incubated with various concentrations of the indicated peptide and 0.14 µM [³H]-AdoMet for 60 min at 25°C. *Closed circle*, methylation activity of human PRMT7 without added ionic strength. *Open circle*, methylation activity of human PRMT7 in the presence of 130 mM KCl. All reactions indicated were run in triplicate. Human histone H2B (23–37) peptide was used as a positive control for all experiments. Mono R, Ac-KKGG**R**GGGGKKY-amide; RGR, Ac-KKGG**R**G**R**GGKKY-amide; KRGR, Ac-KKG**K**R**GR**GGKKY-amide; RKR, Ac-KKGG**R**K**R**GGKKY-amide; RGRK, Ac-KKGG**R**G**R**KGKKY-amide; RER, Ac-KKGG**R**E**R**GGKKY-amide.

lysine and glycine as context. Here, we show that the *in vitro* methylation activity of human PRMT7 decreased dramatically with peptides that either contain a negatively charged Glu within the RXR motif or lack the RXR motif entirely. However, the fact that the highest PRMT7 activity observed with the synthetic peptides is roughly one-fifth of that observed with human histone H2B (23–37) suggests that additional residues in human H2B (23–37)

43

Table 2. Summary of calculated Michaelis-Menten kinetic parameters from the data presented in Fig 8.

Peptide Name	Peptide Sequence	k_m (μM)	95% CI	V_{max} (μM s^{-1})	95% CI
No added salt					
Hs H2B (23–37)	Ac-KKDGKK**R**K**R**S**R**KESY-amide	0.6	[0.3, 1.0]	17000	[15000, 19000]
Mono R	Ac-KKGG**R**GGGGKKY-amide	1.4	[0.9, 2.3]	990	[870, 1100]
RGR	Ac-KKGG**R**G**R**GGKKY-amide	0.7	[0.4, 1.2]	2400	[2200, 2700]
KRGR	Ac-KKGK**R**G**R**GGKKY-amide	0.6	[0.3, 1.0]	1200	[950, 1400]
RKR	Ac-KKGG**R**K**R**GGKKY-amide	0.6	[0.3, 0.9]	1700	[1500, 2000]
RGRK	Ac-KKGG**R**G**R**KGKKY-amide	0.5	[0.3, 0.8]	970	[840, 1100]
RER	Ac-KKGG**R**E**R**GGKKY-amide	2.8	[1.7, 4.6]	750	[640, 880]
+130 mM KCl					
Hs H2B (23–37)	Ac-KKDGKK**R**K**R**S**R**KESY-amide	17	[14, 20]	16000	[15000, 17000]
Mono R	Ac-KKGG**R**GGGGKKY-amide	—*	—*	—*	—*
RGR	Ac-KKGG**R**G**R**GGKKY-amide	6.2	[3.5, 11]	820	[690, 980]
KRGR	Ac-KKGK**R**G**R**GGKKY-amide	3.3	[1.7, 7.0]	550	[440, 700]
RKR	Ac-KKGG**R**K**R**GGKKY-amide	6.9	[3.8, 16]	880	[710, 1200]
RGRK	Ac-KKGG**R**G**R**KGKKY-amide	2.4	[1.3, 4.5]	400	[330, 490]
RER	Ac-KKGG**R**E**R**GGKKY-amide	—*	—*	—*	—*

All kinetic values and their 95% confidence intervals were obtained using the "statistical analysis" function in GraphPad Prism version 8.0.1.

*indicates poor fit of Michaelis-Menten equation

https://doi.org/10.1371/journal.pone.0285812.t002

contribute to PRMT7 catalysis, or that there are additional three-dimensional contacts with residues outside of the motif. Previous mass spectrometry data indicate that PRMT7 methylates human H2B (23–37) at R29, R31, and R33, so it is possible that the third Arg present in human H2B (23–37) also contributes substantially to PRMT7 methylation [8].

We wanted lastly to investigate how the presence of ionic strength inhibited PRMT7 activity. We saw this as a useful next step in identifying possible *in vivo* substrates of human PRMT7, which is challenging in part because PRMT7 lacks significant activity at physiological temperature, pH, and ionic strength [9]. Indeed, observed human PRMT7 activity with human H2B (23–37) peptide substrate decreases by half with the addition of 50 mM NaCl or KCl [9]. By comparison, the intracellular concentration of K$^+$ ions in human HEK293 cells is estimated to be between 120–140 mM [23, 24]. We showed that the addition of 130 mM KCl primarily decreased apparent PRMT7-peptide binding affinity for the human H2B (23–37) peptide, whereas the maximum velocity seemed relatively stable. However, we were intrigued to find a decrease of both apparent binding affinity and maximum velocity in the case of other peptides. This result may suggest that the inhibitory effect of ionic strength on PRMT7 activity is not wholly competitive in nature.

Recently, it has been demonstrated that increases in ionic strength also inhibits the *in vitro* activity of PRMT1 and PRMT5 [9]. However, one earlier study presented evidence that high salt conditions instead increased PRMT1 expression and ADMA formation in the human endothelial cell line EA.hy926, resulting in upregulation of the Ras homolog gene family member A/Rho-associated protein kinase pathway and inhibition of nitric oxide synthetase activity [41]. Extensions of this work in rat-based models further showed that increased ADMA concentration resulted in decreased nitric oxide synthesis, implying that salt-dependent upregulation of PRMT1 expression is ultimately involved in the onset and development of salt-sensitive hypertension [42, 43]. As such, the physiological significance of the effect of ionic strength on PRMT activity remains unclear.

44

Taken together, the results of this study offer additional insight into PRMT7 specificity toward the 29-RKRSR-33 sequence in human histone H2B and, more generally, the effect of disrupting the RXR motif on PRMT7 methylation activity. However, more evidence is needed to elucidate additional substrate factors that contribute to PRMT7 catalysis. In this case, structural evidence could be helpful in determining the origin of the specificity of human PRMT7 toward human H2B. Ultimately, the goal of these studies would be to identify criteria that could accurately predict whether a protein of interest could be a substrate of PRMT7. Such criteria could prove useful for identifying protein substrates of PRMT7 *in vivo* and for further elucidating its role in our physiology.

Supporting information

S1 File.
(XLSX)

S2 File.
(XLSX)

S1 Raw images.
(PDF)

Author Contributions

Conceptualization: Timothy J. Bondoc, Troy L. Lowe, Steven G. Clarke.

Data curation: Timothy J. Bondoc.

Formal analysis: Timothy J. Bondoc.

Funding acquisition: Steven G. Clarke.

Investigation: Timothy J. Bondoc.

Methodology: Timothy J. Bondoc, Troy L. Lowe, Steven G. Clarke.

Resources: Troy L. Lowe, Steven G. Clarke.

Supervision: Troy L. Lowe, Steven G. Clarke.

Writing – original draft: Timothy J. Bondoc.

Writing – review & editing: Timothy J. Bondoc, Troy L. Lowe, Steven G. Clarke.

References

1. Uversky VN. Posttranslational Modification. In: Maloy S and Hughes K, editors. *Brenner's Encyclopedia of Genetics*, 2nd ed. London: Academic Press; 2013. pp. 425–430.

2. Blanc RS and Richard S. Arginine Methylation: The Coming of Age. *Molecular Cell* 2017; 65: 8–24. https://doi.org/10.1016/j.molcel.2016.11.003 PMID: 28061334

3. Jain K, Warmack RA, Debler EW, Hadjikyriacou A, Stavropoulos P, and Clarke SG. Protein Arginine Methyltransferase Product Specificity Is Mediated by Distinct Active-site Architectures. *J. Biol. Chem.* 2016; 291: 18299–18308. https://doi.org/10.1074/jbc.M116.740399 PMID: 27387499

4. Jain K and Clarke SG. PRMT7 as a unique member of the protein arginine methyltransferase family: A review. *Archives of Biochemistry and Biophysics* 2019; 665: 36–45. https://doi.org/10.1016/j.abb.2019.02.014 PMID: 30802433

5. Bedford MT and Clarke SG. Protein Arginine Methylation in Mammals: Who, What, and Why. *Molecular Cell* 2009; 33: 1–13. https://doi.org/10.1016/j.molcel.2008.12.013 PMID: 19150423

6. Paik WK, Lee HW, and Kim S. Analysis of Modified Amino Acids. In: Bhown AS, editor. *Protein/Peptide Sequence Analysis: Current Methodologies*. Boca Raton, FL: CRC Press; 2017. Vol. 61, pp. 220–237.

45

7. Yang Y, Hadjikyriacou A, Xia Z, Gayatri S, Kim D, Zurita-Lopez C, et al. PRMT9 is a Type II methyltrans-ferase that methylates the splicing factor SAP145. *Nat. Commun.* 2015; 6: 6428 https://doi.org/10.1038/ncomms7428 PMID: 25737013

8. Feng Y, Maity R, Whitelegge JP, Hadjikyriacou A, Li Z, Zurita-Lopez C, et al. Mammalian Protein Argi-nine Methyltransferase 7 (PRMT7) Specifically Targets RXR Sites in Lysine- and Arginine-rich Regions. *J. Biol. Chem.* 2013; 288: 37010–37025. https://doi.org/10.1074/jbc.M113.525345 PMID: 24247247

9. Lowe TL and Clarke SG. Human protein arginine methyltransferases (PRMTs) can be optimally active under nonphysiological conditions. *J. Biol. Chem.* 2022; 298: 102290. https://doi.org/10.1016/j.jbc.2022.102290 PMID: 35868559

10. Hadjikyriacou A and Clarke SG. *Caenorhabditis elegans* PRMT-7 and PRMT-9 Are Evolutionarily Con-served Protein Arginine Methyltransferases with Distinct Substrate Specificities. *Biochemistry* 2017; 56: 2612–2626.

11. Feng Y, Hadjikyriacou A, and Clarke SG. Substrate specificity of human protein arginine methyltransfer-ase 7 (PRMT7): the importance of acidic residues in the double E loop. *J. Biol. Chem.* 2014; 289: 32604–32616. https://doi.org/10.1074/jbc.M114.609271 PMID: 25294873

12. Baldwin RM, Haghandish N, Daneshmand M, Amin S, Paris G, Falls TJ., et al. Protein arginine methyl-transferase 7 promotes breast cancer cell invasion through the induction of MMP9 expression. *Oncotar-get* 2015; 6: 3013–3032. https://doi.org/10.18632/oncotarget.3072 PMID: 25605249

13. Bao X, Zhao S, Liu T, Liu YY, Liu YY, and Yang X. Overexpression of PRMT5 Promotes Tumor Cell Growth and Is Associated with Poor Disease Prognosis in Epithelial Ovarian Cancer. *J. Histochem. Cytochem.* 2013; 61: 206–217. https://doi.org/10.1369/0022155413475452 PMID: 23292799

14. Yao R, Jiang H, Ma Y, Wang L, Wang L, Du J, et al. PRMT7 Induces Epithelial-to-Mesenchymal Transi-tion and Promotes Metastasis in Breast Cancer. *Cancer Res.* 2014; 74: 5656–5667. https://doi.org/10.1158/0008-5472.CAN-14-0800 PMID: 25136067

15. Yang T, and Bedford MT. Protein arginine methyltransferases and cancer. *Nature Reviews Cancer* 2013; 13: 37–50. https://doi.org/10.1038/nrc3409 PMID: 23235912

16. Liu C, Zou W, Nie D, Li S, Duan C, Zhou M, et al. Loss of PRMT7 reprograms glycine metabolism to selectively eradicate leukemia stem cells in CML. *Cell Metabolism* 2022; 34: 818–835.e7. https://doi.org/10.1016/j.cmet.2022.04.004 PMID: 35508169

17. Jain K, Jin CY, Clarke SG. Epigenetic control via allosteric regulation of mammalian protein arginine methyltransferases. *Proc. Natl. Acad. Sci. USA.* 2017; 114: 10101–10106. https://doi.org/10.1073/pnas.1706978114 PMID: 28874563

18. Haghandish N, Baldwin RM, Morettin A, Dawit HT, Adhikary H, Masson JY, et al. PRMT7 methylates eukaryotic translation initiation factor 2α and regulates its role in stress granule formation. *Mol. Biol. Cell.* 2019; 30: 778–793.

19. Szewczyk MM, Ishikawa Y, Organ S, Sakai N, Li F, Halabelian L, et al. Pharmacological inhibition of PRMT7 links arginine monomethylation to the cellular stress response. *Nat. Commun.* 2020; 11: 2396. https://doi.org/10.1038/s41467-020-16271-z PMID: 32409666

20. Jelenic P, Stehle JC, and Shaw P. The Testis-Specific Factor CTCFL Cooperates with the Protein Methyltransferase PRMT7 in *H19* Imprinting Control Region Methylation. *PLOS Biol.* 2006; 4: e355.

21. Miranda TB, Miranda M, Frankel A, and Clarke S. PRMT7 Is a Member of the Protein Arginine Methyl-transferase Family with a Distinct Substrate Specificity. *J. Biol. Chem.* 2004; 279: 22902–22907. https://doi.org/10.1074/jbc.M312904200 PMID: 15044439

22. Macadangdang BR, Oberai A, Spektor T, Campos OA, Sheng F, Carey MF, et al. Evolution of histone 2A for chromatin compaction in eukaryotes. *Elife* 2014; 3: e02792. https://doi.org/10.7554/eLife.02792 PMID: 24939988

23. Maguire ME and Cowan JA. Magnesium chemistry and biochemistry. *BioMetals* 2002; 15: 203–210. https://doi.org/10.1023/a:1016058229972 PMID: 12206387

24. Liu B, Poolman B, and Boersma AJ. Ionic Strength Sensing in Living Cells. *ACS Chem. Biol.* 2017; 12: 2510–2514. https://doi.org/10.1021/acschembio.7b00348 PMID: 28853549

25. Price OM and Hevel JM. Toward Understanding Molecular Recognition between PRMTs and their Sub-strates. *Current Protein and Peptide Science* 2020; 21: 713–724. https://doi.org/10.2174/1389203721666200124143145 PMID: 31976831

26. Gary JD, Lin WJ, Yang MC, Herschman HR, and Clarke S. The Predominant Protein-arginine Methyl-transferase from *Saccharomyces cerevisiae*. *J. Biol. Chem.* 1996; 271: 12585–12594.

27. Gary JD and Clarke S. RNA and Protein Interactions Modulated by Protein Arginine Methylation. In: Moldave K, editor. *Progress in Nucleic Acid Research and Molecular Biology.* San Diego: Academic Press; 1998. Vol. 61, pp. 65–131.

46

28. Kim S, Merrill BM, Rajpurohit R, Kumar A, Stone KL, Papov VV, et al. Identification of N^G-Methylarginine Residues in Human Heterogenous RNP Protein A1: Phe/Gly-Gly-Gly-Arg-Gly-Gly-Gly/Phe Is a Preferred Recognition Motif. *Biochemistry* 1997; 36: 5185–5192.

29. Haghandish N and Côté J. The Role of Histone Mark Writers in Chromatin Signaling: Protein Arginine Methyltransferases. In: Binda O and Fernandez-Zapico ME, editors. *Chromatin Signaling and Diseases*. London: Academic Press; 2016. pp. 55–74.

30. Wooderchak WL, Zang T, Zhou ZS, Acuña M, Tahara SM, and Hevel JM. Substrate Profiling of PRMT1 Reveals Amino Acid Sequences That Extend Beyond the "RGG" Paradigm. *Biochemistry* 2008; 47: 9456–9466. https://doi.org/10.1021/bi800984s PMID: 18700728

31. Thiebaut C, Eve L, Poulard C, and Le Romancer M. Structure, Activity, and Function of PRMT1. *Life* 2021; 11: 1147. https://doi.org/10.3390/life11111147 PMID: 34833023

32. Waldmann T, Izzo A, Kamieniarz K, Richter F, Vogler C, Sarg B, et al. Methylation of H2AR29 is a novel repressive PRMT6 target. *Epigenetics & Chromatin* 2011; 4: 11. https://doi.org/10.1186/1756-8935-4-11 PMID: 21774791

33. Wang H, Huang ZQ, Xia L, Feng Q, Erdjument-Bromage H, Strahl BD, et al. Methylation of Histone H4 at Arginine 3 Facilitating Transcriptional Activation by Nuclear Hormone Receptor. *Science* 2001; 293: 853–857. https://doi.org/10.1126/science.1060781 PMID: 11387442

34. Mulvaney KM, Blomquist C, Acharya N, Li R, Ranaghan MJ, O'Keefe M, et al. Molecular basis for substrate recruitment to the PRMT5 methylosome. *Mol. Cell.* 2021; 81:3481–3495.e7. https://doi.org/10.1016/j.molcel.2021.07.019 PMID: 34358446

35. Cáceres TB, Thakur A, Price OM, Ippolito N, Li J, Qu J, et al. Phe71 in Type III Trypanosomal Protein Arginine Methyltransferase 7 (TbPRMT7) Restricts the Enzyme to Monomethylation. *Biochemistry* 2018; 57: 1349–1359. https://doi.org/10.1021/acs.biochem.7b01265 PMID: 29378138

36. Debler EW, Jain K, Warmack RA, Feng Y, Clarke SG, Blobel G, et al. A glutamate/aspartate switch controls product specificity in a protein arginine methyltransferase. *Proc. Natl. Acad. Sci. USA.* 2016; 113: 2068–2073. https://doi.org/10.1073/pnas.1525783113 PMID: 26858449

37. Hadjikyriacou A, Yang Y, Espejo A, Bedford MT, and Clarke SG. Unique Features of Human Protein Arginine Methyltransferase 9 (PRMT9) and Its Substrate RNA Splicing Factor SF3B2. *J. Biol. Chem.* 2015; 290: 16723–16743. https://doi.org/10.1074/jbc.M115.659433 PMID: 25979344

38. Li A, Li F, Eram MS, Bolotokova A, Dela Seña CC, and Vedadi M. Chemical probes for protein arginine methyltransferases. *Methods* 2020; 175: 30–43. https://doi.org/10.1016/j.ymeth.2019.11.017 PMID: 31809836

39. Mendoza M, Mendoza M, Lubrino T, Briski S, Osuji I, Cuala J, et al. Arginine Methylation of the PGC-1α C-Terminus Is Temperature-Dependent. *Biochemistry* 2023; 62: 22–34.

40. Halabelian L and Barsyte-Lovejoy D. Structure and Function of Protein Arginine Methyltransferase PRMT7. *Life* 2021; 11: 768. https://doi.org/10.3390/life11080768 PMID: 34440512

41. Cao Y, Fang Y, Mu J, and Liu X. High salt medium activates RhoA/ROCK and downregulates eNOS expression via the upregulation of ADMA. *Molecular Medicine Reports* 2016; 14: 606–612. https://doi.org/10.3892/mmr.2016.5241 PMID: 27175806

42. Tan X, Li JK, Sun JC, Jiao PL, Wang YK, Wu ZT, et al. The asymmetric dimethylarginine-mediated inhibition of nitric oxide in the rostral ventrolateral medulla contributes to regulation of blood pressure in hypertensive rats. *Nitric Oxide* 2017; 67: 58–67. https://doi.org/10.1016/j.niox.2017.04.002 PMID: 28392446

43. Kawarazaki W and Fujita T. Role of Rho in Salt-Sensitive Hypertension. *Int. J. Mol. Sci.* 2021; 22: 2958. https://doi.org/10.3390/ijms22062958 PMID: 33803946

47

Chapter 4: Supporting information

The exquisite specificity of human protein arginine methyltransferase 7 (PRMT7) toward

Arg-X-Arg sites

Timothy J. Bondoc, Troy L. Lowe and Steven G. Clarke

List of material included:

Figure 1S: Original gel stained with Coomassie Blue from figure 2.

Figure 2S: Original 3H fluorograph 1-day exposure film from figure 2.

Figure 3S: Original 3H fluorograph 74-day exposure film from figure 2.
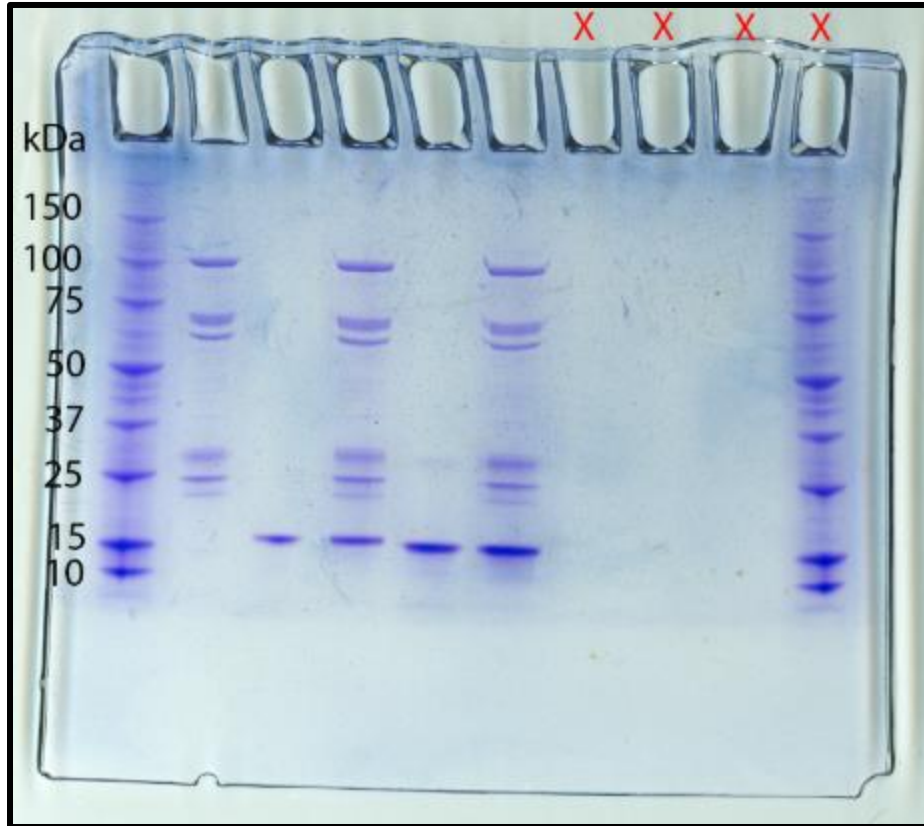
Figure S1: Original gel stained with Coomassie Blue from figure 2. Lane 1: Protein ladder only. Lane 2: 5 μg GST-HsPRMT7. Lane 3: 1 μg full-length human histone H2B. Lane 4: 5 μg GST-HsPRMT7 with 1 μg full-length human histone H2B. Lane 5: 3 μg full-length Xenopus laevis histone H2B. Lane 6: 5 μg GST-HsPRMT7 with 3 μg full-length Xenopus laevis histone H2B. Red (X) lanes were cropped out of figure for presentation purposes and contained either no protein or a duplicate lane 1 protein ladder only.

Figure S2: Original 3H fluorograph 1-day exposure film from figure 2. Autoradiograph scanned backwards of figure S1. Lane 1 labeled L: Ladder. Lane 2 labelled E: 5 µg GST-HsPRMT7. Lane 3 labeled S(Hs): 1 µg full-length human histone H2B. Lane 4 labeled ES (Hs): 5 µg GST-HsPRMT7 with 1 µg full-length human histone H2B. Lane 5: 3 µg full-length Xenopus laevis histone H2B. Lane 6: 5 µg GST-HsPRMT7 with 3 µg full-length Xenopus laevis histone H2B. Red (X) lanes were cropped out of figure for presentation purposes and contained either no protein or a duplicate lane 1 protein ladder only.
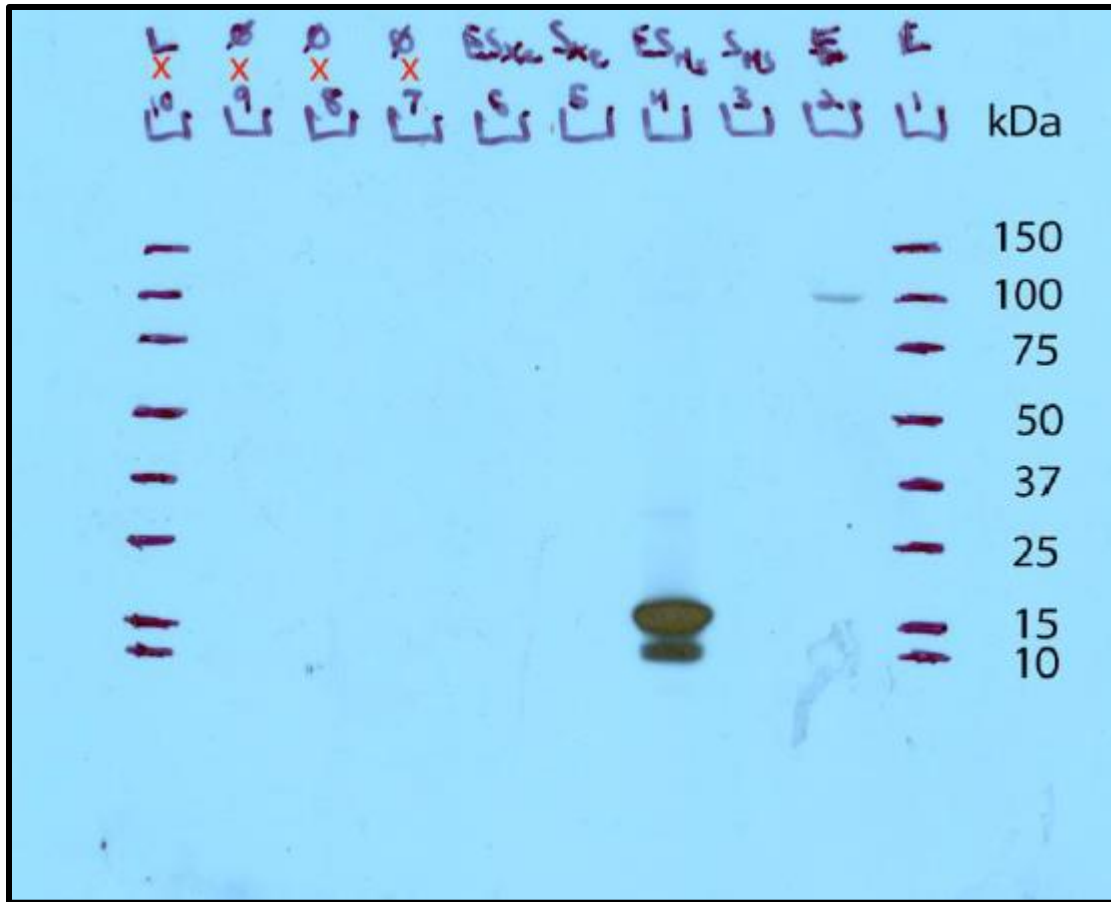
Figure S3: Original 3H fluorograph 74-day exposure film from figure 2. Autoradiograph scanned backwards of figure S1. Lane 1 labeled L: Ladder. Lane 2 labelled E: 5 µg GST-HsPRMT7. Lane 3 labeled S(Hs): 1 µg full-length human histone H2B. Lane 4 labeled ES (Hs): 5 µg GST-HsPRMT7 with 1 µg full-length human histone H2B. Lane 5: 3 µg full-length Xenopus laevis histone H2B. Lane 6: 5 µg GST-HsPRMT7 with 3 µg full-length Xenopus laevis histone H2B. Red (X) lanes were cropped out of figure for presentation purposes and contained either no protein or a duplicate lane 1 protein ladder only. It is noted that the 100 kDa band in land 2 was not included in figure 2.

Chapter 5

Methylation and phosphorylation of formin homology domain proteins (Fhod1 and Fhod3) by protein arginine methyltransferase 7 (PRMT7) and Rho Kinase (ROCK1)

The work described in this chapter is from a manuscript submitted to the Journal of Biological Chemistry, *currently in review*.

Troy L. Lowe, Dylan A. Valencia, Vicente E. Velasquez, Margot E. Quinlan, and Steven G. Clarke

Significance Statement

The idea of the histone code revolves around the idea that specific modifications and combinations of modifications govern biological processes. While combinations of histone modifications, including phosphorylation, acetylation and methylation can work in concert to regulate transcriptional activation and repression, there are fewer examples with non-histone proteins. In this chapter we examine how combinations of phosphorylation and methylation may affect the function of two actin binding proteins Fhod1 and Fhod3.

In this study we deviate from the idea of histones as substrates for PRMTs, and look toward an idea that PRMT7 can recognize RXR motifs and in particular proteins that have similarities to the histone H2B sequence. In theory the same sequence in human histone H2B should be recognized by PRMT7, RKRSR, and the sequence is present in both Fhod1 and Fhod3. This may not be the case as other factors like secondary structure may have a huge influence in

substrate recognition as well as additional modifications. In our particular case we were fortunate to identify the formin homology domain containing proteins (Fhods) as substrates. We identified that these proteins might be novel in vivo substrates for PRMT7 based on cellular localization. However, while our *in vitro* data shows strong evidence of a specific PRMT7 substrate, reconstitution in an *in vivo* system remains unknown. Additionally, this study demonstrates the effects of phosphorylation on methylation, and vice versa.

Attention on how the methylation of Fhods in an *in vivo* system should be monitored for future work on the importance of arginine methylation.

Abstract

Protein post translational modifications (PTMs) can regulate biological processes by altering an amino acid's bulkiness, charge, and hydrogen bonding interactions. Common modifications include phosphorylation, methylation, acetylation and ubiquitylation. Although a primary focus of studying PTMs is understanding the effects of a single amino acid modification, the possibility of additional modifications increases the complexity. For example, substrate recognition motifs for arginine methyltransferases and some serine/threonine kinases overlap, leading to potential enzymatic crosstalk. In this study we have shown that the human family of formin homology domain containing proteins (Fhods) contain a substrate recognition motif specific for human protein arginine methyltransferase 7 (PRMT7). In particular, PRMT7 methylates two arginine residues in the diaphanous autoinhibitory domain (DAD) of the family of Fhod proteins: R1588 and/or R1590 of Fhod3 isoform 4. Additionally, we confirmed that S1589 and S1595 in the DAD domain of Fhod3 can be phosphorylated by Rho/ROCK1 kinase. Significantly, we have determined that if S1589 is phosphorylated then PRMT7 cannot subsequently methylate R1588 or R1590. However, if phosphoserine 1595 is present then PRMT7 is mildly inhibited, but can still methylate R1588 and R1590. Conversely, if R1588 or R1590 of Fhod3 is methylated then ROCK1

phosphorylation activity is slightly affected. Taken together these results suggest that the family of Fhod proteins, a potential *in vivo* substrate for PRMT7, might be regulated by a combination of methylation and phosphorylation.

Introduction

Protein post translational modifications enhance biological diversity. Although a generalized consensus of these individual modifications has been proposed, knowledge about the interplay of multiple modifications on biological function is lacking. However, distinct modifications often occur in close proximity on target substrates, creating potential cross-talk in regulatory pathways. Cross-talk may result from binding competition between enzymes or changes in the recognition motif. In particular, histones and transcription factors are known to display a plethora of modifications ultimately leading to the translational regulation of specific genes. For example, the recruitment of TATA binding proteins (TBPs) and associated factors (TAFs) to the transcriptional start site of some eukaryotic organisms results in the signaling for polymerase II (1). While phosphorylation is the most dominant modification on TBPs and TAFs (2), additional modifications like acetyllysine (3) and methylarginine (4) are also present.

One modification, protein arginine methylation, is catalyzed by a family of nine enzymes in mammals; whether protein arginine demethylases are involved *in vivo* has not been fully resolved (5,6). Methylation occurs on the guanidino side chains of arginine residues, altering charge, increasing the number of potential hydrogen bond donors (7,8) and creating a bulkier side chain (9). PRMT1-4, 6, and 8 are known as type I PRMTs that catalyze asymmetric dimethylarginine (10), PRMT5 and PRMT9 are considered type II that catalyze symmetric dimethylarginine (11), and PRMT7 is the only type III PRMT exclusively catalyzing monomethylarginine (12). While most of the PRMTs recognize substrates containing arginine and

glycine rich motifs (GARs), PRMT4 prefers proline and glycine motifs, and PRMT7 prefers arginine-x-arginine motifs (RXR) (13,14).

Protein phosphorylation is catalyzed by kinases and to date there are an estimated 538 protein kinase encoding genes (15). These protein kinases are classified into eight groups depending on their substrate recognition. In particular, the AKT kinases that phosphorylate serine and threonine residues are known to have a recognition motif sequence of RxRxxS/T and are known to regulate many biological processes including the MAPK pathway and WNT signaling pathway (16). Because PRMT7 and the AKT kinases have overlapping substrate recognition motifs, one might expect some overlap of protein modifications, leading to crosstalk and allosteric regulations. In *Saccharomyces cerevisiae*, proteins Npl3, Ded1, and Sbp1 have been identified to have arginine methylation and phosphorylation co-occur in regions that are highly disordered (17).

PRMT7 has been implicated in many biological processes including the epithelial to mesenchymal transition in breast cancer (18), the regulation of inflammation through the NF-κB pathway in chronic obstructive pulmonary disease patients (19), and the maintenance of stem cells during development (20). To date, 51 patients have been documented to have homozygous or compound heterozygous mutations in the PRMT7 gene, leading to a variety of phenotypes due to the presumed absence of enzyme activity (21,22). These phenotypes are classified as short stature, brachydactyly, intellectual developmental disability, seizures, and hypotonia (23). Additionally, PRMT7 appears to have a major role in skeletal muscle maintenance and formation (24-26).

Actin is one of the most ubiquitous proteins in eukaryotic cells. It is a fundamental element of muscle and plays an important role in cellular architecture and movement (27). Actin nucleators aid in the assembly of actin filaments and are categorized into three classes, Arp2/3 complex, formins, and tandem WASP homology 2 (WH2) (28). In humans,15 genes encode the family of formin proteins and mutations of some of these genes have been linked to cancer, intellectual

disability, and developmental defects of the heart (28,29). All formins contain core formin homology domains unique to the class, FH1 and FH2, (30,31) and sequence similarity can vary between 20-60%, thus creating subclasses. One subfamily of formins, the Formin Homology Domain-containing proteins (Fhods) consist of two proteins in humans, Fhod1 and Fhod3. Fhod1 is highly expressed in many cells, including spleen (32) and skeletal muscle (33). It is found in multiple structures including stress fibers (34), transmembrane actin-associated nuclear (TAN) lines (35), and is linked to a range of diseases (29,36). Fhod3 is mainly expressed in cardiac muscle (37). It is located in the contractile structures, sarcomeres (38,39), and linked to both dilated and hypertrophic cardiomyopathies (40).

In this paper we show that Fhod1 and Fhod3 proteins are newly identified substrates for PRMT7 and that the phosphorylation of nearby serine residues can inhibit the methylation reactions. Additionally, we observed that methylation of an arginine residue in proximity to a phosphorylatable serine has a mild inhibitory effect on ROCK1 kinase.

Results

Human Fhod1 and Fhod3 contain a recognition sequence for PRMT7 similar to human histone H2B.

Human histone H2B has been identified as a particularly effective substrate for PRMT7 methylation (14). Specifically, the arginine residues in the RKRSR motif at residues 29-33 has been identified as PRMT7 targets and the methylation efficiency of this motif is highly dependent upon its sequence (13). To identify additional proteins that may be substrates for PRMT7, we performed a peptide search for human proteins containing an RKRSR motif (Table S1). Based on the apparent importance of PRMT7 in muscle organization (26,41), we narrowed our search to four proteins classified in the "cytoskeleton organization" gene ontology group (Table 1). Since

56

PRMT7 primarily localizes in the cytoplasm (42,43), we further focused our attention on the two proteins that were mainly located in the cytoplasm, FH1/FH2 domain-containing protein 1 and 3.

Table 1: Human cytoskeletal organization proteins containing the specific RKRSR sequence.

Accession	Entry Name	Protein name	Localization	Gene Ontology
O75400	PR40A	Pre-mRNA-processing factor 40 homolog A	Nucleus	Cytoskeleton Organization
P18583	SON	Protein SON	Nucleus	Microtubule Cytoskeleton Organization
Q2V2M9	Fhod3	FH1/FH2 domain-containing protein 3	Cytoplasm	Cortical Actin Cytoskeleton Organization
Q9Y613	Fhod1	FH1/FH2 domain-containing protein 1	Cytoplasm	Cortical Actin Cytoskeleton Organization

The C-terminus of human Fhod1 and Fhod3 are methylated by human PRMT7.

Fhod1 and Fhod3 contain four conserved domains, a diaphanous inhibitory domain (DID), formin homology domains 1 (FH1) and 2 (FH2), and a diaphanous autoregulatory domain (DAD) (Fig. 1A). The latter three domains compose the C-terminal half of the protein, with 52% amino acid identity between Fhod1 and Fhod3 (Fig. 1B). The RKRSR motif is present in the DAD region near the C-terminus. To determine if human Fhod1 and Fhod3 DAD domains can be methylated

by PRMT7, we performed *in vitro* methylation assays. We found that the constructs including the DAD domain of Fhod1 and Fhod3 were, in fact, substrates for PRMT7 (Fig. 1C).

There is an additional sequence in the C-terminal domain of Fhod3 (RTRSR) that closely matches the RKRSR motif of human histone H2B and Fhod1 that may be a methylation site. To determine the localization of PRMT7 methylation site(s), we made mutations where we replaced arginine residues with lysine residues to remove the RXR motif. When we mutated the RTRSR motif to RTKSR we found no loss of methylation, suggesting that this site was not a substrate for PRMT7. On the other hand, when we mutated the RKRSR motif to KKKSR we found that the protein was no longer a substrate for PRMT7. In this case we mutated both of the initial arginine residues because the sequence immediately preceding the motif (RE) might have generated an additional RXR sequence. These results provided evidence that the major sites of arginine methylation reside in the RKRSR sequence exclusively within the DAD domain of Fhod3 (Fig. 2).

Arginine residues at positions 1588 and 1590 of HsFhod3 isoform 4 are major methylation sites for PRMT7 catalysis.

We next identified the specific arginine residues methylated within the canonical Fhod3 target sequence. In the histone H2B RKRSR sequence, all three arginine residues were found to be methylated by PRMT7 through the use of mass spectrometry (14). Evidence was presented that the major activity occurred at the first two arginines in the RKRSR motif, R29 and R31 (14). While both Fhod1 and Fhod3 contained the RKRSR sequence, an additional RXR is present due to the preceding RE amino acids creating a RERKRSR motif (residues 1584-1590) potentially creating 4 arginines that can be methylated by PRMT7. We decided to perform mutagenesis of this region to identify which arginine residues are methylated by PRMT7. Upon performing *in vitro* methylation reactions with the MBP-Fhod3 (1472-1622) R1584K, R1586K, R1588K, and R1590K constructs, we were only able to observe methylation of the R1584K and R1586K constructs,

demonstrating that these two residues are not required for methylation and that both R1588 and R1590 are required (Fig. 3). Because R1588 and R1590 straddle a single RXR motif, we interpret these findings as evidence that one or both of these positions are the major sites of methylation. Interestingly, in the histone H2B sequence the first two arginines are preferentially methylated while in the Fhod3 sequence it is the latter two that are PRMT7 substrates.

Phosphoserine 1589 inhibits methylation by PRMT7, while phosphoserine 1595 only mildly inhibits PRMT7 activity.

It has been established that phosphorylation of Fhod3 at serine 1589 by either ROCK1 or ROCK2 kinase regulates the activity of this protein by alleviating its autoinhibition (44,45). Since we found that the two arginine residues directly adjacent to this serine residue are sites of PRMT7 modification, we asked how phosphorylation of S1589 impacts methylation of R1588 and R1590. Significantly, we found that phosphorylation of a synthetic peptide containing S1589 resulted in little or no methylation by PRMT7 (Fig. 4). On the other hand, phosphorylation of a downstream serine residue at position 1595 decreases the Km four-fold without making a significant change to the Kcat. These results demonstrate that phosphoserine in close proximity to the RXR PRMT7 substrate recognition site inhibits enzyme activity.

Phosphoserine 32 of human histone H2B abolishes PRMT7 activity, while phosphoserine 36 inhibits PRMT7 activity.

The dramatic inhibition of PRMT7 activity by an adjacent phosphoserine residue seen with the Fhod3 peptide led us to ask if a similar effect is seen with the complementary motif of the H2B peptide. In yeast histone H2B, residues 30 to 37 comprise a repressive domain (46,47). Additionally, methylatable arginine residues 31 and 33 flank serine 32 which is known to be

59

phosphorylated by RSK2 (48) and by Aurora B kinase (49). Furthermore, the downstream serine 36 residue can be phosphorylated by S6K1 (50) and AMPK (51). While serine 36 is conserved in higher organisms, serine 32 is only present in mammals and amphibians (Fig. 5). Upon performing *in vitro* methylation assays with PRMT7 and human histone H2B (23-37) synthetic peptides containing either a phosphoserine at position 32 or 36, we observed little to no methylation of the H2B (23-37) peptide containing a phosphoserine at position 32 while the peptide containing a phosphoserine at position 36 had a decreased amount of methylation compared to the wild type (Fig. 6). These results demonstrate that PRMT7 activity inhibition increases as the phosphoserine gets closer to the arginine recognition sequence in Histone H2B, and corroborate the results seen with Fhod3.

Methylarginine 1588 or 1590 minimally affects the phosphorylation of Fhod by ROCK1 in a peptide containing serine 1589 and/or 1595.

Since we found that phosphorylation of the serine residue in the RSR methylation motif resulted in the loss of PRMT7 methylation, we then asked whether methylation of these arginine residues affects phosphorylation of the serine residue. Phosphorylation of serine 1589 and 1595 in the RSR motif of the DAD domain of Fhod1/3 by ROCK1/2 is sufficient to relieve autoinhibition, which then activates actin nucleation (44,45). While the previous ROCK1 phosphorylation studies have been performed both *in vivo* and on truncated C-terminal tail constructs, we first wanted to establish whether ROCK1 could recognize a serine residue in a peptide substrate that we could prepare in methylated and unmethylated forms (45). We thus compared the extent of phosphorylation of Fhod3 peptides containing residues 1581-1595 (VVPRERKRSRANRKS) with ROCK1 in *in vitro* time course assays, for up to 2 hours, analyzed by LC/MS (Fig. 7). We found clear evidence for phosphorylation of the unmethylated peptide and peptides with either a monomethylarginine at positions 1588, 1590, or both. In contrast to the effect of serine

phosphorylation on arginine methylation, we observed no significant decrease in phosphorylation (Fig. 7). These results suggest that methylation of adjacent arginine residues has little effect on ROCK1 phosphorylation, but further work will be needed to validate this.

In the experiment shown in figure 7, we only detected monophosphorylated forms even after 2 h of incubation. We then decided to increase the incubation time in hopes of capturing a diphosphorylated peptide Fhod3. In a 5 h incubation we found that similar amounts of monophosphorylated and diphosphorylated peptides were formed with the unmethylated peptide, the 1588 monomethylated peptide, the 1590 monomethylated peptide, and 1588 and 1590 monomethylated peptide (Fig. S1-S4). These results confirm the general lack of effect of methylation on phosphorylation.

To observe the effect of arginine methylation on the serine residue between the two arginine residues, we designed peptides containing only the Fhod3 sequence 1581-1594 (VVPRERKRSRANRK). In time course experiments with these peptides containing monomethylarginine residues at positions 1588, 1590, or at 1588 and 1590, we detected monophosphorylation at similar levels as the unmethylated peptide (Fig. 8).These results suggest that there is no major effect of methylation on ROCK1 phosphorylation of serine 1589. It is intriguing that phosphorylation has such a powerful negative affect on methylation whereas methylation appears to have a much more limited role on phosphorylation.

Discussion

Previous work has established that PRMT7 can be distinguished from the other members of the mammalian PRMT family both by its specificity for an arginine motif in proteins and by the fact that it is the sole PRMT that catalyzes monomethyl derivatives. This enzyme is characterized by its recognition of certain pairs of arginine residues separated by one residue, the RXR motif (14). A particular variant of this motif found in human histone H2B (RKRSR) has been shown to

be an excellent substrate (14). Searching for other proteins containing this motif identified the formin family of proteins as potential substrates.

In this study we have demonstrated that the family of formin homology domain containing proteins are methylated by PRMT7. Specifically, Fhod1 and Fhod3, are methylated at the RKRSR sequence occurring at residues 1128-1132 in Fhod1 isoform 1 and 1586-1590 in Fhod3 isoform 4, which is identical to the recognition motif in histone H2B. Despite the common sequence we found that different arginines were preferentially methylated in histone H2B and Fhod3. Further, we noted that neither RTRSR nor RERKR were targets for PRMT7. Together these results suggest that additional motif elements beyond the RXR motif contribute to PRMT7 recognition and methylation. We highlight in Table S1 additional proteins with the RKRSR motif. It is noteworthy that none of these proteins have been identified to date in proteomic studies (52).

Methylarginines are known to occur in protein domains enriched with positively charged residues and low structural complexity seen in intrinsically disordered regions (53). The N-terminal regions of histones are highly disordered unless in contact with supercoiled DNA (54). Additionally, another identified substrate for PRMT7, the Peroxisome proliferator-activated receptor gamma (PPARγ) coactivator-1 alpha (PGC-1α), is intrinsically disordered (55). Therefore, we asked if the same is likely to be true for the C-terminal tail of Fhod3. Many if not all formin tails are disordered (56-58). In fact, AlphaFold structural predictions return a folded FH2 domain, as expected, and suggest that the RKRSR sequence in Fhod3 is in a disordered region.

There have been several studies that have demonstrated inhibition of PRMT methylation by adjacent or nearby phosphoserine residues. In histone H3, serine-10 is known to be phosphorylated by a variety of kinases (59) and arginine-8 is methylated by PRMTs (60). However, if serine-10 is phosphorylated, then PRMT1, PRMT4 or PRMT5 catalyzed methylation of arginine-8 is completely inhibited (61). In histones H2A and H4, serine phosphorylation at positions 1 and 4 partially inhibit methylation of arginine-3 by PRMT5 (62,63). We now extend

these observations by showing that PRMT7 methylation is inhibited by a phosphorylated serine in both Fhod3 and histone H2B.

There have been two studies that demonstrate the effect of protein arginine methylation on phosphorylation. For example, methylation of arginine-1199 in the epidermal growth factor receptor stimulates the autophosphorylation of tyrosine-1197 (64). In another study, methylation of CIRBP by PRMT1 reduces the amount of phosphorylation at nearby sites by SRPK1 (65). In contrast, phosphorylation of the PRMT7 methylated site in Fhod3 was minimally impacted. Perhaps a monomethyl group is insufficient to inhibit kinases or the specific kinase is more robust.

The significant inhibitory effect of phosphoserine residues on methylation of nearby arginine residues may be explained on a molecular basis by salt bridges between the positively charged and negatively charged side chains that stabilize proteins (66). Specifically, when a phosphoserine is in close proximity to arginine, the negatively charged oxygens on the phosphate group lead to non-covalent interactions with the positively charged nitrogen atoms of the arginine guanidino group (61).

Interestingly, the inhibition of methylation by phosphorylation may represent a mechanism that can be seen to parallel direct enzymatic demethylation of arginine residues. There is no clear consensus on the existence of protein arginine demethylases but JMJD6, or Jumonji domain containing 6 protein has been proposed as such an enzyme (67). JMJD6 has also been characterized as a lysine hydroxylase (68). However, MALDI-TOF experiments have shown the reduction of 14 kDa or 28 kDa of a monomethylated or dimethylated arginine peptide with the addition of the JMJD6 enzyme (69). Another proposed mechanism of arginine demethylation utilizes the protein arginine deiminase 4 enzyme, PAD4. While the function of this enzyme has been shown to catalyze citrulline from arginine, *in vitro* studies have shown that catalysis of PAD4 on methylarginine histones resulted in methylamine formation (70). However, the rates of demodification of methylarginine by PAD4 were slower in comparison to the formation of

63

methylarginines by PRMTs (71). Thus, inhibition of methylation may be an important way to regulate PRMTs.

While we still lack an understanding of how PRMT7 is regulated *in vivo*, our findings of the crosstalk interactions with Fhod methylation and phosphorylation do suggest a possible regulatory mechanism for formin-mediated actin polymerization. It will be intriguing to learn how the known regulation of PRMT7 by low temperature, a low ionic strength environment, and alkaline conditions (72) may contribute to the physiological process of actin polymerization.

Experimental Procedures

Plasmids and Constructs

Recombinant *H. sapiens* GST-PRMT7 was grown and purified as described (72).

Mammalian Fhod3 C-terminal (963-1622), and Fhod1-tail (1110-1164) constructs were cloned into modified pGEX plasmids with a maltose binding protein (MBP) tag. MBP tagged Fhod3 tail (1472-1622) was cloned via FastCloning using pMAL-Fhod3 wild-type (963-1622) as a template (73). Point mutations of Fhod3-tail (1472-1622) were generated by site-directed mutagenesis as described (74).

Growth and Purification

All Fhod3 constructs were transformed in Rosetta 2 (DE3) cells (Novagen) and grown in 1 L of Terrific Broth supplemented with 100 mg/liter ampicillin and 32 mg/liter chloramphenicol. Expression was induced at OD 0.6-0.8 with 0.5 mM isopropyl-ß-D-1-thiogalactopyranoside (IPTG) and allowed to shake overnight at 18°C, 210 rpm. Cells were harvested by centrifugation at 6,000

x g for 10 minutes, washed in 1X phosphate buffer saline (PBS) containing 1 mM dithiothreitol (DTT), and flash frozen in liquid nitrogen. Cell pellets expressing the MBP-Fhod3 were thawed and resuspended in 20 mM Tris, 200 mM NaCl, 1 mM EDTA, 1 mM DTT, 2 µg/mL DNaseI, 1 mM PMSF, pH 7.5. All subsequent steps were performed on ice or at 4 °C. The cells were lysed by microfluidization (3x) centrifuged at 20,000 x g for 20 minutes. Lysate was incubated with amylose resin (New England Biolabs) for 1 hour at 4 °C. Resin was washed with extraction buffer (20 mM Tris, 200 mM NaCl, 1 mM EDTA, 1 mM DTT, pH 7.5). Protein was eluted using elution buffer (20 mM Tris, 200 mM NaCl, 1 mM EDTA, 1 mM DTT, 10 mM maltose), flash frozen in liquid nitrogen, and stored at -80˚C. MBP-Fhod1 was grown and purified similarly.

Peptide Substrates

Table 2: Arginine Methylation P81 Peptides

Peptide Name	Peptide Sequence	Purity (%)	Theoretical MW
H2B (23-37) WT	Ac-KKDGKKRKRSRKESY-NH$_2$	87.8	1935.25
H2B (23-37) *po*S32	KKDGKKRKR{*po*SER}RKESY	91.0	1974.18
H2B (23-37) *po*S36	KKDGKKRKRSRKE{*po*SER}Y	88.3	1974.18
Fhod3 (1581-1595) WT	VVPRERKRSRANRKSY	98.2	2002.3
Fhod3 (1581-1595) *po*S1589	VVPRERKR{*po*SER}RANRKSY	87.2	2082.28
Fhod3 (1581-1595) *po*S1595	VVPRERKRSRANRK{*po*SER}Y	96.9	2082.28

All peptides were purchased from GenScript. Trifluoroacetic acid removal was performed by company and switched with a standard acetate salt. A tyrosine residue was added at the C-terminus of each Fhod peptide to determine the concentration of the peptide by UV spectra.

Table 3: Serine Phosphorylation Mass Spectrometry Peptides

Peptide Name	Peptide Sequence	Purity (%)	Theoretical MW
Fhod3 (1581-1594) WT	Ac-VVPRERKRSRANRKY-NH$_2$	88.4	1956.33
Fhod3 (1581-1594) R1588Me1	Ac-VVPRERK{RMe1}SRANRKY-NH$_2$	87.2	1970.33
Fhod3 (1581-1594) R1590Me1	Ac-VVPRERKRS{RMe1}ANRKY-NH$_2$	96.9	1970.33
Fhod3 (1581-1594) R1588Me1/R1590Me1	Ac-VVPRERK{RMe1}S{RMe1}ANRKY-NH$_2$	99.1	1984.38
Fhod3 (1581-1595) WT	Ac-VVPRERKRSRANRKSY-NH$_2$	97.6	2043.35
Fhod3 (1581-1595) R1588Me1	Ac-VVPRERK{RMe1}SRANRKSY-NH$_2$	97.6	2057.40
Fhod3 (1581-1595) R1590Me1	Ac-VVPRERKRS{RMe1}ANRKSY-NH$_2$	99.1	2057.40
Fhod3 (1581-1595) R1588Me1/R1590Me1	Ac-VVPRERK{RMe1}S{RMe1}ANRKSY-NH$_2$	94.1	2071.46

All peptides were purchased from GenScript. Trifluoroacetic acid removal was performed by company and switched with a standard acetate salt. A tyrosine residue was added at the C-terminus of each Fhod peptide to determine the concentration of the peptide by UV spectra.

Radioactive Methylation Assay

Gel assays of GST-HsPRMT7, MBP-Fhod1-tail (1110-1164), Fhod3-CT (963-1622), MBP-Fhod3-tail (1472-1622) wild-type and MBP-Fhod3-tail (1472-1622) arginine to lysine mutations were performed as previously described (72).

In Vitro ROCK1 Kinase Assay

N-terminal 6xHis-tagged recombinant human ROKβ/ROCK-I (17-535) was purchased from Eurofins Discoverx (catalog No. 14-601). Kinase reactions were carried out in a reaction buffer containing 8 mM K-HEPES, 200 µM EDTA supplemented with an ATP cocktail mixture of 8 mM MgAc·6H2O and 80 µM ATP. Reactions were allowed to incubate in a 30 °C water bath for the times listed and terminated with 0.5 µL of 100% trifluoroacetic acid.

Mass Spectrometry

In vitro ROCK1 kinase reactions were injected into an Agilent MS Q-TOF model G6545B with a Dual AJS ESI ion source. Scan segments were collected in positive mode with a MS absolute threshold of 200 (0.010% relative threshold), and a MS/MS absolute threshold of 5 (0.010% relative threshold). Sampler auxiliary draw speed was 200 µL/min and an eject speed of 400 µL/min. Binary pump, model G7112B, flow rate was set at 0.800 mL/min with a low-pressure limit of 0.00 bar, and a high-pressure limit of 400.0 bar. The maximum flow gradient was 100.000 mL/min^2 with a stop time of 12.0 min and a post time of 3.0 min. Mobile phase solvent A contained 0.1% FA in water and solvent B contained 0.1% FA in acetonitrile. The first 2 minutes contained 99% solvent A and 1% solvent B then 5% solvent A and 95% solvent B for the remainder of the run. Column composition, model G7116A, temperature was set to 40 °C. Both left and right

temperature control analysis were enabled and set to 0.8 °C with an equilibration temperature time of 0.0 min. DAD, model G7115A, contained a peak width of >0.1 min (2 s response time, 2.5 Hz) with a slit of 4 nm. The analog output was offset by 5% with an attenuation of 1000 mAU and the margin for negative absorbance set to 100 mAU. The spectrum range was from 190 nm to 650 nm with a spectrum step of 2.0 nm.

P81 Methylation Assay

P81 assay of GST-PRMT7, phosphoserine Fhod peptides, and phosphoserine H2B peptides were performed as previously described (72).

Statistical Analysis

Michaelis Menten non-linear regression was performed using GraphPad Prism version 5.01 for Windows, GraphPad Software, San Diego California USA, www.graphpad.com. No constraint was applied to the Vmax while the Km was constrained to a value greater than 0.0. No weighting method was applied and each replicate Y value was considered as an individual point.

Data Availability

All mass spectrometry raw files have been deposited in the MassIVE repository housed at UCSD (http://massive.ucsd.edu/) with the accession number MSV000094470 [http://doi.org/doi:10.25345/C5T14V12K]. FTP files can be directly downloaded from [ftp://massive.ucsd.edu/v07/MSV000094470/]. Additional data are available upon request.

References

1. Hampsey, M., and Reinberg, D. (1997) Transcription: why are TAFs essential? *Curr Biol.* 7, R44-46

2. Whitmarsh, A. J., and Davis, R. J. (2000) Regulation of transcription factor function by phosphorylation. *Cell Mol Life Sci.* 57, 1172–1183

3. Choudhary, C., Kumar, C., Gnad, F., Nielsen, M. L., Rehman, M., Walther, T. C., Olsen, J. V., and Mann, M. (2009) Lysine acetylation targets protein complexes and co-regulates major cellular functions. *Science.* 325, 834–840

4. Guo, A., Gu, H., Zhou, J., Mulhern, D., Wang, Y., Lee, K. A., Yang, V., Aguiar, M., Kornhauser, J., Jia, X., Ren, J., Beausoleil, S. A., Silva, J. C., Vemulapalli, V., Bedford, M. T., and Comb, M. J. (2014) Immunoaffinity enrichment and mass spectrometry analysis of protein methylation. *Mol Cell Proteomics.* 13, 372–387

5. Pham, H. Q. H., Tao, X., and Yang, Y. (2023) Protein arginine methylation in transcription and epigenetic regulation. *Front. Epigenet. Epigenom.* 10.3389/freae.2023.1245832

6. Fuhrmann, J., Clancy, K. W., and Thompson, P. R. (2015) Chemical biology of protein arginine modifications in epigenetic regulation. *Chem Rev*. 115, 5413–5461

7. Bedford, M. T., and Clarke, S. G. (2009) Protein Arginine Methylation in Mammals: Who, What, and Why. *Mol Cell*. 33, 1–13

8. Horowitz, S., and Trievel, R. C. (2012) Carbon-Oxygen Hydrogen Bonding in Biological Structure and Function. *J Biol Chem*. 287, 41576–41582

9. Evich, M., Stroeva, E., Zheng, Y. G., and Germann, M. W. (2016) Effect of methylation on the side-chain pKa value of arginine. *Protein Sci*. 25, 479–486

10. Eram, M. S., Shen, Y., Szewczyk, M., Wu, H., Senisterra, G., Li, F., Butler, K. V., Kaniskan, H. Ü., Speed, B. A., dela Seña, C., Dong, A., Zeng, H., Schapira, M., Brown, P. J., Arrowsmith, C. H., Barsyte-Lovejoy, D., Liu, J., Vedadi, M., and Jin, J. (2016) A Potent, Selective and Cell-active Inhibitor of Human Type I Protein Arginine Methyltransferases. *ACS Chem Biol*. 11, 772–781

11. Fulton, M. D., Brown, T., and Zheng, Y. G. (2018) Mechanisms and Inhibitors of Histone Arginine Methylation. *Chem Rec*. 18, 1792–1807

12. Zurita-Lopez, C. I., Sandberg, T., Kelly, R., and Clarke, S. G. (2012) Human protein arginine methyltransferase 7 (PRMT7) is a type III enzyme forming ω-NG-monomethylated arginine residues. *J Biol Chem*. 287, 7859–7870

13. Bondoc, T. J., Lowe, T. L., and Clarke, S. G. (2023) The exquisite specificity of human protein arginine methyltransferase 7 (PRMT7) toward Arg-X-Arg sites. *PLoS One*. 18, e0285812

14. Feng, Y., Maity, R., Whitelegge, J. P., Hadjikyriacou, A., Li, Z., Zurita-Lopez, C., Al-Hadid, Q., Clark, A. T., Bedford, M. T., Masson, J.-Y., and Clarke, S. G. (2013) Mammalian protein arginine methyltransferase 7 (PRMT7) specifically targets RXR sites in lysine- and arginine-rich regions. *J Biol Chem*. 288, 37010–37025

15. Bhullar, K. S., Lagarón, N. O., McGowan, E. M., Parmar, I., Jha, A., Hubbard, B. P., and Rupasinghe, H. P. V. (2018) Kinase-targeted cancer therapies: progress, challenges and future directions. *Mol Cancer*. 17, 48

16. McKenna, M., Balasuriya, N., Zhong, S., Li, S. S.-C., and O'Donoghue, P. (2020) Phospho-Form Specific Substrates of Protein Kinase B (AKT1). *Front Bioeng Biotechnol*. 8, 619252

17. Separovich, R. J., Wong, M. W. M., Chapman, T. R., Slavich, E., Hamey, J. J., and Wilkins, M. R. (2021) Post-translational modification analysis of Saccharomyces cerevisiae histone methylation enzymes reveals phosphorylation sites of regulatory potential. *J Biol Chem*. 296, 100192

18. Yao, R., Jiang, H., Ma, Y., Wang, L., Wang, L., Du, J., Hou, P., Gao, Y., Zhao, L., Wang, G., Zhang, Y., Liu, D.-X., Huang, B., and Lu, J. (2014) PRMT7 induces epithelial-to-mesenchymal transition and promotes metastasis in breast cancer. *Cancer Res*. 74, 5656–5667

19. Günes Günsel, G., Conlon, T. M., Jeridi, A., Kim, R., Ertüz, Z., Lang, N. J., Ansari, M., Novikova, M., Jiang, D., Strunz, M., Gaianova, M., Hollauer, C., Gabriel, C., Angelidis, I., Doll, S., Pestoni, J. C., Edelmann, S. L., Kohlhepp, M. S., Guillot, A., Bassler, K., Van Eeckhoutte, H. P., Kayalar, Ö., Konyalilar, N., Kanashova, T., Rodius, S., Ballester-López, C., Genes Robles, C. M., Smirnova, N., Rehberg, M., Agarwal, C., Krikki, I., Piavaux, B., Verleden, S. E., Vanaudenaerde, B., Königshoff, M., Dittmar, G., Bracke, K. R., Schultze, J. L., Watz, H., Eickelberg, O., Stoeger, T., Burgstaller, G., Tacke, F., Heissmeyer, V., Rinkevich, Y., Bayram, H., Schiller, H. B., Conrad, M., Schneider, R., and Yildirim, A. Ö. (2022) The arginine methyltransferase PRMT7 promotes extravasation of monocytes resulting in tissue injury in COPD. *Nat Commun*. 13, 1303

20. Wang, B., Zhang, M., Liu, Z., Mu, Y., and Li, K. (2021) PRMT7: A Pivotal Arginine Methyltransferase in Stem Cells and Development. *Stem Cells Int*. 2021, 6241600

21. Agolini, E., Dentici, M. L., Bellacchio, E., Alesi, V., Radio, F. C., Torella, A., Musacchia, F., Tartaglia, M., Dallapiccola, B., Nigro, V., Digilio, M. C., and Novelli, A. (2018) Expanding the clinical and molecular spectrum of PRMT7 mutations: 3 additional patients and review. *Clin Genet.* 93, 675–681

22. Cali, E., Suri, M., Scala, M., Ferla, M. P., Alavi, S., Faqeih, E. A., Bijlsma, E. K., Wigby, K. M., Baralle, D., Mehrjardi, M. Y. V., Schwab, J., Platzer, K., Steindl, K., Hashem, M., Jones, M., Niyazov, D. M., Jacober, J., Littlejohn, R. O., Weis, D., Zadeh, N., Rodan, L., Goldenberg, A., Lecoquierre, F., Dutra-Clarke, M., Horvath, G., Young, D., Orenstein, N., Bawazeer, S., Vulto-van Silfhout, A. T., Herenger, Y., Dehghani, M., Seyedhassani, S. M., Bahreini, A., Nasab, M. E., Ercan-Sencicek, A. G., Firoozfar, Z., Movahedinia, M., Efthymiou, S., Striano, P., Karimiani, E. G., Salpietro, V., Taylor, J. C., Redman, M., Stegmann, A. P. A., Laner, A., Abdel-Salam, G., Li, M., Bengala, M., Müller, A. J., Digilio, M. C., Rauch, A., Gunel, M., Titheradge, H., Schweitzer, D. N., Kraus, A., Valenzuela, I., McLean, S. D., Phornphutkul, C., Salih, M., Begtrup, A., Schnur, R. E., Torti, E., Haack, T. B., Prada, C. E., Alkuraya, F. S., Houlden, H., and Maroofian, R. (2023) Biallelic PRMT7 pathogenic variants are associated with a recognizable syndromic neurodevelopmental disorder with short stature, obesity, and craniofacial and digital abnormalities. *Genet Med.* 25, 135–142

23. Poquérusse, J., Whitford, W., Taylor, J., Alburaiky, S., Snell, R. G., Lehnert, K., and Jacobsen, J. C. (2022) Novel PRMT7 mutation in a rare case of dysmorphism and intellectual disability. *J Hum Genet.* 67, 19–26

24. So, H.-K., Kim, S., Kang, J.-S., and Lee, S.-J. (2021) Role of Protein Arginine Methyltransferases and Inflammation in Muscle Pathophysiology. *Front Physiol.* 12, 712389

25. Jeong, H.-J., Lee, H.-J., Vuong, T. A., Choi, K.-S., Choi, D., Koo, S.-H., Cho, S. C., Cho, H., and Kang, J.-S. (2016) Prmt7 Deficiency Causes Reduced Skeletal Muscle Oxidative Metabolism and Age-Related Obesity. *Diabetes.* 65, 1868–1882

26. Blanc, R. S., Vogel, G., Chen, T., Crist, C., and Richard, S. (2016) PRMT7 Preserves Satellite Cell Regenerative Capacity. *Cell Rep.* 14, 1528–1539

27. Rohn, J. L., and Baum, B. (2010) Actin and cellular architecture at a glance. *J Cell Sci.* 123, 155–158

28. Valencia, D. A., and Quinlan, M. E. (2021) Formins. *Curr Biol.* 31, R517–R522

29. Labat-de-Hoz, L., and Alonso, M. A. (2021) Formins in Human Disease. *Cells.* 10, 2554

30. Shimada, A., Nyitrai, M., Vetter, I. R., Kühlmann, D., Bugyi, B., Narumiya, S., Geeves, M. A., and Wittinghofer, A. (2004) The core FH2 domain of diaphanous-related formins is an elongated actin binding protein that inhibits polymerization. *Mol Cell.* 13, 511–522

31. Xu, Y., Moseley, J. B., Sagot, I., Poy, F., Pellman, D., Goode, B. L., and Eck, M. J. (2004) Crystal structures of a Formin Homology-2 domain reveal a tethered dimer architecture. *Cell.* 116, 711–723

32. Tojo, H., Kaieda, I., Hattori, H., Katayama, N., Yoshimura, K., Kakimoto, S., Fujisawa, Y., Presman, E., Brooks, C. C., and Pilch, P. F. (2003) The Formin family protein, formin homolog overexpressed in spleen, interacts with the insulin-responsive aminopeptidase and profilin IIa. *Mol Endocrinol.* 17, 1216–1229

33. Dwyer, J., Pluess, M., Iskratsch, T., Dos Remedios, C. G., and Ehler, E. (2014) The formin FHOD1 in cardiomyocytes. *Anat Rec (Hoboken).* 297, 1560–1570

34. Schönichen, A., Mannherz, H. G., Behrmann, E., Mazur, A. J., Kühn, S., Silván, U., Schoenenberger, C.-A., Fackler, O. T., Raunser, S., Dehmelt, L., and Geyer, M. (2013) FHOD1 is a combined actin filament capping and bundling factor that selectively associates with actin arcs and stress fibers. *J Cell Sci.* 126, 1891–1901

35. Kutscheidt, S., Zhu, R., Antoku, S., Luxton, G. W. G., Stagljar, I., Fackler, O. T., and Gundersen, G. G. (2014) FHOD1 interaction with nesprin-2G mediates TAN line formation and nuclear movement. *Nat Cell Biol.* 16, 708–715

36. Gardberg, M., Kaipio, K., Lehtinen, L., Mikkonen, P., Heuser, V. D., Talvinen, K., Iljin, K., Kampf, C., Uhlen, M., Grénman, R., Koivisto, M., and Carpén, O. (2013) FHOD1, a formin upregulated in epithelial-mesenchymal transition, participates in cancer cell migration and invasion. *PLoS One*. 8, e74923

37. Antoku, S., Schwartz, T. U., and Gundersen, G. G. (2023) FHODs: Nuclear tethered formins for nuclear mechanotransduction. *Front Cell Dev Biol*. 11, 1160219

38. Ushijima, T., Fujimoto, N., Matsuyama, S., Kan-O, M., Kiyonari, H., Shioi, G., Kage, Y., Yamasaki, S., Takeya, R., and Sumimoto, H. (2018) The actin-organizing formin protein Fhod3 is required for postnatal development and functional maintenance of the adult heart in mice. *J Biol Chem*. 293, 148–162

39. Taniguchi, K., Takeya, R., Suetsugu, S., Kan-O, M., Narusawa, M., Shiose, A., Tominaga, R., and Sumimoto, H. (2009) Mammalian formin fhod3 regulates actin assembly and sarcomere organization in striated muscles. *J Biol Chem*. 284, 29873–29881

40. Walsh, R., Offerhaus, J. A., Tadros, R., and Bezzina, C. R. (2022) Minor hypertrophic cardiomyopathy genes, major insights into the genetics of cardiomyopathies. *Nat Rev Cardiol*. 19, 151–167

41. vanLieshout, T. L., and Ljubicic, V. (2019) The emergence of protein arginine methyltransferases in skeletal muscle and metabolic disease. *Am J Physiol Endocrinol Metab*. 317, E1070–E1080

42. Herrmann, F., Pably, P., Eckerich, C., Bedford, M. T., and Fackelmayer, F. O. (2009) Human protein arginine methyltransferases in vivo--distinct properties of eight canonical members of the PRMT family. *J Cell Sci*. 122, 667–677

43. Haghandish, N., Baldwin, R. M., Morettin, A., Dawit, H. T., Adhikary, H., Masson, J.-Y., Mazroui, R., Trinkle-Mulcahy, L., and Côté, J. (2019) PRMT7 methylates eukaryotic translation initiation factor 2α and regulates its role in stress granule formation. *Mol Biol Cell*. 30, 778–793

44. Zhou, Q., Wei, S.-S., Wang, H., Wang, Q., Li, W., Li, G., Hou, J.-W., Chen, X.-M., Chen, J., Xu, W.-P., Li, Y.-G., and Wang, Y.-P. (2017) Crucial Role of ROCK2-Mediated Phosphorylation and Upregulation of FHOD3 in the Pathogenesis of Angiotensin II-Induced Cardiac Hypertrophy. *Hypertension*. 69, 1070–1083

45. Iskratsch, T., Reijntjes, S., Dwyer, J., Toselli, P., Dégano, I. R., Dominguez, I., and Ehler, E. (2013) Two distinct phosphorylation events govern the function of muscle FHOD3. *Cell Mol Life Sci*. 70, 893–908

46. Parra, M. A., Kerr, D., Fahy, D., Pouchnik, D. J., and Wyrick, J. J. (2006) Deciphering the Roles of the Histone H2B N-Terminal Domain in Genome-Wide Transcription. *Mol Cell Biol*. 26, 3842–3852

47. Mao, P., Kyriss, M. N. M., Hodges, A. J., Duan, M., Morris, R. T., Lavine, M. D., Topping, T. B., Gloss, L. M., and Wyrick, J. J. (2016) A basic domain in the histone H2B N-terminal tail is important for nucleosome assembly by FACT. *Nucleic Acids Res*. 44, 9142

48. Lau, A. T. Y., Lee, S.-Y., Xu, Y.-M., Zheng, D., Cho, Y.-Y., Zhu, F., Kim, H.-G., Li, S.-Q., Zhang, Z., Bode, A. M., and Dong, Z. (2011) Phosphorylation of Histone H2B Serine 32 Is Linked to Cell Transformation. *J Biol Chem*. 286, 26628–26637

49. Monteonofrio, L., Valente, D., Ferrara, M., Camerini, S., Miscione, R., Crescenzi, M., Rinaldo, C., and Soddu, S. (2018) HIPK2 and extrachromosomal histone H2B are separately recruited by Aurora-B for cytokinesis. *Oncogene*. 37, 3562–3574

50. Yi, S. A., Um, S. H., Lee, J., Yoo, J. H., Bang, S. Y., Park, E. K., Lee, M. G., Nam, K. H., Jeon, Y. J., Park, J. W., You, J. S., Lee, S.-J., Bae, G.-U., Rhie, J. W., Kozma, S. C., Thomas, G., and Han, J.-W. (2016) S6K1 Phosphorylation of H2B Mediates EZH2 Trimethylation of H3: A Determinant of Early Adipogenesis. *Mol Cell*. 62, 443–452

51. Bungard, D., Fuerth, B. J., Zeng, P.-Y., Faubert, B., Maas, N. L., Viollet, B., Carling, D., Thompson, C. B., Jones, R. G., and Berger, S. L. (2010) Signaling kinase AMPK activates stress-promoted transcription via histone H2B phosphorylation. *Science*. 329, 1201–1205

52. Szewczyk, M. M., Ishikawa, Y., Organ, S., Sakai, N., Li, F., Halabelian, L., Ackloo, S., Couzens, A. L., Eram, M., Dilworth, D., Fukushi, H., Harding, R., Dela Seña, C. C., Sugo, T., Hayashi, K., McLeod, D., Zepeda, C., Aman, A., Sánchez-Osuna, M., Bonneil, E., Takagi, S., Al-Awar, R., Tyers, M., Richard, S., Takizawa, M., Gingras, A.-C., Arrowsmith, C. H., Vedadi, M., Brown, P. J., Nara, H., and Barsyte-Lovejoy, D. (2020) Pharmacological inhibition of PRMT7 links arginine monomethylation to the cellular stress response. *Nat Commun*. 11, 2396

53. Lorton, B. M., and Shechter, D. (2019) Cellular consequences of arginine methylation. *Cell Mol Life Sci*. 76, 2933–2956

54. Luger, K., and Richmond, T. J. (1998) The histone tails of the nucleosome. *Curr Opin Genet Dev*. 8, 140–146

55. Mendoza, M., Mendoza, M., Lubrino, T., Briski, S., Osuji, I., Cuala, J., Ly, B., Ocegueda, I., Peralta, H., Garcia, B. A., and Zurita-Lopez, C. I. (2023) Arginine Methylation of the PGC-1α C-Terminus Is Temperature-Dependent. *Biochemistry*. 62, 22–34

56. Vizcarra, C. L., Kreutz, B., Rodal, A. A., Toms, A. V., Lu, J., Zheng, W., Quinlan, M. E., and Eck, M. J. (2011) Structure and function of the interacting domains of Spire and Fmn-family formins. *Proc Natl Acad Sci U S A*. 108, 11884–11889

57. Silkworth, W. T., Kunes, K. L., Nickel, G. C., Phillips, M. L., Quinlan, M. E., and Vizcarra, C. L. (2018) The neuron-specific formin Delphilin nucleates nonmuscle actin but does not enhance elongation. *Mol Biol Cell*. 29, 610–621

58. Bremer, K. V., Wu, C., Patel, A. A., He, K. L., Grunfeld, A. M., Chanfreau, G. F., and Quinlan, M. E. (2024) Formin tails act as a switch, inhibiting or enhancing processive actin elongation. *J Biol Chem*. 300, 105557

59. Komar, D., and Juszczynski, P. (2020) Rebelled epigenome: histone H3S10 phosphorylation and H3S10 kinases in cancer biology and therapy. *Clin Epigenetics*. 12, 147

60. Di Lorenzo, A., and Bedford, M. T. (2011) Histone arginine methylation. *FEBS Lett.* 585, 2024–2031

61. Leal, J. A., Estrada-Tobar, Z. M., Wade, F., Mendiola, A. J. P., Meza, A., Mendoza, M., Nerenberg, P. S., and Zurita-Lopez, C. I. (2021) Phosphoserine inhibits neighboring arginine methylation in the RKS motif of histone H3. *Arch Biochem Biophys.* 698, 108716

62. Ho, M.-C., Wilczek, C., Bonanno, J. B., Xing, L., Seznec, J., Matsui, T., Carter, L. G., Onikubo, T., Kumar, P. R., Chan, M. K., Brenowitz, M., Cheng, R. H., Reimer, U., Almo, S. C., and Shechter, D. (2013) Structure of the Arginine Methyltransferase PRMT5-MEP50 Reveals a Mechanism for Substrate Specificity. *PLoS One.* 8, e57008

63. Fulton, M. D., Dang, T., Brown, T., and Zheng, Y. G. (2022) Effects of substrate modifications on the arginine dimethylation activities of PRMT1 and PRMT5. *Epigenetics.* 17, 1–18

64. Hsu, J.-M., Chen, C.-T., Chou, C.-K., Kuo, H.-P., Li, L.-Y., Lin, C.-Y., Lee, H.-J., Wang, Y.-N., Liu, M., Liao, H.-W., Shi, B., Lai, C.-C., Bedford, M. T., Tsai, C.-H., and Hung, M.-C. (2011) Crosstalk between Arg 1175 methylation and Tyr 1173 phosphorylation negatively modulates EGFR-mediated ERK activation. *Nat Cell Biol.* 13, 174–181

65. Lenard, A. J., Hutten, S., Zhou, Q., Usluer, S., Zhang, F., Bourgeois, B. M. R., Dormann, D., and Madl, T. (2021) Phosphorylation Regulates CIRBP Arginine Methylation, Transportin-1 Binding and Liquid-Liquid Phase Separation. *Front Mol Biosci.* 8, 689687

66. Horovitz, A., Serrano, L., Avron, B., Bycroft, M., and Fersht, A. R. (1990) Strength and co-operativity of contributions of surface salt bridges to protein stability. *J Mol Biol.* 216, 1031–1044

67. Chang, B., Chen, Y., Zhao, Y., and Bruick, R. K. (2007) JMJD6 is a histone arginine demethylase. *Science.* 318, 444–447

68. Poulard, C., Corbo, L., and Le Romancer, M. (2016) Protein arginine methylation/demethylation and cancer. *Oncotarget.* 7, 67532–67550

69. Liu, W., Ma, Q., Wong, K., Li, W., Ohgi, K., Zhang, J., Aggarwal, A., and Rosenfeld, M. G. (2013) Brd4 and JMJD6-associated anti-pause enhancers in regulation of transcriptional pause release. *Cell.* 155, 1581–1595

70. Wang, Y., Wysocka, J., Sayegh, J., Lee, Y.-H., Perlin, J. R., Leonelli, L., Sonbuchner, L. S., McDonald, C. H., Cook, R. G., Dou, Y., Roeder, R. G., Clarke, S., Stallcup, M. R., Allis, C. D., and Coonrod, S. A. (2004) Human PAD4 regulates histone arginine methylation levels via demethylimination. *Science.* 306, 279–283

71. Thompson, P. R., and Fast, W. (2006) Histone citrullination by protein arginine deiminase: is arginine methylation a green light or a roadblock? *ACS Chem Biol.* 1, 433–441

72. Lowe, T. L., and Clarke, S. G. (2022) Human protein arginine methyltransferases (PRMTs) can be optimally active under nonphysiological conditions. *J Biol Chem.* 298, 102290

73. Li, C., Wen, A., Shen, B., Lu, J., Huang, Y., and Chang, Y. (2011) FastCloning: a highly simplified, purification-free, sequence- and ligation-independent PCR cloning method. *BMC Biotechnol.* 11, 92

74. Liu, H., and Naismith, J. H. (2008) An efficient one-step site-directed deletion, insertion, single and multiple-site plasmid mutagenesis protocol. *BMC Biotechnol.* 8, 91
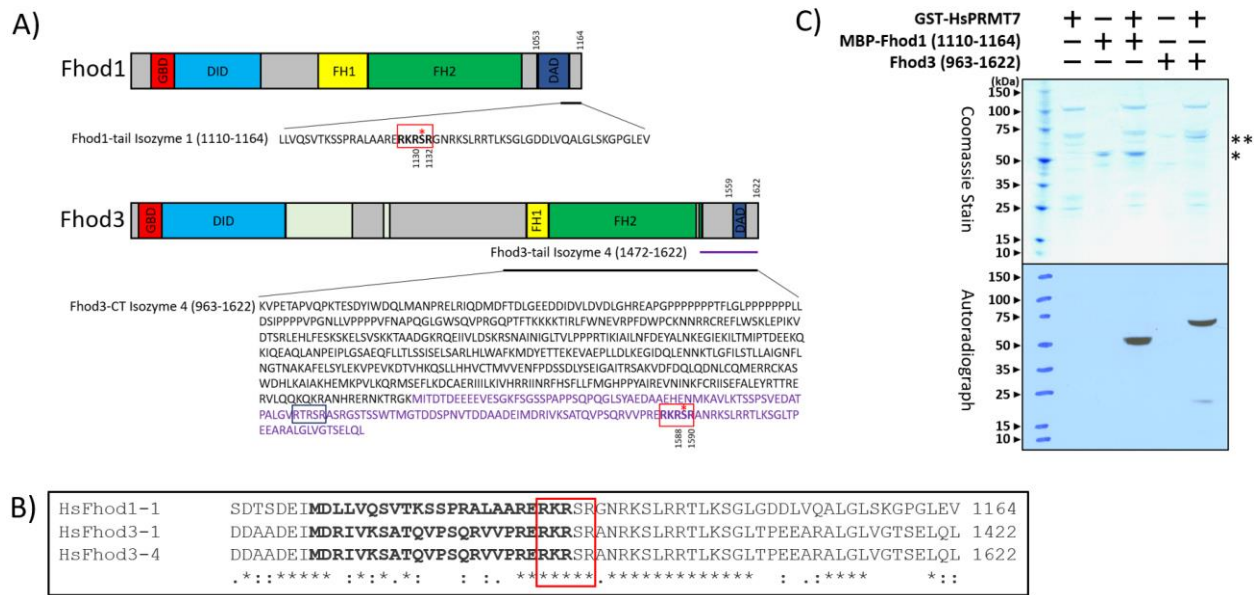
Figure 1: The C-terminal domains of HsFhod1 and HsFhod3 are methylated by HsPRMT7

in vitro. A) Schematic diagram of HsFhod1 and HsFhod3 and constructs used in this paper.

Common domains are indicated. Light green boxes in Fhod3 are inserts that distinguish isozyme

4 from isozyme 1. The dark blue box (RTRSR) contains a sequence similar to the PRMT7

recognition sequence (RKRSR) in the red box. Red asterisk (*) denotes a serine that is

phosphorylated by ROCK1/2. B) Sequence alignment of HsFhod1 and HsFhod3 (isozymes 1 and

4) C-terminal residues including the core DAD domain (bold) and the PRMT7 recognition motif

(red box). C) 7 μg of MBP-Fhod1 DAD domain (1110-1164) or 7 μg of Fhod3-CT (963-1622), 5

μg of GST-HsPRMT7, and 0.7 μM [^{3}H]AdoMet were combined and allowed to incubate for 20 h

at 4 °C in a reaction buffer containing 1 mM DTT, 50 mM K-HEPES, with a final pH of 8.5. Samples

were separated by SDS-PAGE electrophoresis and exposed to autoradiography film for 5 days.

Single asterisk (*) denotes the polypeptide molecular weight of MBP-Fhod1 tail (1110-1164)

double asterisk (**) denotes the polypeptide molecular weight of Fhod3-CT (963-1622).

79
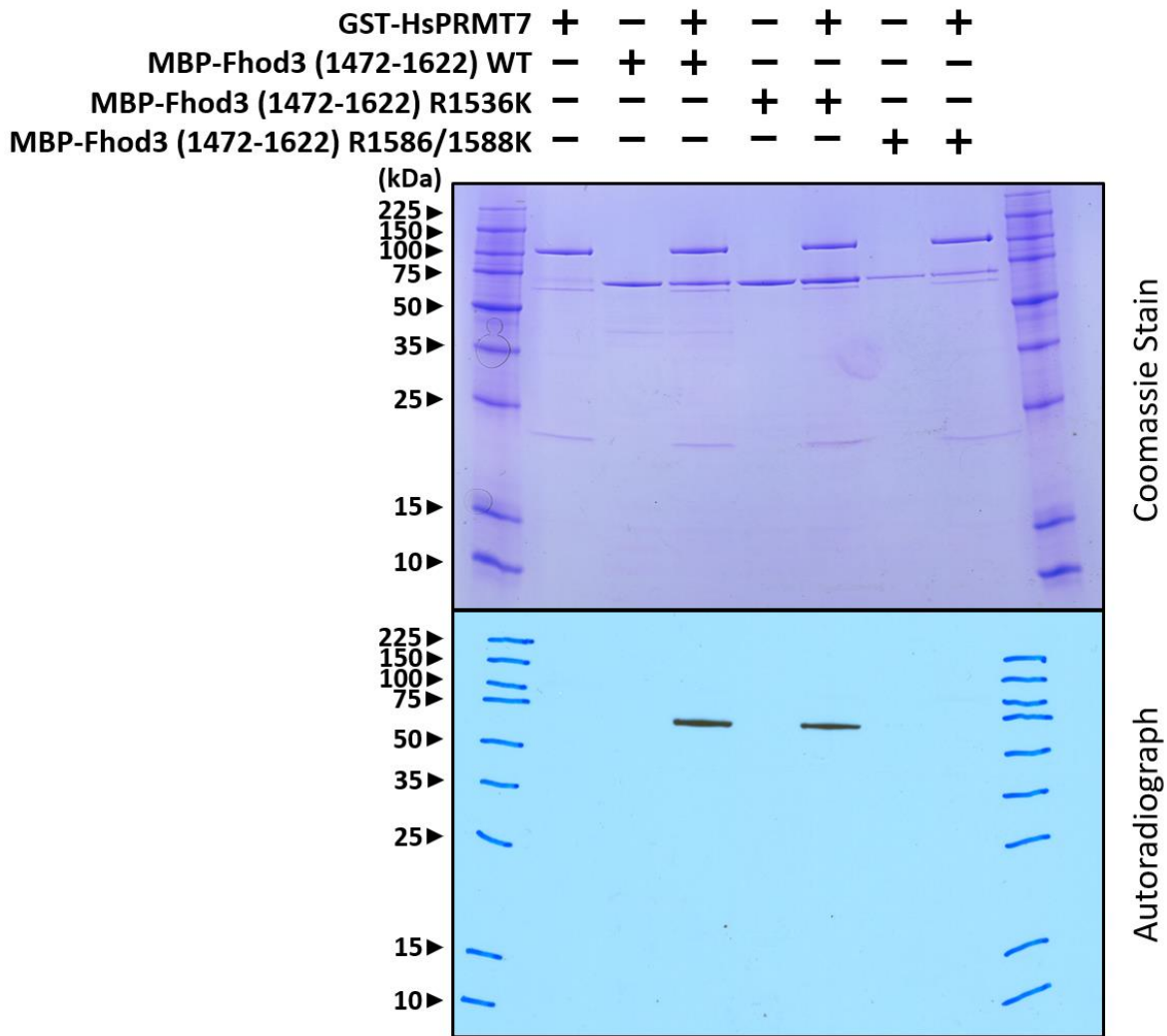
Figure 2: PRMT7 methylates the RKRSR motif of Fhod3 and not the RTRSR motif. 5 µg of GST-HsPRMT7 and 3 µg of MBP-tagged DAD domain Fhod3 constructs was mixed with 0.7 µM [^{3}H]AdoMet. Reactions were incubated for 20 h at 4 °C prior to termination by SDS-sample buffer. Samples were separated by SDS-PAGE electrophoresis and exposed to autoradiography film for 10 days. Fhod3 constructs consisted of amino acid residues (1472-1622) from isozyme 4 as the wildtype (WT) sequence or the mutated R1536K sequence or the double mutant R1586K and R1588K sequence. Protein bands at 100 kDa represents GST-HsPRMT7 and protein bands at 63 kDa represent MBP-Fhod3 (1472-1622) constructs. Total amount of protein and substrate was determined by nanodrop A280 where 1 µg/µL was equal to 1 absorbance unit.
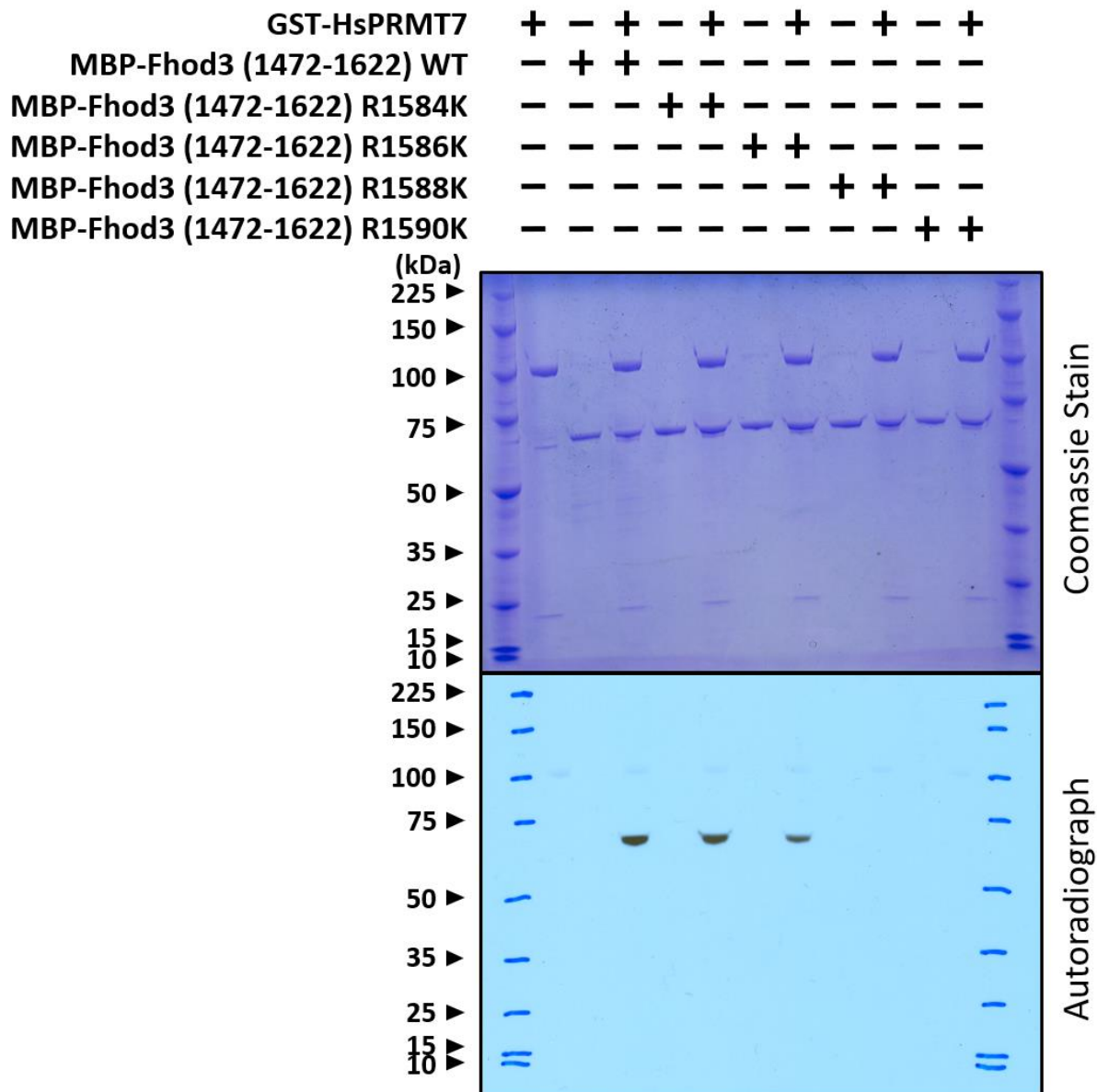
Figure 3: PRMT7 methylates R1588 or R1590 of the Fhod3 C-terminal DAD domain. 5 µg of GST-HsPRMT7 was mixed with 3 µg of MBP-Fhod3 (1472-1622) constructs containing residue mutations of arginine to lysine in the identified RERKRSR motif sequence, and 0.7 µM [³H]AdoMet. Reactions were incubated for 20 h at 4 °C and then terminated with an SDS-PAGE sample buffer. Gel was exposed to an autoradiograph film for 10 days prior to development. Total amount of protein and substrate was determined by nanodrop A280 where 1 µg/µL was equal to 1 absorbance unit.

Peptide Name	Peptide Sequence	Km (μM)	Kcat (min⁻¹)	Kcat/Km (min⁻¹μM⁻¹)
Fhod3 (1581-1595) WT	VVPRERKRSRANRKSY	0.96 ± 0.09	86.7 ± 2.8	90 ± 9
Fhod3 (1581-1595) *po*S1589	VVPRERKR{poS}RANRKSY	1.52 ± 2	1.44 ± 0.82	0.95 ± 1.33
Fhod3 (1581-1595) *po*S1595	VVPRERKRSRANRK{poS}Y	4.06 ± 0.99	84 ± 11	20.8 ± 5.8
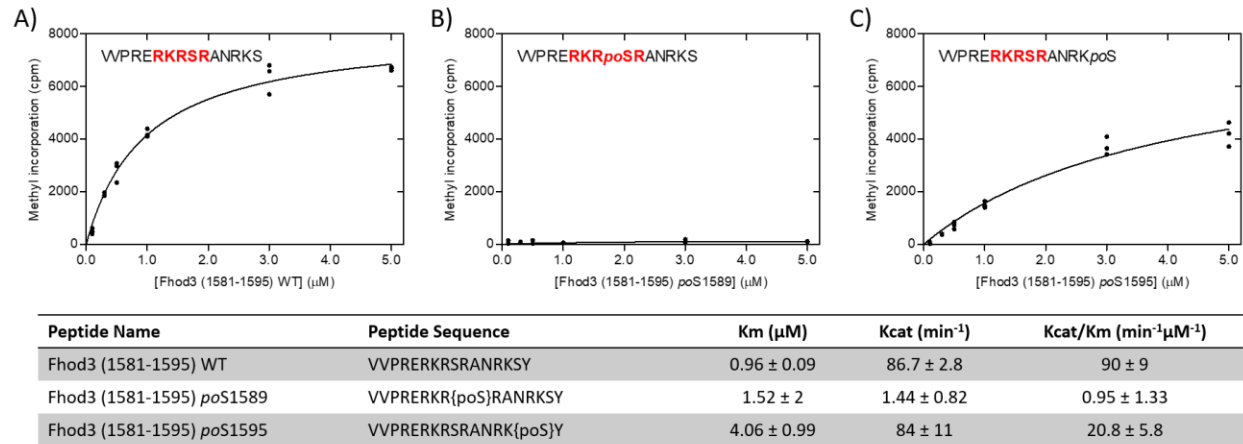
Figure 4: Phosphoserine 1589 of Fhod3 inhibits PRMT7 activity. 5 μg of GST-HsPRMT7, 0.14 μM of [³H]AdoMet and indicated Fhod3 (1581-1595) peptides incubated at 20 °C for 1 h in a reaction mixture of 50 mM K-HEPES, 1 mM DTT, and pH of 8.5. *A)* Fhod3 (1581-1595) WT, *B)* Fhod3 (1581-1595) *po*S1589, *C)* Fhod3 (1581-1595) *po*S1595. Curves were fitted to a standard Michaelis-Menten equation using GraphPad PRISM, n=3.

```
                                     29  31   36
                                        32
                                        33
H. sapiens          KAQKKDGKK**RKRSR**KESYSIYVYK
B. taurus           KAQKKDGKK**RKRSR**KESYSVYVYK
M. musculus         KVQKKDGKK**RKRSR**KESYSVYVYK
X. laevis           KTQKKDGKK**RRKSR**KESYAIYVYK
D. rerio            KTQKKGDKK**RRKTR**KESYAIYVYK
D. melanogaster     NITKT-DKK**KKRKR**KESYAIYIYK
A. thaliana         KEAGDKKKK**RSKKN**VETYKIYIFK
S. cerevisiae       TSTSTDGKK**RSKAR**KETYSSYIYK
H. vulgaris         KIAGTGDKK**RKKKR**RESYAIYIYN
```

Figure 5: The RKRSR motif of histone H2B is highly conserved among higher order species. The human histone H2B sequence containing PRMT7 recognition residues RKRSR aligned with common model organism histone H2Bs. Higher organisms only contain a serine at position 32. Serine 36 is highly conserved but is altered to threonine in some lower organisms.
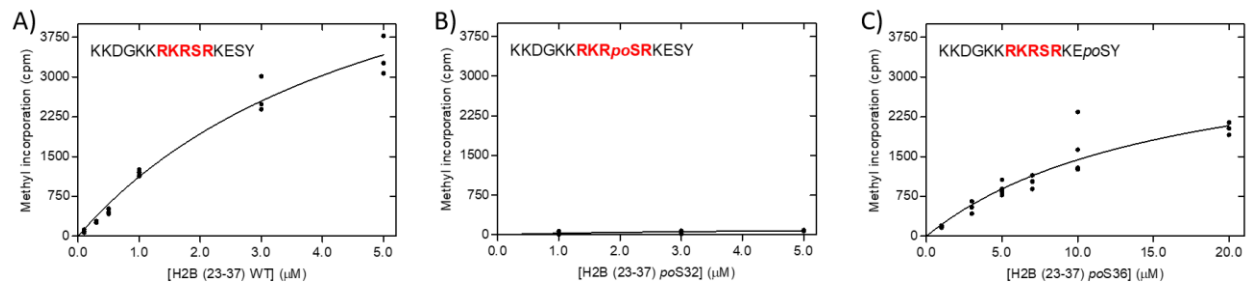
Peptide Name	Peptide Sequence	Km (µM)	Kcat (min^{-1})	Kcat/Km (min^{-1}µM^{-1})
H2B (23-37) WT	Ac-KKDGKKRKRSRKESY-NH$_2$	5.3 ± 1.3	75 ± 11	14 ± 4
H2B (23-37) poS32	KKDGKKRKR{poS}RKESY	3.5 ± 4.7	1.4 ± 0.9	0.4 ± 0.6
H2B (23-37) poS36	KKDGKKRKRSRKE{poS}Y	16.2 ± 6.1	40.0 ± 9	2.5 ± 1.1

Figure 6: Phosphoserine 32 of human histone H2B abolishes PRMT7 activity. 5 µg of GST-HsPRMT7 was mixed with either *A)* H2B (23-37) WT, *B)* H2B (23-37) *po*S32 or *C)* H2B (23-37) *po*S36, and 0.7 µM [^{3}H]AdoMet. Reaction mixtures contained 50 mM K-HEPES, 1 mM DTT, pH = 8.5. Reactions were incubated at 20 °C for 1 h prior to termination with 100% TFA. Points were fitted to a standard Michaelis Menten fit equation using GraphPad PRISM, n=3.

Fhod3 WT (1581-1595); Ac-VVPRERKR**S**RANRK**S**Y-NH$_2$

A)

B)
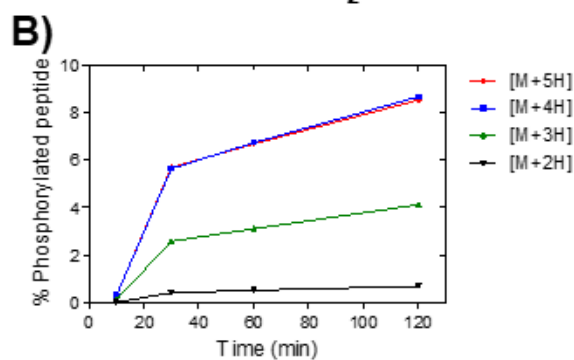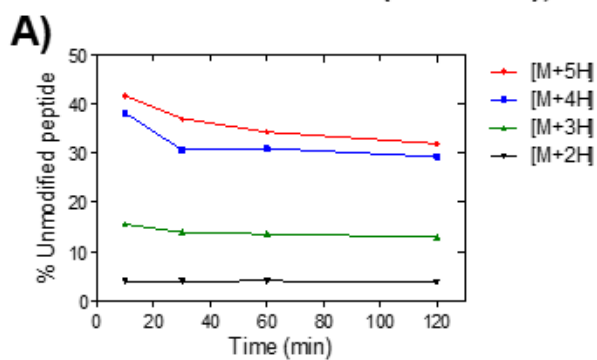
Fhod3 R1588Me1 (1581-1595); Ac-VVPRERKR**R****S**RANRK**S**Y-NH$_2$

C)

D)
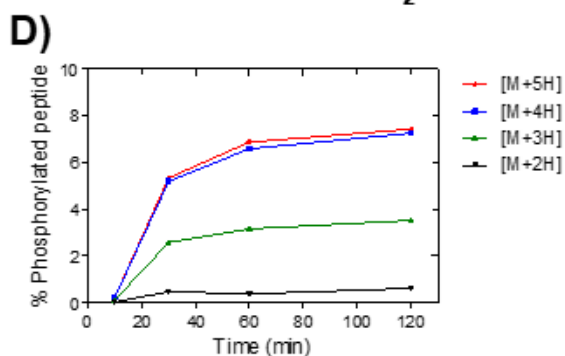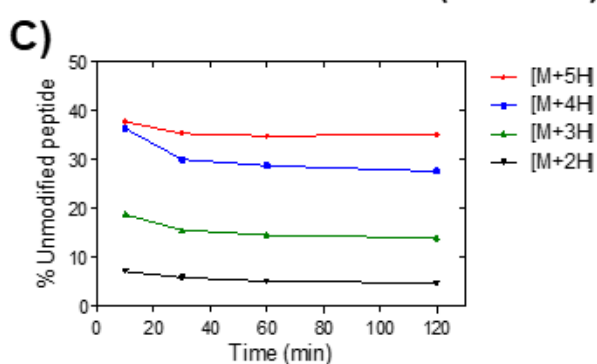
Fhod3 R1590Me1 (1581-1595); Ac-VVPRERKR**S****R**ANRK**S**Y-NH$_2$

E)

F)
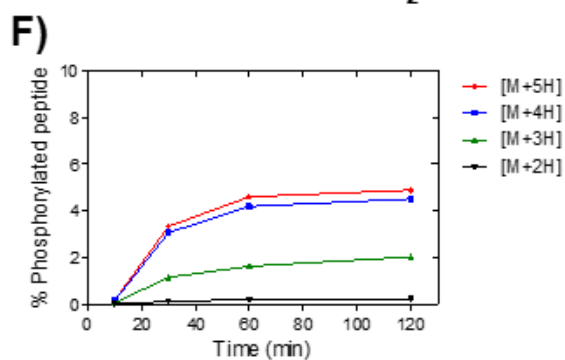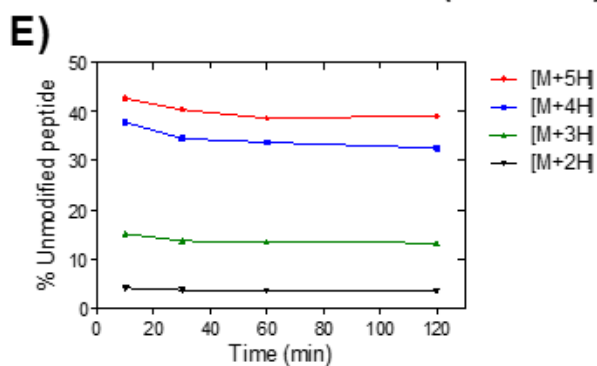
Fhod3 1588Me1/1590Me1 (1581-1595); Ac-VVPRERKR**S****R**ANRK**S**Y-NH$_2$

G)

H)
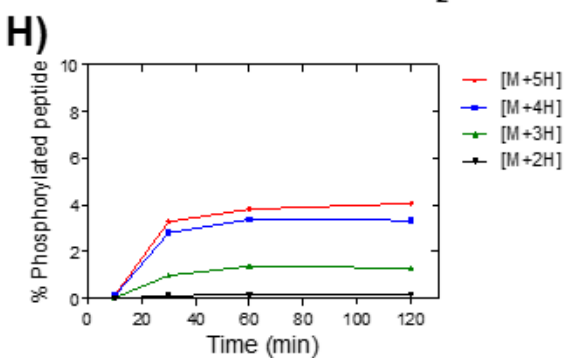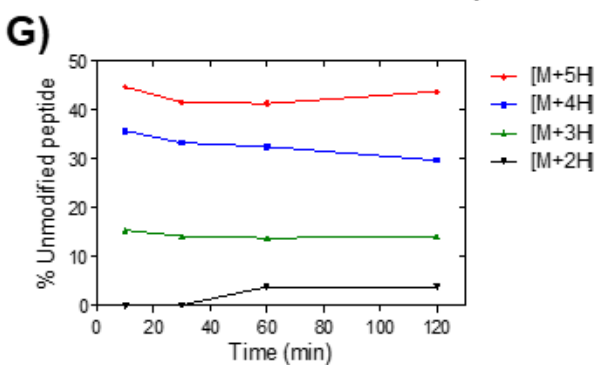
Figure 7: ROCK1 enzymatic activity is minimally affected by the presence of methylarginine residues in a peptide containing serine 1589 and serine 1595. 130 ng of ROCK1, 1 mM ATP and 10 μM Fhod3 (1581-1595) peptides was incubated in a water bath at 30 °C for the specified time. Reactions were terminated with TFA and loaded into a vial for mass spectrometry analysis. 10 μL of sample was injected into an Agilent QTOF 6545 with a run time of 12 mins. *A-B)* Fhod3 WT, *C-D)* Fhod3 R1588Me1, *E-F)* Fhod3 R1590Me1, *G-H)* Fhod3 R1588Me1/R1590Me1. Change in the total amount of unmodified or phosphorylated peptide in reaction mixtures from charge states [M+2H] (black line), [M+3H] (green line), [M+4H] (blue line), and [M+5H] (red line) with time.

Fhod3 WT (1581-1594); Ac-VVPRERKR**S****RANRKY-NH₂**

A)

B)
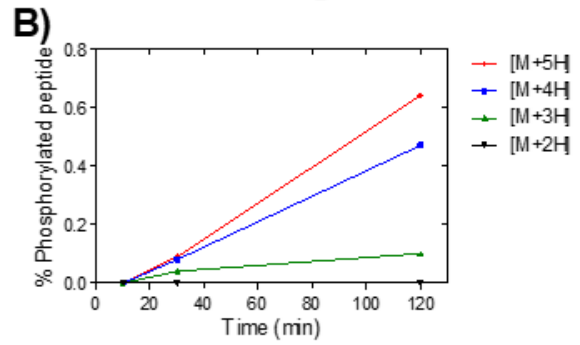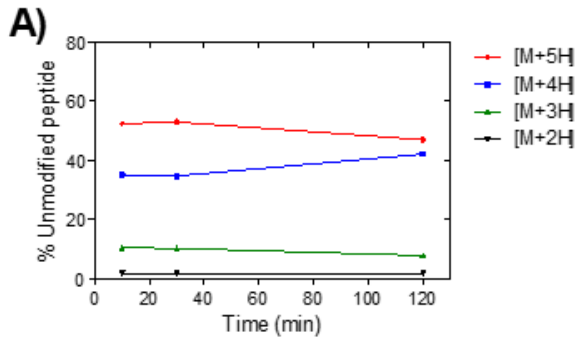
Fhod3 R1588Me1 (1581-1594); Ac-VVPRERKR**R****S****RANRKY-NH₂**

C)

D)

Fhod3 R1590Me1 (1581-1594); Ac-VVPRERKR**S****RANRKY-NH₂**

E)

F)
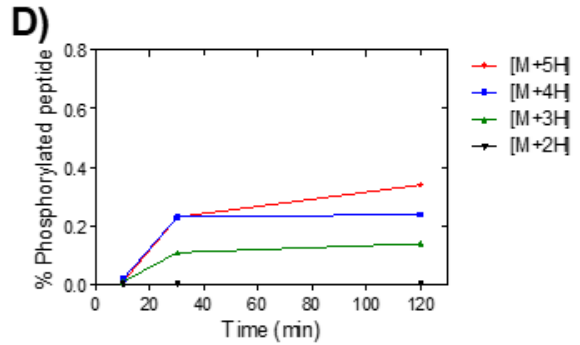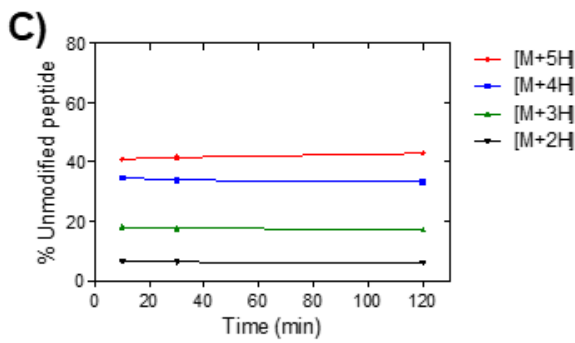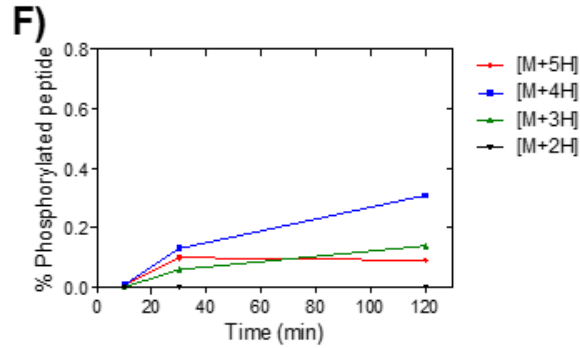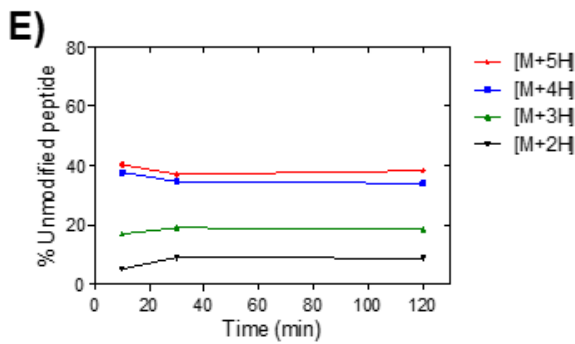
Fhod3 R1588Me1/R1590Me1 (1581-1594); Ac-VVPRERKR**R****S****RANRKY-NH₂**

G)

H)
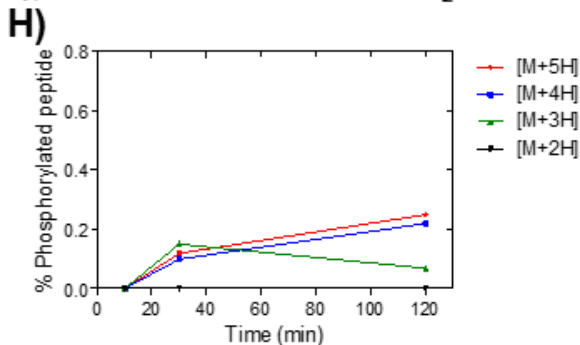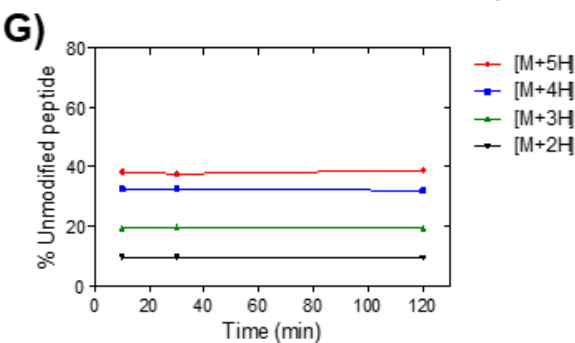
Figure 8: ROCK1 enzymatic activity is minimally affected by the presence of methylarginine residues in a peptide containing serine 1589. 130 ng of ROCK1, 1 mM ATP, and 10 µM Fhod3 (1581-1594) peptides was incubated in a water bath at 30 °C for the specified time. Reactions were terminated with TFA and loaded into a vial for mass spectrometry analysis. 10 µL of sample was injected into an Agilent QTOF 6545 with a run time of 12 mins. *A-B)* Fhod3 WT, *C-D)* Fhod3 R1588Me1, *E-F)* Fhod3 R1590Me1, *G-H)* Fhod3 R1588Me1/R1590Me1. Change in the total amount of unmodified or phosphorylated peptide in reaction mixtures from charge states [M+2H] (black line), [M+3H] (green line), [M+4H] (blue line), and [M+5H] (red line) with time.

Chapter 5: Supporting information

Methylation and phosphorylation of formin homology domain proteins (Fhod1 and Fhod3) by protein arginine methyltransferase 7 (PRMT7) and Rho Kinase (ROCK1)

Troy L. Lowe, Dylan A. Valencia, Vicente E. Velasquez, Margot E. Quinlan and Steven G. Clarke

List of material included:

Table S1: *H. Sapiens* proteins containing an RKRSR sequence

Figure S1: Fhod3 (1581-1595) can be phosphorylated by ROCK1 *in vitro*.

Figure S2: Methylarginine at 1588 of Fhod3 (1581-1595) minimally affects phosphorylation by ROCK1.

Figure S3: Methylarginine at 1590 of Fhod3 (1581-1595) minimally affects phosphorylation by ROCK1.

Figure S4: Methylarginine at 1588 and 1590 of (1581-1595) minimally affects phosphorylation by ROCK1.

Table S1: *H. Sapiens* proteins containing an RKRSR sequence

Accession Entry	Protein	Position
P57053	Histone H2B type F-S	30-34
O94913	Pre-mRNA cleavage complex 2 protein Pcf11	477-481
P23527	Histone H2B type 1-O	30-34
Q9HAZ1	Dual specificity protein kinase	133-137
Q6PH81	UPF0547 protein C16orf87	84-88
Q96IZ7	Serine/Arginine-related protein 53	80-84
Q8IZU1	Protein FAM9A	6-10 49-53
Q3KR37	Protein Aster-B	25-29
O95696	Bromodomain-containing protein 1	798-802
Q7RTU1	Transcription factor 23	32-36
O43290	U4/U6.U5 tri-snRNP-associated protein 1	53-57
Q9NV56	MRG/MORF4L-binding protein	177-181
P56182	Ribosomal RNA processing protein 1 homolog A	388-392
Q3LXA3	Triokinase/FMN cyclase	347-351
O60814	Histone H2B type 1-K	30-34
Q0VF96	Cingulin-like protein 1	383-387
Q93079	Histone H2B type 1-H	30-34
P33778	Histone H2B type 1-B	30-34
P62807	Histone H2B type 1-C/E/F/G/I	30-34
Q5QNW6	Histone H2B type 2-F	30-34
P06899	Histone H2B type 1-J	30-34
Q99877	Histone H2B type 1-N	30-34

P53801	Pituitary tumor-transforming gene 1 protein-interacting protein	123-127
Q99879	Histone H2B type 1-M	30-34
Q16778	Histone H2B type 2-E	30-34
Q99880	Histone H2B type 1-L	30-34
P58876	Histone H2B type 1-D	30-34
Q9UPN6	SR-related and CTD-associated factor 8	428-432
Q66PJ3	ADP-ribosylation factor-like protein 6-interaction protein 4	7-11
Q5VTL8	Pre-mRNA-splicing factor 38B	498-502
Q95218	Zinc finger Ran-binding domain-containing protein 2	285-289
Q9HCG8	Pre-mRNA-splicing factor CWC22 homology	85-89
Q9H8W3	Protein FAM204A	102-106
P46695	Radiation-inducible immediate-early gene IEX-1	59-63
Q9HCI7	E3 ubiquitin-protein ligase MSL2	340-344
Q8TC41	E3 ubiquitin-protein ligase RNG217	533-537
O95232	Luc7-like protein 3	290-294
O75400	Pre-mRNA-processing factor 40 homolog A	796-800
Q9HBE1	POZ-, AT hook-, and zinc finger-containing protein 1	346-350
Q9Y3A4	Ribosomal RNA-processing protein 7 homolog A	231-235
P47901	Vasopressin V1b receptor	64-68
O75182	Paired amphipathic helix protein Sin3b	267-271
Q08170	Serine/Arginine-rich splicing factor 4	357-361
Q9Y5U2	U5 small nuclear ribonucleoprotein TSSC4	308-312
Q9UQ35	Serine/arginine repetitive matrix protein 2	245-249 1849-1853

		2039-2043
P18583	Protein SON	2035-2039
Q9BUQ8	Probable ATP-dependent RNA helicase	20-24
Q86U06	Probably RNA-binding protein 23	73-77
Q96G42	Kelch domain-containing protein 7B	772-776
Q8IX12	Cell division cycle and apoptosis regulator	336-340
Q12955	Ankyrin-3	29-33
O43502	DNA repair protein RAD51 homolog 3	366-370
Q8NBI3	Draxin	133-137
Q15637	Splicing factor 1	17-21
Q14498	RNA-binding protein 39	55-59 71-75
Q9Y613	FH1/FH2 domain-containing protein 1	1128-1132
Q2V2M9	FH1/FH2 domain-containing protein 3	1386-1390
Q6PL18	ATPase family AAA domain-containing protein 2	376-380
Q92560	Ubiquitin carboxyl-terminal hydrolase BAP1	718-722
Q8N7W2	BEN domain-containing protein 7	6-10
Q6DN03	Putative histone H2B type 2-C	30-34
Q6DRA6	Putative histone H2B type 2-D	30-34
O95218	Zinc finger Ran-binding domain-containing protein 2	285-289

Proteins identified using MOTIF search (http://www.genome.jp/tools/motif/MOTIF2.html) and Expasy's ScanProsite (http://prosite.expasy.org/scanprosite) using the UniProtKB/SWISS-Prot Database.
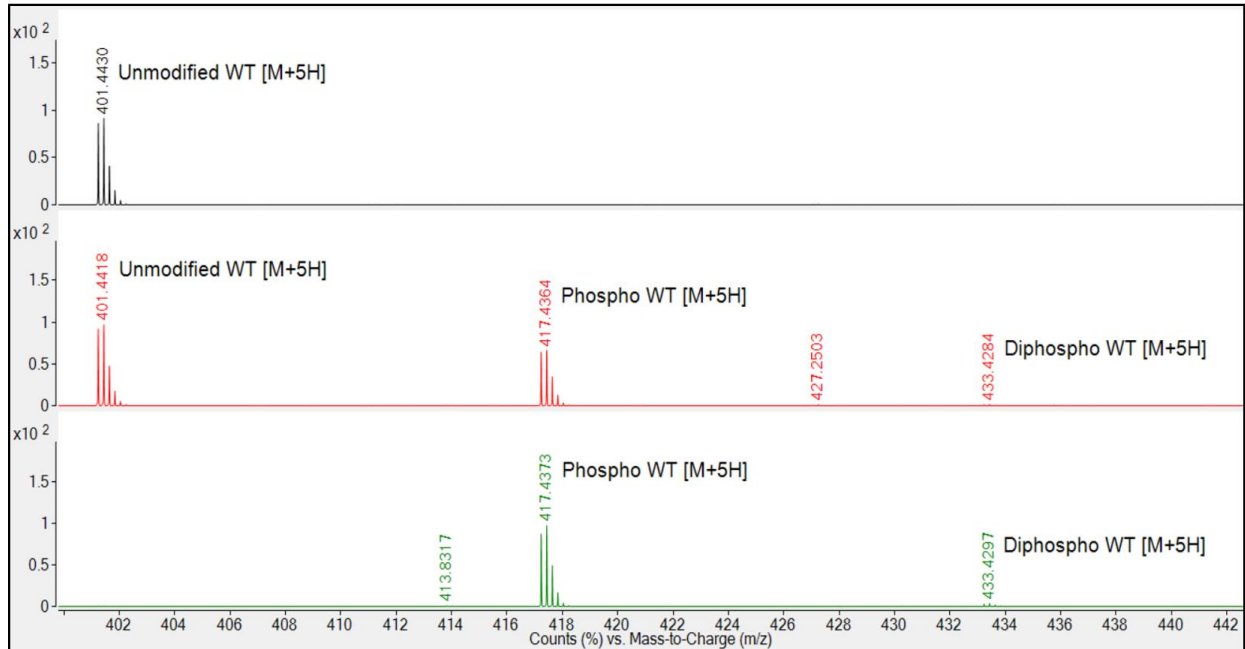
Figure S1: Fhod3 (1581-1595) can be phosphorylated by ROCK1 *in vitro*. 130 ng of ROCK1, 1 mM ATP, 10 µM Fhod3 (1581-1595) WT unmodified peptide was incubated for 5 h in a water bath at 30 °C. Reactions were terminated with TFA and loaded into a vial for mass spectrometry analysis. 10 µL of sample was injected into an Agilent QTOF 6545 with a run time of 12 mins. *Top Panel:* [M+5H] charge state of Fhod3 (1581-1595) unmodified peptide only control of an extracted MS result with a TIC retention time of 4.520 – 8.508 mins, WT unmodified labeled peak of 401.4430 m/z. *Middle Panel:* [M+5H] charge state of Fhod3 (1581-1595) unmodified peptide with ROCK1 reaction from an extracted MS result with a TIC retention time of 4.469 – 8.406 mins, WT unmodified labeled peak of 401.4418 m/z, monophosphorylation labeled peak of 417.4364 m/z, and diphosphorylation labeled peak of 433.4284 m/z. Peak at 427.2503 m/z is an unidentified contaminate. *Bottom panel:* [M+5H] charge state of Fhod3 (1581-1595) unmodified peptide with ROCK1 reaction from an extracted MS result with a TIC retention time of 4.485 – 4.601 mins, monophosphorylation labeled peak of 417.4373 m/z, and diphosphorylation labeled peak of 433.4297 m/z. Peak at 413.8317 m/z is an unidentified contaminate. ATP = adenosine

triphosphate, TFA = trifluoroacetic acid, MS = mass spectrometry, TIC = total ion current, WT = wild-type.
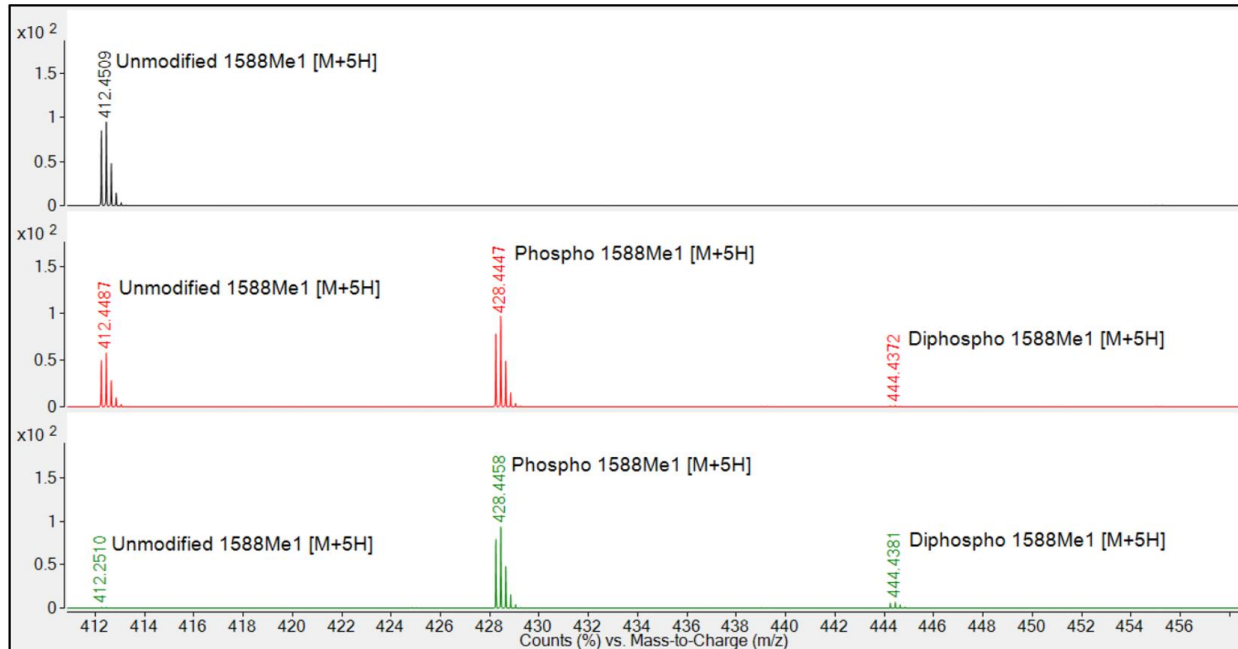
Figure S2: Methylarginine at 1588 of Fhod3 (1581-1595) minimally affects phosphorylation by ROCK1. 130 ng of ROCK1, 1 mM ATP, 10 µM Fhod3 (1581-1595) R1588Me1 unmodified peptide was incubated for 5 h in a water bath at 30 °C. Reactions were terminated with TFA and loaded into a vial for mass spectrometry analysis. 10 µL of sample was injected into an Agilent QTOF 6545 with a run time of 12 mins. *Top Panel:* [M+5H] charge state of Fhod3 (1581-1595) R1588Me1 unmodified peptide only control of an extracted MS result with a TIC retention time of 4.643 – 9.278 mins, R1588Me1 unmodified labeled peak of 412.4509 m/z. *Middle Panel:* [M+5H] charge state of Fhod3 (1581-1595) R1588Me1 unmodified peptide with ROCK1 reaction from an extracted MS result with a TIC retention time of 4.682 – 9.301 mins, R1588Me1 unmodified labeled peak of 412.4487 m/z, monophosphorylation R1588Me1 labeled peak of 428.4447 m/z, and R1588Me1 diphosphorylation labeled peak of 444.4372 m/z. *Bottom panel:* [M+5H] charge state of Fhod3 (1581-1595) R1588Me1 unmodified peptide with ROCK1 reaction from an extracted MS result with a TIC retention time of 4.682 – 4.765 mins, R1588Me1 unmodified labeled peak of 412.2510 m/z, monophosphorylation R1588Me1 labeled peak of 428.4458 m/z, and R1588Me1 diphosphorylation labeled peak of 444.4381 m/z. ATP = adenosine triphosphate,

TFA = trifluoroacetic acid, MS = mass spectrometry, TIC = total ion current, 1588Me1 = Fhod3 (1581-1595) R1588Me1.
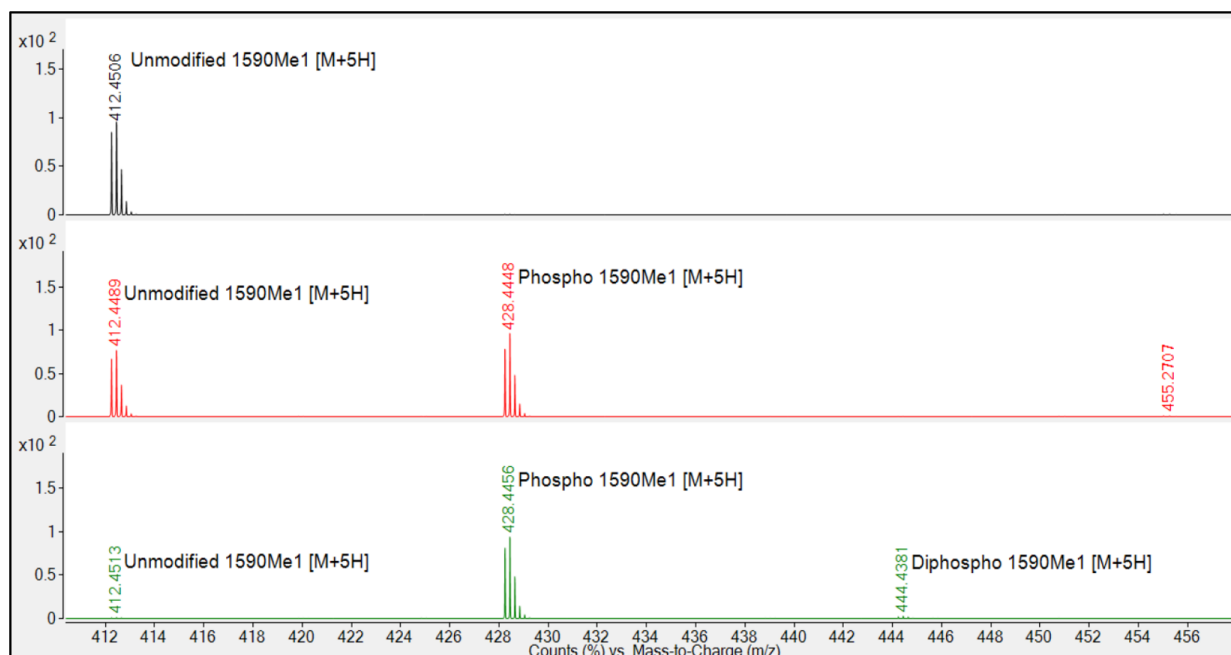
Figure S3: Methylarginine at 1590 of Fhod3 (1581-1595) minimally affects phosphorylation by ROCK1. 130 ng of ROCK1, 1 mM ATP, 10 µM Fhod3 (1581-1595) R1590Me1 unmodified peptide was incubated for 5 h in a water bath at 30 °C. Reactions were terminated with TFA and loaded into a vial for mass spectrometry analysis. 10 µL of sample was injected into an Agilent QTOF 6545 with a run time of 12 mins. *Top Panel:* [M+5H] charge state of Fhod3 (1581-1595) R1590Me1 unmodified peptide only control of an extracted MS result with a TIC retention time of 4.643 – 9.278 mins, R1590Me1 unmodified labeled peak of 412.4509 m/z. *Middle Panel:* [M+5H] charge state of Fhod3 (1581-1595) R1590Me1 unmodified peptide with ROCK1 reaction from an extracted MS result with a TIC retention time of 4.682 – 9.301 mins, R1590Me1 unmodified labeled peak of 412.4489 m/z, and monophosphorylation R1590Me1 labeled peak of 428.4448 m/z. Peak at 455.2707 m/z is an unidentified contaminate. *Bottom panel:* [M+5H] charge state of Fhod3 (1581-1595) R1590Me1 unmodified peptide with ROCK1 reaction from an extracted MS result with a TIC retention time of 4.682 – 4.765 mins, R1590Me1 unmodified labeled peak of 412.4513 m/z, monophosphorylation R1590Me1 labeled peak of 428.4456 m/z, and R1590Me1 diphosphorylation labeled peak of 444.4381 m/z. ATP = adenosine triphosphate, TFA =

97

trifluoroacetic acid, MS = mass spectrometry, TIC = total ion current, 1590Me1 = Fhod3 (1581-1595) R1590Me1.
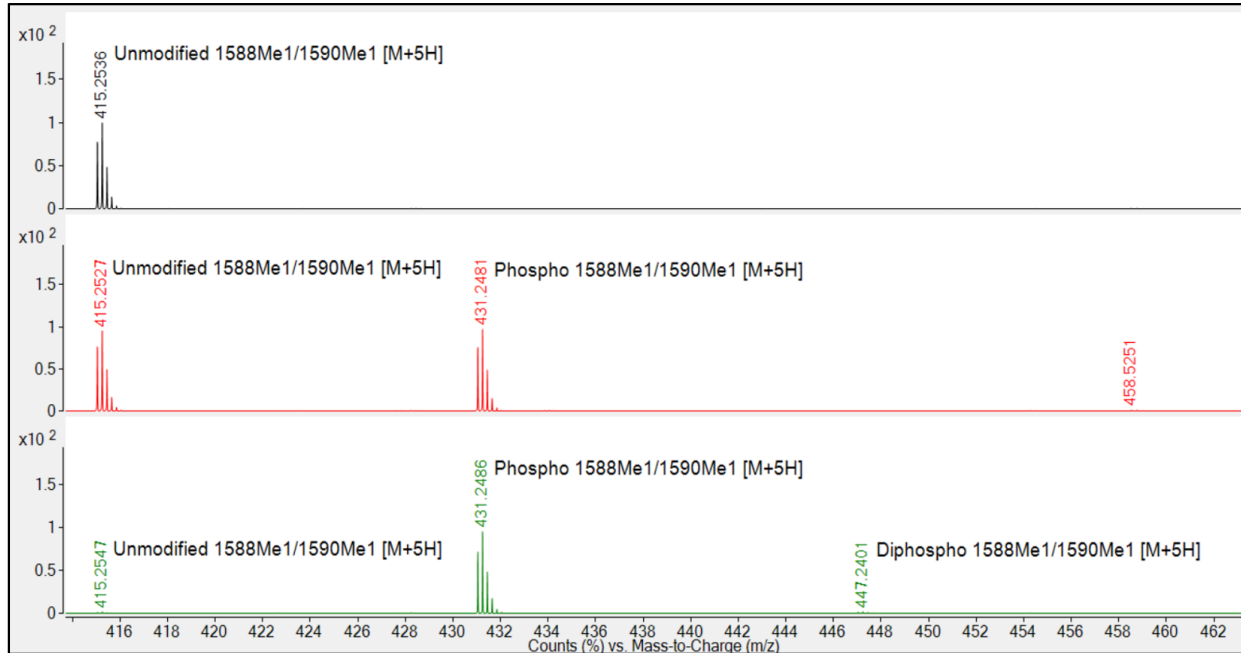
Figure S4: Methylarginine at 1588 and 1590 of Fhod3 (1581-1595) minimally affects phosphorylation by ROCK1. 130 ng of ROCK1, 1 mM ATP, 10 µM Fhod3 (1581-1595) R1588Me1/R1590Me1 unmodified peptide was incubated for 5 h in a water bath at 30 °C. Reactions were terminated with TFA and loaded into a vial for mass spectrometry analysis. 10 µL of sample was injected into an Agilent QTOF 6545 with a run time of 12 mins. *Top Panel:* [M+5H] charge state of Fhod3 (1581-1595) R1588Me1/R1590Me1 unmodified peptide only control of an extracted MS result with a TIC retention time of 4.710 – 9.245 mins, R1590Me1 unmodified labeled peak of 415.2536 m/z. *Middle Panel:* [M+5H] charge state of Fhod3 (1581-1595) R1588Me1/R1590Me1 unmodified peptide with ROCK1 reaction from an extracted MS result with a TIC retention time of 4.749 – 9.252 mins, R1588Me1/R1590Me1 unmodified labeled peak of 415.2527 m/z, and monophosphorylation R1588Me1/R1590Me1 labeled peak of 431.2481 m/z. Peak at 458.5251 m/z is an unidentified contaminate. *Bottom panel:* [M+5H] charge state of Fhod3 (1581-1595) R1588Me1/R1590Me1 unmodified peptide with ROCK1 reaction from an extracted MS result with a TIC retention time of 4.783 – 4.799 mins, R1588Me1/R1590Me1 unmodified labeled peak of 415.2547 m/z, monophosphorylation R1588Me1/R1590Me1 labeled peak of

431.2486 m/z, and R1588Me1/R1590Me1 diphosphorylation labeled peak of 447.2401 m/z. ATP = adenosine triphosphate, TFA = trifluoroacetic acid, MS = mass spectrometry, TIC = total ion current, 1588Me1/1590Me1 = Fhod3 (1581-1595) R1588Me1/R1590Me1.

Chapter 6

Asymmetric and symmetric protein arginine methylation in methionine-addicted human cancer cells

The work described in this chapter has been reproduced from:

Holtz, A. G., Lowe, T. L., Aoki, Y., Kubota, Y., Hoffman, R. M., and Clarke, S. G. (2023) "Asymmetric and symmetric protein arginine methylation in methionine-addicted human cancer cells" Plos one. 18, article e0296291, pp. 1-21. (http://doi.org/10.1371/journal.pone.0296291). PMCID: PMC10745221. PMID: 38134182.

Significance Statement

Cancer cells have been associated with elevated levels of transmethylation reactions through the uptake of dietary methionine. While an original research study noted that a diet depleted of methionine resulted in inhibited tumor growth in mice, it wasn't until years later that methionine dependence was considered a hallmark of cancer. Methionine is an essential amino acid and a precursor for the formation of *S*-adenosylmethionine. *S*-adenosylmethionine is utilized by many methyltransferases including RNA methyltransferases, DNA methyltransferases, and protein methyltransferases. Protein arginine methyltransferases are known to be overexpressed in cancer, however the biological interplay is still unknown.

These results suggest a connection between PRMT function and cancer. Because of the direct link between methionine, *S*-adenosylmethionine, and PRMTs, we were curious as to whether we could observe a difference in methylation patterns between cancer cells that were restricted to methionine or not. In this study we utilize a parental and methionine revertant osteosarcoma cell line to identify whether revertant cell lines had lower transmethylation marks compared to parental.

Our results ultimately showed that the amounts of asymmetric and symmetric dimethylarginine marks were indistinguishable between both cell lines, suggesting the possibility that the relationship between PRMTs and cancer may be more complex.

RESEARCH ARTICLE

Asymmetric and symmetric protein arginine methylation in methionine-addicted human cancer cells

Ashley G. Holtz[1], Troy L. Lowe[1], Yusuke Aoki[2,3,4], Yutaro Kubota[2,3], Robert M. Hoffman[2,3], Steven G. Clarke[1] *

1 Department of Chemistry and Biochemistry, University of California, Los Angeles, Los Angeles, CA, United States of America, 2 AntiCancer, Inc, San Diego, CA, United States of America, 3 Department of Surgery, University of California, San Diego, La Jolla, CA, United States of America, 4 Department of Orthopedic Surgery, Graduate School of Medicine, University of the Ryukyus, Nishihara, Japan

* clarke@chem.ucla.edu

Abstract

The methionine addiction of cancer cells is known as the Hoffman effect. While non-cancer cells in culture can utilize homocysteine in place of methionine for cellular growth, most cancer cells require exogenous methionine for proliferation. It has been suggested that a biochemical basis of this effect is the increased utilization of methionine for S-adenosyl-methionine, the major methyl donor for a variety of cellular methyltransferases. Recent studies have pointed to the role of S-adenosylmethionine-dependent protein arginine methyltransferases (PRMTs) in cell proliferation and cancer. To further understand the biochemical basis of the methionine addiction of cancer cells, we compared protein arginine methylation in two previously described isogenic cell lines, a methionine-addicted 143B human osteosarcoma cell line and its less methionine-dependent revertant. Previous work showed that the revertant cells were significantly less malignant than the parental cells. In the present study, we utilized antibodies to detect the asymmetric dimethylarginine (ADMA) and symmetric dimethylarginine (SDMA) products of PRMTs in polypeptides from cellular extracts and purified histone preparations of these cell lines fractionated by SDS-PAGE. Importantly, we observed little to no differences in the banding patterns of ADMA- and SDMA-containing species between the osteosarcoma parental and revertant cell lines. Furthermore, enzymatic activity assays using S-adenosyl-L-[methyl-^{3}H] methionine, recombinantly purified PRMT enzymes, cell lysates, and specific PRMT inhibitors revealed no major differences in radiolabeled polypeptides on SDS-PAGE gels. Taken together, these results suggest that changes in protein arginine methylation may not be major contributors to the Hoffman effect and that other consequences of methionine addiction may be more important in the metastasis and malignancy of osteosarcoma and potentially other cancers.

Introduction

Methionine is an essential amino acid whose metabolites are involved in a variety of cellular pathways. Methionine addiction of cancer cells is a phenomenon where cancer cells require

exogenous methionine to grow and are unable to survive when methionine in the culture medium is replaced with homocysteine, methionine's precursor [1–6]. However, paradoxically cancer cells have the ability to produce large amounts of methionine from homocysteine and can use endogenously synthesized methionine for cellular processes [1, 7, 8]. In contrast, normal cells can grow in culture when homocysteine is substituted for methionine [6, 7]. The methionine addiction of cancer cells is known as the Hoffman effect and is a target for cancer treatment [2, 3, 9].

Studies in xenograft mouse models show that treatment with recombinant methioninase, an enzyme that depletes plasma methionine levels, and/or a methionine-restricted diet can decrease tumor volume [10–14]. Clinically, the enhanced usage of methionine in cancer cells can be used to localize tumors with [^{11}C]-methionine positron emission tomography (MET--PET), particularly for cancers in the brain as well as organ cancers [15–17]. Additionally, methionine restriction has been used as a combination treatment with chemotherapy in cancer patients [9]. A methionine-restricted diet in Phase I clinical trials as well as a Phase I study of methioninase with cancer patients have been shown to reduce plasma methionine levels without major complications [18, 19]. In initial studies of three patients with metastatic breast cancer, i.v. infusion of methioninase reduced serum methionine levels without any significant side effects [20]. Oral methioninase given to three patients with advanced prostate cancer decreased prostate-specific antigen levels, and has had beneficial effects in several patients with pancreatic cancer, rectal cancer, and breast cancer [21–26]. Overall, methionine restriction appears to be safe for patients and is potentially effective for reducing the severity of cancer.

Methionine is not only used in protein synthesis but also for polyamine metabolism, purine and pyrimidine synthesis, glutathione synthesis, and methylation reactions [27]. Because methionine is required for a wide variety of cellular functions, the exogenous requirement for methionine in cancer cells despite their capacity to synthesize and use methionine endogenously at high levels is incompletely understood [1, 5, 7, 8]. As methionine addiction of cancer is becoming more clinically relevant, it is important to understand how methionine affects cancer progression at a molecular level. To elucidate the molecular mechanism of methionine addiction, Aoki et. al derived a less methionine-dependent revertant cell line from the methionine-addicted human osteosarcoma 143B cell line that demonstrated improved survival at high levels of recombinant methioninase (rMETase) treatment [28]. After culturing the cells in rMETase, methionine was depleted from the culture medium, so most of the cancer cells did not survive. The cells cultured with rMETase that survived after four cycles of selection were designated as less methionine-dependent revertant cells. In cell culture with rMETase, the cell viability of the 143B revertant (143B-R) cells was higher than that of the 143B parent (143B-P) cells [28]. At higher concentrations of rMETase, the 143B-P cells were unable to survive in culture while the 143B-R cells still could grow [28]. Additionally, the morphology between the two cell lines differed, with the 143B-R cells appearing more normal fibroblast-like, larger, and aligned in one direction compared to the 143B-P cells. With a wound-healing assay and a cell-invasion assay, the 143B-R cells showed significantly lower cell migration and invasion ability, respectively, than the 143B-P cells. In orthotopic xenograft mouse models, the 143B-R cells grew smaller tumors than the 143B-P cells and did not metastasize unlike the 143B-P cells. There were no histological differences observed between primary tumors arising from 143B-P and 143B-R cells. The 143B-R cells had increased protein expression of ZO-1, an epithelial marker, and decreased expression of the mesenchymal markers vimentin, Snail, and Slug, compared to the 143B-P cells upon immunoblotting [28]. Taken together, the results of this previous study show that the 143B-R cells are less malignant than their parental cells. Revertant cells of other methionine-addicted cancers have also been shown to lose their malignancy with their methionine dependence [29].

104

Methionine addiction of cancer cells is due at least in part to elevated transmethylation reactions [5, 29–35]. In the previous study, it was found that the 143B-R cells had differences in histone lysine methylation [28], suggesting that this modification may be one of the links between the simultaneous loss of methionine addiction and malignancy in the 143B-R cells, possibly by changing the expression of important genes for cancer progression. In the present work, we wanted to determine the effect of the reversion of methionine addiction on protein arginine methylation, a methionine-dependent modification that is often affected in cancer [36–45]. Protein arginine methylation is a post-translational modification catalyzed by methyltransferases (PRMTs) that are involved in a variety of biological processes, including transcriptional regulation, the immune response, RNA splicing, and DNA repair [36, 37, 46, 47]. The methyl donor of these enzymes is S-adenosylmethionine (AdoMet), a direct product of methionine. In mammals, nine PRMTs have been identified and are categorized by the products that they form. While all PRMTs initially form monomethylarginine (MMA), Type I PRMTs (PRMTs 1–4, 6, and 8) produce asymmetric dimethylarginine (ADMA) and Type II PRMTs (PRMTs 5 and 9) produce symmetric dimethylarginine (SDMA) [47]. PRMT7 is a Type III enzyme, which only forms MMA [47, 48]. PRMT1 and PRMT5 are the major Type I and Type II enzymes and are responsible for the majority of ADMA and SDMA marks on proteins, respectively [49, 50]. Of the three types of protein arginine methylation, ADMA is the most abundant in cells, followed by SDMA and then MMA [51]. Significantly, the overexpression of PRMTs in cancer is often linked to poor prognosis [36, 37, 39, 40, 42, 44, 45], and PRMT inhibitors, especially against PRMT5, are currently being tested in clinical trials with cancer patients [52–56]. Because the formation of AdoMet requires methionine and PRMTs are commonly upregulated in cancer, we hypothesized that cancer cells would more extensively utilize methionine in the biosynthesis of AdoMet and in PRMT-dependent methylation reactions of cellular proteins. To test this hypothesis, we wanted to compare protein arginine methylation levels in the previously described methionine-addicted parent and less methionine-dependent revertant cell lines.

Using antibodies against ADMA and SDMA in immunoblots, we show that the 143B-P and 143B-R cells had no major differences in the level of ADMA or SDMA on proteins in cellular extracts and on purified histones. Additionally, enzymatic activity assays with S-adenosyl-L-[methyl-^{3}H] methionine ([^{3}H]-AdoMet), recombinantly purified PRMT1, 5, and 7 enzymes, and intracellular substrates showed a similar banding pattern of radiolabeled polypeptides between the parent and revertant cells. Overall, no significant changes in PRMT activity were observed in the revertant cells, suggesting that the involvement of PRMTs in cancer may be through a mechanism distinct from the Hoffman effect.

Results

Revertant human 143B osteosarcoma cells are less sensitive to methionine restriction with recombinant methioninase

We first analyzed whether the 143B-P and 143B-R cells responded differently to methionine restriction with rMETase. The revertant cells had greater cell viability at high concentrations of rMETase concentrations compared to their parental cells, indicating their relative independence from methionine, consistent with previous results [28] (Fig 1). The IC$_{50}$ of rMETase was 0.46 U/mL in the revertant cells and 0.29 U/mL in the parental cells. Therefore, we would possibly see the effects of different degrees of methionine dependence on S-adenosylmethionine-dependent methyltransferases, including those involved in protein arginine methylation. Thus, we began to explore how the difference in methionine dependence between the parental and revertant cells may affect the activity of PRMTs.

105
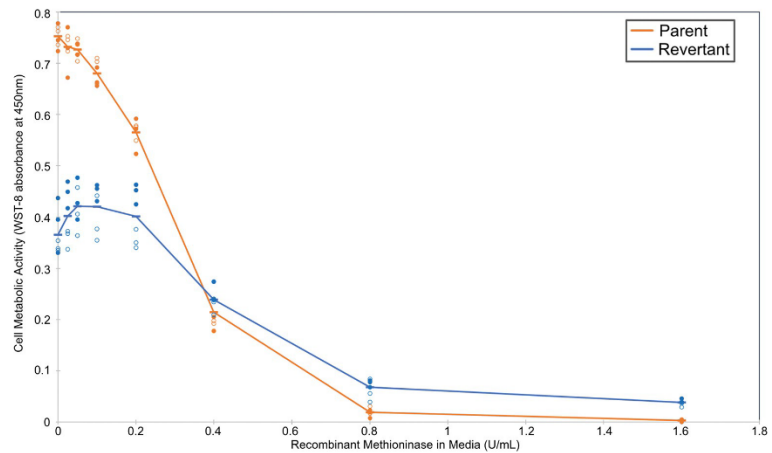
Fig 1. Analysis of methionine dependence in human osteosarcoma 143B parent cells and in revertant cells grown on low-methionine media.

Cells were grown in normal media and then cultured for three days in media containing various concentrations of recombinant methioninase to lower the methionine level, as previously described [28]. Cell viability was measured in an assay using water-soluble tetrazolium-8 (WST-8) as previously described [28]. The absorbance at 450 nm after subtracting a no-cell blank is indicated on the y-axis. The results represent two separate experiments performed in triplicate. The closed circles represent one experiment and the open circles represent a second individual experiment following the same procedure. The measurements from the parent 143B are shown in orange, and those from the revertant 143B cells are shown in blue. The average values are denoted by a dash and connected by the line.

The 143B-P and 143B-R cells have no major differences in the levels of proteins marked with ADMA or SDMA

We employed polyclonal antibodies raised against synthetic peptides containing SDMA and ADMA within glycine rich regions [57] to mimic the common substrate sites recognized by PRMT1, -3, -5, -6, and -8 [36, 50, 58]. SDMA is predominantly produced by PRMT5, and ADMA is predominantly produced by PRMT1. We found that neither the anti-SDMA nor the anti-ADMA antibodies had specific reactivity against negative controls compared to mammalian cell lysates and histone fractions, which were used as positive controls (S1 Fig). Negative controls included an unmethylated protein with a glycine and arginine rich region and *Escherichia coli* (*E. coli*) lysate, which does not contain PRMTs [59].

Next, we explored differences in protein arginine methylation, specifically ADMA and SDMA, in the parent and revertant cancer cell lines. Whole cell extracts of the 143B-P and 143B-R cells were fractionated onto a sodium dodecyl-sulfate polyacrylamide gel electrophoresis (SDS-PAGE) gel, and Coomassie staining was performed as a loading control to compare ADMA and SDMA levels between 143B-P and 143B-R cells (Fig 2). Significantly, no differences in the polypeptide Coomassie staining pattern were observed in two independent experiments, suggesting that there were no major differences in protein expression in the parent and

106
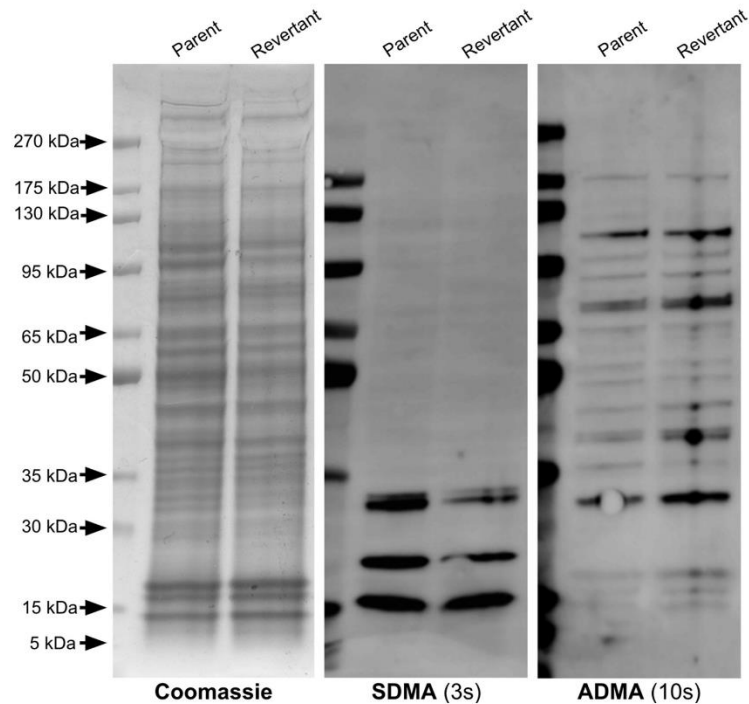
Fig 2. Identification of proteins containing SDMA and ADMA in human parent and revertant 143B osteosarcoma cells.

revertant cells (Fig 2). Three proteins with molecular weights of near 30 kDa, 20 kDa, and 15 kDa had an SDMA modification and were at a similar intensity level between the 143B-P and 143B-R cell extracts. In both cell lines, multiple proteins with ADMA modifications are present between approximately 175 kDa and 15 kDa at similar intensity levels. These results indicate that no observable changes in protein arginine methylation accompany the reversion from the methionine-addicted and metastatic phenotype of the parent cells.

The leftmost panel shows a Coomassie-stained SDS-PAGE gel. The middle panel shows an anti-SDMA immunoblot with a 3 second exposure time. The rightmost panel shows an anti-ADMA immunoblot with a 10 second exposure time. Molecular weight markers are shown at the left in the Coomassie-stained gel and as fluorescent bands on the left margin of the immunoblots.

The proteins with ADMA and with SDMA near 15 kDa could represent methylated arginine on histones. Multiple studies have shown the importance of histone arginine methylation in transcriptional controls in cancer cells [37, 60, 61]. While we established that there were no large-scale differences in overall protein arginine methylation, it was difficult to determine whether there were differences in arginine methylation on histones since the whole cell extract contained histones as well as other low-molecular weight cellular proteins. Because histone modifications can affect gene expression, which may affect the mechanism of reversion, we

107
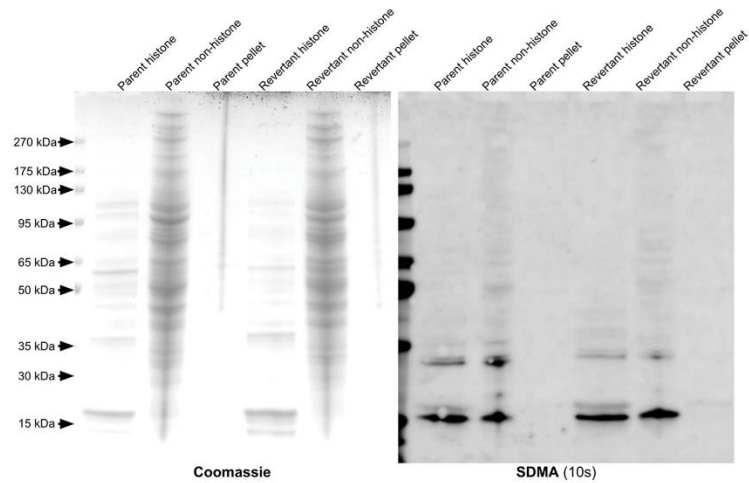
Fig 3. Identification of SDMA-containing polypeptides in histone and non-histone fractions of parent and revertant human osteosarcoma 143B cells.

next investigated whether there were observable differences in SDMA and ADMA on histones in the 143B-P and 143B-R cells.

Extracted histones were analyzed with SDS-PAGE and used in immunoblots against SDMA and ADMA (Fig 3). In the SDMA immunoblot, a band appears slightly above 15kDa in the histone fractions of the 143B-P and 143B-R cells but is not present in the non-histone supernatant, indicating that this protein is a histone. When comparing this histone band between the 143B-P and 143B-R histones, the signal is at a similar intensity, indicating no major differences in SDMA on histones. In the ADMA immunoblot, a histone band near 15 kDa appears more strongly in the 143B-P cells than in the 143B-R cells (Fig 4). However, the
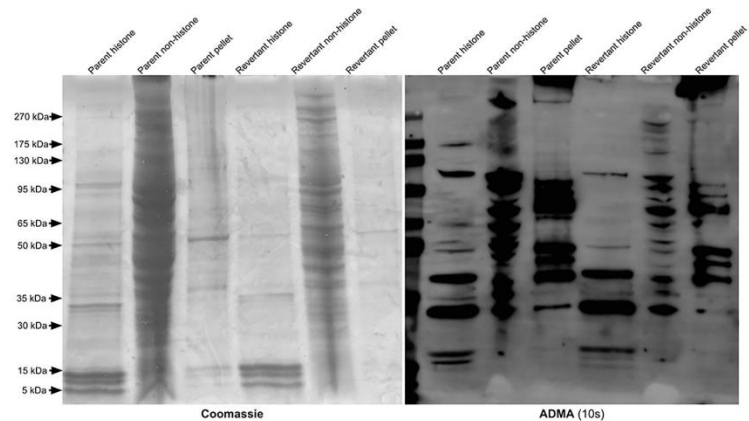
Fig 4. Identification of ADMA-containing polypeptides in histone and non-histone fractions of parent and revertant human osteosarcoma 143B cells.

108

Coomassie-stained SDS-PAGE gel shows that the histones are slightly more enriched in the 143B-P cells than in the 143B-R cells, which may reflect the higher level of ADMA on histones of 143B-P cells. Additionally, a difference in ADMA in this molecular weight region was not observed in replicate anti-ADMA immunoblots of cell lysates (S2 Fig). Therefore, we did not find any large-scale differences in ADMA on histones between the 143B-P and 143B-R cells.

The leftmost panel shows a Coomassie-stained SDS-PAGE gel, and the rightmost panel shows an anti-SDMA immunoblot with an exposure time of 10 seconds.

The leftmost panel shows a Coomassie-stained SDS-PAGE gel, and the rightmost panel shows an anti-ADMA immunoblot with an exposure time of 10 seconds.

The 143B-P and 143B-R cells share similar substrates for PRMT1, PRMT5, and PRMT7

We next performed in vitro enzymatic assays to examine whether there was a difference in substrate availability for PRMTs within the 143B-P and 143B-R cell lysates. Reactions were set up by incubating either the 143B-P or 143B-R cell lysates with [^{3}H]-AdoMet, recombinantly purified PRMT1, -5, or -7, and PRMT inhibitors. Highly selective PRMT inhibitors, including the PRMT7 inhibitor SGC8158, the PRMT5 inhibitor EPZ015666, and the Type I PRMT inhibitor MS023, were used to parse out the activity of individual classes of PRMTs. For example, using PRMT5 along with the inhibitors SGC8158 and MS023 should show methylation in lysates due to PRMT5 activity. Separation of the polypeptides within the reaction mixtures by SDS-PAGE was followed by fluorography. In both the 143B-P and 143B-R lysates incubated only with [^{3}H]-AdoMet, there are two major bands indicating methylated proteins near 50 kDa and 15 kDa, as well as two minor bands near 35 kDa and 25 kDa (Fig 5). These four bands remain present in the lysates with PRMT1 and PRMT5 added, but no additional bands are shown that would indicate additional methylation by the PRMT enzymes. All four of these major bands decrease upon addition of the PRMT inhibitors. When PRMT5 is added with MS023 and SGC8158, it appears that there is less signal intensity in the revertant cell lysates than in the parent cell lysates, indicating that there may be less substrate availability for PRMT5 in the revertant cell lysates. However, the 50 kDa and 15 kDa proteins appear in both cell lysates under these conditions, indicating that these proteins may be PRMT5 substrates. A protein with SDMA near 15 kDa was also detected in the 143B lysates in Fig 2. Interestingly, when PRMT7 was added with Type I and PRMT5 inhibitors, these four bands were not present while a single band near 20 kDa appeared. PRMT7 is unique from other PRMTs because it is optimally active at the nonphysiological temperature of 15°C [62]. The band observed near 20 kDa in both 143B-P and 143B-R lysates with PRMT7 added may be a PRMT7 substrate. However, the reactions with PRMT7 were performed at 20°C, so this substrate may not be methylated within a cell at 37°C. While there may be slightly less substrates methylated by PRMT5 in the revertant cells, no major differences in substrate availability for the PRMT1, PRMT5, and PRMT7 enzymes were observed between the 143B-P and 143B-R cells. Therefore, these results strengthen our conclusion from the immunostaining experiments shown in Figs 2–4 that protein arginine methylation is unlikely to play a major role in the reversion of the 143B cells following methionine restriction with recombinant methioninase. We note, however, that the parent and revertant cells were grown in high-methionine medium that may mask differences in the expression of PRMTs.

Cell lysates were incubated for one hour with 0.14 μM [^{3}H]-AdoMet, recombinant PRMTs (0.20 μg PRMT1, 0.076 μg PRMT5, or 5.5 μg PRMT7), and their inhibitors (2 μM MS023, 20 μM EPZ015666, or 200 nM SGC8158). The inhibitors are abbreviated with their letters at the top of each lane. The images on the top show Coomassie-stained SDS-PAGE gels, and the

109
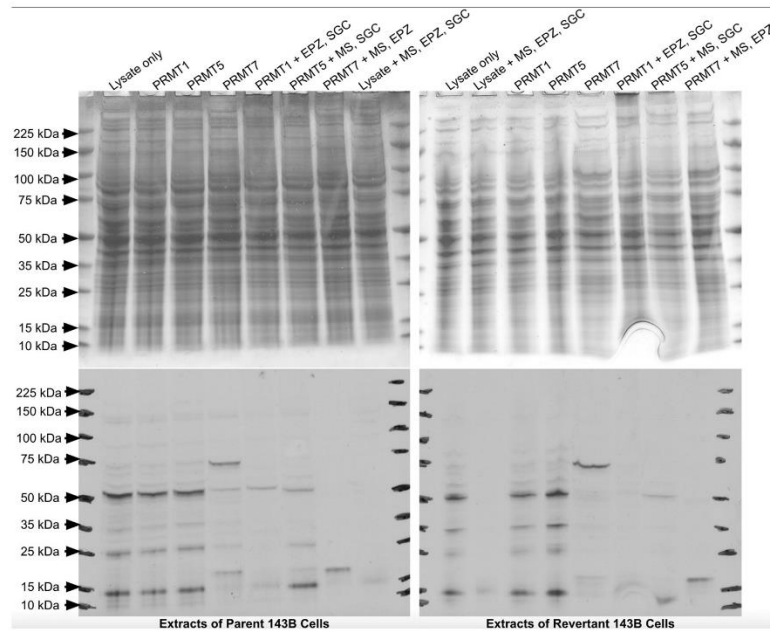
Fig 5. In vitro methylation of polypeptides from extracts of human parent and revertant osteosarcoma 143B cells.

images on the bottom show films exposed for fluorography for 63 days. All incubations were carried out at 37°C, except for those with PRMT7 which were carried out at 20°C. To separate the activity of each PRMT, the PRMT enzyme was added in addition to inhibitors of the other types of PRMTs. For example, in order to measure activity mainly from PRMT1, PRMT1 was added along with a PRMT5 inhibitor and a PRMT7 inhibitor.

A similar constellation of SDMA and ADMA modified polypeptides are seen in various human cancer cell lines, including 143B, H460, HCT116, and HeLa cells

Despite their dysregulation in multiple types of cancer and connection to the methionine metabolic pathway, PRMTs did not seem to heavily contribute to the reversion of the 143B cells to a methionine-independent phenotype. Next, we compared the proteins with SDMA and ADMA found in the bone-derived 143B cells to those in other methionine-addicted cancer cell lines to determine if there are common substrates observed in multiple cancer types. Lung-derived H460 cells and colon-derived HCT116 cells also have the capacity to revert to a less malignant phenotype upon methionine restriction [29], and cervix-derived HeLa cells have been shown to undergo cell cycle arrest when grown in methionine-depleted medium [63].

Overall, the H460 cells had the lowest amount of protein arginine methylation compared to the 143B, the HCT116, and the HeLa cells (Figs 2 and 6). The 143B cells also had a lower amount of proteins with SDMA compared to the HCT116 and HeLa cells. The HCT116 and

110
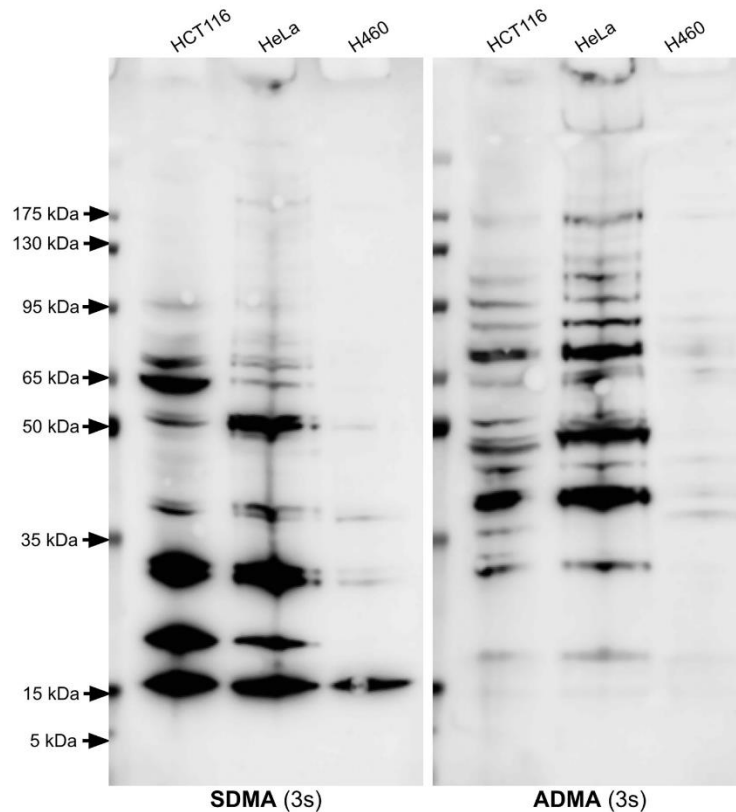
Fig 6. Identification of proteins containing SDMA and ADMA in whole cell extracts of the human colorectal cancer HCT116 cell line, human cervical cancer HeLa cell line, and human non-small cell lung cancer H460 cell line.

HeLa cells showed a very similar banding pattern with both the SDMA and ADMA antibodies. ADMA seemed to be most abundant in proteins above 35 kDa in all four cell lines, while SDMA was most abundant in proteins below 100 kDa. A protein with ADMA slightly above 15 kDa was observed in the HCT116 and HeLa cells. Proteins with SDMA with molecular weights of approximately 15 kDa, 20 kDa, and 30 kDa were observed at a high level in the 143B, HCT116, and HeLa cells, while multiple proteins with ADMA were observed in these three cell lines.

Extracts loaded on the gel represented approximately 250,000 cells. The left panel is an anti-SDMA immunoblot, and the right panel is an anti-ADMA immunoblot. Each has an exposure time of 3 seconds. These images are representative of two individual experiments.

Because arginine methylation on histones can affect gene expression, we wanted to analyze any differences in SDMA and ADMA modifications on histones between each cell line. Upon histone enrichment in the HCT116 and H460 cells, a histone with SDMA with a molecular

111
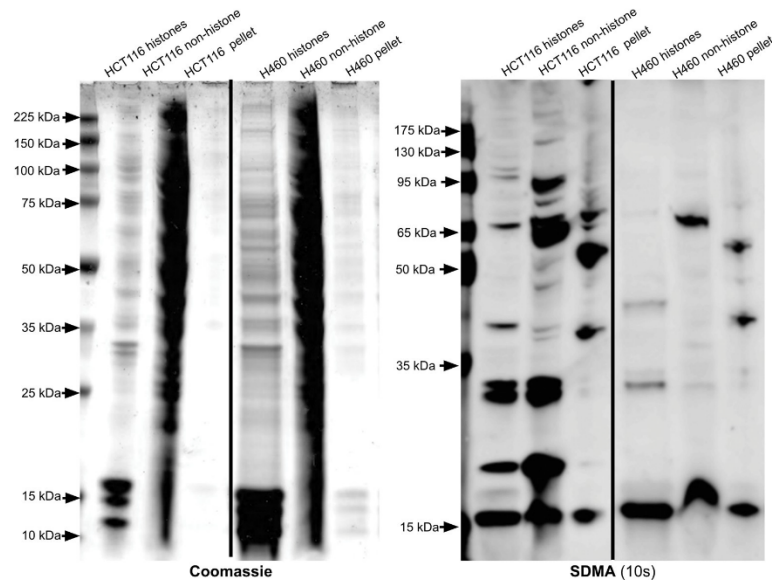
Fig 7. Identification of SDMA-containing polypeptides in histone and non-histone fractions of HCT116 and H460 cell extracts.

weight slightly above 15 kDa was observed (Fig 7 and S5 Fig). A similar result was seen in the 143B cells, where a non-histone 15 kDa protein and a histone protein slightly above 15 kDa both had the SDMA mark (Fig 3). A low signal for ADMA on a histone was seen in the HCT116 cells at slightly above 15 kDa (Fig 8). Meanwhile, the H460 cells do not appear to contain histones with ADMA, as there is little to no signal upon immunoblotting (Fig 8). The 143B histones also showed a signal near 15 kDa in the ADMA immunoblot (Fig 4). Overall, similarities in ADMA and SDMA on histones were observed between the HCT116 and 143B cells, while H460 cells seemed to lack ADMA on histones and non-histone proteins. These results support common patterns of protein arginine methylation in distinct cancer cell lines derived from various tissues. The significance of these common bands on anti-SDMA and anti-ADMA immunoblots is unknown and requires further experiments to elucidate their identity.

The left panel is a Coomassie-stained SDS-PAGE gel, and the right panel is an anti-SDMA immunoblot with an exposure time of 10 seconds. In this case, we utilized 12% SDS-PAGE gels (GenScript catalog #M01215). These images are representative of two individual experiments. Lanes from a single gel or blot were spliced together, as shown by the vertical black line, to remove irrelevant lanes.

The left panel is a Coomassie-stained SDS-PAGE gel, and the right panel is an anti-ADMA immunoblot with an exposure time of 30 seconds. In this case, we utilized 12% SDS-PAGE gels (GenScript catalog #M01215). These images are representative of two individual experiments. Lanes from a single gel or blot were spliced together, as shown by the vertical black line, to remove irrelevant lanes.

112
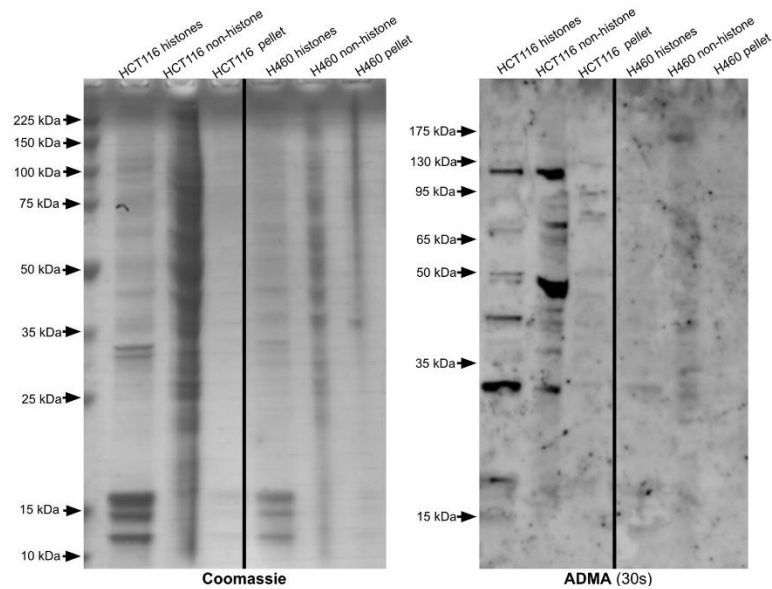
Fig 8. Identification of ADMA-containing polypeptides in histone and non-histone fractions of HCT116 and H460 cell extracts.

Discussion

Whether there exists a link between methionine addiction and PRMT activity in cancer cells is still unknown, but the results presented here suggest that there is no large-scale direct connection in an osteosarcoma cell line. The rationale for initiating this study included the fact that methionine is the direct precursor of AdoMet, itself the substrate for PRMTs, as well as the known overexpression of PRMTs in many types of cancer cells [36–45]. Additionally, methionine-independent revertants of other cancer cell lines have greatly reduced transmethylation reactions compared to their parental cells [29, 30]. In the present study, we examined the levels of methylated proteins resulting from PRMT activity and substrate availability in methionine-independent revertant 143B human osteosarcoma cells and their parent cells to understand the mechanism behind the revertants' loss of malignancy. Because the 143B-P cells relied more heavily on methionine than the 143B-R cells, different expression levels in protein arginine methylation were thought to be possible between parent and revertant cells. With the changes observed in markers of the epithelial-to-mesenchymal transition (EMT) and reported association between PRMTs and EMT, we expected there to be variations in proteins with ADMA and SDMA [28, 64]. Additionally, histone lysine methylation differed between the 143B-P and 143B-R cells, so we expected changes specifically in histone arginine methylation [28]. However, no major changes in protein arginine methylation were observed between the 143B-P and 143B-R cells, which suggests that changes in protein arginine methylation may not be central to the mechanism of reversion from methionine addiction to methionine independence.

In Fig 2, three proteins with SDMA with approximate molecular weights of 30 kDa, 20 kDa, and 15 kDa were seen at similar levels in the 143B-P and 143B-R cells. However, previous

113

literature using a different SDMA antibody on an immunoblot of 143B cells also shows one major band near 85 kDa and a minor band near 128 kDa, which differs from the results presented here [65]. This may be due to differences in the antibody detection or differences in the method of cell culture. In both the 143B-P and 143B-R cells, multiple proteins with ADMA modifications are present between approximately 175 kDa and 30 kDa at similar intensity levels. Arginine methylation on histones can affect gene expression, so we hypothesized that SDMA and ADMA on histones may play a role in the mechanism of reversion. However, no major differences were observed in ADMA or SDMA on histones between the 143B-P and 143B-R cells (Figs 4 and 5).

While there appears to be some PRMT5 substrates that are methylated less in the revertant than the parent cell lysates, no major differences were found in substrate availability with an enzymatic assay using 143B-P and 143B-R cell lysates, [^{3}H]-AdoMet, and PRMT enzymes (Fig 5). Because the banding pattern is similar between reactions with lysates only and those with PRMT enzymes added, it is possible that these bands show other types of protein methylation that are not catalyzed by PRMTs. While only arginine methylation was directly tested here, there appears to be no major differences in cytoplasmic protein methylation as a whole because the 143B-P and 143B-R cell lysates without PRMTs and with [^{3}H]-AdoMet show the same radioactive banding pattern. Although changes in histone lysine methylation between the 143B-P and 143B-R cells were seen previously, the method of cell lysis may not have lysed the nuclear membrane and did not solubilize histones, as shown in the Coomassie-stained gel that lacks histone bands [28]. Other than in protein methylation, AdoMet is the methyl donor in DNA and RNA methylation, which both can be deregulated in cancer [60, 66]. Twenhafel et. al has reviewed how epigenetic changes are associated with disease progression in osteosarcoma [67]. DNA methylation can suppress miRNAs, whose underexpression in osteosarcoma tissue is correlated with higher-stage tumors. Additionally, DNA methylation of tumor-suppressing genes can silence their transcription and therefore allow for further cancer progression. Methylation of RNA at adenosine bases leads to N6-methyladenosine (m6a), which is recognized by "reader" proteins, promoting translation of the mRNA. In osteosarcoma, methyltransferase-like protein 3, which adds a methyl group to form m6a, is linked to tumor progression. A methionine-restricted diet in a mouse model of colorectal carcinoma was shown to decrease m6a mRNA methylation in cancer cells [68]. DNA and RNA methylation were not explored in this study, but they could be altered as a result of a lower dependence on methionine. Because methionine metabolism includes pathways besides protein methylation, there are many possibilities for the mechanism of reversion from methionine addiction to methionine independence. These results suggest that protein arginine methylation may not be important in altering the osteosarcoma cells' methionine addiction. Interestingly, a previous study has shown that PRMT1 and methionine are both required for Wnt signaling activity in HeLa cells [69]. Methionine deprivation decreased PRMT1 colocalization with glycogen synthase kinase 3, an essential enzyme in Wnt signaling [69]. Thus, the association between methionine addiction and PRMT function may vary among different types of cancer cells.

PRMTs are generally overexpressed in cancer, and this study showed a direct comparison of proteins with SDMA and ADMA within various cancer cell lines. In the 143B, HCT116, and HeLa cells, many proteins with ADMA are present upon immunoblotting across a wide range of molecular weights (Fig 6). In previous literature, multiple bands ranging from 25 kDa to 150 kDa are also shown in an anti-ADMA immunoblot of an HCT116 cell lysate [70]. Additionally, human embryonic kidney 293T cells have multiple proteins with ADMA between 20kDa and 250 kDa, as well as three SDMA-containing proteins near 15 kDa, 20 kDa, and 30 kDa [57]. A previous report of ADMA in breast tumors found 403 ADMA sites on 213 proteins in patient-derived xenograft tumors, which highlights the extensive methylation by Type

114

I PRMTs in cancerous tissues [43]. The HCT116 and HeLa cells had the highest abundance of proteins with SDMA. HCT116 cells express the methylthioadenosine phosphorylase (MTAP) protein at a higher level than H460 cells, while 143B cells do not express MTAP [29, 71]. HeLa cells do express MTAP [72]. Without the MTAP enzyme, methylthioadenosine can accumulate since it cannot be phosphorylated by MTAP [54, 73]. Methylthioadenosine can inhibit PRMT5, which is the enzyme responsible for most SDMA in the cell [73]. This endogenous inhibition of PRMT5 mediated by *MTAP* deletion may affect SDMA levels because there are only three major bands on the SDMA immunoblot of the 143B cells. The relatively low abundance of proteins with SDMA in the 143B cells may be due to *MTAP* deletion. *MTAP*-deleted cell lines are more sensitive to methioninase treatment than those containing the *MTAP* gene, so it is surprising that the 143B-P and 143B-R cells did not have any major differences in PRMT5 activity [71]. Because they are more sensitive to PRMT inhibition, *MTAP*-deleted cancers can be selectively targeted [73]. Identifying the major substrates of PRMT5 that are still methylated in *MTAP*-deleted cancers may be important to understanding what reactions PRMT inhibitors are acting on in these cancers. Further experiments are necessary to elucidate the identity and importance of the common proteins with SDMA and ADMA found in the several cancer cell lines studied here.

While we have shown that PRMT activity may not be connected to methionine addiction as well as similarities in PRMT substrates between cancer cell lines, which are also methionine-addicted [29, 74], there are a few limitations to this study. Methionine-addicted cancer cell lines grown in methionine-depleted medium have low levels of free intracellular methionine as shown in Table 1 of Stern et. al, 1983 [8]. Whether there are differences in methionine concentrations between the 143B-P and 143-R cells remains unknown; however, it appears that any potential differences did not affect protein arginine methylation. Also, protein arginine methylation is stable in cells [75, 76]. HeLa cell extracts treated with adenosine dialdehyde, a methyltransferase inhibitor, still had many proteins with SDMA and ADMA present, although at a slightly lower level than HeLa cells cultured without any inhibitor [75]. Using [^{3}H]-Ado-Met, recombinantly purified PRMTs, and cell lysates to identify substrates may not account for stable proteins that have been modified by endogenous PRMTs during cell culture. Analyzing PRMT activity with similar methods but in synchronized cells would clarify whether variations exist in protein arginine methylation at different points in the cell cycle. PRMT3, 6, and 7 are differentially expressed depending on the stage of the cell cycle in synchronized HeLa cells [77]. While no differences in protein arginine methylation between the 143B-P and 143B-R cells were observed, it is possible that changes in ADMA may occur at specific points during cell growth and be observed in synchronized cells. Because overexpression of the PRMT enzymes is common in cancer cells, measuring the expression levels of each PRMT within the 143B-P and 143B-R cells would be an important future study to further elucidate the mechanisms of methionine addiction. Additionally, PRMT substrates may be different in vivo. A study analyzing ADMA on proteins in ER- and ER+ breast cancer showed a low amount of shared ADMA sites between tumor samples and in vitro samples [43]. While this study compared the abundance of SDMA and ADMA on proteins between various human cancer cell lines, a similar comparison among primary tumors in different tissues may produce distinct results. Finally, immunohistochemistry analyses could determine the localization of SDMA and ADMA containing proteins within parent and revertant cells. While this study has suggested no association between methionine addiction and protein arginine methylation in osteosarcoma, the mechanism of methionine addiction remains unknown. Future studies could use proteomics and RNAseq analyses in parent and revertant cells to elucidate the pathways important for methionine dependency.

115

Overall, elucidating the mechanism in which methionine restriction can affect cancer malignancy will be useful in developing targeted cancer therapeutics. With PRMT inhibitors entering clinical trials for cancer patients, it is important to understand how methionine deprivation on its own and in combination with these drugs may affect PRMT activity. The present results suggest that methionine addiction and the upregulation of PRMTs are distinct characteristics of osteosarcoma cells because the revertant cells with lowered methionine dependence showed no changes in PRMT activity.

Materials and methods

Preparation of cells and other materials

The 143B parent and revertant cell lines were cultured as previously described [28]. The HCT116 and H460 cells used in this study were the parent cell lines previously described in Yamamoto et. al [29]. Approximately 2,000,000 cells each of the HCT116, H460, 143B-P, and 143B-R grown in high-methionine medium were shipped to UCLA as a cell pellet on ice at 0°C from AntiCancer, Inc. A frozen cell pellet of approximately 500,000,000 cells of the HeLa-S3 epithelial suspension adapted cell line (C3 PN:HA48) was purchased from the Cell Culture Company (Minneapolis, MN). Upon arrival, the cells were either frozen at -80°C or were kept at 0°C. Cells were aliquoted by suspending them in 1 mL of 1X PBS (Phosphate Buffered Saline 10X Solution, Fisher Scientific, catalog #BP3991, lot #124561) and divided into approximately 250,000-cell aliquots for the HCT116, H460, and HeLa cells, and 200,000-cell aliquots for the 143B-P and 143B-R cells. In each case, the cells were spun down at 180 g for 5 min at 4°C. The new cell pellets and their PBS supernatants were stored separately at -80°C for future use. Uninduced, untransformed BL21 $E. coli$ were cultured in 10 mL LB media overnight at 37°C, leaving a final OD600 of 1.29. The cells were divided into 500 µL aliquots, which were lysed at 13,000 g at 4°C for 5 min.

Histone extraction

The EpiQuick Total Histone Extraction Kit (EpiGentek, catalog #OP-0006) was used to extract the histones from each cell line. One aliquot (250,000 cells for H460 and HCT116, and 200,000 cells for 143B-P and 143B-R cells) was used for each histone extraction, which resulted in 26 µL of histone material. The supernatant with non-histone proteins and the unextracted pellet that remained after using the kit were saved, and their proteins were fractionated on SDS-PAGE along with the histone-containing supernatants. For SDS-PAGE, the volume of sample applied was normalized to the protein concentration of histones measured using 3 µL of the histone fraction on a NanoDrop 2000c spectrophotometer. The absorption at 280 nm was calculated, where 1 mg/mL was assumed to give 1 A.

SDS-PAGE and immunoblotting

Each 200,000-cell 143B pellet, 250,000-cell H460 pellet, 250,000-cell HCT116 pellet, or 250,000-cell HeLa pellet was suspended in 200 µL 2X sample buffer (4% SDS, 20% glycerol, 120 mM Tris-HCl pH 6.8, 0.02% bromophenol blue, 5% beta-mercaptoethanol). Histone extraction fractions were diluted in 2X sample buffer or 5X sample buffer (10% SDS, 50% glycerol, 250 mM Tris-HCl pH 6.8, 0.05% bromophenol blue, 12.5% beta-mercaptoethanol). A 1.3 mg/mL solution of GST-GAR, prepared as described in Lowe et. al [62], was diluted in 2X sample buffer, and 6.5 µg were loaded onto the gel. Each $E. coli$ pellet was resuspended in 130 µL 2X sample buffer, and 15 µL were loaded onto the gel. For the purified histones, samples were analyzed of the histone fraction, the non-histone soluble fraction, and the non-

116

histone pellets obtained from the histone extraction kit described above. In Figs 3 and 4, histones and non-histone supernatants were diluted in 5X sample buffer at a 1:4 ratio, and non-histone pellets were resuspended in 50 μL 5X sample buffer. 15 μL of the non-histone supernatant and non-histone pellet were loaded into each well. For Fig 3, the 143B-P and 143B-R histones contained 1.6 mg/mL and 2.1 mg/mL, respectively, so 15 μL 143B-P histones and 11 μL 143B-R histones (19 μg) were loaded onto the gel. For Fig 4, the 143B-P and 143B-R histones contained 1.2 mg/mL and 0.7 mg/mL, respectively, so 11 μL 143B-P histones and 20 μL 143B-R histones (11 μg) were loaded onto the gel. In Figs 7 and 8, histones and non-histone supernatants were diluted in 2X sample buffer at a 1:1 ratio, and non-histone pellets were resuspended in 200 μL 2X sample buffer. 15 μL of the non-histone supernatant and non-histone pellet were loaded into each well. For Fig 7, the HCT116 and H460 histones contained 5.8 mg/mL and 2.3 mg/mL, respectively, so 8 μL HCT116 histones and 20 μL H460 histones (23 μg) were loaded onto the gel. For Fig 8, the HCT116 and H460 histones contains 2.2 mg/mL and 3.9 mg/mL, respectively, so 15 μL HCT116 histones and 9 μL H460 histones (17 μg) were loaded onto the gel. Whole cell extracts in 2X sample buffer were drawn up and down 20 times in a 1 mL syringe with luer-lock and a 20 gauge needle (BD PrecisionGlide™ Needle; 20G * 1 ½ (0.9mm * 40mm)) to shear the DNA. Each sample was heated at 95°C for 3 minutes. The whole cell extract was separated with 35 μL in each well on a 4–20% (unless otherwise mentioned) ExpressPlus PAGE gel (GenScript catalog #M42010) at 140V for 1 hour using a BioRad PowerPac 300 electrophoresis Power supply with Tris-MOPS-SDS running buffer (GenScript Tris-MOPS-SDS Running Buffer Powder; 50 mM Tris Base, 50 mM MOPS, 0.1% SDS, 1 mM EDTA). Coomassie staining was performed on a separate gel with identical loading as a control for the amount of protein. Gels were stained for 1 hour with Coomassie (0.1% (w/v) Brilliant Blue R-250, 10% (v/v) glacial acetic acid, and 50% (v/v) methanol) and destained overnight with 10% (v/v) acetic acid and 15% (v/v) methanol. For immunoblotting, gels were transferred onto a PVDF membrane with transfer buffer (10% (v/v) Tris-glycine, 10% (v/v) methanol) at 30V for 2 hours with ice using a BioRad PowerPac 300 electrophoresis Power supply. The blocking buffer used was 5% bovine serum albumin (BSA) in TBS-T (20 mM Tris, 137 mM NaCl, 0.1% (v/v) Tween-20, pH 7.6). The primary antibodies used in this study were rabbit polyclonal anti-SDMA, anti-ADMA, and anti-MMA (1:2000, generously gifted from Dr. Mark T. Bedford [57]). The immunogens were short GAR motifs with either the SDMA, ADMA, or MMA modification separated by polyethylene glycol linkers. The secondary antibody used was goat anti-rabbit IgG (H + L) Alexa Fluor Plus 647 (1:2000, Thermo Fisher, catalog #A32733). All antibody solutions were diluted in 5% BSA in TBS-T. Molecular weights of proteins were calculated using ImageJ (Version 2.1.0/1.53c).

SDS-PAGE fluorography with [^{3}H]AdoMet

Approximately 1,000,000 cells were lysed in 100 μL of NP-40 cell lysis buffer (1 EDTA-free protease inhibitor tablet per 50 mL (Catalog No. PIA32965, Thermo Scientific), 50 mM HEPES, pH 7.6, 150 mM NaCl, 7% beta-mercaptoethanol, 1% NP-40). Cells were lysed at 13,000 g for 1 minute. Each reaction mixture contained 33.3% (v/v) cell lysate, 50 mM HEPES pH = 9.0 (9.5 for PRMT7), 1 mM DTT, and 0.14 μM S-adenosyl-L-[methyl-^{3}H] methionine ([^{3}H]AdoMet; Catalog No. NET155H001MC, PerkinElmer Life Sciences; 81.9 Ci/mmol, 7 μM in 9:1 10 mM H_2SO_4:ethanol). Reactions with PRMTs contained either 0.20 μg PRMT1, 0.076 μg PRMT5, or 5.5 μg PRMT7. Each reaction also contained 2 μM MS023 (MedChemExpress, catalog # HY-19615) [78], 20 μM EPZ015666 (MedChemExpress, catalog # HY-12727) [79], 200 nM SGC8158 [80], or 3.33% (v/v) DMSO. Incubation temperature was 37°C for PRMT1, PRMT5, and controls, and 20°C for PRMT7. Incubation time was one hour.

117

Reactions were terminated with 5X sample buffer, and 30 μL of the reaction were fractionated with SDS-PAGE as described above. Gels were incubated with EN^{3}HANCE (PerkinElmer Life Sciences, catalog #6NE9701) for 1 hour, incubated in water for 30 minutes, and dried before the gels were exposed to film (Denville Scientific, 8 X 10 in. Hyblot Cl) at -80°C for 63 days. The eight reactions consisted of the following: lysate only; PRMT1, lysate; PRMT5, lysate; PRMT7, lysate; PRMT1, lysate, EPZ015666, SGC8158; PRMT5, lysate, MS023, SGC8158; PRMT7, lysate, MS023, EPZ015666; lysate, no enzyme, MS023, EPZ015666, SGC8158.

Supporting information

S1 Fig. Validating antibodies against SDMA and ADMA. 143B-R whole cell extracts were used as positive controls, and GST-GAR and *E. coli* extracts were used as negative controls. To ensure the antibodies recognized the arginine methylation modification rather than the glycine and arginine rich regions, an unmethylated GST-tagged protein, based on the N-terminus of human fibrillarin that contains a glycine and arginine rich region (GST-GAR), was used as a negative control. Another negative control was an extract of untransformed and uninduced BL21 *Escherichia coli* (*E. coli*) lysate. The first and third panels show Coomassie-stained SDS-PAGE gels. The second and fourth panels are immunoblots using the SDMA antibody or ADMA antibody with exposure times of 3 seconds or 10 seconds, respectively. Lanes from a single gel or blot were spliced together, as shown by the vertical black line, to remove irrelevant lanes. The same lanes for the parent cells and parent histones are shown in Figs 2 and 4, respectively.
(TIF)

S2 Fig. Identification of proteins containing SDMA and ADMA in human parent and revertant 143B osteosarcoma cells: Replicate experiment. This shows an individual replicate experiment of the same conditions as in Fig 2. The leftmost panel shows a Coomassie-stained SDS-PAGE gel. The middle panel and rightmost panel show an anti-SDMA immunoblot and an anti-ADMA immunoblot, respectively, each with a 30 second exposure time. Molecular weight markers are shown at the left in the Coomassie-stained gel and as fluorescent bands on the left margin of the immunoblots.
(TIF)

S3 Fig. Identification of SDMA-containing polypeptides in histone and non-histone fractions of parent and revertant human osteosarcoma 143B cells. This shows a higher exposure (30 seconds) of the immunoblot in Fig 3 to show the histone band more clearly.
(TIF)

S4 Fig. Identification of proteins containing SDMA and ADMA in whole cell extracts of the human colorectal cancer HCT116 cell line, human cervical cancer HeLa cell line, and human non-small cell lung cancer H460 cell line. This shows a higher exposure (10 seconds) of the immunoblots in Fig 6. The left panel is an anti-SDMA immunoblot, and the right panel is an anti-ADMA immunoblot.
(TIF)

S5 Fig. Identification of SDMA-containing polypeptides in histone and non-histone fractions of HCT116 and H460 cell extracts. This shows a higher exposure (30 seconds) of the anti-SDMA immunoblot in Fig 7.
(TIF)

S1 Raw images. Original data for all immunoblots.
(PDF)

118

S1 File. Original data for <u>Fig 1</u> graph.
(XLSX)

Acknowledgments

Author Contributions

Conceptualization: Ashley G. Holtz, Troy L. Lowe, Robert M. Hoffman, Steven G. Clarke.

Data curation: Ashley G. Holtz, Yusuke Aoki, Yutaro Kubota.

Formal analysis: Ashley G. Holtz.

Funding acquisition: Robert M. Hoffman, Steven G. Clarke.

Investigation: Ashley G. Holtz.

Methodology: Ashley G. Holtz, Troy L. Lowe, Yusuke Aoki, Yutaro Kubota, Robert M. Hoffman, Steven G. Clarke.

Resources: Troy L. Lowe, Robert M. Hoffman, Steven G. Clarke.

Supervision: Troy L. Lowe, Robert M. Hoffman, Steven G. Clarke.

Writing – original draft: Ashley G. Holtz.

Writing – review & editing: Ashley G. Holtz, Troy L. Lowe, Yusuke Aoki, Yutaro Kubota, Robert M. Hoffman, Steven G. Clarke.

References

1. Hoffman RM, Erbe RW. High in vivo rates of methionine biosynthesis in transformed human and malignant rat cells auxotrophic for methionine. Proc Natl Acad Sci U S A. 1976 May; 73(5):1523–7. https://doi.org/10.1073/pnas.73.5.1523 PMID: 179090

2. Kaiser P. Methionine Dependence of Cancer. Biomolecules. 2020 Apr; 10(4):568. https://doi.org/10.3390/biom10040568 PMID: 32276408

3. Yamamoto J, Han Q, Simon M, Thomas D, Hoffman RM. Methionine Restriction: Ready for Prime Time in the Cancer Clinic? Anticancer Res. 2022 Feb; 42(2):641–4. https://doi.org/10.21873/anticanres.15521 PMID: 35093861

4. Chello PL, Bertino JR. Dependence of 5-Methyltetrahydrofolate Utilization by L5178Y Murine Leukemia Cells in Vitro on the Presence of Hydroxycobalamin and Transcobalamin II1. Cancer Res. 1973 Aug 1; 33(8):1898–904.

5. Wang Z, Yip LY, Lee JHJ, Wu Z, Chew HY, Chong PKW, et al. Methionine is a metabolic dependency of tumor-initiating cells. Nat Med. 2019 May; 25(5):825–37. https://doi.org/10.1038/s41591-019-0423-5 PMID: 31061538

6. Halpern BC, Clark BR, Hardy DN, Halpern RM, Smith RA. The Effect of Replacement of Methionine by Homocystine on Survival of Malignant and Normal Adult Mammalian Cells in Culture. Proc Natl Acad Sci U S A. 1974 Apr; 71(4):1133–6. https://doi.org/10.1073/pnas.71.4.1133 PMID: 4524624

7. Coalson DW, Mecham JO, Stern PH, Hoffman RM. Reduced availability of endogenously synthesized methionine for S-adenosylmethionine formation in methionine-dependent cancer cells. Proc Natl Acad Sci. 1982 Jul; 79(14):4248–51. https://doi.org/10.1073/pnas.79.14.4248 PMID: 6289297

8. Stern PH, Mecham JO, Wallace CD, Hoffman RM. Reduced free-methionine in methionine-dependent SV40-transformed human fibroblasts synthesizing apparently normal amounts of methionine. J Cell Physiol. 1983; 117(1):9–14. https://doi.org/10.1002/jcp.1041170103 PMID: 6311851

119

9.   Kubota Y, Han Q, Aoki Y, Masaki N, Obara K, Hamada K, et al. Synergy of Combining Methionine Restriction and Chemotherapy: The Disruptive Next Generation of Cancer Treatment. Cancer Diagn Progn. 2023; 3(3):272–81. https://doi.org/10.21873/cdp.10212 PMID: 37168964

10. Sugisawa N, Yamamoto J, Han Q, Tan Y, Tashiro Y, Nishino H, et al. Triple-Methyl Blockade With Recombinant Methioninase, Cycloleucine, and Azacitidine Arrests a Pancreatic Cancer Patient-Derived Orthotopic Xenograft Model. Pancreas. 2021 Jan; 50(1):93. https://doi.org/10.1097/MPA.0000000000001709 PMID: 33370029

11. Hens JR, Sinha I, Perodin F, Cooper T, Sinha R, Plummer J, et al. Methionine-restricted diet inhibits growth of MCF10AT1-derived mammary tumors by increasing cell cycle inhibitors in athymic nude mice. BMC Cancer. 2016 Jun 3; 16(1):349.

12. Hoffman RM, Hoshiya Y, Guo W. Efficacy of Methionine-Restricted Diets on Cancers In Vivo. In: Hoffman RM, editor. Methionine Dependence of Cancer and Aging: Methods and Protocols [Internet]. New York, NY: Springer; 2019 [cited 2023 Mar 11]. p. 75–81. (Methods in Molecular Biology). Available from: https://doi.org/10.1007/978-1-4939-8796-2_7

13. Higuchi T, Han Q, Sugisawa N, Yamamoto J, Yamamoto N, Hayashi K, et al. Combination Methionine-methylation-axis Blockade: A Novel Approach to Target the Methionine Addiction of Cancer. Cancer Genomics Proteomics. 2021; 18(2):113–20. https://doi.org/10.21873/cgp.20246 PMID: 33608308

14. Miyake K, Han Q, Murakami T, Kiyuna T, Kawaguchi K, Igarashi K, et al. Colon-cancer liver metastasis is effectively targeted by recombinant methioninase (rMETase) in an orthotopic mouse model. Tissue Cell. 2023 Aug 1; 83:102125. https://doi.org/10.1016/j.tice.2023.102125 PMID: 37320867

15. Kubota Y, Sato T, Hozumi C, Han Q, Aoki Y, Masaki N, et al. Superiority of [11C]methionine over [18F] deoxyglucose for PET Imaging of Multiple Cancer Types Due to the Methionine Addiction of Cancer. Int J Mol Sci. 2023 Jan 18; 24(3):1935.

16. Park YJ, Lee JW, Cho HW, Choe YS, Lee KH, Choi JY, et al. Value of C-11 methionine PET/CT in patients with intracranial germinoma. PLOS ONE. 2022 Feb 7; 17(2):e0263690. https://doi.org/10.1371/journal.pone.0263690 PMID: 35130327

17. Tomura N, Saginoya T, Goto H. PET findings in lymphomatosis and gliomatosis of the brain: a comparison of C-11 methionine PET/CT and F-18 FDG PET/CT. Acta Radiol. 2021 Oct 1; 62(10):1391–6. https://doi.org/10.1177/0284185120966710 PMID: 33081486

18. Hoffman RM. Clinical Studies of Methionine-Restricted Diets for Cancer Patients. In: Hoffman RM, editor. Methionine Dependence of Cancer and Aging: Methods and Protocols [Internet]. New York, NY: Springer; 2019 [cited 2023 Mar 11]. p. 95–105. (Methods in Molecular Biology). Available from: https://doi.org/10.1007/978-1-4939-8796-2_9

19. Tan Y, Zavala J, Han Q, Xu M, Sun X, Tan X, et al. Recombinant methioninase infusion reduces the biochemical endpoint of serum methionine with minimal toxicity in high-stage cancer patients. Anticancer Res. 1997; 17(5B):3857–60. PMID: 9427792

20. Tan Y, Zavala J, Xu M, Zavala J, Hoffman RM. Serum methionine depletion without side effects by methioninase in metastatic breast cancer patients. Anticancer Res. 1996; 16(6C):3937–42. PMID: 9042316

21. Han Q, Tan Y, Hoffman RM. Oral dosing of Recombinant Methioninase Is Associated With a 70% Drop in PSA in a Patient With Bone-metastatic Prostate Cancer and 50% Reduction in Circulating Methionine in a High-stage Ovarian Cancer Patient. Anticancer Res. 2020 May 1; 40(5):2813–9. https://doi.org/10.21873/anticanres.14254 PMID: 32366428

22. Han Q, Hoffman RM. Chronic Treatment of an Advanced Prostate-cancer Patient With Oral Methioninase Resulted in Long-term Stabilization of Rapidly Rising PSA Levels. In Vivo. 2021 Jul 1; 35(4):2171–6. https://doi.org/10.21873/invivo.12488 PMID: 34182494

23. Han Q, Hoffman RM. Lowering and Stabilizing PSA Levels in Advanced-prostate Cancer Patients With Oral Methioninase. Anticancer Res. 2021 Apr 1; 41(4):1921–6. https://doi.org/10.21873/anticanres.14958 PMID: 33813397

24. Kubota Y, Han Q, Hamada K, Aoki Y, Masaki N, Obara K, et al. Long-term Stable Disease in a Rectal-cancer Patient Treated by Methionine Restriction With Oral Recombinant Methioninase and a Low-methionine Diet. Anticancer Res. 2022 Aug 1; 42(8):3857–61. https://doi.org/10.21873/anticanres.15877 PMID: 35896248

25. Kubota Y, Han Q, Masaki N, Hozumi C, Hamada K, Aoki Y, et al. Elimination of Axillary-Lymph-Node Metastases in a Patient With Invasive Lobular Breast Cancer Treated by First-line Neo-adjuvant Chemotherapy Combined With Methionine Restriction. Anticancer Res. 2022 Dec 1; 42(12):5819–23. https://doi.org/10.21873/anticanres.16089 PMID: 36456116

26. Kubota Y, Han Q, Hozumi C, Masaki N, Yamamoto J, Aoki Y, et al. Stage IV Pancreatic Cancer Patient Treated With FOLFIRINOX Combined With Oral Methioninase: A Highly-Rare Case With Long-term

120

Stable Disease. Anticancer Res. 2022 May 1; 42(5):2567–72. https://doi.org/10.21873/anticanres. 15734 PMID: 35489727

27. Sanderson SM, Gao X, Dai Z, Locasale JW. Methionine metabolism in health and cancer: a nexus of diet and precision medicine. Nat Rev Cancer. 2019 Nov; 19(11):625–37. https://doi.org/10.1038/ s41568-019-0187-8 PMID: 31515518

28. Aoki Y, Han Q, Tome Y, Yamamoto J, Kubota Y, Masaki N, et al. Reversion of methionine addiction of osteosarcoma cells to methionine independence results in loss of malignancy, modulation of the epithe-lial-mesenchymal phenotype and alteration of histone-H3 lysine-methylation. Front Oncol [Internet]. 2022 [cited 2023 Jan 11];12. Available from: https://www.frontiersin.org/articles/10.3389/fonc.2022. 1009548 PMID: 36408173

29. Yamamoto J, Inubushi S, Han Q, Tashiro Y, Sugisawa N, Hamada K, et al. Linkage of methionine addic-tion, histone lysine hypermethylation, and malignancy. iScience. 2022 Apr 15; 25(4):104162. https://doi. org/10.1016/j.isci.2022.104162 PMID: 35434545

30. Judde JG, Ellis M, Frost P. Biochemical Analysis of the Role of Transmethylation in the Methionine Dependence of Tumor Cells1. Cancer Res. 1989 Sep 1; 49(17):4859–65.

31. Stern PH, Wallace CD, Hoffman RM. Altered methionine metabolism occurs in all members of a set of diverse human tumor cell lines. J Cell Physiol. 1984; 119(1):29–34. https://doi.org/10.1002/jcp. 1041190106 PMID: 6707100

32. Stern PH, Hoffman RM. Elevated overall rates of transmethylation in cell lines from diverse human tumors. In Vitro. 1984 Aug; 20(8):663–70. https://doi.org/10.1007/BF02619617 PMID: 6500606

33. Yamamoto J, Aoki Y, Inubushi S, Han Q, Hamada K, Tashiro Y, et al. Extent and Instability of Trimethy-lation of Histone H3 Lysine Increases With Degree of Malignancy and Methionine Addiction. Cancer Genomics Proteomics. 2022; 19(1):12–8. https://doi.org/10.21873/cgp.20299 PMID: 34949655

34. AOKI Y, YAMAMOTO J, TOME Y, HAMADA K, MASAKI N, INUBUSHI S, et al. Over-methylation of Histone H3 Lysines Is a Common Molecular Change Among the Three Major Types of Soft-tissue Sar-coma in Patient-derived Xenograft (PDX) Mouse Models. Cancer Genomics Proteomics. 2021 Nov 3; 18(6):715–21. https://doi.org/10.21873/cgp.20292 PMID: 34697064

35. Yamamoto J, Han Q, Inubushi S, Sugisawa N, Hamada K, Nishino H, et al. Histone methylation status of H3K4me3 and H3K9me3 under methionine restriction is unstable in methionine-addicted cancer cells, but stable in normal cells. Biochem Biophys Res Commun. 2020 Dec 17; 533(4):1034–8. https:// doi.org/10.1016/j.bbrc.2020.09.108 PMID: 33019978

36. Yang Y, Bedford MT. Protein arginine methyltransferases and cancer. Nat Rev Cancer. 2013 Jan; 13 (1):37–50. https://doi.org/10.1038/nrc3409 PMID: 23235912

37. Xu J, Richard S. Cellular pathways influenced by protein arginine methylation: Implications for cancer. Mol Cell. 2021 Nov 4; 81(21):4357–68. https://doi.org/10.1016/j.molcel.2021.09.011 PMID: 34619091

38. Li S, Cheng D, Zhu B, Yang Q. The Overexpression of CARM1 Promotes Human Osteosarcoma Cell Proliferation through the pGSK3β/β-Catenin/cyclinD1 Signaling Pathway. Int J Biol Sci. 2017 Jul 18; 13 (8):976–84.

39. Wu K, Li W, Liu H, Niu C, Shi Q, Zhang J, et al. Metabolome Sequencing Reveals that Protein Arginine-N-Methyltransferase 1 Promotes the Progression of Invasive Micropapillary Carcinoma of the Breast and Predicts a Poor Prognosis. Am J Pathol [Internet]. 2023 Jun 9 [cited 2023 Aug 2]; Available from: https://www.sciencedirect.com/science/article/pii/S000294402300202X PMID: 37301537

40. Liao Y, Luo Z, Lin Y, Chen H, Chen T, Xu L, et al. PRMT3 drives glioblastoma progression by enhancing HIF1A and glycolytic metabolism. Cell Death Dis. 2022 Nov 9; 13(11):1–14. https://doi.org/10.1038/ s41419-022-05389-1 PMID: 36351894

41. Suresh S, Huard S, Brisson A, Némati F, Dakroub R, Poulard C, et al. PRMT1 Regulates EGFR and Wnt Signaling Pathways and Is a Promising Target for Combinatorial Treatment of Breast Cancer. Can-cers. 2022 Jan; 14(2):306. https://doi.org/10.3390/cancers14020306 PMID: 35053470

42. Huang T, Yang Y, Song X, Wan X, Wu B, Sastry N, et al. PRMT6 methylation of RCC1 regulates mito-sis, tumorigenicity, and radiation response of glioblastoma stem cells. Mol Cell. 2021 Mar 18; 81 (6):1276–1291.e9. https://doi.org/10.1016/j.molcel.2021.01.015 PMID: 33539787

43. Ma M, Liu F, Miles HN, Kim EJ, Fields L, Xu W, et al. Proteome-wide Profiling of Asymmetric Dimethy-lated Arginine in Human Breast Tumors. J Am Soc Mass Spectrom [Internet]. 2023 Jul 18 [cited 2023 Jul 24]; Available from: https://doi.org/10.1021/jasms.3c00154 PMID: 37463068

44. Amano Y, Matsubara D, Yoshimoto T, Tamura T, Nishino H, Mori Y, et al. Expression of protein arginine methyltransferase-5 in oral squamous cell carcinoma and its significance in epithelial-to-mesenchymal transition. Pathol Int. 2018; 68(6):359–66. https://doi.org/10.1111/pin.12666 PMID: 29603824

121

45. Xie F, Zhang H, Zhu K, Jiang C, Zhang X, Chang H, et al. PRMT5 promotes ovarian cancer growth through enhancing Warburg effect by methylating ENO1. MedComm. 2023 Mar 28; 4(2):e245. https://doi.org/10.1002/mco2.245 PMID: 36999124

46. Brobbey C, Liu L, Yin S, Gan W. The Role of Protein Arginine Methyltransferases in DNA Damage Response. Int J Mol Sci. 2022 Aug 29; 23(17):9780. https://doi.org/10.3390/ijms23179780 PMID: 36077176

47. Bedford MT, Clarke SG. Protein Arginine Methylation in Mammals: Who, What, and Why. Mol Cell. 2009 Jan 16; 33(1):1–13.

48. Jain K, Clarke SG. PRMT7 as a unique member of the protein arginine methyltransferase family: A review. Arch Biochem Biophys. 2019 Apr 15; 665:36–45. https://doi.org/10.1016/j.abb.2019.02.014 PMID: 30802433

49. Tang J, Frankel A, Cook RJ, Kim S, Paik WK, Williams KR, et al. PRMT1 Is the Predominant Type I Protein Arginine Methyltransferase in Mammalian Cells*. J Biol Chem. 2000 Mar 17; 275(11):7723–30. https://doi.org/10.1074/jbc.275.11.7723 PMID: 10713084

50. Branscombe TL, Frankel A, Lee JH, Cook JR, Yang Z hong, Pestka S, et al. PRMT5 (Janus Kinase-binding Protein 1) Catalyzes the Formation of Symmetric Dimethylarginine Residues in Proteins *. J Biol Chem. 2001 Aug 1; 276(35):32971–6. https://doi.org/10.1074/jbc.M105412200 PMID: 11413150

51. Dhar S, Vemulapalli V, Patananan AN, Huang GL, Di Lorenzo A, Richard S, et al. Loss of the major Type I arginine methyltransferase PRMT1 causes substrate scavenging by other PRMTs. Sci Rep. 2013; 3:1311. https://doi.org/10.1038/srep01311 PMID: 23419748

52. Wu Q, Schapira M, Arrowsmith CH, Barsyte-Lovejoy D. Protein arginine methylation: from enigmatic functions to therapeutic targeting. Nat Rev Drug Discov. 2021 Jul; 20(7):509–30. https://doi.org/10.1038/s41573-021-00159-8 PMID: 33742187

53. Dong J, Duan J, Hui Z, Garrido C, Deng Z, Xie T, et al. An updated patent review of protein arginine N-methyltransferase inhibitors (2019–2022). Expert Opin Ther Pat. 2022 Dec; 32(12):1185–205. https://doi.org/10.1080/13543776.2022.2163162 PMID: 36594709

54. Clarke SG. 16 Inhibition of mammalian protein methyltransferases by 5′-methylthioadenosine (MTA): A mechanism of action of dietary same? In: Clarke SG, Tamanoi F, editors. The Enzymes [Internet]. Academic Press; 2006 [cited 2023 Jan 11]. p. 467–93. (Protein Methyltransferases; vol. 24). Available from: https://www.sciencedirect.com/science/article/pii/S1874604706800181

55. El-Khoueiry AB, Clarke J, Neff T, Crossman T, Ratia N, Rathi C, et al. Phase 1 study of GSK3368715, a type I PRMT inhibitor, in patients with advanced solid tumors. Br J Cancer. 2023 May 26;1–9. https://doi.org/10.1038/s41416-023-02276-0 PMID: 37237172

56. Vieito M, Moreno V, Spreafico A, Brana I, Wang JS, Preis M, et al. Phase 1 Study of JNJ-64619178, a Protein Arginine Methyltransferase 5 Inhibitor, in Advanced Solid Tumors. Clin Cancer Res. 2023 Aug 1;OF1–11. https://doi.org/10.1158/1078-0432.CCR-23-0092 PMID: 37491846

57. Wang Y, Person MD, Bedford MT. Pan-methylarginine antibody generation using PEG linked GAR motifs as antigens. Methods. 2022 Apr 1; 200:80–6. https://doi.org/10.1016/j.ymeth.2021.06.005 PMID: 34107353

58. Thandapani P, O'Connor TR, Bailey TL, Richard S. Defining the RGG/RG Motif. Mol Cell. 2013 Jun 6; 50(5):613–23. https://doi.org/10.1016/j.molcel.2013.05.021 PMID: 23746349

59. Liu Q, Dreyfuss G. In vivo and in vitro arginine methylation of RNA-binding proteins. Mol Cell Biol. 1995 May; 15(5):2800–8. https://doi.org/10.1128/MCB.15.5.2800 PMID: 7739561

60. Michalak EM, Burr ML, Bannister AJ, Dawson MA. The roles of DNA, RNA and histone methylation in ageing and cancer. Nat Rev Mol Cell Biol. 2019 Oct; 20(10):573–89. https://doi.org/10.1038/s41580-019-0143-1 PMID: 31270442

61. Di Lorenzo A, Bedford MT. Histone arginine methylation. FEBS Lett. 2011; 585(13):2024–31. https://doi.org/10.1016/j.febslet.2010.11.010 PMID: 21074527

62. Lowe TL, Clarke SG. Human protein arginine methyltransferases (PRMTs) can be optimally active under nonphysiological conditions. J Biol Chem. 2022 Sep; 298(9):102290. https://doi.org/10.1016/j.jbc.2022.102290 PMID: 35868559

63. Homma T, Kobayashi S, Fujii J. Methionine Deprivation Reveals the Pivotal Roles of Cell Cycle Progression in Ferroptosis That Is Induced by Cysteine Starvation. Cells. 2022 Jan; 11(10):1603. https://doi.org/10.3390/cells11101603 PMID: 35626640

64. Qin J, Xu J. Arginine methylation in the epithelial-to-mesenchymal transition. FEBS J. 2022 Dec; 289(23):7292–303. https://doi.org/10.1111/febs.16152 PMID: 34358413

65. Mu H, Liu C, Zhang Q, Meng H, Yu S, Zeng K, et al. Magnetic-Driven Hydrogel Microrobots Selectively Enhance Synthetic Lethality in MTAP-Deleted Osteosarcoma. Front Bioeng Biotechnol [Internet]. 2022 [cited 2023 Mar 17];10. Available from: https://www.frontiersin.org/articles/10.3389/fbioe.2022.911455

122

66. Diala ES, Hoffman RM. Hypomethylation of hela cell DNA and the absence of 5-methylcytosine in SV40 and adenovirus (type 2) DNA: Analysis by HPLC. Biochem Biophys Res Commun. 1982 Jul 16; 107 (1):19–26. https://doi.org/10.1016/0006-291x(82)91663-1 PMID: 6289818

67. Twenhafel L, Moreno D, Punt T, Kinney M, Ryznar R. Epigenetic Changes Associated with Osteosarcoma: A Comprehensive Review. Cells. 2023 Jun 9; 12(12):1595. https://doi.org/10.3390/cells12121595 PMID: 37371065

68. Li T, Tan YT, Chen YX, Zheng XJ, Wang W, Liao K, et al. Methionine deficiency facilitates antitumour immunity by altering m6A methylation of immune checkpoint transcripts. Gut. 2023 Mar 1; 72(3):501–11. https://doi.org/10.1136/gutjnl-2022-326928 PMID: 35803704

69. Albrecht LV, Bui MH, De Robertis EM. Canonical Wnt is inhibited by targeting one-carbon metabolism through methotrexate or methionine deprivation. Proc Natl Acad Sci. 2019 Feb 19; 116(8):2987–95. https://doi.org/10.1073/pnas.1820161116 PMID: 30679275

70. Lim Y, Lee JY, Ha SJ, Yu S, Shin JK, Kim HC. Proteome-wide identification of arginine methylation in colorectal cancer tissues from patients. Proteome Sci. 2020 May 19; 18:6. https://doi.org/10.1186/s12953-020-00162-8 PMID: 32467672

71. Aoki Y, Tome Y, Han Q, Yamamoto J, Hamada K, Masaki N, et al. Deletion of MTAP Highly Sensitizes Osteosarcoma Cells to Methionine Restriction With Recombinant Methioninase. Cancer Genomics Proteomics. 2022 May 1; 19(3):299–304. https://doi.org/10.21873/cgp.20321 PMID: 35430564

72. Tang B, Kadariya Y, Chen Y, Slifker M, Kruger WD. Expression of MTAP Inhibits Tumor-Related Phenotypes in HT1080 Cells via a Mechanism Unrelated to Its Enzymatic Function. G3 GenesGenomesGenetics. 2014 Nov 11; 5(1):35–44.

73. Marjon K, Cameron MJ, Quang P, Clasquin MF, Mandley E, Kunii K, et al. MTAP Deletions in Cancer Create Vulnerability to Targeting of the MAT2A/PRMT5/RIOK1 Axis. Cell Rep. 2016 Apr 19; 15(3):574–87. https://doi.org/10.1016/j.celrep.2016.03.043 PMID: 27068473

74. Mecham JO, Rowitch D, Wallace CD, Stern PH, Hoffman RM. The metabolic defect of methionine dependence occurs frequently in human tumor cell lines. Biochem Biophys Res Commun. 1983 Dec 16; 117(2):429–34. https://doi.org/10.1016/0006-291x(83)91218-4 PMID: 6661235

75. Chen DH, Wu KT, Hung CJ, Hsieh M, Li C. Effects of adenosine dialdehyde treatment on in vitro and in vivo stable protein methylation in HeLa cells. J Biochem (Tokyo). 2004 Sep; 136(3):371–6. https://doi.org/10.1093/jb/mvh131 PMID: 15598895

76. Najbauer J, Johnson BA, Aswad DW. Analysis of stable protein methylation in cultured cells. Arch Biochem Biophys. 1992 Feb 14; 293(1):85–92. https://doi.org/10.1016/0003-9861(92)90369-8 PMID: 1731643

77. Kim C, Lim Y, Yoo BC, Won NH, Kim S, Kim G. Regulation of post-translational protein arginine methylation during HeLa cell cycle. Biochim Biophys Acta BBA—Gen Subj. 2010 Sep 1; 1800(9):977–85. https://doi.org/10.1016/j.bbagen.2010.06.004 PMID: 20541591

78. Eram MS, Shen Y, Szewczyk M, Wu H, Senisterra G, Li F, et al. A Potent, Selective and Cell-active Inhibitor of Human Type I Protein Arginine Methyltransferases. ACS Chem Biol. 2016 Mar 18; 11 (3):772–81. https://doi.org/10.1021/acschembio.5b00839 PMID: 26598975

79. Chan-Penebre E, Kuplast KG, Majer CR, Boriack-Sjodin PA, Wigle TJ, Johnston LD, et al. A selective inhibitor of PRMT5 with in vivo and in vitro potency in MCL models. Nat Chem Biol. 2015 Jun; 11 (6):432–7. https://doi.org/10.1038/nchembio.1810 PMID: 25915199

80. Szewczyk MM, Ishikawa Y, Organ S, Sakai N, Li F, Halabelian L, et al. Pharmacological inhibition of PRMT7 links arginine monomethylation to the cellular stress response. Nat Commun. 2020 May 14; 11 (1):2396. https://doi.org/10.1038/s41467-020-16271-z PMID: 32409666

123

Chapter 6: Supporting information

Asymmetric and symmetric protein arginine methylation in methionine-addicted human cancer cells

Ashley G. Holtz, Troy L. Lowe, Yusuke Aoki, Yutaro Kubota, Robert M. Hoffman, and Steven G. Clarke

List of material included:

Figure S1: Validating antibodies against SDMA and ADMA.

Figure S2: Identification of proteins containing SDMA and ADMA in human parent and revertant 143B osteosarcoma cells: Replicate experiment.

Figure S3: Identification of SDMA-containing polypeptides in histone and non-histone fractions of parent and revertant human osteosarcoma 143B cells

Figure S4: Identification of proteins containing SDMA and ADMA in whole cell extracts of the human colorectal cancer HCT116 cell line, human cervical cancer HeLa cell line, and human non-small cell lung cancer H460 cell line.

Figure S5: Identification of SDMA-containing polypeptides in histone and non-histone fractions of HCT116 and H460 cell extracts

Figure S1: Validating antibodies against SDMA and ADMA. 143B-R whole cell extracts were used as positive controls, and GST-GAR and *E. coli* extracts were used as negative controls. To ensure the antibodies recognized the arginine methylation modification rather than the glycine and arginine rich regions, an unmethylated GST-tagged protein, based on the N-terminus of human fibrillarin that contains a glycine and arginine rich region (GST-GAR), was used as a negative control. Another negative control was an extract of untransformed and uninduced BL21 *Escherichia coli* (*E. coli*) lysate. The first and third panels show Coomassie-stained SDS-PAGE gels. The second and fourth panels are immunoblots using the SDMA antibody or ADMA antibody with exposure times of 3 seconds or 10 seconds, respectively. Lanes from a single gel or blot were spliced together, as shown by the vertical black line, to remove irrelevant lanes. The same lanes for the parent cells and parent histones are shown in Figs 2 and 4, respectively.

Figure S2: Identification of proteins containing SDMA and ADMA in human parent and revertant 143B osteosarcoma cells: Replicate experiment. This shows an individual replicate experiment of the same conditions as in Fig 2. The leftmost panel shows a Coomassie-stained SDS-PAGE gel. The middle panel and rightmost panel show an anti-SDMA immunoblot and an anti-ADMA immunoblot, respectively, each with a 30 second exposure time. Molecular weight markers are shown at the left in the Coomassie-stained gel and as fluorescent bands on the left margin of the immunoblots.

SDMA (30s)

Figure S3: Identification of SDMA-containing polypeptides in histone and non-histone fractions of parent and revertant human osteosarcoma 143B cells. This shows a higher exposure (30 seconds) of the immunoblot in Fig. 3 to show the histone band more clearly.

127

Figure S4: Identification of proteins containing SDMA and ADMA in whole cell extracts of the human colorectal cancer HCT116 cell line, human cervical cancer HeLa cell line, and human non-small cell lung cancer H460 cell line. This shows a higher exposure (10 seconds) of the immunoblots in Fig. 6. The left panel is an anti-SDMA immunoblot, and the right panel is an anti-ADMA immunoblot.

SDMA (30s)

Figure S5: Identification of SDMA-containing polypeptides in histone and non-histone fractions of HCT116 and H460 cell extracts. This shows a higher exposure (30 seconds) of the anti-SDMA immunoblot in Fig. 7.

Chapter 7

Identification of a Protein Arginine Methyltransferase 7 (PRMT7)/Protein Arginine Methyltransferase 9 (PRMT9) inhibitor

The work described in this chapter has been reproduced from:

Significance Statement

Protein arginine methyltransferases have been identified as targets for cancer therapeutics. While the goal of many drug and inhibitor designs are to target specific molecular binding sites, even well-constructed inhibitors may have off target sights limiting their usefulness.

Protein methyltransferases bind *S*-adenosylmethionine at motifs I, post motif I, motif II, and motif III. Protein arginine methyltransferase contains an additional double E loop, and THW loop which specifically binds the guanidino arginine. Previous inhibitors fall into three classes. The first type defined involves a *S*-adenosylmethionine analog, the second type defined involves a peptide or guanidino analog, or a third type which involves a mixture of these structures.

To date there have been many successful inhibitors identified including MS023 which is defined as a type I PRMT inhibitor, EPZ015666 which is a PRMT5 specific inhibitor, as well as SGC8158 which is PRMT7 specific. While additional inhibitors are present and currently undergoing clinical trials, a general inhibitor for PRMT9 has not yet been identified.

The activity of PRMTs have been noted to be regulated by dimerization. While two monomers of PRMT 1-5, 6 and 8 are needed for activity, PRMT7 and PRMT9 just need one monomer. The structures of PRMT7 and PRMT9 are pseudo dimers containing duplicate motifs thus the need for just one copy for enzyme activity. Because of a similar structural design basis, in theory a PRMT7 inhibitor design could be applied to PRMT9. In collaboration with the Sbardella group, we were able to identify a novel inhibitor for both PRMT7 and PRMT9. While also uncovering small differences in both PRMT7 and PRMT9 active sites, which may aid in future PRMT drug designs.

Identification of a Protein Arginine Methyltransferase 7 (PRMT7)/ Protein Arginine Methyltransferase 9 (PRMT9) Inhibitor

Alessandra Feoli, Giulia Iannelli, Alessandra Cipriano, Ciro Milite, Lei Shen, Zhihao Wang, Andrea Hadjikyriacou, Troy L. Lowe, Cyrus Safaeipour, Monica Viviano, Giuliana Sarno, Elva Morretta, Maria Chiara Monti, Yanzhong Yang, Steven G. Clarke, Sandro Cosconati,* Sabrina Castellano,* and Gianluca Sbardella*

ABSTRACT: Less studied than the other protein arginine methyltransferase isoforms, PRMT7 and PRMT9 have recently been identified as important therapeutic targets. Yet, most of their biological roles and functions are still to be defined, as well as the structural requirements that could drive the identification of selective modulators of their activity. We recently described the structural requirements that led to the identification of potent and selective PRMT4 inhibitors spanning both the substrate and the cosubstrate pockets. The reanalysis of the data suggested a PRMT7 preferential binding for shorter derivatives and prompted us to extend these structural studies to PRMT9. Here, we report the identification of the first potent PRMT7/9 inhibitor and its binding mode to the two PRMT enzymes. Label-free quantification mass spectrometry confirmed significant inhibition of PRMT activity in cells. We also report the setup of an effective AlphaLISA assay to screen small molecule inhibitors of PRMT9.
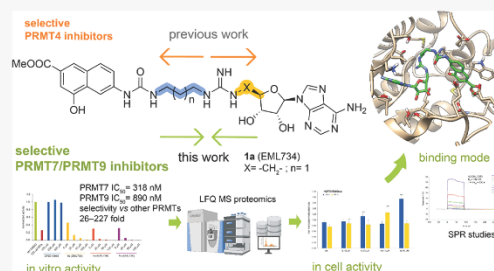
■ INTRODUCTION

Protein arginine methylation has recently attracted growing interest from the scientific community for its role in cell biology and its involvement in physiological and physiopathological processes. As a consequence, the enzymes responsible for this post-translational modification, protein arginine methyltransferases (PRMTs), are increasingly considered promising and relevant targets for drug discovery.[1]

In mammals, nine sequence-related PRMT isoforms (PRMT1−PRMT9) have been identified, and they are classified into three subfamilies (Type I, Type II, and Type III) based on the product of the methylation reaction they catalyze. In particular, type I PRMTs (PRMT1, PRMT2, PRMT3, PRMT4, PRMT6, and PRMT8) catalyze the formation of monomethylarginine (Rme1)[2] and asymmetric dimethylarginine (Rme2a), type II PRMTs (PRMT5 and PRMT9) catalyze the formation of Rme1 and symmetric dimethylarginine (Rme2s), whereas type III PRMT (PRMT7) catalyzes only the formation of Rme1.[3,4] The nine members of the PRMT family share a common Rossmann-like fold seven-stranded β-sheet connected by α-helices and a β-barrel domain. They have been classified as class I S-adenosylmethionine (SAM)-dependent methyltransferases, together with some non-SET domain lysine methyltransferases (e.g., DOT1L; Figure 1) also featuring the same elements.[5,6]

Several PRMT inhibitors have been identified to date, mostly type I PRMT inhibitors, both selective and unselective, and PRMT5 inhibitors.[1,7,8] Only recently the first PRMT7 selective inhibitor, SGC8158, was reported,[9] while no inhibitor for PRMT9 has been described so far.[10] However, very little is known about these two methyltransferases. While all the other PRMTs contain only one methyltransferase domain, both PRMT7 and PRMT9 contain two tandem domains resulting from ancestral duplication (Figure 1). The single C-terminal domain is catalytically inactive, yet it is necessary for enzyme activity being folded together with the N-terminal one to form a pseudodimer.[11−13,14,15,16,17] PRMT7 is associated with metastasis and DNA damage and is considered a potential target for treating breast cancer,[18,19] but important questions regarding its major role in cell biology are still open since it does not prime for dimethylation by type I and type II PRMTs.[15]

13665
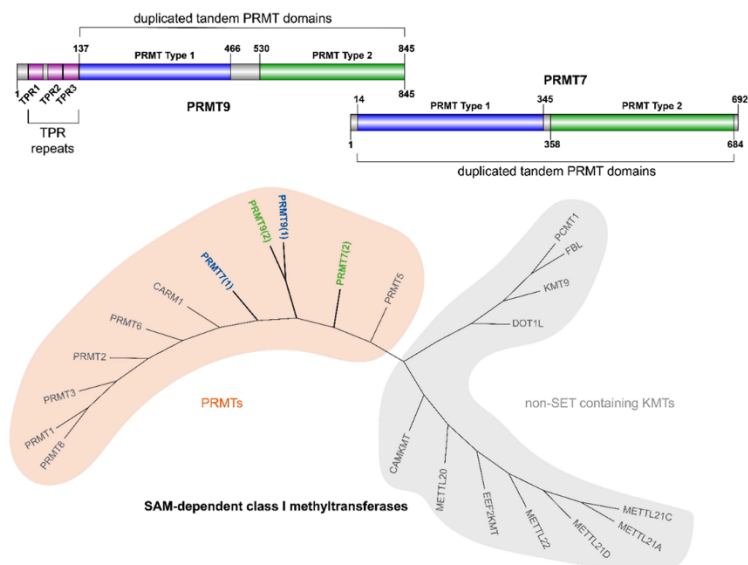
Figure 1. Architecture of PRMT7 and PRMT9 (prepared using Illustrator for Biological Sequences, IBS)[20] and phylogenetic tree of SAM-dependent class I methyltransferases (obtained with the Structural Genomic Consortium ChromoHub[21] and modified with Adobe Illustrator CC 2023). PRMTs are highlighted in the orange area, whereas non-SET domain-containing KMTs are in the gray area.

Seemingly, most of the biological roles of PRMT9 remain to be further defined along with its substrates.[13]

Nonetheless, PRMT9 has been identified as a potential target for treating hepatocellular carcinoma,[22,23] for suppressing acute myeloid leukemia maintenance,[24] and it is required for androgen-dependent proliferation of LNCaP prostate cancer cells.[25] It has been reported to play a role in the regulation of alternative splicing.[11,13] Very recently, it has been shown that PRMT9 attenuates activation of mitochondrial antiviral signaling protein (MAVS) through arginine methylation (R41 and R43), thus reducing innate antiviral immune response.[26]

Pursuing our interest in the identification of potent and selective PRMT inhibitors,[27−29,30,31,32,33,34,35,36,37,38] we were intrigued by the identification of hits for the development of PRMT9 inhibitors.

Identification of potent and selective PRMT9 inhibitors is a challenge due to several factors. Crystal structures of PRMTs have provided extensive amounts of information to aid in the development of selective inhibitors[1] but only recently a crystal structure of PRMT9 has become available (PDB ID: 6PDM),[39] and no literature report has been published up to date. In addition, the discovery of PRMT inhibitors requires efficient and effective biochemical screening assays for measuring their methyltransferase activity. However, in the case of PRMT9, there are only a limited number of screening techniques,[8] and no commercially available antibody can recognize R508me2s resulting from the enzymatic activity of PRMT9 on its specific substrate splicing factor 3B subunit 2 (SF3B2, also known as spliceosome-associated protein 145 SAP145).[13]

Overall, although many potent small molecule inhibitors have been reported for PRMTs, selectivity remains a challenge for individual PRMT isoforms because of a conserved SAM binding site and similar substrate recognition motif. On the other hand, even subtle modifications of chemical structure can greatly influence selectivity, and even close analogs of SAM can be surprisingly selective. Moreover, several lines of evidence support the essential role of the distance between the pharmacophore groups in PRMTs inhibition potency and selectivity.[31,40−42,43,44]

In SGC8158, for instance, changing the methylene linker length between the terminal amine moiety and the adenosine core resulted in a decrease in selectivity.[9]

In a recent study, we demonstrated that modulating the distance between pharmacophoric moieties leads to potent and selective PRMT4 inhibitors.[31] On the contrary, PRMT7 seems to preferentially bind derivatives with shorter linkers.

Based on the abovementioned considerations, we resolved to extend these structural studies to PRMT9 and to further explore the features of the binding of compounds spanning both the substrate and the cosubstrate pockets for the further development of inhibitors.

Herein, we report the identification of the first potent PRMT7/9 inhibitor and its binding mode to the two PRMT enzymes. We also report the setup of an effective assay to screen small molecule inhibitors of PRMT9.

■ RESULTS AND DISCUSSION

Optimization of Alpha-Based Screening for PRMT9 Inhibitor Identification. To date, radiometric assays represent the only standard for biochemically measuring the methyltransferase activity of PRMT9. Yet, the cost, the difficulty to automate, and the danger associated with their usage and the generation of radioactive waste are huge deterrents for random or target-based screening. Recently, a

133

PRMT9 homogeneous assay kit in an AlphaLISA format has become commercially available (BPS Bioscience #52069) and, even if, to the best of our knowledge, no evidence of its effectiveness in small molecules screening has been reported in the literature so far,[45] at first we decided to use it for the evaluation of the inhibitory effect of our compounds against PRMT9. The assay was based on PRMT9-mediated methylation of the GST-tagged substrate (an unspecified SF3B2 peptide) in the presence of the SAM cosubstrate. The modification resulting from the enzymatic reaction was detected by adding a primary antibody (specifically recognizing the substrate methylated arginine), antirabbit IgG acceptor beads (capturing the Fc region of the primary antibody), and glutathione donor beads (capturing the GST tag of the substrate).

Unfortunately, following the protocol reported for this assay, we obtained low alpha counts and an unacceptable signal/noise ratio, with a blank higher than the controls (Figure S1A, Supporting Information). We assumed that this unexpected behavior could be due to a nonspecific recognition of the substrate and/or to an interference from the GST tag of the substrate. Accordingly, we tried to optimize the assay by diluting the substrate 1:10, but we did not observe any improvement (Figure S1B). We reported the issue to the BPS Technical Support, which suggested an 8-fold increase in the enzyme amount to obtain a signal/noise ratio of 2.3. However, this was still unacceptable and also resulted in the need for significantly larger amounts of enzyme. Therefore, we redesigned the assay using a biotinylated 20-amino acid peptide of SF3B2 (aa 500−519) instead of the GST-substrate of the kit and streptavidin donor beads instead of glutathione ones. Thanks to these modifications, we were finally able to obtain a good signal/noise ratio, avoiding the previously reported problems with blanks (Figure S1C). Accordingly, all the enzymatic inhibition data were obtained by performing the assays in these optimized conditions. Noteworthy, while writing this manuscript, we were pleased to find out that BPS changed the kit, replacing the GST-tagged substrate with a biotinylated one and including a 5-fold higher amount of the enzyme (with a higher level of purity), substantially confirming our modifications to the assay.[46]

Recently, we successfully applied a deconstruction−reconstruction and fragment-growing approach to achieve potency and selectivity against PRMT4 starting from non-selective PRMT inhibitors. This approach allowed us to investigate the structural features of the binding to PRMT enzymes and we found that the overall length of synthesized compounds 1a−h (Figure 2) and, even more, the length of the linkers between the 4-hydroxy-2-naphthoate-6-urea and the guanidine group and between the latter and the adenosine moiety resulted to be crucial for the inhibitory activity especially against PRMT4 and, at a minor extent, against PRMT1.[31] On the contrary, the study showed that increasing the linker length is detrimental for the inhibition of PRMT6 because the resulting compounds are forced to adopt an odd distorted U-shaped conformation that reduces the favorable binding interactions with the enzyme double-E loop clamp and the arginine substrate pocket.[31] Interestingly, we observed a different trend for the inhibitory activity against PRMT7, with the shorter compound (1a, EML 734) showing an IC$_{50}$ value of 0.32 μM and a certain selectivity compared to other tested PRMTs (SI values in the range 26−227; see Figure 2).
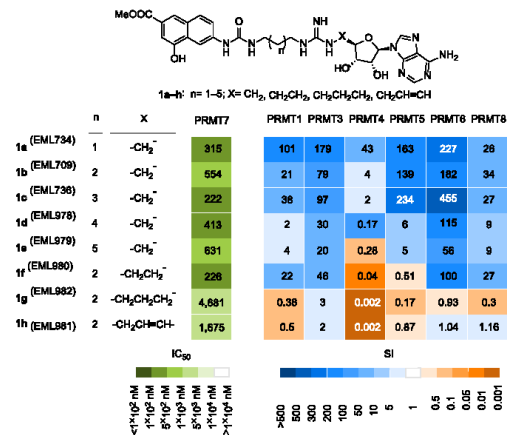
Figure 2. Inhibitory activities of compounds **1a−h** against PRMT7:[31] the heatmaps depict the IC$_{50}$ values (nM) for compounds **1a−1h** against PRMT7 (left panel, in shades of green) and the selectivity index (fold) for PRMT7 over the specified PRMT (right, shades of blue and orange).

This is consistent with the restrictive and narrow active site described for PRMT7.[15,47] Therefore, we decided to start our structural studies on PRMT9 by investigating the capability of **1a** (EML734) to inhibit the enzyme in our AlphaLISA assay. For comparison, we also selected a few compounds from our in-house libraries of PRMT modulators[27,28,31,35] among those featuring some structural similarities with **1a** (e.g., the hydroxy-carboxy-naphthyl-urea portion, or the bioisosteric carboxy-indolyl-urea or carboxy-indolyl-amide moieties) and tested them for their ability to inhibit PRMT9 (Figure 3).

Selection of Compounds for Preliminary Screening and Hit Identification. Both bis-4-hydroxy-2-naphthoic compounds (EML107 and EML108)[27] and bis-indolecarboxylate compounds (EML145, EML147, and EML148),[28] previously identified as class I PRMT inhibitors, as well as the aryl acetamido ureido indole carboxylate ("uracandolate") EML105 (an enhancer of PRMT4 activity),[28] showed no activity against PRMT9. On the contrary, compound **1a** exhibited good inhibitory activity against PRMT9, with a submicromolar IC$_{50}$ value (0.89 μM).

Prompted by this result, we turned back our attention to the derivatives of **1a** previously synthesized by us (compounds **1b−h**) and tested them in our in-house AlphaLISA assay, with the aim of investigating the effect of the modulation of the distance between the pharmacophoric moieties on the inhibiting activity against PRMT9.

We found that in the case of PRMT9, the distance between the methyl 4-hydroxy-2-naphthoate moiety and the arginine-mimetic group does not significantly affect the inhibitory activity of the compounds, with all the compounds **1a−e** (n= 1−5; Table 1) showing comparable and relatively good inhibiting properties (IC$_{50}$ values around 1 μM) against PRMT9. A decrease in the inhibitory activity was observed when the linker between the guanidine group and the adenosine moiety was more than two-carbon atoms long. In fact, compounds **1g** and **1h** were the least effective inhibitors, with an opposite trend with respect to what we previously observed for PRMT4.[31] Compound **1a**, featuring a propyl

134
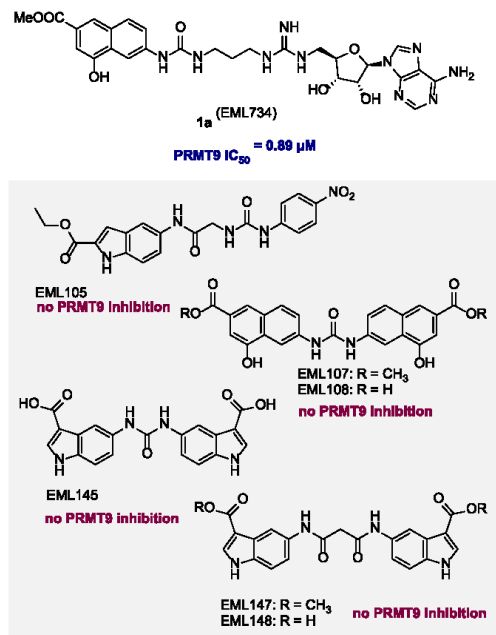
Figure 3. Inhibitory activities of selected PRMT modulators (from in-house libraries) against PRMT9.

Table 1. Inhibitory Activities of Compounds 1a–h against PRMT9

compound	n	X	PRMT9 IC$_{50}$^{a,b} (μM)
1a (EML734)	1	$-CH_2-$	0.89
1b (EML709)	2	$-CH_2-$	1.32
1c (EML736)	3	$-CH_2-$	5.80
1d (EML978)	4	$-CH_2-$	1.02
1e (EML979)	5	$-CH_2-$	1.30
1f (EML980)	2	$-CH_2-CH_2-$	1.20
1g (EML982)	2	$-CH_2-CH_2-CH_2-$	>10.00
1h (EML981)	2	$-CH_2-CH=CH-$	9.30

^{a}Obtained in AlphaLISA assay, using human recombinant PRMT9 (0.105 μM, final concentration). SF3B2 (500–519) peptide, biotinylated (100 nM, final concentration), and SAM (25 μM, final concentration) were used as substrate and cosubstrate, respectively. ^{b}Compounds were tested in 10-concentration IC$_{50}$ mode with 3-fold serial dilutions starting at 100 μM. Data were analyzed with GraphPad Prism software (version 6.0) for IC$_{50}$ curve fitting.

spacer between the 4-hydroxy-2-naphthoate moiety and the guanidine group, was the most potent derivative with a submicromolar activity against PRMT9 and a good selectivity profile against the other PRMTs.

Design, synthesis, and inhibitory activity of **1i** (EML1102), the lower homologue of **1a** (EML734).

Based on these outcomes, we resolved to explore the effect on the capability to inhibit PRMT9 enzymatic activity of further reduction of the distance between the pharmacophoric moieties. Therefore, we synthesized compound **1i** (EML1102) in which the propyl spacer of **1a** was replaced with the shorter ethyl group and tested it against PRMT9 as well as against all the other PRMTs (with the only exception of PRMT2; Table 2). As shown in Table 2, compound **1i** confirmed the general trend previously observed for compound **1a–h** against type I PRMTs. In fact, the reduction of the spacer length further reduced the inhibitory potency against PRMT1, PRMT3, PRMT6, and PRMT8 (compare the activities of **1i** and **1a** in Table 2). Consistent with the geometric restriction of the enzyme active site,[15,47] compound **1i** substantially maintained the inhibitory activity of **1a** against PRMT7. On the contrary, the further reduction of the length of the alkyl spacer between the 4-hydroxy-2-naphthoate moiety and the guanidine group resulted in being detrimental to the inhibition of PRMT9. In fact, as reported in Table 2, compound **1i** exhibited a 3-fold reduction in potency compared to its next higher homologue **1a**. To confirm the activity of the compounds against PRMT9, we then used a radioisotope-based assay as a secondary screening approach.[48,49] In these experiments, *Hs*PRMT9 was incubated with ^{3}H-SAM and SF3B2 (401–550) peptide with and without inhibitors **1a–c** at the reported concentrations, and then the reaction products were analyzed by SDS gel electrophoresis followed by fluorography and densitometric analysis. 5′-Deoxy-5′-(methylthio)adenosine (methylthioadenosine, MTA), the polyamine byproduct in the methionine salvage pathway that is reported to be a SAM-competitive inhibitor of PRMTs,[50–52,53,54] and the PRMT5 inhibitor EPZ015666 (GSK3235025)[50,55] were used as reference drugs. As shown in Figure 4a and consistent with the results of the AlphaLISA assay, all three compounds induced half inhibition of PRMT9 at a concentration lower than 5 μM. The effect is concentration-dependent, and almost complete inhibition was observed at 100 μM. On the contrary, MTA was able to give a good inhibition only at 100 μM, whereas EPZ015666 was inactive up to 500 μM. For comparison, compounds **1a–c** were tested in the same assay also against *Hs*PRMT7, in the presence of recombinant *Hs*H2B as a substrate (Figure 4b). As expected, the inhibiting activities were consistent with those reported in Figure 2. Both PRMT7 and PRMT9 are evolutionarily conserved proteins, with distinct orthologs in plants, invertebrates, and vertebrates, and human enzymes have much in common with their orthologs from the soil nematode worm *Caenorhabditis elegans*,[48] which has developed into an important model for the functional characterization of various drug targets,[56] including PRMTs.[57] Nonetheless, important differences in terms of active site architecture and substrate specificity have been reported between human and nematode PRMT7 proteins, whereas the two PRMT9 orthologs appear to be biochemically indistinguishable.[48] Therefore, we decided to investigate the effects of compounds **1a–c** also on the enzymes from *C. elegans*. A nearly full inhibition of *Ce*PRMT9 was observed with each of the three inhibitors at 100 μM concentration, while the half inhibition was observed between 25 and 50 μM, suggesting that the inhibitors have maybe 5–10-fold less binding affinity for the worm enzyme than for the human enzyme (Figure 4c). On the contrary, consistent with the previously reported differences, not much inhibition was seen with the *Ce*PRMT7 enzyme using histone H2B as a

135

Table 2. Inhibitory Activities of Compound 1i against PRMTs

1i (EML1102)

cmpd	IC$_{50}$[a,b] (μM)							
	PRMT1	PRMT3	PRMT4	PRMT5	PRMT6	PRMT7	PRMT8	PRMT9
1a (EML734)	32.27[c]	57.19[c]	13.84[c]	52.13[c]	72.77[c]	0.32[c]	8.29[c]	0.89[d]
1i (EML1102)	>100	>100	22.8	9.4	70	0.54	42	2.47[d]

[a]Compounds were tested in 10-concentration IC$_{50}$ mode with 3-fold serial dilutions starting at 100 μM. Data were analyzed with GraphPad Prism software (version 6.0) for IC$_{50}$ curve fitting. [b]Unless differently indicated, the values were obtained in a radioisotope-based filter assay, using 5 μM histone H4 (for PRMT1, PRMT3, and PRMT8), histone H3 (for PRMT4), histone H2A (for PRMT5), or GST-GAR (for PRMT6 and PRMT7) as the substrate and S-adenosyl-L-[methyl-^{3}H]methionine (1 μM) as a methyl donor. [c]Data from ref 31. [d]Obtained in AlphaLISA assay, using human recombinant PRMT9 (0.105 μM, final concentration). SF3B2 (500−519) peptide, biotinylated (100 nM, final concentration) and SAM (25 μM, final concentration) were used as substrate and cosubstrate, respectively.
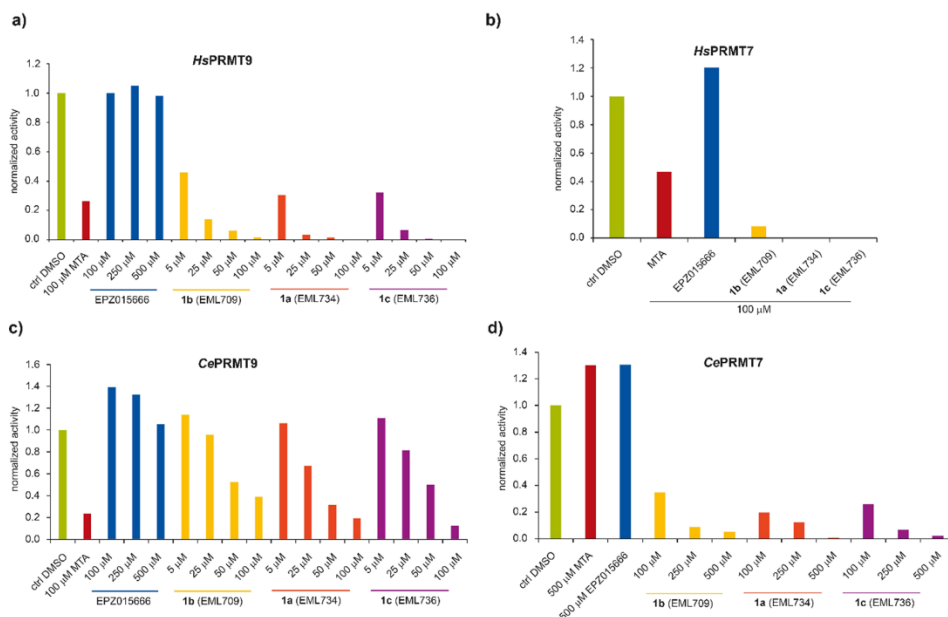
Figure 4. Inhibition of GST-tagged HsPRMT9 and HsPRMT7 (panels a and b, respectively) or CePRMT7 and CePRMT9 (panels c and d, respectively) by compounds 1a−c as detected by a radioisotope-based assay. The experiments were performed as reported in the Experimental procedures section. GST-HsPRMT9 (a) and GST-HsPRMT7 (b) were incubated with human GST-SF3B2 (401−550) peptide or recombinant HsH2B, respectively (1 μg of enzyme, 5 μg of substrate), 0.14 μM [^{3}H]SAM, and the indicated concentrations of tested compounds at the corresponding optimal reaction temperature (37 °C for HsPRMT9, 15 °C for HsPRMT7). $C.$ $elegans$ GST-tagged enzymes PRMT9 (c) and PRMT7 (d) were incubated with GST-CeSFTB-2 (99−248) fragment or recombinant HsH2B, respectively (1 μg of enzyme, 5 μg of substrate), 0.14 μM [^{3}H]SAM, and the indicated concentrations of tested compounds at the corresponding optimal reaction temperature (25 °C for CePRMT9, 15 °C for CePRMT7). After SDS-PAGE, the gels were treated as previously described[48] and densitometry analysis was done using ImageJ software, and data was plotted as normalized activity to the no inhibitor controls.

substrate at 100 μM concentrations. After the experiment was repeated with 100, 250, and 500 μM concentrations of each inhibitor, half inhibition was observed only at a concentration of roughly 250 μM (Figure 4d).

Docking and Structure-Based Ligand Design Studies. Prompted by the results of preliminary structure−activity relationship (SAR) studies, molecular modeling calculations were attempted to propose a viable binding interaction model between our most potent and sufficiently selective PRMT9 ligand, 1a (EML734), and the enzyme and prospectively suggest possible modifications that could enhance the ligand/enzyme recognition. In particular, 1a was subjected to docking calculations employing the latest OpenCL implementation of AutoDock4, called AutoDock-GPU (AD4-GPU),[58] and the recently released cocrystal structure of the human PRMT9 in complex with another adenosine-based inhibitor (MT556,

136
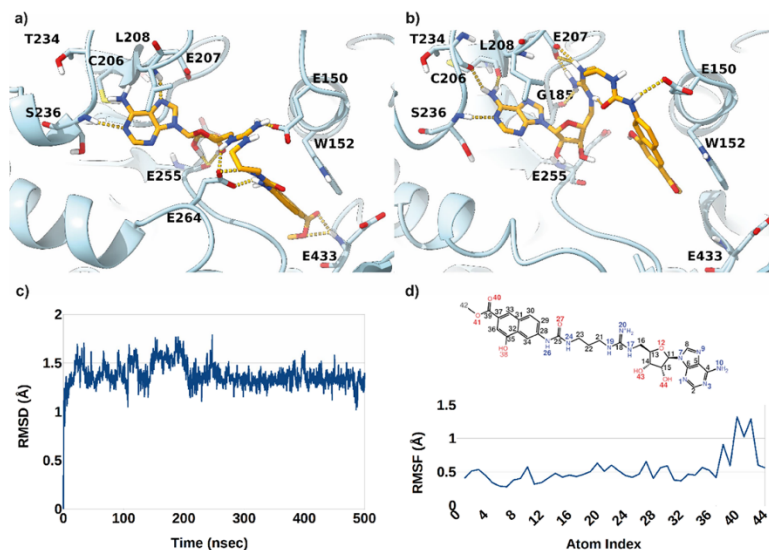
Figure 5. Binding mode of **1a** in complex with the PRMT9 3D structure (PDB entry 7RBQ) as predicted by docking calculations (a) and representative frame of the 500 ns long MD simulation (b). The ligand and enzyme are represented as orange and cyan stick and ribbons, respectively. L-RMSD (c) and L-RMSF (d) plots obtained from the analysis of MD simulations.

PDB code 7RBQ).[59] Results of docking analysis revealed that in the predicted lowest-energy binding orientation (ΔG_{AD4} = −14.4 kcal/mol), the ligand adenine ring is able to occupy the protein region engaged by the same ring in the cocrystal ligand. Here, H-bond interactions are established with the L208 and S236 backbone NHs groups. Additional H-bonds are formed by the sugar OH groups with the E255 backbone CO, while the arginine-mimetic group is involved in ionic contacts with the E150 and E264 negatively charged side chains. This latter residue is also involved in charged-reinforced hydrogen bonds with the ligand urea moiety. Finally, the 4-hydroxy-2-naphthoate group is inserted in a rather lipophilic cleft establishing a $\pi-\pi$ interaction with the W152 side chain, while the methyl ester in position 6 is H-bonding E433 backbone NH. On the contrary, no specific contacts were predicted for the 4-OH group of the naphthyl ring. To probe the stability of the interactions predicted by AD4 as well as include the effect of the solvent in mediating the ligand/protein contacts, the above-described **1a**/PRMT9 complex was subjected to a 500 ns long molecular dynamics simulations employing the Desmond MD software.[60] Analysis of the achieved results demonstrated that the predicted binding pose is fairly stable over the simulation time, as demonstrated by the ligand root-mean-square deviations and fluctuations plots (L-RMSD and L-RMSF, respectively, Figure 5c,d). Indeed, the average RMSD value is fairly low (1.38 Å with a standard deviation of 0.12) with the most flexible part residing in the ligand naphthyl tail which experiences a partial relocation probably induced by the flexible linking spacer between this ring and the adenine one. This relocation is made possible by a rather stable intramolecular charge-reinforced H-bond established by the urea carbonyl oxygen and the positively charged guanidinium group. While relocating the terminal moieties of the ligand are still able to establish the same sort of interactions with the

protein counterpart. In particular, the adenine ring engages H-bonds with C206, T234, and S236 backbone atoms while the naphthyl ring π-stacking contacts with W152. While this latter contact seems to be stable throughout the simulation, the naphthyl hydroxy and methyl ester substituents do not seem to have direct and stable interactions with PRMT9. Compound **1a** is demonstrated to be a proficient PRMT7 inhibitor. Therefore, molecular modeling studies were also attempted on this latter enzyme. Unfortunately, up to date no experimental structure of the human PRMT7 enzyme has been reported, while the structure of the murine orthologue has been solved in complex with the SGC8158 chemical probe. We resolved to analyze the structure of the human protein as calculated by AlphaFold[61] and compared it to the mouse one, demonstrating no substantial difference in the overall folding (data not shown). Therefore, also considering that the activity data were obtained using the human PRMT7, in this inspection, we decided to utilize the human protein. In particular, the same protocol of docking + MD simulations used for PRMT9 was employed, demonstrating a comparable interaction pattern. More precisely, as happened for the predicted binding pose in the human PRMT9, also for the PRMT7 enzyme, the ligand adenosine and sugar rings are involved in H-bond interactions reminiscent of the interactions established by the same rings in the SAM cosubstrate.

Additionally, the guanidine portion is involved in ionic contacts with negatively charged residues. The main differences, however, are recorded for the terminal 4-hydroxy-2-naphthoate group that in this case is pointing toward a rather solvent-exposed and hydrophilic protein region. This set of interactions is well preserved throughout the entire 500 ns MD simulation (Figure S2, Supporting Information). To further validate the presented ligand/PRMT9 interaction model, we decided to design an analogue of **1a** capable of further

137

enhancing recognition with this latter enzyme. Specifically, we wanted to reinforce the contact with W152 of the naphthyl ring by decorating it with an electron-withdrawing group capable of strengthening the π–π contact with this residue. We decided to synthesize compound **1j** (EML1219; Figure 6)
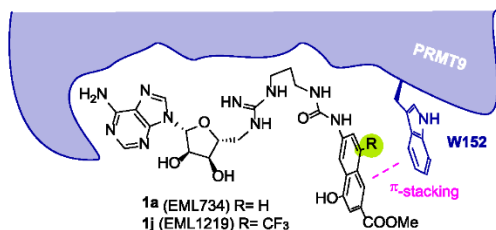

Figure 6. Design of compound **1j** to strengthen π-stacking interaction with the PRMT9 W152 residue (in blue).

featuring a trifluoromethyl group at position 8 of the above-mentioned ring. This position was selected because, being solvent exposed, no unwanted steric clash with the enzyme binding site was expected.

To characterize the effect of compound **1j** on PRMT9, we resolved to evaluate its direct binding to the target protein using surface plasmon resonance (SPR). To this aim, human recombinant PRMT9 (2−845; N-terminal FLAG-tag, C-terminal His6-tag) was covalently immobilized on a sensor chip surface using an amine coupling approach and compound **1j** was injected over the active and reference cells at 10 different concentrations (2-fold dilution series) from 25 to 0.05 μM using the multicycle modality. Each injection was performed with an association and a dissociation time of 90 and 180 s, respectively, and with a flow rate of 30 μL/min. To reduce false positives from detergent-sensitive, nonspecific aggregation-based binding, detergents (0.05% Tween20) were added to the running buffer in all experiments. The corrected sensorgrams were fitted simultaneously by kinetic analysis using the 1:1 Langmuir model of the BIAevaluation software to obtain equilibrium dissociation constants (K_D) and kinetic dissociation (k_{off}) and association (k_{on}) constants, and the curve-fitting efficiency was evaluated by chi-square (χ^2). The χ^2 value of **1j** was calculated to be 0.650, indicating a good fit.

SPR studies demonstrated a specific and strong binding interaction between PRMT9 and the compound, with an equilibrium dissociation constant (K_D) value in the sub-micromolar range (K_D = 188 nM; Figure 7) and a rather high in vitro residence time value (τ_R = 500 s).

Next, we tested **1j** against PRMT9 as well as the other PRMTs (with the only exception being PRMT2; Table 3).

As shown in Table 3, the introduction of the trifluoromethyl substituent at position 8 of the naphthyl ring resulted in a 4-fold increased inhibitory potency against PRMT9, thus confirming the predicted binding mode. However, the gain in target affinity comes at a cost in selectivity, particularly against the other type II enzyme, PRMT5 (Table 3).

The selectivity of compound **1j** was further assessed against a panel of eight lysine methyltransferases (KMTs), including the SET-domain-containing proteins ASH1L/KMT2H, EZH2/KMT6 (5 component complex), G9a/KMT1C, MLL1/KMT2A (5 component complex), SET7/9/KMT7, SMYD3/KMT3E, SUV39H2/KMT1B, and the non-SET
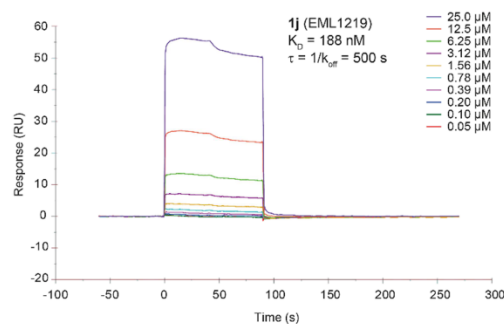
Figure 7. Sensorgrams obtained from the SPR interaction analysis of compound **1j** binding to immobilized PRMT9. The compound was injected at different concentrations (from 25 to 0.05 mM) with an association and a dissociation time of 90 and 180 s, respectively, and with a flow rate of 30 μL/min. The equilibrium dissociation constant (K_D) was derived from the ratio between kinetic dissociation (k_{off}) and association (k_{on}) constants.

domain containing DOT1L/KMT4.[6] To this aim, the inhibition of **1j** toward these selected enzymes was assessed at two different concentrations (10 and 100 μM, respectively, >50 and >500 fold higher than the IC$_{50}$ value against PRMT9) using SAH,[62−64] or chaetocin (for ASH1L)[65] as reference compounds. Noteworthy, we found that none of the SET-domain-containing enzymes was inhibited by **1j** even at the highest tested concentration (Figure S3 and Table S1, Supporting Information), whereas the non-SET domain containing DOT1L/KMT4 was significantly inhibited even at 10 μM, thus confirming that the introduction of the trifluoromethyl group gives a reduction in selectivity within class I SAM-dependent methyltransferases.

Assessment of in Cell Functional Potency. As mentioned above, compounds **1a−h** were originally designed to probe the structural differences among the various PRMTs in order to gain important information for the development of potent and selective inhibitors and nonoptimized for cell permeability. Yet, we previously reported that, regardless of its low cell permeability, **1h** is able to induce an evident reduction of PRMT4-catalyzed arginine methylation levels in MCF-7 cells and a marked reduction of proliferation.[31]

Therefore, we resolved to investigate whether the compounds can reduce the cellular level of arginine methylation catalyzed by PRMT9. Note that when SF3B2 was characterized as the methylation substrate of PRMT9, a homemade methyl-specific antibody was developed to detect PRMT9-catalyzed SF3B2 methylation site (R508), namely, SF3B2 R508me2s.[13] This antibody was validated as very specific and not affected by the low reproducibility issues that often plague many antibodies used for detection of PTMs.[66,67] To test the effect of compounds **1a**, **1c**, **1e**, and **1f** on PRMT9 activity in vivo, we treated MCF-7 and MDA-MB-436 breast cancer cell lines with these compounds at indicated concentrations for 72 h, and the total cell lysates were then immunoblotted with the αSF3B2 R508me2s methyl-specific antibody.

However, as shown in Figure 8, in both cell lines and for all of the tested compounds, we were not able to see a convincing inhibition on the levels of SF3B2 R508 methylation. As mentioned above, this is not surprising considering the low cell permeability of these compounds.

138

Table 3. Inhibitory Activities of Compound 1j against PRMTs

1a (EML734) R= H
1j (EML1219) R= CF3

	$IC_{50}^{a,b}$ (μM)							
cmpd	PRMT1	PRMT3	PRMT4	PRMT5	PRMT6	PRMT7	PRMT8	PRMT9
1a (EML734)	32.27^c	57.19^c	13.84^c	52.13^c	72.77^c	0.32^c	8.29^c	0.89^d
1j (EML1219)	48.9	14.9	1.46	1.01	49.7	5.6	1.97	0.2^d

[a]Compounds were tested in 10-concentration IC_{50} mode with 3-fold serial dilutions starting at 100 μM. Data were analyzed with GraphPad Prism software (version 6.0) for IC_{50} curve fitting. [b]Unless differently indicated, the values were obtained in a radioisotope-based filter assay, using 5 μM histone H4 (for PRMT1, PRMT3, and PRMT8), histone H3 (for PRMT4), histone H2A (for PRMT5) or GST-GAR (for PRMT6 and PRMT7) as substrate and S-adenosyl-L-[methyl-^{3}H]methionine (1 μM) as the methyl donor. [c]Data from ref 31. [d]Obtained in AlphaLISA assay, using human recombinant PRMT9 (0.105 μM, final concentration). SF3B2 (500−519) peptide, biotinylated (100 nM, final concentration), and SAM (25 μM, final concentration) were used as substrate and cosubstrate, respectively.
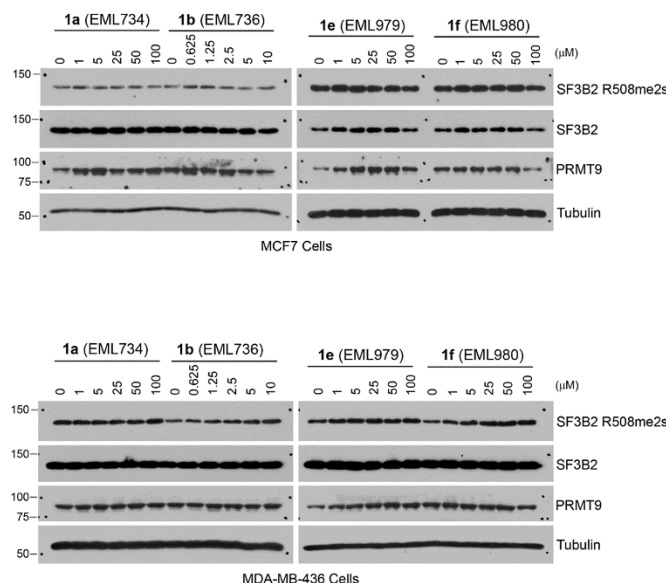
Figure 8. Testing the effects of compounds **1a** (EML734), **1b** (EML736), **1e** (EML979), and **1f** (EML980) on PRMT9 activity in MCF7 (top) and MDA-MB-436 breast cancer cell lines. MCF7 and MDA-MB-436 cells were treated with 4 candidate inhibitors at indicated concentrations for 72 h. The total cell lysates were harvested in RIPA buffer and the levels of SF3B2 R508me2s, SF3B2, and PRMT9 were detected by using Western blot assays. Anti-Tubulin antibody was used as a loading control.

Quantification of in Cell Methylation by Mass Spectrometry. Antibody-based methods such as enzyme-linked immunosorbent assay (ELISA) or Western blot are widely used to detect PTMs, yet they are significantly less sensitive than methods based on mass spectrometry, in which resolution is based on mass changes and includes a variety of PTMs within a certain mass range in a single measurement. This is even more evident in the case of the combination of state-of-the-art spectrometers with high resolving power and powerful bioinformatic tools, that made very popular the use of "label-free" quantification methods (LFQ) as an alternative to stable isotope labeling strategies.[68,69] Therefore, we decided to

investigate whether variations in the level of arginine methylation of specific substrates of PRMT7 and PRMT9 could be detected by LFQ mass spectrometry. To this aim, we focused on the heat shock 70 kDa protein 1B (HSP70) and the heterogeneous nuclear ribonucleoprotein A1 (HNRNPA1), which are methylated by PRMT7 on R469 and R194, respectively,[9,70] and on SF3B2, symmetrically dimethylated on R508 by PRMT9.[11,13]

Briefly, HEK293T cells treated with compounds **1a** or **1j** or untreated were lysed through sonication, and then proteins from each lysate were denatured and digested with a protease (trypsin/LysC) into a peptide mixture, which was subse-

139
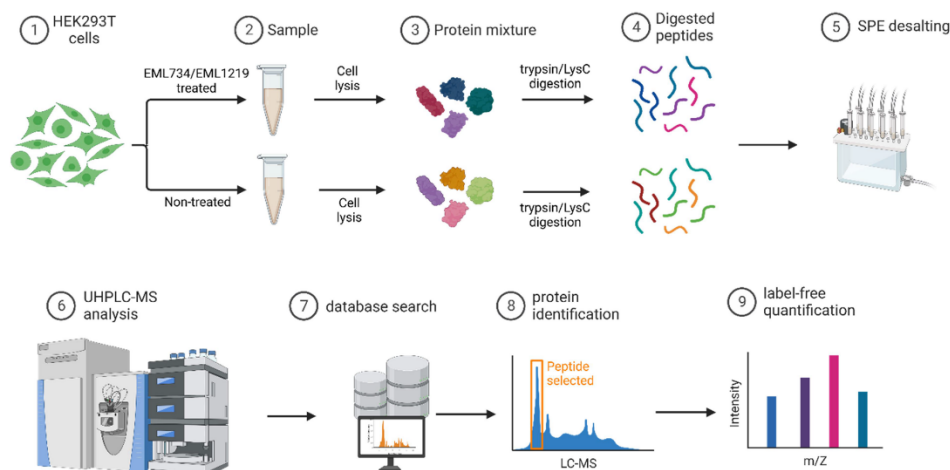
Figure 9. Schematic description of the MS proteomic experiment. Created with BioRender.com.

quently analyzed by tandem MS (MS/MS), identified by database searching, and quantified (Figure 9; see Experimental Section for details).

For both untreated and compound-treated samples, the ratio between the abundance of the nonmethylated over the monomethylated peptides was calculated and plotted as bar graphs. As shown in Figure 10, for both substrates of PRMT7,
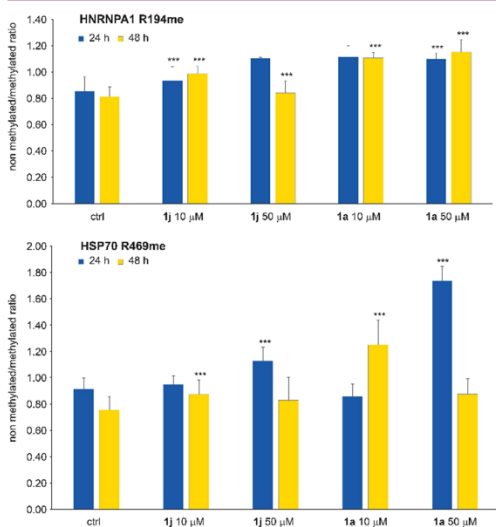
Figure 10. Compounds **1a** and **1j** inhibit PRMT7 in cells. The bar graphs plot the ratio between the abundance of nonmethylated over methylated peptides in HEK392T cells treated with compounds **1a** or **1j** or untreated for 24 h (blue) or 48 h (yellow). The top panel shows the ratio between HNRNPA1 unmethylated over R194me peptides, and the bottom panel shows the ratio between HSP70 unmethylated over R469me peptides.

HNRNPA1, and HSP70, the ratio increased in treated samples compared to control, indicating an increasing prevalence of unmethylated over methylated peptides, thus revealing a slight but significant inhibition of the enzyme catalytic activity even in cells. The effect is concentration- and time-dependent.

Unfortunately, after trypsin/Lys-C digestion, we were not able to identify the SF3B2 peptide(s) including R508 but only peptides preceding or following it (e.g., 496−507 or 515−530). Therefore, we resolved to repeat the experiments using digestion by the alternative protease Glu-C or a digestion with trypsin/Lys-C and Glu-C in parallel and subsequent MS-proteomics analysis.[71] Alas, both attempts were not successful, and again we identified the protein but not the peptide(s) including R508. Nonetheless, the results obtained for two distinct substrates of PRMT7 confirmed that, although nonoptimized for cell permeability, compounds **1a** and **1j** inhibit PRMT activity also in a cellular context.

■ CONCLUSIONS

Compared to other PRMTs, PRMT7 and PRMT9 are relatively underinvestigated and, although they have been recently identified as potential therapeutic targets for the treatment of various diseases, including different types of cancer,[18,19,22−24,25] much is still to be understood on their biological roles, as well as on the structural requirements that could drive the development of selective modulators of their methyltransferase activity.

Prompted by our longstanding interest in PRMTs, we recently demonstrated that modulating the distance between pharmacophoric moieties of compounds spanning both the substrate and the cosubstrate pockets leads to potent and selective PRMT4 inhibitors.[31] In this work, starting from the reanalysis of those data, we observed that, differently from PRMT4, PRMT7 seems to preferentially bind derivatives with shorter linkers, consistently with its previously described restrictive and narrow active site.[15,47] The shortest compound in the series (**1a**, EML 734), featuring a propyl spacer between the 4-hydroxy-2-naphthoate moiety and the guanidine group, showed an IC_{50} value of 0.32 μM and a certain selectivity

140

Scheme 1. Synthesis of Compounds 1i and 1j

2a: R = -H
2b: R = -CF$_3$

3a: R = -H
3b: R = -CF$_3$

4a: R = -H
4b: R = -CF$_3$

5a: R = -H; R$_1$ = -Boc; n = 1
5b: R = -CF$_3$; R$_1$ = -Boc; n = 2
6a: R = -H; R$_1$ = -H; n = 1
6b: R = -CF$_3$; R$_1$ = -H; n = 2

7

8a: R = -H; n = 1
8b: R = -CF$_3$; n = 2

1i (EML1102): R = -H; n = 1
1j (EML1219): R = -CF$_3$; n = 2
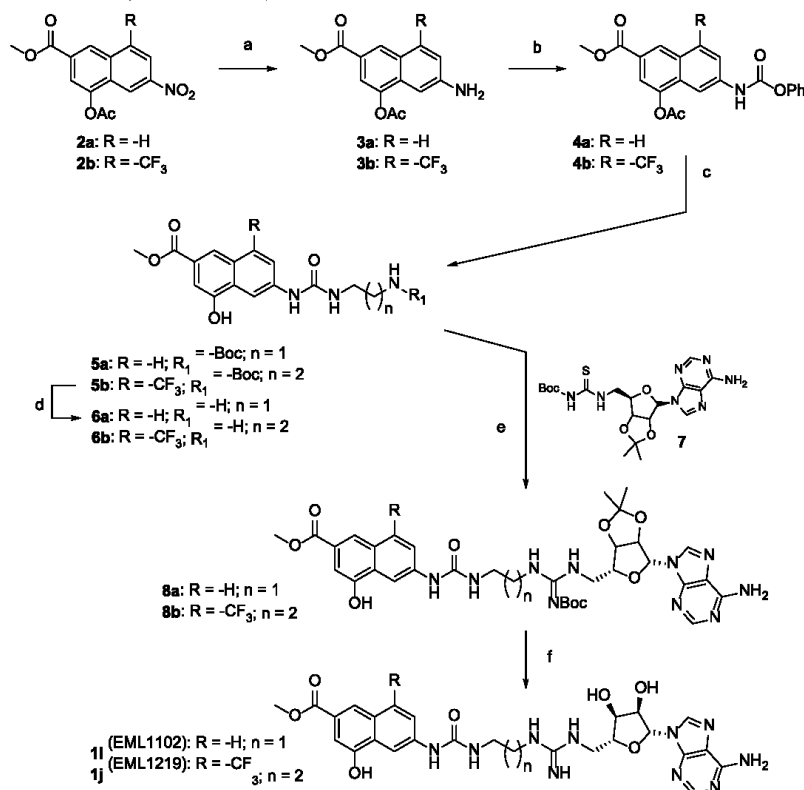
Reagents and conditions: (a) zinc dust, acetic acid, 1 h (97–98%); (b) phenyl chloroformate, TEA, AcOEt, r. t., 12 h (65–70%); (c) TEA, dry DMF, r. t., 2 h (68–70%); (d) DCM/TFA 9:1, r. t., 2 h (80–92%); (e) EDC hydrochloride, TEA, dry DCM, r. t., 18 h (60–74%); (f) DCM/TFA 1:1, r. t., 2 h (60–76%).

compared to other tested PRMTs (SI values in the range 26–227). The trend was confirmed by the lower homologue **1i** (EML1102), in which the reduction of the spacer length (propyl to ethyl) further reduced the inhibitory potency against PRMT1, PRMT3, PRMT6, and PRMT8 but substantially maintained the inhibitory activity of **1a** against PRMT7.

This prompted us to extend the study to PRMT9, and we decided to gauge the inhibitory activity of compounds **1a–i**. As a primary screening assay, we used an in-house custom-developed AlphaLISA assay employing a biotinylated 20-amino acid peptide of SF3B2 (aa 500–519) as a substrate. We found that compound **1a** is also a very good inhibitor of PRMT9 with an IC$_{50}$ value in the submicromolar range (IC$_{50}$ = 0.89 μM) and a good selectivity profile against the other PRMTs. In the case of PRMT9, the distance between the methyl 4-hydroxy-2-naphthoate moiety and the arginine-mimetic group does not significantly affect the inhibitory activity of the compounds, with all the compounds **1a–e** (n = 1–5) showing comparably good inhibiting properties (IC$_{50}$ values around 1 μM) against this enzyme. Differently from what we observed for PRMT7, the further reduction of the length of the alkyl spacer between

the 4-hydroxy-2-naphthoate moiety and the guanidine group as featured by compound **1i** was detrimental for the inhibition of PRMT9, with a 3-fold reduction in potency. Similarly, a decrease of the inhibitory activity was observed when the linker between the guanidine group and the adenosine moiety was more than a two-carbon atom long, with compounds **1g** and **1h** being the least effective PRMT9 inhibitors in the series.

A radioisotope-based assay was used as a secondary screening approach and confirmed the PRMT9-inhibiting activity of the compounds. Docking calculations with the crystal structures of PRMT9 and PRMT7 proposed binding modes for **1a** that were confirmed by 500 ns long molecular dynamics simulations. In the interaction with PRMT9, the ligand adenine ring is able to occupy the SAM cofactor binding pocket, establishing H-bond interactions with the L208 and S236 backbone NHs groups.

Additional H-bonds are formed by the sugar OH groups with the E255 backbone CO, while the arginine-mimetic group is involved in ionic contacts with the negatively charged side chains of the double E loop (E150 and E264). E264 is also involved in charged-reinforced H-bonds with the urea moiety. Finally, the 4-hydroxy-2-naphthoate group is inserted in a

141

rather lipophilic cleft establishing a π−π interaction with the W152 side chain, while the methyl ester in position 6 is H-bonding E433 backbone NH. Also in the binding with PRMT7, the ligand adenosine and sugar rings are involved in H-bond interactions reminiscent of the interactions established by the same rings in the SAM cosubstrate. Additionally, the guanidine portion is involved in ionic contacts with negatively charged residues. The main differences, however, are recorded for the terminal 4-hydroxy-2-naphthoate group that in this case is pointing toward a rather solvent-exposed and hydrophilic protein region.

To further validate the ligand/PRMT9 interaction model, we designed and synthesized a trifluoromethylated analogue of **1a** (namely, **1j**, EML1219) with the aim to strengthen the π−π contact with the W152 side chain of the enzyme without altering the overall conformation. SPR studies confirmed a specific and strong binding interaction between PRMT9 and **1j** with a K_D value in the submicromolar range and a relatively high in vitro residence time value (K_D = 188 nM; τ_R = 500 s).

However, this gain in affinity was paid by selectivity against the other PRMTs, particularly against the other type II enzyme PRMT5, as well as against related methyltransferases like the non-SET domain containing DOT1L. On the contrary, **1j** was found to be selective against a panel of SET-domain-containing proteins including ASH1L/KMT2H, EZH2/KMT6, MLL1/KMT2A, SET7/9/KMT7, SETD8/KMT5A, SUV39H2/KMT1B, and SUV420H1/KMT5B, which were not inhibited even at the higher tested concentration (100 μM, > 500 fold higher than the IC$_{50}$ value against PRMT9).

Similar to what we previously observed for compound **1h**, LFQ mass spectrometry revealed that compounds **1a** and **1j** are able to affect PRMT activity even in a cellular context, regardless of their low cell permeability.

In conclusion, this study sheds more light on the binding interactions with PRMT7 and PRMT9 of inhibitors spanning both the substrate and the cosubstrate pockets and provides structural information that could inform the development of potent and selective inhibitors of these two enzymes.

Chemistry. The synthetic protocol adopted for the preparation of compounds **1i** and **1j** is depicted in Scheme 1.

4-acetoxy-6-nitro-2-naphthoate (**2a**) and 4-acetoxy-6-nitro-8-(trifluoromethyl)-2-naphthoate (**2b**) were prepared according to the synthetic procedures previously reported by us (Scheme 2).[31] Reduction of the nitro group with zinc dust in acetic acid (**3a, 3b**), followed by treatment with phenyl chloroformate, allowed us to obtain compounds **4a, 4b**, which straightforwardly reacted with the proper mono-Boc-protected alkyldiamines to yield ureidic compounds **5a, 5b**. After trifluoroacetic acid (TFA) deprotection, the corresponding amines **6a, 6b** were coupled with the adenosine derivative **7**[31] in the presence of EDC hydrochloride as an activating agent. The obtained derivatives **8a,8b** were finally subjected to acidic deprotection to give the desired compounds **1i** and **1j**.

■ EXPERIMENTAL SECTION

Chemistry. *General Directions.* All chemicals purchased from Merck KGaA and Fluorochem Ltd. were of the highest purity. All solvents were reagent grade and, when necessary, were purified and dried by standard methods. All reactions requiring anhydrous conditions were conducted under a positive atmosphere of nitrogen in oven-dried glassware. Standard syringe techniques were used for the anhydrous addition of liquids. Reactions were routinely monitored by TLC performed on aluminum-backed silica gel plates (Merck KGaA, Alufolien Kieselgel 60 F254) with spots visualized by UV light

Scheme 2. Synthesis of Derivative 2b
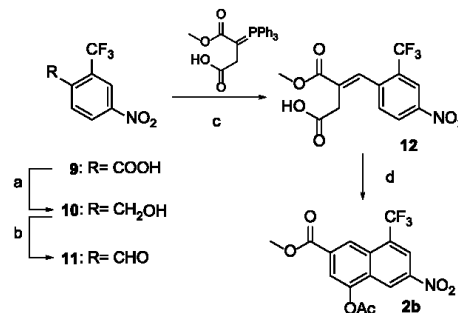
Reagents and conditions: (a) NaBH$_4$, I$_2$, dry THF, 0 °C to reflux, 18 h (88%); (b) Dess-Martin periodinane, dry DCM, 2 h, r.t. (74%); (c) toluene, r. t., 48 h (63%); (d) sodium acetate, acetic anhydride, 120 °C (MW), 25 min (67%).

(λ = 254, 365 nm) or using a KMnO4 alkaline solution. Solvents were removed by using a rotary evaporator operating at a reduced pressure of ∼10 Torr. Organic solutions were dried over anhydrous Na$_2$SO$_4$. Chromatographic purification was done on an automated flash-chromatography system (Isolera Dalton 2000, Biotage) using cartridges packed with KPSIL, 60 Å (40−63 μm particle size). All microwave-assisted reactions were conducted in a CEM Discover SP microwave synthesizer equipped with a vertically focused IR temperature sensor. Analytical high-performance liquid chromatography (HPLC) was performed on a Shimadzu SPD 20A UV/vis detector (λ = 220 and 254 nm) using a C-18 column Phenomenex Synergi Fusion-RP 80A (75 × 4.60 mm; 4 μm) at 25 °C using mobile phases A (water + 0.1% TFA) and B (ACN + 0.1% TFA) at a flow rate of 1 mL/min. Preparative HPLC was performed using a Shimadzu Prominence LC-20AP instrument with the UV detector set to 220 and 254 nm. Samples were injected into a Phenomenex Synergi Fusion-RP 80A (150 × 21 mm; 4 mm) C-18 column at room temperature. Mobile phases A (water + 0.05% TFA) and B (ACN + 0.03% TFA) were used at a flow rate of 20 mL/min. ^{1}H and ^{19}F spectra were recorded at 400 MHz on a Bruker Ascend 400 spectrometer, while ^{13}C NMR spectra were obtained by distortionless enhancement by polarization transfer quaternary (DEPTQ) spectroscopy on the same spectrometer. Chemical shifts are reported in δ (ppm) relative to the internal reference tetramethylsilane (TMS). For ^{19}F spectra, trifluorotoluene (−62.74 ppm) was used as an external standard. Low-resolution and high-resolution mass spectra were recorded on a ThermoFisher Scientific Orbitrap XL mass spectrometer in electrospray positive ionization modes (ESI-MS). All tested compounds possessed a purity of at least 95% established by HPLC unless otherwise noted.

Methyl 6-(3-(2-(3-(((2R,3S,4R,5R)-5-(6-Amino-9H-purin-9-yl)-3,4-dihydroxytetrahydrofuran-2-yl)methyl)guanidino)ethyl)-ureido)-4-hydroxy-2-naphthoate (1i). Compound **8a** (0.100 g, 0.120 mmol) was dissolved in a 1:1 DCM/TFA solution (0.1 M), and then a drop of water was added. The resulting mixture was stirred at room temperature for 2 h. Then, the solvent was evaporated and the crude material was purified by reversed-phase high-performance liquid chromatography (RP-HPLC) to afford the TFA salt of **1i** as a white solid (54.0 mg, 76%). ^{1}H NMR (400 MHz, DMSO-d_6) δ 10.34 (s, 1H, exchangeable with D$_2$O), 9.17 (s, 1H, exchangeable with D$_2$O), 8.52 (s, 1H), 8.34 (s, 1H), 8.27−8.21 (m, 1H), 7.97 (s, 1H), 7.89 (d, J = 9.0 Hz, 1H), 7.63−7.38 (m, 6H, 4H, exchangeable with D$_2$O), 7.30 (s, 1H), 6.49 (br t, J = 5.7 Hz, 1H, exchangeable with D$_2$O), 5.95 (d, J = 5.7 Hz, 1H), 4.69 (t, J = 5.5 Hz, 1H), 4.18−4.12 (m, 1H), 4.09−4.00 (m, 1H), 3m.86 (s, 3H), 3.28−3.17 (m, 4H). ^{13}C NMR (100 MHz, DMSO-d_6) δ: 167.1, 156.6, 156.0, 153.1, 150.3, 149.4, 141.6, 140.0, 130.3, 129.4, 128.3, 125.3, 121.7, 120.7, 119.6, 115.1,

142

108.0, 107.0, 88.3, 82.8, 73.3, 71.6, 52.5, 43.7, 41.9, 38.8. HRMS (ESI): m/z [M + H]$^+$ calcd for $C_{26}H_{30}N_{10}O_7$ + H$^+$: 595.2372. Found: 595.2376.

Methyl 6-(3-(3-(3-(((2R,3S,4R,5R)-5-(6-Amino-9H-purin-9-yl)-3,4-dihydroxytetrahydrofuran-2-yl)methyl)guanidino)propyl)ureido)-4-hydroxy-8-(trifluoromethyl)-2-naphthoate (1j). The TFA salt of compound **1j** was obtained as a white solid (22.0 mg, 60%), starting from compound **8b** (38.0 mg, 0.046 mmol), following the procedure described for **1i**. ^{1}H NMR (400 MHz, DMSO-d_6) δ 10.80 (s, 1H, exchangeable with D$_2$O), 9.36 (s, 1H, exchangeable with D$_2$O), 8.47 (d, J = 2.2 Hz, 1H), 8.43 (s, 1H), 8.26 (d, J = 2.3 Hz, 1H), 8.25 (s, 1H), 8.09 (s, 1H), 7.82 (s, 2H, exchangeable with D$_2$O), 7.51−7.45 (m, 1H, exchangeable with D$_2$O), 7.45−7.39 (m, 3H, 2H, exchangeable with D$_2$O), 6.55 (br t, J = 5.7 Hz, 1H, exchangeable with D$_2$O), 5.93 (d, J = 5.8 Hz, 1H), 4.71 (t, J = 5.4 Hz, 1H), 4.16 (t, J = 4.5 Hz, 1H), 4.05−4.00 (m, 1H), 3.89 (s, 3H), 3.19−3.10 (m, 4H), 1.69−1.61 (m, 2H). ^{19}F NMR (377 MHz, DMSO-d_6) δ: −58.57 (s, 3F), −73.97 (s, 3F). ^{13}C NMR (101 MHz, DMSO-d_6) δ: 166.5, 158.8, 158.5, 156.2, 155.5, 154.4, 153.5, 150.6, 149.2, 141.2, 138.6, 128.9, 127.0, 123.8, 119.8, 119.4, 116.3, 111.9, 107.6, 88.2, 82.7, 73.0, 71.2, 52.7, 43.4, 36.8, 29.4. HRMS (ESI): m/z [M + H]$^+$ calcd for $C_{28}H_{31}F_3N_{10}O_7$ + H$^+$: 677.2402. Found: 677.2401.

Methyl 4-Acetoxy-6-nitro-8-(trifluoromethyl)-2-naphthoate (2b). A 10 mL CEM pressure vessel equipped with a stir bar was charged with **12** (0.350 g, 1.05 mmol), acetic anhydride (2.5 mL), and sodium acetate (0.129 g, 1.58 mmol). The microwave vial was sealed and heated in a CEM Discover microwave synthesizer to 120 °C (measured by the vertically focused IR temperature sensor) for 25 min. After cooling to room temperature, the reaction mixture was filtered, and the filtrate was concentrated under reduced pressure. The title product was obtained as a yellow solid (0.250 g, 67%) after recrystallization from AcOEt. ^{1}H NMR (400 MHz, DMSO-d_6) δ 9.17 (d, J = 1.4 Hz, 1H), 8.70 (d, J = 2.2 Hz, 1H), 8.67 (s, 1H), 8.22 (d, J = 1.4 Hz, 1H), 3.99 (s, 3H), 2.55 (s, 3H). MS (ESI) m/z: 358 (M + H)$^+$.

Methyl 4-Acetoxy-6-amino-8-(trifluoromethyl)-2-naphthoate (3b). To a solution of **2b** (0.150 g, 0.420 mmol) in acetic acid (9 mL) was added Zn dust (0.275 g, 4.20 mmol). The resulting mixture was stirred for 1 h at room temperature, filtered, and concentrated in vacuo. The acid residue was dissolved in a saturated aqueous solution of NaHCO$_3$ (30 mL) and extracted with AcOEt (3 × 30 mL). The collected organic phases were washed with brine (30 mL), dried over Na$_2$SO$_4$, filtered, and concentrated under reduced pressure. The title compound **3b** (0.134 g, 97%) was obtained as a pale-yellow solid, which was used in the next step without further purification. ^{1}H NMR (400 MHz, DMSO-d_6) δ 8.39 (s, 1H), 7.69 (d, J = 1.4 Hz, 1H), 7.59 (d, J = 2.2 Hz, 1H), 7.09−7.04 (m, 1H), 6.39 (s, 2H, exchangeable with D$_2$O), 3.89 (s, 3H), 2.44 (s, 3H). MS (ESI) m/z: 328 (M + H)$^+$.

Methyl 4-Acetoxy-6-((phenoxycarbonyl)amino)-8-(trifluoromethyl)-2-naphthoate (4b). To a solution of **3b** (0.134 g, 0.409 mmol) in 1.7 mL of AcOEt was added TEA (0.063 mL, 0.45 mmol). The resulting mixture was cooled at 0 °C, and phenyl chloroformate (0.057 mL, 0.45 mmol) was added dropwise. The resulting yellow suspension was allowed to warm at room temperature and stirred for 16 h. Then, the reaction mixture was diluted with AcOEt (30 mL) and washed with water (3 × 20 mL), HCl 1N (3 × 20 mL), saturated aqueous solution of NaHCO$_3$ (3 × 20 mL), and brine (30 mL). The organic phase was dried in Na$_2$SO$_4$, filtered, and concentrated under reduced pressure. The title compound was obtained as a pale-yellow solid (0.122 g, 65%) after recrystallization from AcOEt. ^{1}H NMR (400 MHz, DMSO-d_6) δ 10.99 (s, 1H, exchangeable with D$_2$O), 8.55 (s, 1H), 8.43 (s, 1H), 8.37−8.32 (m, 1H), 7.94 (d, J = 1.4 Hz, 1H), 7.51−7.41 (m, 2H), 7.35−7.26 (m, 3H), 3.94 (s, 3H), 2.44 (s, 3H). MS (ESI) m/z: 448 (M + H)$^+$.

Methyl 6-(3-(2-((tert-Butoxycarbonyl)amino)ethyl)ureido)-4-hydroxy-2-naphthoate (5a). To a stirring solution of compound **4a** (0.400 g, 1.05 mmol) in dry DMF (5 mL) were added a solution of tert-butyl (2-aminoethyl)carbamate (0.336 g, 2.10 mmol) and TEA

(0.294 mL, 2.10 mmol) in dry DMF (5 mL). The resulting reaction mixture was stirred at room temperature for 2 h. Then, a saturated aqueous solution of NaHCO$_3$ was added (50 mL) and the resulting mixture was extracted with AcOEt (3 × 30 mL). The combined organic phases were washed with a saturated aqueous solution of NaHCO$_3$ (3 × 20 mL) and brine (10 mL), dried over Na$_2$SO$_4$, filtered, and concentrated under reduced pressure. The crude material was purified by flash chromatography to afford the title compound as an orange solid (0.290 g, 68%). ^{1}H NMR (400 MHz, DMSO-d_6) δ 10.28 (s, 1H, exchangeable with D$_2$O), 8.91 (s, 1H, exchangeable with D$_2$O), 8.27 (d, J = 2.1 Hz, 1H), 7.97 (s, 1H), 7.89 (d, J = 8.9 Hz, 1H), 7.55 (dd, J = 8.9, 2.1 Hz, 1H), 7.30 (s, 1H), 6.85 (t, J = 5.0 Hz, 1H, exchangeable with D$_2$O), 6.25 (t, J = 5.7 Hz, 1H, exchangeable with D$_2$O), 3.87 (s, 3H), 3.14−3.08 (m, 2H), 3.01−2.94 (m, 2H), 1.40 (s, 9H). MS (ESI) m/z: 404 (M + H)$^+$.

Methyl 6-(3-(3-((tert-Butoxycarbonyl)amino)propyl)ureido)-4-hydroxy-8-(trifluoromethyl)-2-naphthoate (5b). Compound **5b** was obtained as a pale-yellow solid (67.0 mg, 70%), starting from compound **4b** (88.0 mg, 0.197 mmol) and tert-butyl (3-aminopropyl)carbamate (68.0 mg, 0.390 mmol), following the procedure described for **5a**. ^{1}H NMR (400 MHz, DMSO-d_6) δ 10.76 (s, 1H, exchangeable with D$_2$O), 9.27 (s, 1H, exchangeable with D$_2$O), 8.47 (d, J = 2.2 Hz, 1H), 8.24 (d, J = 2.2 Hz, 1H), 8.09 (s, 1H), 7.42 (d, J = 1.4 Hz, 1H), 6.83 (t, J = 5.7 Hz, 1H, exchangeable with D$_2$O), 6.34 (t, J = 5.8 Hz, 1H, exchangeable with D$_2$O), 3.89 (s, 3H), 3.15−3.08 (m, 2H), 3.01−2.94 (m, 2H), 1.60−1.52 (m, 2H), 1.38 (s, 9H). MS (ESI) m/z: 486 (M + H)$^+$.

Methyl 6-(3-(2-Aminoethyl)ureido)-4-hydroxy-2-naphthoate (6a). Compound **5a** (0.700 g, 1.73 mmol) was dissolved in 10 mL of a solution of DCM/TFA (9:1), and the mixture was stirred at room temperature for 2 h. Then, the solvent was evaporated, and the resulting solid was washed with CHCl$_3$ to give the TFA salt of compound **6a** as a white solid (0.558 g, 80%). ^{1}H NMR (400 MHz, DMSO-d_6) δ 10.33 (s, 1H, exchangeable with D$_2$O), 9.19 (s, 1H, exchangeable with D$_2$O), 8.29 (d, J = 2.2 Hz, 1H), 7.98−7.95 (m, 1H), 7.90 (d, J = 8.9 Hz, 1H), 7.76 (br s, 3H, exchangeable with D$_2$O), 7.58 (dd, J = 8.9, 2.1 Hz, 1H), 7.30 (s, 1H), 6.47 (br t, 1H, J = 5.8 Hz, exchangeable with D$_2$O), 3.86 (s, 3H), 3.29−3.12 (m, 2H), 2.98−2.89 (m, 2H). MS (ESI) m/z: 303 (M + H)$^+$.

Methyl 6-(3-(3-Aminopropyl)ureido)-4-hydroxy-8-(trifluoromethyl)-2-naphthoate (6b). The TFA salt of compound **6b** was obtained as a white solid (63.4 mg, 92%), starting from compound **5b** (67.0 mg, 0.138 mmol), following the procedure described for **6a**. ^{1}H NMR (400 MHz, DMSO-d_6) δ 10.80 (s, 1H, exchangeable with D$_2$O), 9.42 (s, 1H, exchangeable with D$_2$O), 8.49 (d, J = 2.2 Hz, 1H), 8.27 (d, J = 2.2 Hz, 1H), 8.10 (s, 1H), 7.76−7.63 (m, 3H, exchangeable with D$_2$O), 7.43 (d, J = 1.4 Hz, 1H), 6.65 (t, J = 5.9 Hz, 1H, exchangeable with D$_2$O), 3.89 (s, 3H), 3.24−3.17 (m, 2H), 2.88−2.80 (m, 2H), 1.79−1.72 (m, 2H). MS (ESI) m/z: 386 (M + H)$^+$.

Methyl 6-(3-(2-((E)-3-(((3aR,4R,6R,6aR)-6-(6-Amino-9H-purin-9-yl)-2,2-dimethyltetrahydrofuro[3,4-d][1,3]dioxol-4-yl)methyl)-2-(tert-butoxycarbonyl)guanidino)ethyl)ureido)-4-hydroxy-2-naphthoate (8a). To a stirred suspension of **6a** (0.147 g, 0.354 mmol) and **7** (100 mg, 0.177 mmol) in dry DCM, EDC hydrochloride (69.0 mg, 0.354 mmol) and TEA (0.074 mL, 0.531 mmol) were added, and the resulting mixture was stirred at room temperature for 18 h. Then, the solvent was evaporated under reduced pressure, and the resulting oil was taken up with water. The aqueous phase was extracted with AcOEt (3 × 25 mL), and the collected organic phases were washed with brine, dried over Na$_2$SO$_4$, filtered, and concentrated under reduced pressure. The crude material was purified by flash chromatography, yielding **8a** as a white solid (0.109 g, 74%). ^{1}H NMR (400 MHz, DMSO-d_6) δ 10.28 (s, 1H, exchangeable with D$_2$O), 9.01−8.90 (m, 1H, exchangeable with D$_2$O), 8.35 (s, 1H), 8.23 (d, J = 2.2 Hz, 1H), 8.18 (s, 1H), 7.96 (d, J = 1.4 Hz, 1H), 7.88 (d, J = 8.9, 1H), 7.59 (dd, J = 8.9, 2.2 Hz, 1H), 7.33 (s, 2H, exchangeable with D$_2$O), 7.29 (d, J = 1.4 Hz, 1H), 6.42−6.32 (m, 1H, exchangeable with D$_2$O), 6.15 (s, 1H), 5.47−5.39 (m, 1H), 5.10−4.93 (m, 1H), 4.35−4.24 (m, 1H), 3.86 (s, 3H), 3.52−

143

3.40 (m, 2H), 3.28−3.22 (m, 4H), 1.52 (s, 3H), 1.36 (s, 9H), 1.31 (s, 3H); MS (ESI) m/z: 835 (M + H)⁺.

Methyl 6-(3-(3-((E)-3-(((3aR,4R,6R,6aR)-6-(6-Amino-9H-purin-9-yl)-2,2-dimethyltetrahydrofuro[3,4-d][1,3]dioxol-4-yl)methyl)-2-(tert-butoxycarbonyl)guanidino)propyl)ureido)-4-hydroxy-8-(trifluoromethyl)-2-naphthoate (8b). The compound **8b** was obtained as a white solid (42.0 mg, 60%), starting from compound **6b** (63.4 mg, 0.127 mmol) and compound **7** (39.3 mg, 0.085 mmol), following the procedure described for **8a**. ¹H NMR (400 MHz, DMSO-d_6) δ 10.76 (s, 1H, exchangeable with D₂O), 9.21 (s, 1H, exchangeable with D₂O), 8.47 (d, J = 2.4 Hz, 1H), 8.35 (d, J = 2.2 Hz, 1H), 8.25 (d, J = 2.4 Hz, 1H), 8.18 (d, J = 2.2 Hz, 1H), 8.09 (s, 1H), 7.42 (d, J = 1.4 Hz, 1H), 7.34 (s, 2H, exchangeable with D₂O), 6.50−6.42 (m, 1H, exchangeable with D₂O), 6.15 (s, 1H,), 5.78−5.73 (m, 1H), 5.07−4.97 (m, 1H), 4.33−4.25 (m, 1H), 3.89 (s, 3H), 3.49−3.41 (m, 2H), 3.22−3.11 (m, 4H), 1.68−1.60 (m, 2H), 1.53 (s, 3H), 1.35 (s, 9H), 1.32 (s, 3H). MS (ESI) m/z: 817 (M + H)⁺.

(4-Nitro-2-(trifluoromethyl)phenyl)methanol (10). To a cooled solution of 4-nitro-2-(trifluoromethyl)benzoic acid (**9**; 3.00 g, 12.76 mmol) in dry THF (26 mL) was added NaBH₄ (1.21 g, 31.9 mmol) portion-wise. Subsequently, a solution of I₂ (3.24 g, 12.76 mmol) in 13 mL of dry THF was added over 1 h, and the resulting mixture was stirred at room temperature for 1 h and then refluxed for 12 h. The mixture was cooled at room temperature, and a solution of KOH 20% (100 mL) was added and stirred for 1 h: the aqueous phase was extracted with AcOEt (3 × 40 mL), and the collected organic phases were washed with brine, dried over Na₂SO₄, filtered, and concentrated under reduced pressure. The crude product was purified by flash chromatography, yielding **10** as a yellow solid (2.50 g, 88%). ¹H NMR (400 MHz, DMSO-d_6) δ 8.55 (dd, J = 8.6, 2.4 Hz, 1H), 8.39 (d, J = 2.4 Hz, 1H), 8.08 (d, J = 8.6 Hz, 1H), 5.95−5.88 (m, 1H, exchangeable with D₂O), 4.78 (s, 2H). MS (ESI) m/z: 222 (M + H)⁺.

4-Nitro-2-(trifluoromethyl)benzaldehyde (11). To a cooled solution of **10** (1.3 g, 5.88 mmol) in dry DCM (25 mL) was added Dess-Martin periodinane (2.47 g, 6.47 mmol) portion-wise, and the resulting mixture was stirred at room temperature for 3 h. The formed-white precipitate was filtered off, and the filtrate was taken up with DCM (60 mL). The organic phase was washed with saturated aqueous solution of NaHCO₃ (3 × 30 mL) and brine (30 mL), dried over Na₂SO₄, filtered, and concentrated under reduced pressure. The crude was purified by flash chromatography, yielding **11** as a pale-yellow solid (0.950 g, 74%). ¹H NMR (400 MHz, DMSO-d_6) δ 10.34 (s, 1H), 8.69 (dd, J = 8.5, 2.2 Hz, 1H), 8.57 (d, J = 2.2 Hz, 1H), 8.33 (d, J = 8.5 Hz, 1H). MS (ESI) m/z: 220 (M + H)⁺.

(E)-3-(Methoxycarbonyl)-4-(4-nitro-2-(trifluoromethyl)-phenyl)but-3-enoic acid (12). To a suspension of 4-methoxy-4-oxo-3-(triphenyl-l5-phosphaneylidene)butanoic acid (1.13 g, 2.88 mmol) in toluene (20 mL) was added compound **11** (0.630 g, 2.88 mmol). The resulting mixture was stirred at room temperature for 48 h and then concentrated under reduced pressure. The residue was taken up with saturated aqueous solution of NaHCO₃ (60 mL), washed with Et₂O (3 × 30 mL), and acidified with HCl 6 N until pH 2. The aqueous phase was extracted with AcOEt (3 × 30 mL), and the collected organic phases were washed with brine, dried over Na₂SO₄, filtered, and concentrated in vacuo to afford **12** (0.600 g, 63%) as a yellow solid. ¹H NMR (400 MHz, DMSO-d_6) δ 8.59 (dd, J = 8.5, 2.4 Hz, 1H), 8.50 (d, J = 2.4 Hz, 1H), 7.86 (d, J = 2.4 Hz, 1H), 7.72 (d, J = 8.5 Hz, 1H), 3.79 (s, 3H), 3.23 (s, 2H); MS (ESI) m/z: 334 (M+H)⁺.

AlphaLISA PRMT9 Activity Assay. PRMT9 activity assays were performed by AlphaLISA using the "PRMT9 Homogeneous assay Kit" (BPS BioScience, #52069), as opportunely modified by us (see above in the text).

The assays were performed in white opaque OptiPlate-384 (PerkinElmer, no. 6007299) at 22 °C in a final volume of 30 μL, using the HMT assay buffer 2A (BPS-BioScience #52170-A).

In each well, 2 μL of human recombinant PRMT9 (BPS BioScience, no. 79124) (50 ng/μL) was first incubated for 30 min

with 3 μL of each compound (dissolved in DMSO and diluted in assay buffer to obtain 1% DMSO). Then, each well was added with 0.5 μL of the biotinylated substrate peptide SF3B2 (aa 500−519) (Pepmic, custom synthesis) (final concentration, 100 nM), 1 μL of SAM 250 μM, 1.5 μL of water, and 2 μL of 4× HMT assay buffer 2A to reach the final volume of 10 μL. The reaction was incubated for 60 min. Afterward, in each well, 5 μL of a 1:100 dilution of Primary antibody 28 (BPS BioScience, #52140Z3) in Detection buffer (BPS BioScience) and 5 μL of anti-Rabbit acceptor beads (PerkinElmer, #AL104C) were added to obtain a final concentration of 20 μg/mL. After an incubation of 60 min, 10 μL of streptavidin donor beads (PerkinElmer, # 6760002) diluted in detection buffer was added in each well (final concentration, 20 μg/mL). After an incubation of 30 min, signals were read in Alpha mode with a PerkinElmer EnSight multimode microplate reader (excitation at 680 nm and emission at 615 nm).

For each incubation step, the OptiPlate was sealed with a protective foil to prevent evaporation and contamination. Donor and Acceptor beads were added to the mixture in subdued light.

The 100% activity (positive control) was reached using vehicle (DMSO), while 0% activity (negative control) was obtained without the protein. Data were analyzed by using Excel and Prism software. Values obtained for each compound are mean ± SD determined for three separate experiments.

PRMT7 and PRMT9 Radioisotope-Based Activity Assay. *Protein Purification and Inhibitors.* Human PRMT9, *C. elegans* PRMT9, human PRMT7, and *C. elegans* PRMT7 plasmids were sequenced, expressed in *E. coli* as GST-fusion proteins, and purified as previously described.[48] Substrates were also sequenced and purified as described [human GST-SF3B2 (401−550);[13] *C. elegans* SFTB-2;[48] human histone H2B (New England Biolabs, M2505S)]. *Xenopus laevis* histone H2B was expressed in *E. coli* and purified similarly to what was previously reported by Luger et al.[72]

Inhibitors used were 5′-deoxy-5′-(methylthio)adenosine (methyl-thioadenosine, MTA; Sigma, cat. no. D5011) and EPZ015666 (APEx Bio, Cat. No. B4989).

In Vitro Methylation Reactions with MTA and EPZ015666. Reactions consisting of approximately 1 μg of enzyme (human or *C. elegans* GST-tagged enzymes PRMT9 and PRMT7), reacted with approximately 5 μg of substrate [for human PRMT9, human GST-SF3B2 401−550 fragment; *C. elegans* PRMT9 with *C. elegans* GST-SFTB-2 (99−248) fragment, or recombinant human histone H2B from New England Biolabs (M2505S)], were incubated for the indicated time in reaction buffer {50 mM potassium HEPES buffer, 10 mM NaCl, 1 mM dithiothreitol (DTT), pH 8.0 with 0.7 μM S-adenosyl-L-[methyl-³H]methionine (³H-AdoMet, PerkinElmer Life Sciences, 82.7 Ci/mmol, 0.55 mCi/mL in 10 mM H₂SO₄/EtOH [9:1 (v/v)])} in a final reaction volume of 60 μL. Each reaction was incubated at the corresponding optimal reaction temperature (37 °C for human PRMT9, 25 °C for *C. elegans* PRMT9, and 15 °C for *C. elegans* and human PRMT7 enzymes. MTA was dissolved in water, and a wavelength scan was taken to determine the final concentration using the extinction coefficient. The final concentrations used are indicated in the figure legends. EPZ015666 was dissolved in DMSO to a final concentration of 13.04 mM, and further dilutions were made in DMSO to achieve the final concentrations used as indicated in the figure legends. EML734, EML736, and EML709 were also dissolved in DMSO, and further dilutions were made in DMSO for the working stocks. For controls, no inhibitor reactions were created by the addition of the respective solvent (water for MTA and DMSO for EPZ015666 and EML inhibitors).

Detection of Inhibition Activity after SDS-PAGE. After the reaction incubations with the various concentrations of inhibitors, the reactions were quenched by adding 0.2 volume of 5× SDS sample loading buffer, and subsequently, the reactions were run on a 12.6% polyacrylamide Tris gel. To collect the radioactive signal, the gels were then treated in the same way as previously described.[48]

Analysis of Densitometric Data. After various exposures were collected to ensure linear detection, densitometry analysis was done

using ImageJ software, and data were plotted as normalized activity to the no inhibitor controls.

Molecular Modeling and Molecular Dynamics Methods. Docking experiments were attained for compound **1a** on the X-ray structure of the human PRMT9 in complex with the adenosine-based inhibitor (MT556, PDB code 7RBQ)[59] and on the Alphafold structure of the human PRMT7 enzyme. Before these receptor structures could be utilized in docking calculations, they required preparation using the Protein Preparation Wizard[73,74] utility within the Maestro software package.[75] The receptor structures were prepared by assigning bond orders, adding hydrogens, and generating physiological pH states using the EPIK tool. Subsequently, the "Minimize and Delete Waters" tool was employed to minimize the overall protein structures, with heavy atoms restrained and all water molecules removed. In order to prepare **1a** for docking calculations, a separate tool within the Schrödinger software suite known as "LigPrep" was utilized. Specifically, all the hydrogen atoms were added, all the tautomeric states were generated, and the specified chiralities were retained. The AUTODOCK-GPU (AD4-GPU)[58] is an accelerated version of AutoDock 4.2.6 able to increase docking calculation speed.[76] Before launching all docking calculations, for every ligand/receptor complex, a 60 Å × 60 Å × 60 Å with a 0.375 Å spacing grid was calculated around the binding site for ligand atom types using AutoGrid4. In the context of performing docking calculations, a crucial preliminary step involves the conversion of ligand structures from the PDB to the PDBQT format, which is required by AutoDock software. This conversion is typically accomplished using the AutoDock Tools (ADT) utility known as "prepare_ligand4.py". All docking calculations were accomplished on our GPUs (NVIDIA RTX A6000 and Quadro RTX 8000). To improve the accuracy and speed of the docking calculations, a heuristic parameter was incorporated into the AutoDock GPU algorithm. This parameter guides the search algorithm toward the most promising solutions based on previous docking experiments. During the automated docking process, only ".xml" output files were generated to reduce the amount of storage required and simplify the data analysis. 200 independent docking simulations were carried out for each docking experiment to ensure the comprehensive exploration of the conformational space and enhance the likelihood of identifying potential drug candidates. Finally, a .csv file was created from .xml files, returning for **1a** the lowest binding free energy, number of runs, mean binding energy, and numbers in the lowest energy cluster.

The latter conformation was considered for the MD simulations. We conducted all-atom molecular dynamics (MD) simulations using the Desmond module[60] of the Schrödinger software package to study the **1a**/hPRMT9 and **1a**/hPRMT7 complexes. To set up the initial system for the MD calculation, we utilized the system builder panel. The complexes were placed within a parallelepiped box and solvated with TIP3P water models.[77] To neutralize the system's charge, Na+ ions were added. The equilibration of the systems was carried out using the *NPT* ensemble following the default Desmond protocol, which involved a total of eight steps. The first seven steps were short simulations that gradually increased the temperature and decreased restraints on the solute, aiming to reach an equilibrated state. Subsequently, the equilibrated systems underwent a 500 ns MD production run under periodic boundary conditions (PBC) and the *NPT* ensemble, utilizing the OPLSe force field.[78] The simulation was conducted at 1 atm pressure and a temperature of 300 K. To maintain these conditions, a Martyna–Tobias–Klein barostat[79] and a Nose-Hoover chain thermostat[80] were employed.

Radioisotope-Based IC$_{50}$ Profiling against PRMTs. The effects of compounds **1i,j** on the catalytic activity of PRMT1, PRMT3, PRMT4, PRMT5, PRMT6, PRMT7, and PRMT8 were determined with a HotSpot PRMT activity assay by Reaction Biology Corporation (Malvern, PA, USA) according to the company's standard operating procedure.[81,82] Briefly, the full-length human recombinant proteins PRMT1 (residues 2–371, C-terminus; with an N-terminal GST-tag; M_W = 68.3 kDa; Genbank Accession # NM_001536) or PRMT3 (residues 2–531, C-terminus; with an N-terminal His-tag; M_W = 62.0 kDa; Genbank Accession #

NM_005788), or PRMT4 (residues 2–608, C-terminus; with an N-terminal GST-tag; M_W = 91.7 kDa; Genbank Accession # NM_199141), or PRMT5/MEP50 complex[83,84] (residues PRMT5 2–637, C-terminus, and MEP50 2–342, C-terminus; with an N-terminal FLAG-tag, PRMT5, or His-tag, MEP50; M_W = 73.7/39.9 kDa; Genbank Accession # NM_006109, NM_006109), or PRMT6 (residues 2–375, C-terminus; with an N-terminal GST-tag; MW = 67.8 kDa; Genbank Accession # NM_018137), or PRMT7 (residues 2–692, C-terminus; with an N-terminal His-tag; M_W = 81.7 kDa; Genbank Accession # NM_019023), or ΔN(1–60)-PRMT8[85] (residues 61–394, C-terminus; with C- and N-terminal His-tags; M_W = 43.2 kDa; Genbank Accession # NM_019854) were added to a solution of the proper substrate (histone H4 for PRMT1, PRMT3, and PRMT8; histone H3.3 for PRMT4; histone H2A for PRMT5/MEP50; GST-GAR for PRMT6 and PRMT7; final concentration 5 μM) in freshly prepared reaction buffer (50 mM Tris-HCl (pH 8.5), 5 mM MgCl$_2$, 50 mM NaCl, 1 mM DTT, 1 mM PMSF, 1% DMSO) and gently mixed. The proper solution of compound **1i–j** in DMSO was delivered into the PRMT reaction mixture by using Acoustic Technology (Echo 550, LabCyte Inc. Sunnyvale, CA) in nanoliter range, and incubated for 20 min at room temperature. Then, ^{3}H-SAM (final concentration of 1 μM) was delivered into the reaction mixture to initiate the reaction. After incubation for 60 min at 30 °C, the reaction mixture was delivered to filter-paper for detection (as assessed by scintillation). Data were analyzed using Excel and GraphPad Prism 6.0 software (GraphPad Software Inc., San Diego, CA) for IC$_{50}$ curve fits using sigmoidal dose vs response - variable slope (four parameters) equations.

Selectivity Assay against KMTs. The effects of compound **1j** on the catalytic activity of ASH1L/KMT2H, EZH2/KMT6, G9a/KMT1C, MLL1/KMT2A, SET7/9/KMT7, SMYD3/KMT3E, SUV39H2/KMT1B, and DOT1L/KMT4 were determined with a HotSpot KMT activity assay by Reaction Biology Corporation (Malvern, PA, USA) according to the company's standard operating procedure.[81,82] Briefly, the human recombinant ASH1L (residues 2046–2330, with an N-terminal His-tag; M_W = 35.4 kDa; Genbank Accession # NM_018489), or the human recombinant EZH2-containing five-member polycomb repressive complex 2 (including EZH2 residues 2–746, AEBP2 2–517, EED 2–441, RbAp48 2–425, SUZ12 2–739; all full-length; with N-terminal Flag-tag on EED and N-terminal His-tag on all others; M_W = 333.8 kDa; Genbank Accession # NM_001203247, NM_001114176, NM_003797, NM_005610, NM_015355), or the human recombinant G9a (residues 913–1193, C-terminus; with an N-terminal His-tag; M_W = 34.6 kDa; Genbank Accession # NM_006709.3), or the human recombinant MLL1 complex (including MLL1 residues 3745–3969, C-terminus, WDR5 22–334, C-terminus, RbBP5 1–538, C-terminus, ASH2L 2–534, C-terminus, DPY-30 1–99, C-terminus; N-terminal His-tag on all subunits; M_W = 212.0 kDa; Genbank Accession # NM_005933, NM_017588, NM_005057, NM_001105214, NM_0325742), or the human recombinant SET7/9 (residues 2–366, C-terminus; with a N-terminal GST-tag and a C-terminal His-tag; M_W = 68.5 kDa; Genbank Accession # NM_030648), or the human recombinant SMYD3 (residues 2–428, C-terminus; C-terminal His-tag; M_W = 50.1 kDa; Genbank Accession # NM_001167740), or the human recombinant SUV39H2 (residues 46–410, C-terminus; N-terminal fusion protein with a C-terminal His-tag; M_W = 98.8 kDa; GenBank Accession No. NM_001193424), or the human recombinant DOT1L (residues 1–416; N-terminal GST-tag; M_W = 80.0 kDa; Genbank Accession # NM_032482) was added to a solution of the proper substrate (oligo nucleosomes for ASH1L, MLL1 complex, and DOT1L, final concentration 0.05 mg/mL; core histone for EZH2 complex and SET7/9, final concentration 0.05 mg/mL; histone H3 for SUV39H2, final concentration 5 μM; histone H3 1–21 for G9a, final concentration 2.5 μM) in freshly prepared reaction buffer (50 mM Tris-HCl (pH 8.5), 5 mM MgCl$_2$, 50 mM NaCl, 1 mM DTT, 1 mM PMSF, 1% DMSO) and gently mixed. The proper solution (1 or 10 μM fixed concentrations) of compound **1j** in DMSO was delivered into the KMT reaction mixture by using Acoustic Technology (Echo 550, LabCyte Inc. Sunnyvale,

145

CA) in the nanoliter range and incubated for 20 min at room temperature. Then, ^{3}H-SAM (final concentration 1 μM) was delivered into the reaction mixture to initiate the reaction. After incubation for 60 min at 30 °C, the reaction mixture was delivered to filter paper for detection (as assessed by scintillation). SAH[62−64] or chaetocin (for ASH1L)[65] was used as reference compounds and tested in 10-dose IC$_{50}$ mode with 3-fold serial dilution starting at 100 μM. No inhibitor control (DMSO) was considered as showing 100% enzyme activity. Data were analyzed using Excel and GraphPad Prism 6.0 software (GraphPad Software Inc., San Diego, CA). Values obtained for each compound are mean ± SD determined for two separate experiments.

PRMT9 SPR Experiments. SPR experiments were performed on a Biacore T200 biosensor (Cytiva). PBS buffer (phosphate buffered saline, pH 7.5) supplemented with 0.05% Tween-20 was used as the running buffer. Full-length recombinant PRMT9 (2−285, BPS Bioscience, # BPS-79124) was covalently immobilized on the carboxymethylated surface of a Series S Sensor Chip CM5 by amine coupling. In detail, 50 μg/mL of protein in phosphate buffer (40 mM NaH$_2$PO$_4$/Na$_2$HPO$_4$ pH 8.0, 110 mM NaCl, 2.2 mM KCl, 0.04% Tween-20, and 2 mM TCEP) was preconcentrated on the surface with 10 mM of sodium acetate pH 4.5 after surface activation with EDC/NHS (1:1) was covalently immobilized using the running buffer 1X HBS − 0.05% Tween20 at a flow rate of 10 μL/min to obtain densities of 8.3 kRU. The compound of interest was diluted in PBS supplemented with 0.05% Tween-20 and injected over the active and reference cells at 10 different concentrations (2-fold dilution series) from 25 μM to 0.05 μM, keeping a final 2% DMSO concentration, using the multicycle modality. Binding experiments were performed at 25 °C by using a flow rate of 30 μL/min, with 90 s of monitoring of association and 180 s of monitoring of dissociation. Regeneration of the surfaces was performed, when necessary, by a 10 s injection of 5 mM NaOH. The sensorgrams obtained at the 10 concentrations of the compound were first corrected taking advantage of the solvent correction performed by the instrument (correction range from 1.5 to 2.8% DMSO), and then they were double-referenced. The corrected sensorgrams were fitted simultaneously by kinetic analysis using the 1:1 Langmuir model of the BIAevaluation software to obtain equilibrium dissociation constants (K_D) and kinetic dissociation (k_{off}) and association (k_{on}) constants. The curve-fitting efficiency was evaluated by the chi-square (χ^2). The χ^2 value denotes the fitting degree between the estimative and experimental curves.

PAINS Analysis. Compounds **1i** and **1j** were analyzed for known classes of assay interference compounds.[86] All derivatives were not recognized as PAINS according to the SwissADME web tool (http://www.swissadme.ch),[87] the Free ADME-Tox Filtering Tool (FAF-Drugs4) program (http://fafdrugs4.mti.univ-paris-diderot.fr/),[70] and the "False Positive Remover" software (http://www.cbligand.org/PAINS/);[88] neither were they recognized as aggregators according to the software "Aggregator Advisor" (http://advisor.bkslab.org/).[89]

Western Blotting Methods. To test the effect of compounds **1a**, **1c**, **1e**, and **1f** on PRMT9 activity, MCF cells or MDA-MB-436 cells were treated with 4 candidate inhibitors at indicated concentrations. After 72 h, cells were harvested in ice-cold PBS and were lysed in radio immune-precipitation assay (RIPA) buffer (50 mM Tris [pH 8.0], 150 mM NaCl, 1% Triton X-100, 0.5% sodium deoxycholate, 0.1% SDS, 2 mM EDTA, and protease inhibitors). For immunoblotting, an equal amount of each sample was resolved by sodium dodecyl sulfate-polyacrylamide gel electrophoresis (SDS-PAGE) and transferred to a polyvinylidene difluoride (PVDF) western membrane. Following blocking with 5% nonfatty milk in PBS-T, membranes were incubated with indicated primary antibodies at 4 °C overnight. The HRP-conjugated secondary antibodies were used against respective primary antibodies. The antibody−antigen complexes were visualized by the chemiluminescence method by using X-ray films.

Proteomic Analysis. Control and **1a**- and **1j**-treated HEK293T cell pellets were suspended in 200 μL of 8 M urea/50 mM ammonium bicarbonate (AmBic, pH 8.5), 0.5% w/v sodium deoxycholate, and 1× protease inhibitor cocktail (GeneSpin); the suspensions were lysed through sonication (Vibra cell; SONICS; 1

min, 30% amplitude, 9.9 s pulses) and then centrifuged (21,000 rcf, 18 °C, 30 min). Protein concentration was determined through Bradford assay (Bio-Rad).

For each sample, 300 μg of proteins were submitted to our optimized *in-solution* digestion protocol,[90] reducing disulfide bridges with 1,4-dithiothreitol (DTT, 10 mM) for 1 h at 25 °C and 800 rpm and then alkylating them with iodoacetamide (IAA, 20 mM) for 30 min, at 25 °C and 800 rpm, in the dark. Then, IAA was quenched with 10 mM DTT, urea was diluted to 1 M with 50 mM AmBic and a trypsin/LysC solution (Promega, Madison, Wisconsin) was added at the enzyme to proteins ratio of 1:100 w/w, overnight at 37 °C.

The peptidic mixtures were then desalted through Sep-Pak C18 1 cc (50 mg) cartridges (Waters, Milford, USA), as reported by the manufacturer, and redissolved in 10% TFA for the subsequent analysis.

1.5 μg sample of each digest was analyzed on an Orbitrap Q-Exactive Classic Mass Spectrometer (ThermoFisher Scientific, Bremen, Germany) coupled to an UltiMate 3000 Ultra-High-Pressure Liquid Chromatography (UHPLC) system (ThermoFisher Scientific, Bremen, Germany), equipped with an EASY-Spray PepMAP RSLC C18 column (3 μm, 100 Å, 75 μm × 50 cm, ThermoFisher Scientific, Bremen, Germany) at a flow rate of 300 nL/min with the following gradient: 1 min at 3% B, 1 to 100 min to 38% B, 100 to 101 min to 80% B, then held at 80% B for 10 min, and re-equilibrated for 8 min at 3% B (A: 95% H$_2$O, 5% CH$_3$CN, 0.1% AcOH; B: 95% CH$_3$CN, 5% H$_2$O, 0.1% AcOH). The mass spectrometer was operated in data-dependent acquisition mode. Full-scan MS spectra were acquired with the scan range 375−1500 *m/z*, a full-scan automatic gain control (AGC) target 3e6 at 70,000 resolution, and a maximum injection time of 50 ms. MS2 spectra were generated for up to 8 precursors (normalized collision energy of 28%), and the fragment ions were acquired at a resolution of 17,500 with an AGC target of 1e5 and a maximum injection time of 80 ms. Protein identification and label-free quantification were then achieved through Proteome Discoverer (version 2.4.1.15). A spectral library search (NIST Human Orbitrap HCD Library, 1127970 spectra, September 2016) was performed through MSPepSearch, and then MS/MS spectra were searched by Sequest against a reviewed *Homo sapiens* database (SwissProt, February 2022, 20,594 entries) with the following parameters: trypsin digestion; maximum of 5 missed cleavages; cysteine carboxyamido-methylation as fixed modification; arginine mono- or dimethylation, methionine oxidization, protein N-terminal acetylation and/or demethylation as variable modifications. Mass tolerances were 50 ppm for MS1 and 0.02 Da for MS/MS. Label-free quantification was achieved by using both unique and razor peptides for peptides and protein abundance calculation, and a pairwise ratio-based approach was used to evaluate the EML-treated vs control peptides and protein abundance. For each calculated ratio, a background-based *t*-test was performed.

■ ASSOCIATED CONTENT

ⓢ Supporting Information

The Supporting Information is available free of charge at https://pubs.acs.org/doi/10.1021/acs.jmedchem.3c01030.

> Optimization of the PRMT9 AlphaLISA assay, docking studies on PRMT9, results of the selectivity assay against KMTs, and copies of ^{1}H NMR,^{13}C NMR, and ^{19}F NMR spectra of all final compounds (PDF)
>
> The output of the computational studies (PDB) (PDB)
>
> Molecular formula strings (CSV)

■ AUTHOR INFORMATION

Corresponding Authors

Sandro Cosconati − *DiSTABiF, University of Campania "Luigi Vanvitelli", 81100 Caserta, Italy;* ⦿ orcid.org/0000-0002-8900-0968; Email: sandro.cosconati@unicampania.it

Sabrina Castellano − *Department of Pharmacy, Epigenetic Med Chem Lab, University of Salerno, Fisciano I-84084 SA, Italy;* orcid.org/0000-0002-7449-3704; Email: scastellano@unisa.it

Gianluca Sbardella − *Department of Pharmacy, Epigenetic Med Chem Lab, University of Salerno, Fisciano I-84084 SA, Italy;* orcid.org/0000-0003-0748-1145; Email: gsbardella@unisa.it

Authors

Alessandra Feoli − *Department of Pharmacy, Epigenetic Med Chem Lab, University of Salerno, Fisciano I-84084 SA, Italy;* orcid.org/0000-0002-8960-7858

Giulia Iannelli − *Department of Pharmacy, Epigenetic Med Chem Lab and PhD Program in Drug Discovery and Development, University of Salerno, Fisciano I-84084 SA, Italy*

Alessandra Cipriano − *Department of Pharmacy, Epigenetic Med Chem Lab, University of Salerno, Fisciano I-84084 SA, Italy*

Ciro Milite − *Department of Pharmacy, Epigenetic Med Chem Lab, University of Salerno, Fisciano I-84084 SA, Italy;* orcid.org/0000-0003-1000-1376

Lei Shen − *Department of Cancer Genetics and Epigenetics, Beckman Research Institute, Duarte, California 91010, United States*

Zhihao Wang − *Department of Cancer Genetics and Epigenetics, Beckman Research Institute, Duarte, California 91010, United States*

Andrea Hadjikyriacou − *Department of Chemistry and Biochemistry, and the Molecular Biology Institute, University of California, Los Angeles, California 90095, United States;* orcid.org/0000-0002-3420-367X

Troy L. Lowe − *Department of Chemistry and Biochemistry, and the Molecular Biology Institute, University of California, Los Angeles, California 90095, United States*

Cyrus Safaeipour − *Department of Chemistry and Biochemistry, and the Molecular Biology Institute, University of California, Los Angeles, California 90095, United States*

Monica Viviano − *Department of Pharmacy, Epigenetic Med Chem Lab, University of Salerno, Fisciano I-84084 SA, Italy;* orcid.org/0000-0003-1118-790X

Giuliana Sarno − *Department of Pharmacy, Epigenetic Med Chem Lab and PhD Program in Drug Discovery and Development, University of Salerno, Fisciano I-84084 SA, Italy*

Elva Morretta − *Department of Pharmacy, ProteoMass Lab, University of Salerno, Fisciano I-84084 SA, Italy*

Maria Chiara Monti − *Department of Pharmacy, ProteoMass Lab, University of Salerno, Fisciano I-84084 SA, Italy;* orcid.org/0000-0002-1337-2909

Yanzhong Yang − *Department of Cancer Genetics and Epigenetics, Beckman Research Institute, Duarte, California 91010, United States*

Steven G. Clarke − *Department of Chemistry and Biochemistry, and the Molecular Biology Institute, University of California, Los Angeles, California 90095, United States*

Complete contact information is available at:
https://pubs.acs.org/10.1021/acs.jmedchem.3c01030

Author Contributions

The manuscript was written through contributions of all authors. All authors have given approval to the final version of the manuscript. A.F. and G.I. contributed equally to this work and are listed in alphabetical order.

◼ ACKNOWLEDGMENTS

◼ ABBREVIATIONS

AcOEt, ethyl acetate; ACN, acetonitrile; AEBP2, zinc finger protein AEBP2, also known as Adipocyte enhancer-binding protein 2; ALPHA, amplified luminescent proximity homogeneous assay; ASH1L, absent small and homeotic disks protein 1 homologue; ASH2L, Set1/Ash2 histone methyltransferase complex subunit ASH2, also known as absent small and homeotic disks protein 2 homologue; CA150, also known as TCERG1; CARM1, coactivator-associated arginine methyltransferase 1; CBP, CREB-binding protein; CREB, cAMP response element-binding protein; DEPTQ, distortionless enhancement by polarization transfer quaternary; DOT1L, DOT1-like (disruptor of telomeric silencing 1-like); DPY30, protein dpy-30 homologue also known as Dpy-30-like protein; EDC, 1-ethyl-3-(3-(dimethylamino)propyl)carbodiimide; ECL, enhanced chemiluminescence; EED, Polycomb protein EED, also known as Embryonic ectoderm development

protein; ELAV, embryonic lethal, abnormal vision, Drosophila; ELAVL1, ELAV like RNA binding protein 1; ELAVL4, ELAV like RNA binding protein 4; EZH2, enhancer of zeste homologue 2; GAR, glycine- and arginine-rich motif; GST, glutathioneS-transferase; HNRNPA1, heterogeneous nuclear ribonucleoprotein A1; HSP70, heat shock 70 kDa protein 1B; HuD, human antigen D, also known as ELAVL4; HuR, human antigen R, also known as ELAVL1; LFQ, label-free quantification method in mass spectrometry; LNCaP, lymph node carcinoma of the prostate cell line; MAVS, mitochondrial antiviral signaling protein; MED12, mediator of RNA polymerase II transcription subunit 12; MLL1, histone-lysine N-methyltransferase 2A, also known as myeloid/lymphoid or mixed-lineage leukemia protein 1; MTA, methylthioadenosine; MTT, 3-(4,5-dimethylthiazol-2-yl)-2,5-diphenyltetrazolium bromide; NFIB-Me, nuclear factor 1 B-type; p300, E1A-associated protein of 300 kDa; P_{app}, apparent permeability; PABP1, poly(A)-binding protein 1; Pbf, 2,2,4,6,7-pentam-ethyldihydrobenzofuran-5-sulfonyl; PBST, phosphate buffered saline with Tween 20; PMSF, phenylmethylsulfonyl fluoride; PRMT, protein arginine methyltransferase; PRMT1, protein arginine methyltransferase 1; PRMT3, protein arginine methyltransferase 3; PRMT4, protein arginine methyltransfer-ase 4; PRMT5, protein arginine methyltransferase 5; PRMT6, protein arginine methyltransferase 6; PRMT7, protein arginine methyltransferase 7; PRMT8, protein arginine methyltransfer-ase 8; PVDF, polyvinylidene difluoride; RBAP48, histone-binding protein RBBP4, also known as retinoblastoma-binding protein p48; RBBP5, retinoblastoma-binding protein 5; SAH, S-5′-adenosyl-L-homocysteine; SAM, S-adenosyl-L-methionine; SD, standard deviation; SRC-3, steroid receptor coactivator-3; SET, suppressor of variegation 3–9 enhancer-of-zeste trithorax; SET7/9, SET domain-containing protein 7; SETD8, SET domain-containing protein 8, also known as PR/SET domain-containing protein 07; siRNA, small inter-ference ribonucleic acid; SF3B2, splicing factor 3B subunit 2 also known as spliceosome-associated protein 145, SAP145; SMYD3, SET (Suppressor of variegation Enhancer of Zeste Trithorax) and MYND (myeloid-Nervy-DEAF-1) domain-containing protein 3; SUV39H2, suppressor of variegation 3–9 homologue 2 also known as Su(var.)3–9 homologue 2; SUV420H1-TV2, Suppressor of variegation 4–20 homologue 1 -transcription variant 2; SUZ12, polycomb protein SUZ12 also known as suppressor of zeste 12 protein homologue; TCERG1, transcription elongation regulator 1; WDR5, WD repeat-containing protein 5

■ REFERENCES

(1) Wu, Q.; Schapira, M.; Arrowsmith, C. H.; Barsyte-Lovejoy, D. Protein arginine methylation: from enigmatic functions to therapeutic targeting. *Nat. Rev. Drug Discovery* **2021**, *20* (7), 509–530.

(2) Turner, B. M. Reading signals on the nucleosome with a new nomenclature for modified histones. *Nat. Struct. Mol. Biol.* **2005**, *12* (2), 110–112.

(3) Bedford, M. T.; Clarke, S. G. Protein Arginine Methylation in Mammals: Who, What, and Why. *Mol. Cell* **2009**, *33* (1), 1–13.

(4) Yang, Y.; Bedford, M. T. Protein arginine methyltransferases and cancer. *Nat. Rev. Cancer* **2013**, *13* (1), 37–50.

(5) Schubert, H. L.; Blumenthal, R. M.; Cheng, X. Many paths to methyltransfer: a chronicle of convergence. *Trends Biochem. Sci.* **2003**, *28* (6), 329–335.

(6) Feoli, A.; Viviano, M.; Cipriano, A.; Milite, C.; Castellano, S.; Sbardella, G. Lysine methyltransferase inhibitors: where we are now. *RSC Chem. Biol.* **2022**, *3* (4), 359–406.

(7) Hwang, J. W.; Cho, Y.; Bae, G.-U.; Kim, S.-N.; Kim, Y. K. Protein arginine methyltransferases: promising targets for cancer therapy. *Exp. Mol. Med.* **2021**, *53* (5), 788–808.

(8) Li, A. S. M.; Li, F.; Eram, M. S.; Bolotokova, A.; Dela Seña, C. C.; Vedadi, M. Chemical probes for protein arginine methyltrans-ferases. *Methods* **2020**, *175*, 30–43.

(9) Szewczyk, M. M.; Ishikawa, Y.; Organ, S.; Sakai, N.; Li, F.; Halabelian, L.; Ackloo, S.; Couzens, A. L.; Eram, M.; Dilworth, D.; et al. Pharmacological inhibition of PRMT7 links arginine monomethylation to the cellular stress response. *Nat. Commun.* **2020**, *11* (1), 2396.

(10) Szewczyk, M. M.; Vu, V.; Barsyte-Lovejoy, D. Quantitative Methods to Study Protein Arginine Methyltransferase 1–9 Activity in Cells. *J. Vis. Exp.* **2021**, *174*, No. e62418.

(11) Hadjikyriacou, A.; Yang, Y.; Espejo, A.; Bedford, M. T.; Clarke, S. G. Unique Features of Human Protein Arginine Methyltransferase 9 (PRMT9) and Its Substrate RNA Splicing Factor SF3B2*. *J. Biol. Chem.* **2015**, *290* (27), 16723–16743.

(12) Feng, Y.; Hadjikyriacou, A.; Clarke, S. G. Substrate Specificity of Human Protein Arginine Methyltransferase 7 (PRMT7): THE IMPORTANCE OF ACIDIC RESIDUES IN THE DOUBLE E LOOP*. *J. Biol. Chem.* **2014**, *289* (47), 32604–32616.

(13) Yang, Y.; Hadjikyriacou, A.; Xia, Z.; Gayatri, S.; Kim, D.; Zurita-Lopez, C.; Kelly, R.; Guo, A.; Li, W.; Clarke, S. G.; et al. PRMT9 is a Type II methyltransferase that methylates the splicing factor SAP145. *Nat. Commun.* **2015**, *6*, 6428. https://www.natur-e.com/articles/ncomms7428#supplementary-information

(14) Miranda, T. B.; Miranda, M.; Frankel, A.; Clarke, S. PRMT7 Is a Member of the Protein Arginine Methyltransferase Family with a Distinct Substrate Specificity. *J. Biol. Chem.* **2004**, *279* (22), 22902–22907.

(15) Jain, K.; Clarke, S. G. PRMT7 as a unique member of the protein arginine methyltransferase family: A review. *Arch. Biochem. Biophys.* **2019**, *665*, 36–45.

(16) Cura, V.; Troffer-Charlier, N.; Wurtz, J.-M.; Bonnefond, L.; Cavarelli, J. Structural insight into arginine methylation by the mouse protein arginine methyltransferase 7: a zinc finger freezes the mimic of the dimeric state into a single active site. *Acta Crystallogr., D* **2014**, *70* (9), 2401–2412.

(17) Hasegawa, M.; Toma-Fukai, S.; Kim, J.-D.; Fukamizu, A.; Shimizu, T. Protein arginine methyltransferase 7 has a novel homodimer-like structure formed by tandem repeats. *FEBS Lett.* **2014**, *588* (10), 1942–1948.

(18) Karkhanis, V.; Wang, L.; Tae, S.; Hu, Y.-J.; Imbalzano, A. N.; Sif, S. Protein Arginine Methyltransferase 7 Regulates Cellular Response to DNA Damage by Methylating Promoter Histones H2A and H4 of the Polymerase δ Catalytic Subunit Gene, POLD1*. *J. Biol. Chem.* **2012**, *287* (35), 29801–29814.

(19) Yao, R.; Jiang, H.; Ma, Y.; Wang, L.; Wang, L.; Du, J.; Hou, P.; Gao, Y.; Zhao, L.; Wang, G.; et al. PRMT7 Induces Epithelial-to-Mesenchymal Transition and Promotes Metastasis in Breast Cancer. *Cancer Res.* **2014**, *74* (19), 5656–5667.

(20) Liu, W.; Xie, Y.; Ma, J.; Luo, X.; Nie, P.; Zuo, Z.; Lahrmann, U.; Zhao, Q.; Zheng, Y.; Zhao, Y.; et al. IBS: an illustrator for the presentation and visualization of biological sequences. *Bioinformatics* **2015**, *31* (20), 3359–3361. (acccessed 23 April, 2023).

(21) Liu, L.; Zhen, X. T.; Denton, E.; Marsden, B. D.; Schapira, M. ChromoHub: a data hub for navigators of chromatin-mediated signalling. *Bioinformatics* **2012**, *28* (16), 2205–2206.

(22) Lei, Y.; Han, P.; Tian, D. Protein arginine methyltransferases and hepatocellular carcinoma: A review. *Transl. Oncol.* **2021**, *14* (11), No. 101194.

(23) Jiang, H.; Zhou, Z.; Jin, S.; Xu, K.; Zhang, H.; Xu, J.; Sun, Q.; Wang, J.; Xu, J. PRMT9 promotes hepatocellular carcinoma invasion and metastasis via activating PI3K/Akt/GSK-3β/Snail signaling. *Cancer Sci.* **2018**, *109* (5), 1414–1427.

(24) Dong, H.; He, X.; Zhang, L.; Chen, W.; Wu, Y.; Zhu, Y.; Wang, H.; Huang, W.; Lin, Y.; Zhang, L.; et al. Targeting PRMT9 Suppresses Acute Myeloid Leukemia Maintenance. *Blood* **2021**, *138*, 358.

148

(25) Harada, N.; Takagi, T.; Nakano, Y.; Yamaji, R.; Inui, H. Protein arginine methyltransferase 10 is required for androgen-dependent proliferation of LNCaP prostate cancer cells. *Biosci., Biotechnol., Biochem.* **2015**, *79* (9), 1430−1437. (acccessed 18 Oct, 2021).

(26) Bai, X.; Sui, C.; Liu, F.; Chen, T.; Zhang, L.; Zheng, Y.; Liu, B.; Gao, C. The protein arginine methyltransferase PRMT9 attenuates MAVS activation through arginine methylation. *Nat. Commun.* **2022**, *13* (1), 5016.

(27) Castellano, S.; Milite, C.; Ragno, R.; Simeoni, S.; Mai, A.; Limongelli, V.; Novellino, E.; Bauer, I.; Brosch, G.; Spannhoff, A.; et al. Design, Synthesis and Biological Evaluation of Carboxy Analogues of Arginine Methyltransferase Inhibitor 1 (AMI-1). *ChemMedChem* **2010**, *5* (3), 398−414.

(28) Castellano, S.; Spannhoff, A.; Milite, C.; Dal Piaz, F.; Cheng, D.; Tosco, A.; Viviano, M.; Yamani, A.; Cianciulli, A.; Sala, M.; et al. Identification of small-molecule enhancers of arginine methylation catalyzed by coactivator-associated arginine methyltransferase 1. *J. Med. Chem.* **2012**, *55* (22), 9875−9890.

(29) Cheng, D.; Valente, S.; Castellano, S.; Sbardella, G.; Di Santo, R.; Costi, R.; Bedford, M. T.; Mai, A. Novel 3,5-bis-(bromohydroxybenzylidene)piperidin-4-ones as coactivator-associated arginine methyltransferase 1 inhibitors: enzyme selectivity and cellular activity. *J. Med. Chem.* **2011**, *54* (13), 4928−4932.

(30) Franek, M.; Legartova, S.; Suchankova, J.; Milite, C.; Castellano, S.; Sbardella, G.; Kozubek, S.; Bartova, E. CARM1 modulators affect epigenome of stem cells and change morphology of nucleoli. *Physiol. Res.* **2015**, *64* (5), 769−782.

(31) Iannelli, G.; Milite, C.; Marechal, N.; Cura, V.; Bonnefond, L.; Troffer-Charlier, N.; Feoli, A.; Rescigno, D.; Wang, Y.; Cipriano, A.; et al. Turning Nonselective Inhibitors of Type I Protein Arginine Methyltransferases into Potent and Selective Inhibitors of Protein Arginine Methyltransferase 4 through a Deconstruction−Reconstruction and Fragment-Growing Approach. *J. Med. Chem.* **2022**, *65* (17), 11574−11606.

(32) Legartova, S.; Sbardella, G.; Kozubek, S.; Bartova, E. Ellagic Acid-Changed Epigenome of Ribosomal Genes and Condensed RPA194-Positive Regions of Nucleoli in Tumour Cells. *Folia Biol.* **2015**, *61* (2), 49−59.

(33) Mai, A.; Cheng, D.; Bedford, M. T.; Valente, S.; Nebbioso, A.; Perrone, A.; Brosch, G.; Sbardella, G.; De Bellis, F.; Miceli, M.; et al. epigenetic multiple ligands: mixed histone/protein methyltransferase, acetyltransferase, and class III deacetylase (sirtuin) inhibitors. *J. Med. Chem.* **2008**, *51* (7), 2279−2290.

(34) Mai, A.; Valente, S.; Cheng, D.; Perrone, A.; Ragno, R.; Simeoni, S.; Sbardella, G.; Brosch, G.; Nebbioso, A.; Conte, M.; et al. Synthesis and biological validation of novel synthetic histone/protein methyltransferase inhibitors. *ChemMedChem* **2007**, *2* (7), 987−991.

(35) Ragno, R.; Simeoni, S.; Castellano, S.; Vicidomini, C.; Mai, A.; Caroli, A.; Tramontano, A.; Bonaccini, C.; Trojer, P.; Bauer, I.; et al. Small Molecule Inhibitors of Histone Arginine Methyltransferases: Homology Modeling, Molecular Docking, Binding Mode Analysis, and Biological Evaluations. *J. Med. Chem.* **2007**, *50* (6), 1241−1253.

(36) Tsai, W. C.; Gayatri, S.; Reineke, L. C.; Sbardella, G.; Bedford, M. T.; Lloyd, R. E. Arginine Demethylation of G3BP1 Promotes Stress Granule Assembly. *J. Biol. Chem.* **2016**, *291* (43), 22671−22685.

(37) van Haren, M. J.; Marechal, N.; Troffer-Charlier, N.; Cianciulli, A.; Sbardella, G.; Cavarelli, J.; Martin, N. I. Transition state mimics are valuable mechanistic probes for structural studies with the arginine methyltransferase CARM1. *Proc. Natl. Acad. Sci. U. S. A.* **2017**, *114* (14), 3625−3630.

(38) Zeng, H.; Wu, J.; Bedford, M. T.; Sbardella, G.; Hoffmann, F. M.; Bi, K.; Xu, W. A TR-FRET-based functional assay for screening activators of CARM1. *ChemBioChem* **2013**, *14* (7), 827−835.

(39) Halabelian, L.; Tempel, W.; Zeng, H.; Li, Y.; Seitova, A.; Hutchinson, A.; Bountra, C.; Edwards, A. M.; Arrowsmith, C. H.; Structural Genomics, C. RCSB PDB - 6PDM: Crystal structure of Human Protein Arginine Methyltransferase 9 (PRMT9), 2019.

(40) Cai, X.-C.; Zhang, T.; Kim, E.-J.; Jiang, M.; Wang, K.; Wang, J.; Chen, S.; Zhang, N.; Wu, H.; Li, F.; et al. A chemical probe of CARM1 alters epigenetic plasticity against breast cancer cell invasion. *eLife* **2019**, *8*, No. e47110.

(41) Boriack-Sjodin, P. A.; Jin, L.; Jacques, S. L.; Drew, A.; Sneeringer, C.; Scott, M. P.; Moyer, M. P.; Ribich, S.; Moradei, O.; Copeland, R. A. Structural Insights into Ternary Complex Formation of Human CARM1 with Various Substrates. *ACS Chem. Biol.* **2016**, *11* (3), 763−771.

(42) Sack, J. S.; Thieffine, S.; Bandiera, T.; Fasolini, M.; Duke, G. J.; Jayaraman, L.; Kish, K. F.; Klei, H. E.; Purandare, A. V.; Rosettani, P.; et al. Structural basis for CARM1 inhibition by indole and pyrazole inhibitors. *Biochem. J.* **2011**, *436* (2), 331−339.

(43) Troffer-Charlier, N.; Cura, V.; Hassenboehler, P.; Moras, D.; Cavarelli, J. Functional insights from structures of coactivator-associated arginine methyltransferase 1 domains. *EMBO J.* **2007**, *26* (20), 4391−4401.

(44) Yue, W. W.; Hassler, M.; Roe, S. M.; Thompson-Vale, V.; Pearl, L. H. Insights into histone code syntax from structural and biochemical studies of CARM1 methyltransferase. *EMBO J.* **2007**, *26* (20), 4402−4412. Research Support, Non-U.S. Gov't.

(45) Although the BPS Bioscience web site reports the following reference for this kit, the paper only mentions chemoluminescent assay kits for PRMT1, PRMT3, PRMT4, PRMT5, PRMT6, and PRMT8. No ALPHAScreen or ALPHALisa assay kit is mentioned nor any kind of assay for PRMT9: Li, Y.; Zhu, R.; Wang, W.; Fu, D.; Hou, J.; Ji, S.; Chen, B.; Hu, Z.; Shao, X.; Yu, X.; et al. Arginine Methyltransferase 1 in the Nucleus Accumbens Regulates Behavioral Effects of Cocaine. *J. Neurosci.* **2015**, *35* (37), 12890−12902.

(46) All the differences between the old and the new version of the BPS Biosciences assay kit can be gauged by comparing the new datasheet (https://bpsbioscience.com/media/wysiwyg/HMT/52069.pdf) and the old one, still reported on the websites of a few international distributors (e.g., https://www.tebu-bio.com/Product/14952069/PRMT9_Homogeneous_Assay_Kit.html; https://bpsbioscience.com/pub/media/wysiwyg/52069_1.pdf).

(47) Jain, K.; Warmack, R. A.; Debler, E. W.; Hadjikyriacou, A.; Stavropoulos, P.; Clarke, S. G. Protein Arginine Methyltransferase Product Specificity Is Mediated by Distinct Active-site Architectures*. *J. Biol. Chem.* **2016**, *291* (35), 18299−18308.

(48) Hadjikyriacou, A.; Clarke, S. G. Caenorhabditis elegans PRMT-7 and PRMT-9 Are Evolutionarily Conserved Protein Arginine Methyltransferases with Distinct Substrate Specificities. *Biochemistry* **2017**, *56* (20), 2612−2626.

(49) Lowe, T. L.; Clarke, S. G. Human protein arginine methyltransferases (PRMTs) can be optimally active under non-physiological conditions. *J. Biol. Chem.* **2022**, *298* (9), No. 102290.

(50) Kryukov, G. V.; Wilson, F. H.; Ruth, J. R.; Paulk, J.; Tsherniak, A.; Marlow, S. E.; Vazquez, F.; Weir, B. A.; Fitzgerald, M. E.; Tanaka, M.; et al. MTAP deletion confers enhanced dependency on the PRMT5 arginine methyltransferase in cancer cells. *Science* **2016**, *351* (6278), 1214.

(51) Marjon, K.; Cameron, M. J.; Quang, P.; Clasquin, Michelle F.; Mandley, E.; Kunii, K.; McVay, M.; Choe, S.; Kernytsky, A.; Gross, S.; et al. MTAP Deletions in Cancer Create Vulnerability to Targeting of the MAT2A/PRMT5/RIOK1 Axis. *Cell Rep.* **2016**, *15* (3), 574−587.

(52) Mavrakis, K. J.; McDonald, E. R.; Schlabach, M. R.; Billy, E.; Hoffman, G. R.; deWeck, A.; Ruddy, D. A.; Venkatesan, K.; Yu, J.; McAllister, G.; et al. Disordered methionine metabolism in MTAP/CDKN2A-deleted cancers leads to dependence on PRMT5. *Science* **2016**, *351* (6278), 1208.

(53) Tang, B.; Lee, H.-O.; Gupta, S.; Wang, L.; Kurimchak, A. M.; Duncan, J. S.; Kruger, W. D. Extracellular 5′-methylthioadenosine inhibits intracellular symmetric dimethylarginine protein methylation of FUSE-binding proteins. *J. Biol. Chem.* **2022**, *298* (9), No. 102367.

(54) Williams-Ashman, H. G.; Seidenfeld, J.; Galletti, P. Trends in the biochemical pharmacology of 5′-deoxy-5′-methylthioadenosine. *Biochem. Pharmacol.* **1982**, *31* (3), 277−288.

149

(55) Chan-Penebre, E.; Kuplast, K. G.; Majer, C. R.; Boriack-Sjodin, P. A.; Wigle, T. J.; Johnston, L. D.; Rioux, N.; Munchhof, M. J.; Jin, L.; Jacques, S. L.; et al. A selective inhibitor of PRMT5 with in vivo and in vitro potency in MCL models. *Nat. Chem. Biol.* **2015**, *11* (6), 432−437.

(56) Kaletta, T.; Hengartner, M. O. Finding function in novel targets: C. elegans as a model organism. *Nat. Rev. Drug Discovery* **2006**, *5* (5), 387−399.

(57) Yang, M.; Sun, J.; Sun, X.; Shen, Q.; Gao, Z.; Yang, C. Caenorhabditis elegans Protein Arginine Methyltransferase PRMT-5 Negatively Regulates DNA Damage-Induced Apoptosis. *PLOS Genet.* **2009**, *5* (6), No. e1000514.

(58) Santos-Martins, D.; Solis-Vasquez, L.; Tillack, A. F.; Sanner, M. F.; Koch, A.; Forli, S. Accelerating AutoDock4 with GPUs and Gradient-Based Local Search. *J. Chem. Theory Comput.* **2021**, *17* (2), 1060−1073.

(59) Zeng, H.; Dong, A.; Hutchinson, A.; Seitova, A.; Li, Y.; Gao, Y. D.; Schneider, S.; Siliphaivanh, P.; Sloman, D.; Nicholson, B.; et al. RCSB PDB - 7RBQ: Co-crystal structure of human PRMT9 in complex with MT556 inhibitor, 2021.

(60) Bowers, K. J.; Chow, D. E.; Xu, H.; Dror, R. O.; Eastwood, M. P.; Gregersen, B. A.; Klepeis, J. L.; Kolossvary, I.; Moraes, M. A.; Sacerdoti, F. D.; et al. Scalable Algorithms for Molecular Dynamics Simulations on Commodity Clusters. In *SC '06: Proceedings of the 2006 ACM/IEEE Conference on Supercomputing*, 11−17 Nov. 2006, 2006; pp 43−43.

(61) Jumper, J.; Evans, R.; Pritzel, A.; Green, T.; Figurnov, M.; Ronneberger, O.; Tunyasuvunakool, K.; Bates, R.; Žídek, A.; Potapenko, A.; et al. Highly accurate protein structure prediction with AlphaFold. *Nature* **2021**, *596* (7873), 583−589.

(62) Borchardt, R. T.; Huber, J. A.; Wu, Y. S. Potential inhibitors of S-adenosylmethionine-dependent methyltransferases. 2. Modification of the base portion of S-adenosylhomocysteine. *J. Med. Chem.* **1974**, *17* (8), 868−873.

(63) Coward, J. K.; Slisz, E. P. Analogs of S-adenosylhomocysteine as potential inhibitors of biological transmethylation. Specificity of the S-adenosylhomocysteine binding site. *J. Med. Chem.* **1973**, *16* (5), 460−463.

(64) Richon, V. M.; Johnston, D.; Sneeringer, C. J.; Jin, L.; Majer, C. R.; Elliston, K.; Jerva, L. F.; Scott, M. P.; Copeland, R. A. Chemogenetic Analysis of Human Protein Methyltransferases. *Chem. Biol. Drug Des.* **2011**, *78* (2), 199−210.

(65) Coussens, N. P.; Kales, S. C.; Henderson, M. J.; Lee, O. W.; Horiuchi, K. Y.; Wang, Y.; Chen, Q.; Kuznetsova, E.; Wu, J.; Chakka, S.; et al. High-throughput screening with nucleosome substrate identifies small-molecule inhibitors of the human histone lysine methyltransferase NSD2. *J. Biol. Chem.* **2018**, *293* (35), 13750−13765.

(66) Kungulovski, G.; Jeltsch, A. Quality of histone modification antibodies undermines chromatin biology research [version 2; peer review: 3 approved]. *F1000Res.* **2015**, *4*, 1160.

(67) Pillai-Kastoori, L.; Heaton, S.; Shiflett, S. D.; Roberts, A. C.; Solache, A.; Schutz-Geschwender, A. R. Antibody validation for Western blot: By the user, for the user. *J. Biol. Chem.* **2020**, *295* (4), 926−939.

(68) Hermann, J.; Schurgers, L.; Jankowski, V. Identification and characterization of post-translational modifications: Clinical implications. *Mol. Aspects Med.* **2022**, *86*, No. 101066.

(69) Bloom, J.; Triantafyllidis, A.; Quaglieri, A.; Burton Ngov, P.; Infusini, G.; Webb, A. Mass Dynamics 1.0: A Streamlined, Web-Based Environment for Analyzing, Sharing, and Integrating Label-Free Data. *J. Proteome Res.* **2021**, *20* (11), 5180−5188.

(70) Li, W.-J.; He, Y.-H.; Yang, J.-J.; Hu, G.-S.; Lin, Y.-A.; Ran, T.; Peng, B.-l; Xie, B.-l.; Huang, M.-F.; Gao, X.; et al. Profiling PRMT methylome reveals roles of hnRNPA1 arginine methylation in RNA splicing and cell growth. *Nat. Commun.* **2021**, *12* (1), 1946.

(71) Giansanti, P.; Tsiatsiani, L.; Low, T. Y.; Heck, A. J. R. Six alternative proteases for mass spectrometry−based proteomics beyond trypsin. *Nat. Protoc.* **2016**, *11* (5), 993−1006.

(72) Luger, K.; Rechsteiner, T. J.; Flaus, A. J.; Waye, M. M. Y.; Richmond, T. J. Characterization of nucleosome core particles containing histone proteins made in bacteria11Edited by A Klug. *J. Mol. Biol.* **1997**, *272* (3), 301−311.

(73) Madhavi Sastry, G.; Adzhigirey, M.; Day, T.; Annabhimoju, R.; Sherman, W. Protein and ligand preparation: parameters, protocols, and influence on virtual screening enrichments. *J. Comput. Aided Mol. Des.* **2013**, *27* (3), 221−234.

(74) *Schrödinger Release 2021−4: Protein Preparation Wizard*, 2021.

(75) *Schrödinger Release 2023−1: Maestro.* 2023.

(76) Morris, G. M.; Huey, R.; Lindstrom, W.; Sanner, M. F.; Belew, R. K.; Goodsell, D. S.; Olson, A. J. AutoDock4 and AutoDockTools4: Automated docking with selective receptor flexibility. *J. Comput. Chem.* **2009**, *30* (16), 2785−2791.

(77) Mark, P.; Nilsson, L. Structure and Dynamics of the TIP3P, SPC, and SPC/E Water Models at 298 K. *J. Phys. Chem. A* **2001**, *105* (43), 9954−9960.

(78) *OPLSe*, 2018.

(79) Martyna, G. J.; Tuckerman, M. E.; Tobias, D. J.; Klein, M. L. Explicit reversible integrators for extended systems dynamics. *Mol. Phys.* **1996**, *87* (5), 1117−1157.

(80) Hoover, W. G. Canonical dynamics: Equilibrium phase-space distributions. *Phys. Rev. A* **1985**, *31* (3), 1695−1697.

(81) Anastassiadis, T.; Deacon, S. W.; Devarajan, K.; Ma, H.; Peterson, J. R. Comprehensive assay of kinase catalytic activity reveals features of kinase inhibitor selectivity. *Nat. Biotechnol.* **2011**, *29* (11), 1039−1045.

(82) Horiuchi, K. Y.; Eason, M. M.; Ferry, J. J.; Planck, J. L.; Walsh, C. P.; Smith, R. F.; Howitz, K. T.; Ma, H. Assay Development for Histone Methyltransferases. *Assay Drug Dev. Technol.* **2013**, *11* (4), 227−236. (acccessed 24 June, 2021).

(83) Antonysamy, S.; Bonday, Z.; Campbell, R. M.; Doyle, B.; Druzina, Z.; Gheyi, T.; Han, B.; Jungheim, L. N.; Qian, Y.; Rauch, C.; et al. Crystal structure of the human PRMT5:MEP50 complex. *Proc. Natl. Acad. Sci. U. S. A.* **2012**, *109* (44), 17960−17965.

(84) Eddershaw, A. R.; Stubbs, C. J.; Edwardes, L. V.; Underwood, E.; Hamm, G. R.; Davey, P. R. J.; Clarkson, P. N.; Syson, K. Characterization of the Kinetic Mechanism of Human Protein Arginine Methyltransferase 5. *Biochemistry* **2020**, *59* (50), 4775−4786.

(85) Sayegh, J.; Webb, K.; Cheng, D.; Bedford, M. T.; Clarke, S. G. Regulation of Protein Arginine Methyltransferase 8 (PRMT8) Activity by Its N-terminal Domain*. *J. Biol. Chem.* **2007**, *282* (50), 36444−36453.

(86) Aldrich, C.; Bertozzi, C.; Georg, G. I.; Kiessling, L.; Lindsley, C.; Liotta, D.; Merz, K. M.; Schepartz, A.; Wang, S. The Ecstasy and Agony of Assay Interference Compounds. *J. Med. Chem.* **2017**, *60* (6), 2165−2168.

(87) Daina, A.; Michielin, O.; Zoete, V. SwissADME: a free web tool to evaluate pharmacokinetics, drug-likeness and medicinal chemistry friendliness of small molecules. *Sci. Rep.* **2017**, *7*, 42717. https://www.nature.com/articles/srep42717#supplementary-information

(88) Lagorce, D.; Sperandio, O.; Baell, J. B.; Miteva, M. A.; Villoutreix, B. O. FAF-Drugs3: a web server for compound property calculation and chemical library design. *Nucleic Acids Res.* **2015**, *43* (W1), W200−W207.

(89) Baell, J. B.; Holloway, G. A. New Substructure Filters for Removal of Pan Assay Interference Compounds (PAINS) from Screening Libraries and for Their Exclusion in Bioassays. *J. Med. Chem.* **2010**, *53* (7), 2719−2740.

(90) Belvedere, R.; Morretta, E.; Pessolano, E.; Novizio, N.; Tosco, A.; Porta, A.; Whiteford, J.; Perretti, M.; Filippelli, A.; Monti, M. C.; et al. Mesoglycan exerts its fibrinolytic effect through the activation of annexin A2. *J. Cell. Physiol.* **2021**, *236* (7), 4926−4943.

150

Identification of a Protein Arginine Methyltransferase 7 (PRMT7)/Protein Arginine Methyltransferase 9 (PRMT9) Inhibitor

Alessandra Feoli,[‡,∥] Giulia Iannelli,[‡,∫,†,∥] Alessandra Cipriano,[‡] Ciro Milite,[‡] Lei Shen,[Δ] Zhihao Wang,[Δ] Andrea Hadjikyriacou,[§] Troy L. Lowe,[§] Cyrus Safaeipour,[§] Monica Viviano,[‡] Giuliana Sarno,[‡,∫] Elva Morretta,[∩] Maria Chiara Monti,[∩] Yanzhong Yang,[Δ] Steven G. Clarke,[§] Sandro Cosconati,[,¥] Sabrina Castellano,[*,‡] and Gianluca Sbardella[*,‡]*

[‡]Department of Pharmacy, Epigenetic Med Chem Lab, [∩]Department of Pharmacy, ProteoMass Lab, and [∫]PhD Program in Drug Discovery and Development, University of Salerno, via Giovanni Paolo II 132, I-84084 Fisciano (SA), Italy

[§]Department of Chemistry and Biochemistry, and the Molecular Biology Institute, University of California, Los Angeles, California 90095, USA

[Δ]Department of Cancer Genetics and Epigenetics, Beckman Research Institute, City of Hope National Cancer Center, Duarte, California 91010, USA

[¥]DiSTABiF, University of Campania "Luigi Vanvitelli", Via Vivaldi 43, 81100 Caserta, Italy

*S.C.: E-mail, sandro.cosconati@unicampania.it; *S.C.: E-mail, scastellano@unisa.it; *G.S.: E-mail, gsbardella@unisa.it

Table of Contents:

Figure S1. Optimization of the ALPHA-based screening protocol for PRMT9
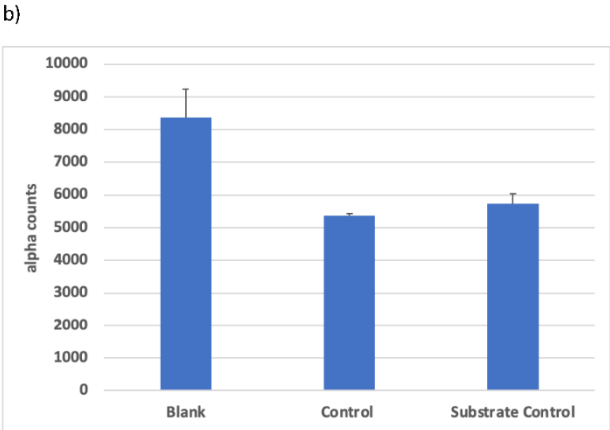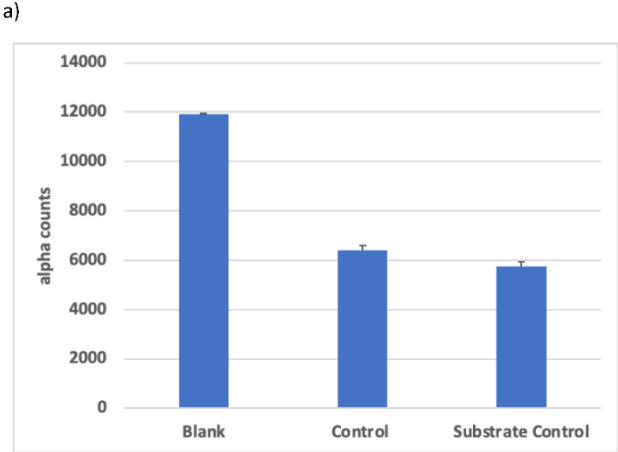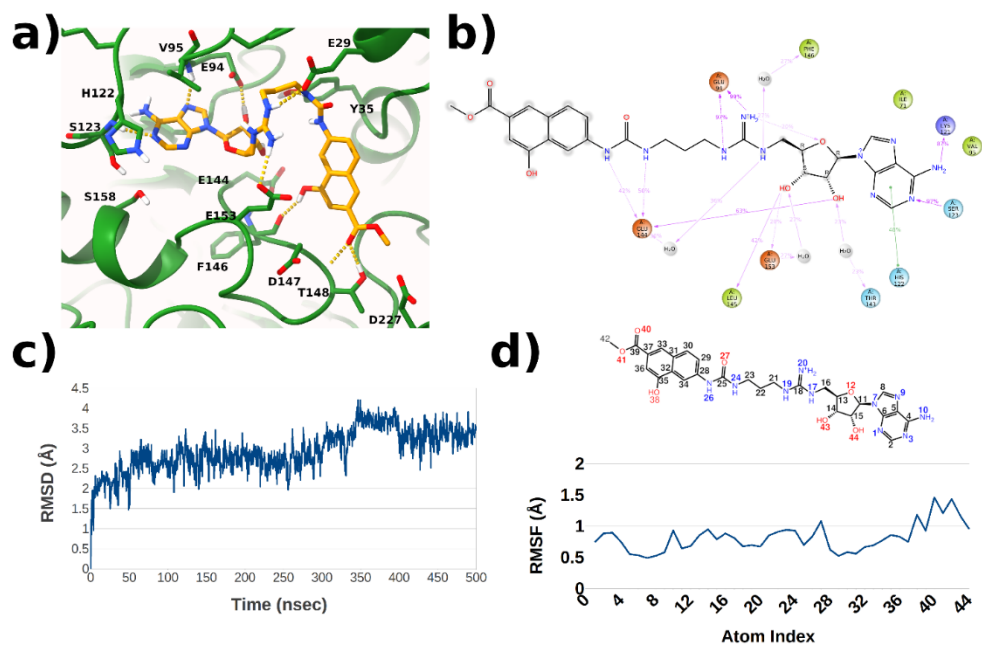
a)

b)

c)

S2

152
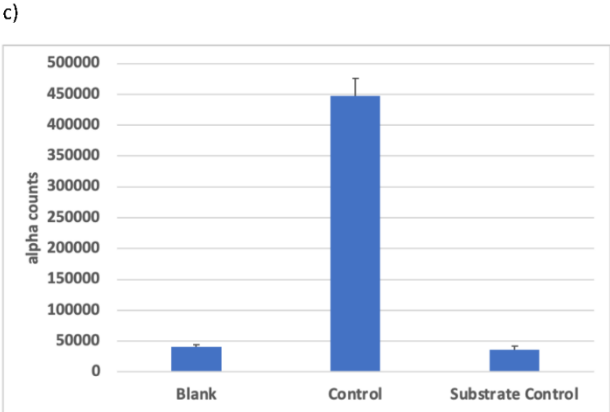
Figure S2

Binding mode of **1a** in complex with PRMT7 3D structure as predicted by docking calculations (a) and 2D representation of ligand/protein interactions through the 500 ns long MD simulation (b). The ligand and enzyme are represented as orange and green sticks and ribbons, respectively. L-RMSD (c) and L-RMSF (d) plots obtained from the analysis of MD simulations.

Figure S3
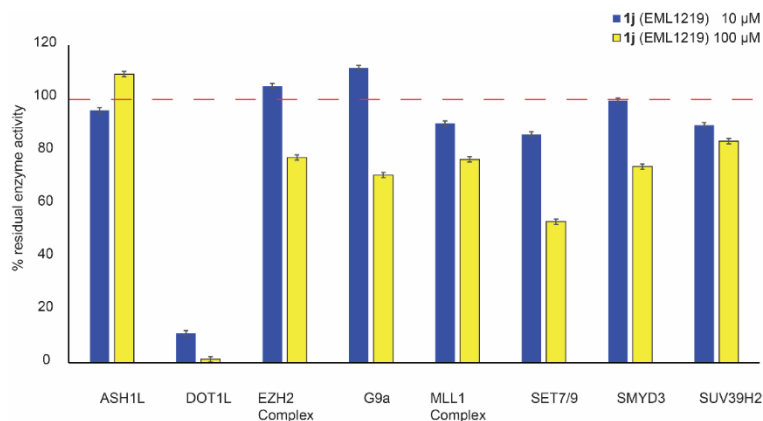
Inhibitory activity profiles of compound **1j** towards ASH1L, DOT1L, EZH2, G9a, MLL1, SET7/9, SMYD3, and SUV39H2 at two different fixed concentrations (10 and 100 μM).

Table S1. Inhibitory activity values of compound **1j** against a panel of KMTs

	% enzyme residual activ. after treatment with 1j[a,b,]		ref. cmpd. $IC_{50}(\mu M)^{b,c}$	
	10 μM	100 μM	SAH	chaetocin
ASH1L	95.38±1.49	109.06±3.80	-	0.025
DOT1L	11.21±0.88	1.35±0.17	0.20	-
EZH2	104.55±0.99	77.56±3.43	43.7	-
G9a	111.35±4.30	70.93±0.31	1.39	-
MLL1	90.45±2.83	76.86±3.96	0.30	-
SET7/9	86.32±1.40	53.33±0.38	70.4	-
SMYD3	99.09±1.41	74.15±1.80	15.9	-
SUV39H2	89.74±1.08	83.76±0.22	37.3	-

[a]Compounds were tested at 10 and 100 μM fixed concentrations; values obtained for each compound are mean ± SD determined for two separate experiments.in duplicate; [b]values were obtained in a radioisotope-based filter assay, using 0.05 mg/mL oligo nucleosomes (for ASH1L, DOT1L, and MLL1 complex), 0.05 mg/mL core histone (for EZH2 complex and SET7/9), 5 μM histone H3 (for SUV39H2) or 2.5 μM histone H3 1–21 (for G9a) as substrate and *S*-adenosyl-L-[methyl-³H]methionine (1 μM) as methyl donor; [c]reference compounds were tested in 10-dose IC_{50} mode with 3-fold serial dilution starting at 10 or 100 μM; data were analyzed using Excel and GraphPad Prism 6.0 software (GraphPad Software Inc., San Diego, CA) for IC_{50} curve fits using sigmoidal dose *vs.* response - variable slope (four parameters) equations.

S4

154

Chapter 8

Future directions and concluding statements of protein arginine methyltransferase research

The work described in this chapter includes my unpublished experiments that maybe entry points to further work in the field.

Abstract

This chapter includes preliminary work in four areas. First we analyzed peptide sequences that have been previously assessed as PRMT7 methylation sites in two proteomic studies. We find that some of these sites do not appear to be methylatable raising questions on the original identification of these sites, or suggesting that tertiary structural conformations may strongly affect substrate site recognition. Secondly, we followed up on the results of Chapter 4 to demonstrate the effect of the serine residue in the RKRSR motif of histone H2B and Fhod1/Fhod3. Thirdly, we describe experiments that originate from results in a previous paper describing the allosteric regulation of PRMTs (Jain 2017). Here we show the effects of amino acid changes at positions 1, 3, 17 and 19 on histone H4 methylation by PRMT7. Finally, we show that an amino acid change in PRMT7 that results in human pathology also results in the loss of enzyme activity.

While the current thesis in its whole describes the work performed throughout my graduate career, additional research experiments were performed yet will remain unpublished. The purpose of this chapter is to document these unpublished studies in the hopes that future protein arginine methyltransferase researchers can advance the ideas presented.

First we pursued our investigation of the substrate specificity of PRMT7. We selected peptide sequences from identified proteins from two separate PRMT7 proteomics studies

containing RXR motifs (Ma 2023)(Szewczyk 2020). While we expected that PRMT7 would methylate each of these peptides, we found that many of these peptides were not substrates at all using the P81 phosphocellulose assay (Figures 1-3). We confirmed the absence of substrate activity in all of these peptides using the radioactive gel assay and mass spectrometry analysis (data not shown). We suggest two reasons why we saw little or no methylation in peptides from proteins that had been previously been identified as containing PRMT7 dependent methylated sites. In first place the three-dimensional structure of the protein may be required for the PRMT7 recognition of particular arginine residues. Secondly, it is possible that the some of the proteomic identifications by mass spectrometry were simply incorrect. Further work will be necessary to validate the proteomic studies and to determine how three-dimensional structures may control the recognition of sites by PRMT7.

In an extension of the work of Chapter 4 we studied the effect of the serine residue in the RKRSR PRMT7 substrate motif of histone H2B and Fhod1/Fhod3. We showed that switching the lysine and serine residues, or substituting a serine residue for the lysine residue, or substituting a lysine residue for the serine residue all had little effect on the ability of a peptide substrate to be methylated by PRMT7 (Figure 4). We were surprised by these results in light of the total loss of substrate activity when the lysine and central arginine residue were switched as seen in Chapter 4. These results now will allow for a more extensive study to try to explain why some changes in this motif affect substrate activity and some don't.

One of the biggest breakthroughs that has come out of the Clarke Lab that has yet to further be investigated is the idea of allosteric regulation. Histone H4 can be methylated by PRMT1, PRMT5, and PRMT7. While initial characterization suggested H4R3 to be methylated by PRMT7 (Ying 2015), further studies revealed that H4R3 is not PRMT7 specific. Additionally, studies have shown that H4R17 and H4R19 are PRMT7 specific while H4R3 has been identified as a substrate for PRMT1 (Huang 2005) and PRMT5 (Dhar 2012). Jain and colleagues identified that if a predeposited methyl mark occurs at H4R17 then H4R3 methylation by PRMT1 or PRMT5

is enhanced (Jain 2017). Unfortunately, these results have not been recapitulated *in vivo*. However, with the discovery of PRMT5 specific inhibitor EPZ015666 (Liu 2021) and the PRMT7 specific inhibitor SGC8158 (Szewczyk 2020), these *in vivo* studies are now possible. Ultimately these results have opened up doors for researchers to question whether other substrates that may be methylated by multiple PRMTs simultaneously, operate in an allosteric fashion. In efforts to recapitulate this finding as well as add to the knowledge we selectively tested N-terminal histone H4 peptides that contained phosphoserine modifications, as well as methylarginine modifications and tested how these affect PRMT1, PRMT5 and PRMT7 activities. The Zhang lab at the University of Georgia performed a similar study with PRMT1 and PRMT5 and concluded that if a modification in the -2 or +2 position occurred next to the R3 histone H4 peptide, then PRMT1 or PRMT5 activity would be mildly inhibited (Fulton 2022). Results of our experiments are presented in Figure 5. In this figure we show that amino acid substitutions at residues 1 and 3 do not largely effect PRMT7 activity. However, we were surprised to find that the loss of either arginine 17 or arginine 19 completely abolished the substrate activity of H4 peptides. This work provides the framework for future studies of the allosteric regulation of PRMT5 by methylation modifications catalyzed by PRMT7.

Late into my PhD we were contacted by a doctor who had a patient with a PRMT7 mutation that showed a phenotype similar to those described by Cali 2023. The doctor identified a deletion mutation of one of the leucine residues in motif II and we were able to identify that this mutation leads to an abolishment of PRMT7 activity (Figure 6). It will be very interesting to examine the three-dimensional structure of the PRMT7 enzyme with the deleted leucine residue to determine the molecular basis for the loss of activity.

References

1. Evich, Marina, et al. "Effect of methylation on the side-chain pKa value of arginine." *Protein science* 25.2 (2016): 479-486.

2. Ying, Zhengzhou, et al. "Histone arginine methylation by PRMT7 controls germinal center formation via regulating Bcl6 transcription." *The Journal of Immunology* 195.4 (2015): 1538-1547.

3. Huang, Suming, Michael Litt, and Gary Felsenfeld. "Methylation of histone H4 by arginine methyltransferase PRMT1 is essential in vivo for many subsequent histone modifications." *Genes & development* 19.16 (2005): 1885-1893.

4. Dhar, Shilpa S., et al. "Trans-tail regulation of MLL4-catalyzed H3K4 methylation by H4R3 symmetric dimethylation is mediated by a tandem PHD of MLL4." *Genes & development* 26.24 (2012): 2749-2762.

5. Jain, Kanishk, Cyrus Y. Jin, and Steven G. Clarke. "Epigenetic control via allosteric regulation of mammalian protein arginine methyltransferases." *Proceedings of the National Academy of Sciences* 114.38 (2017): 10101-10106.

6. Liu, Xing, et al. "EPZ015666, a selective protein arginine methyltransferase 5 (PRMT5) inhibitor with an antitumour effect in retinoblastoma." *Experimental Eye Research* 202 (2021): 108286.

7. Szewczyk, Magdalena M., et al. "Pharmacological inhibition of PRMT7 links arginine monomethylation to the cellular stress response." *Nature communications* 11.1 (2020): 2396.

8. Fulton, Melody D., et al. "Effects of substrate modifications on the arginine dimethylation activities of PRMT1 and PRMT5." *Epigenetics* 17.1 (2022): 1-18.

9. Cali, Elisa, et al. "Biallelic PRMT7 pathogenic variants are associated with a recognizable syndromic neurodevelopmental disorder with short stature, obesity, and craniofacial and digital abnormalities." *Genetics in Medicine* 25.1 (2023): 135-142.

10. Ma, Min, et al. "Proteome-wide Profiling of Asymmetric Dimethylated Arginine in Human Breast Tumors." *Journal of the American Society for Mass Spectrometry* 34.8 (2023): 1692-1700.
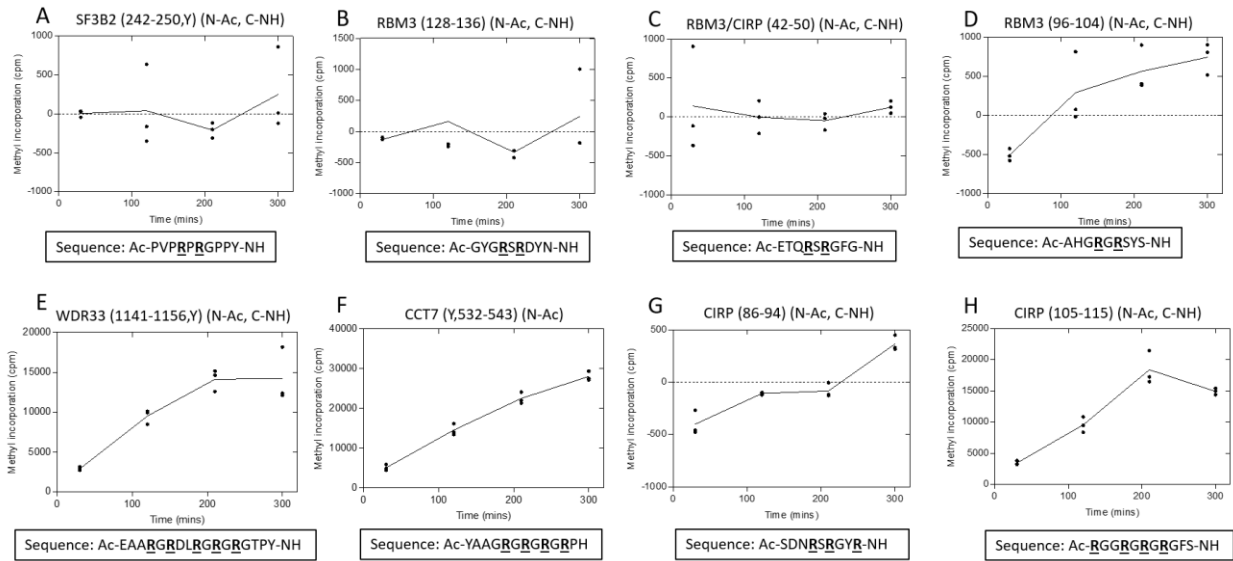
Figure 1: Time course methylation assays of peptides containing RXR motifs identified from PRMT7 proteomic studies. 1.5 µg of GST-HsPRMT7, 10 µM of described peptide and 0.14 µM ^{3}H-AdoMet was incubated in a reaction mixture containing 50 mM HEPES, 1 mM DTT at a pH of 8.5 for the varied time indicated. Methylation reactions were subjected to P81 phosphocellulose analysis.
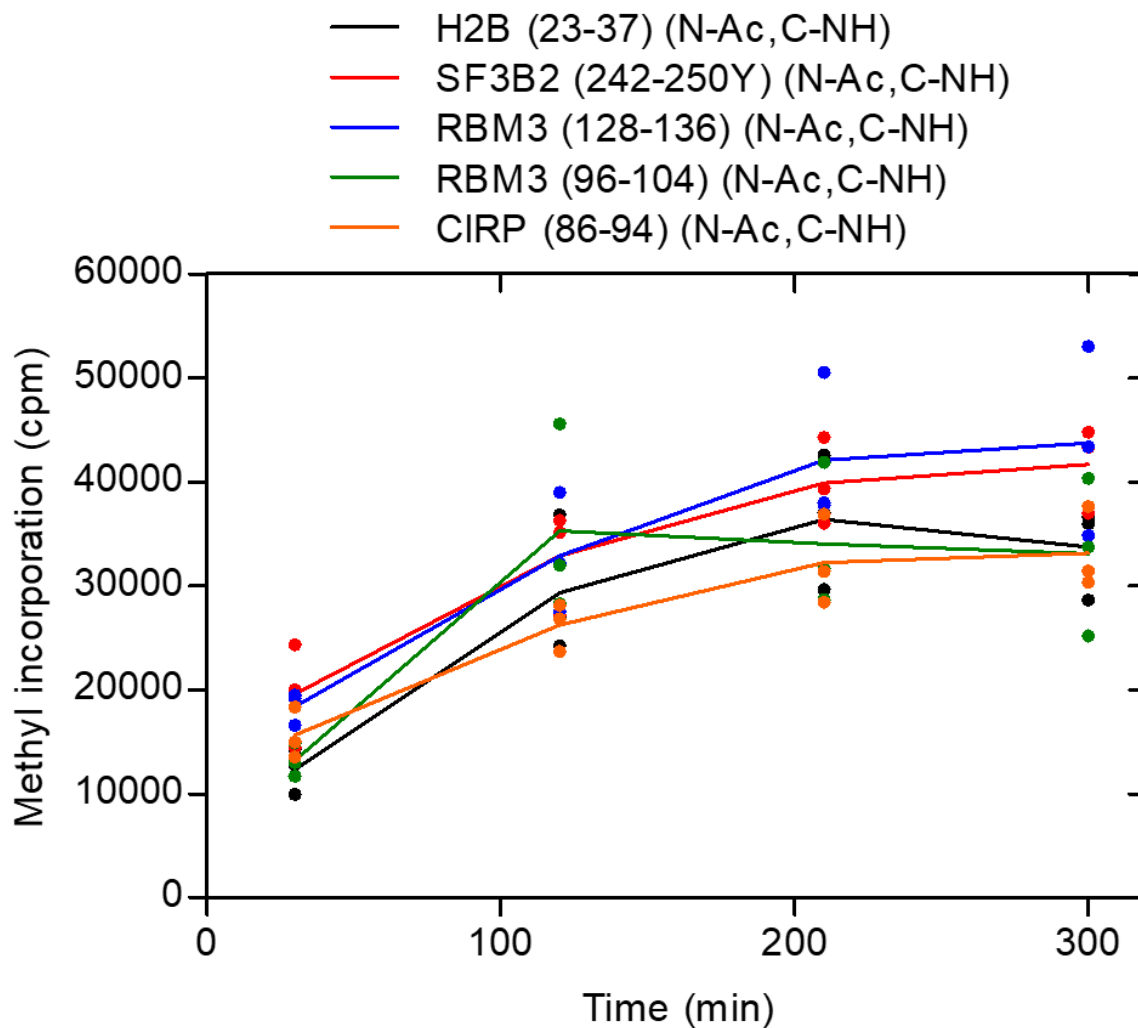
Figure 2: Competition experiments the verify if peptides that were not considered substrates with histone H2B (23-37). 1.5 µg of GST-HsPRMT7, 10 µM of described peptide, and 10 µM of histone H2B (23-37) and 0.14 µM ^{3}H-AdoMet was incubated in a reaction mixture containing 50 mM HEPES, 1 mM DTT at a pH of 8.5 for the varied time indicated. Methylation reactions were subjected to P81 phosphocellulose analysis.
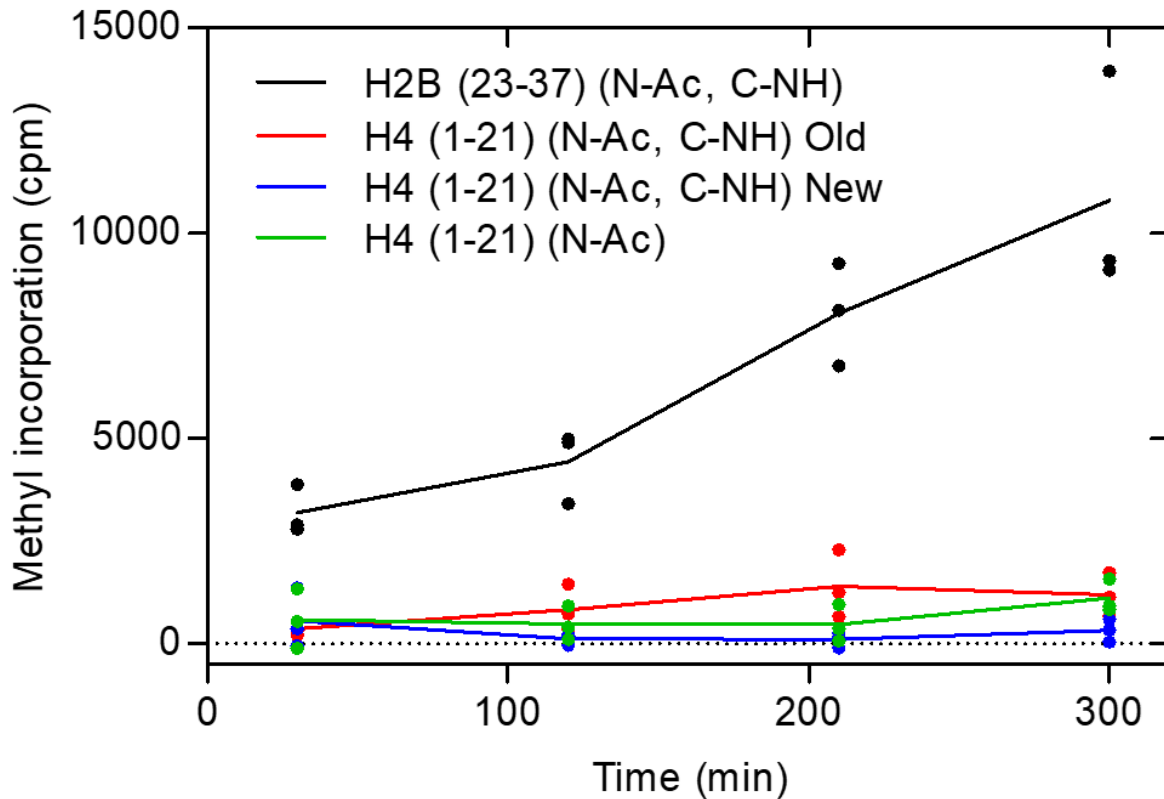
Figure 3: Time course methylation experiments of histone peptides H2B and H4. 1.5 µg of GST-HsPRMT7, 10 µM of described peptide, and 0.14 µM ^{3}H-AdoMet was incubated in a reaction mixture containing 50 mM HEPES, 1 mM DTT at a pH of 8.5 for the varied time indicated. Reaction mixtures were assayed using our P81 Phosphocellulose assay. For the H4 (1-21) peptides we tested a stock sample that we used in previous experiments as well a freshly made peptide purchased from GenScript. Additionally, we compared these peptides toward a non-amidated peptide to see if this altered PRMT7 activity.
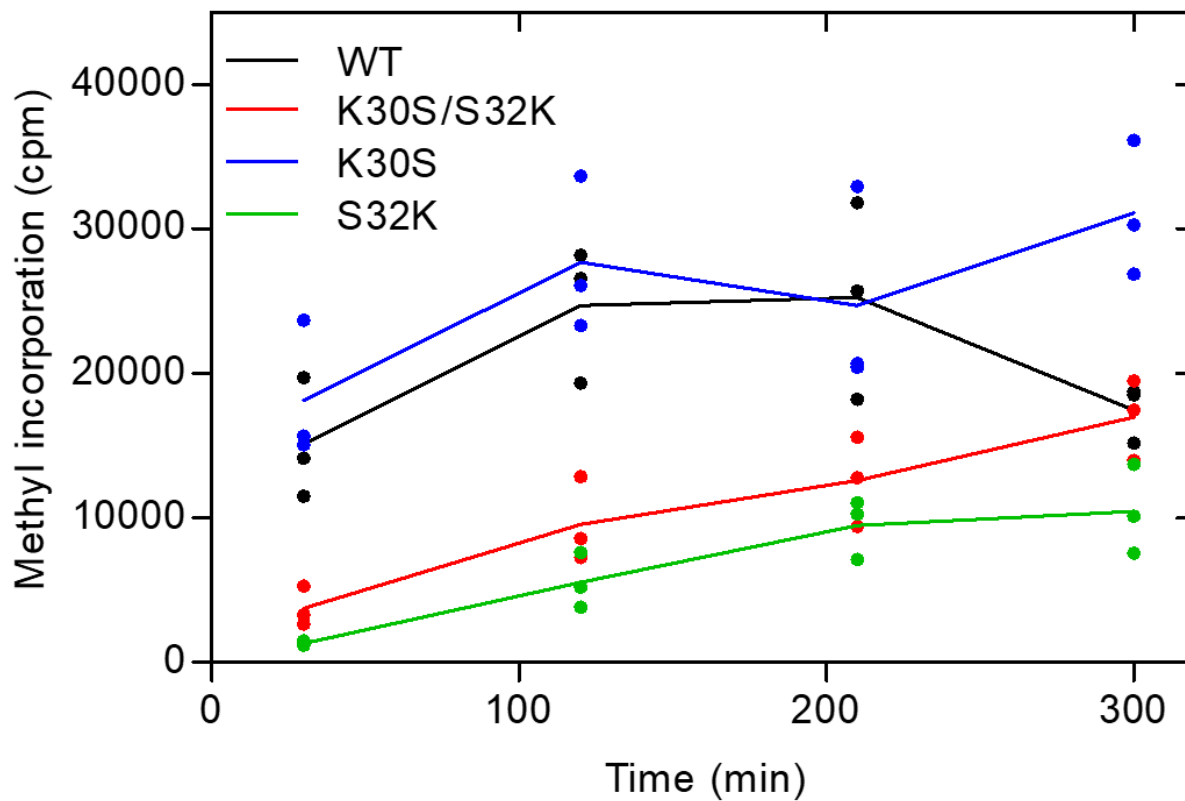
Figure 4: Mutations and rearrangements of residues of histone H2B (23-37) and PRMT7.
1.5 μg of GST-HsPRMT7, 10 μM of described peptide, and 0.14 μM ^{3}H-AdoMet was incubated in a reaction mixture containing 50 mM HEPES, 1 mM DTT at a pH of 8.5 for the varied time indicated. Reaction mixtures were assayed using our P81 Phosphocellulose assay
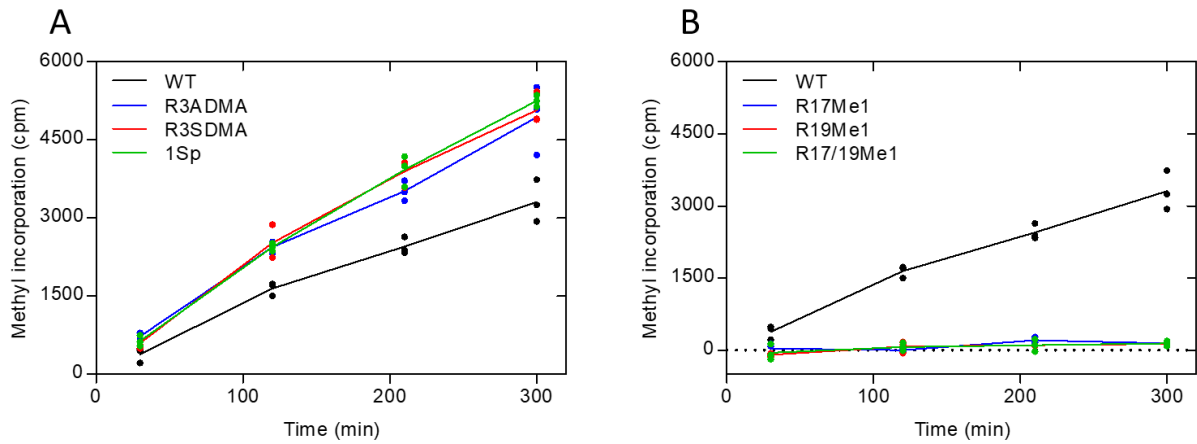
Figure 5: Modifications of Histone H4 (1-21) peptide and PRMT7 activity. 1.5 μg of GST-HsPRMT7, 10 μM of described peptide, and 0.14 μM ^{3}H-AdoMet was incubated in a reaction mixture containing 50 mM HEPES, 1 mM DTT at a pH of 8.5 for the varied time indicated. Reaction mixtures were assayed using our P81 Phosphocellulose assay.
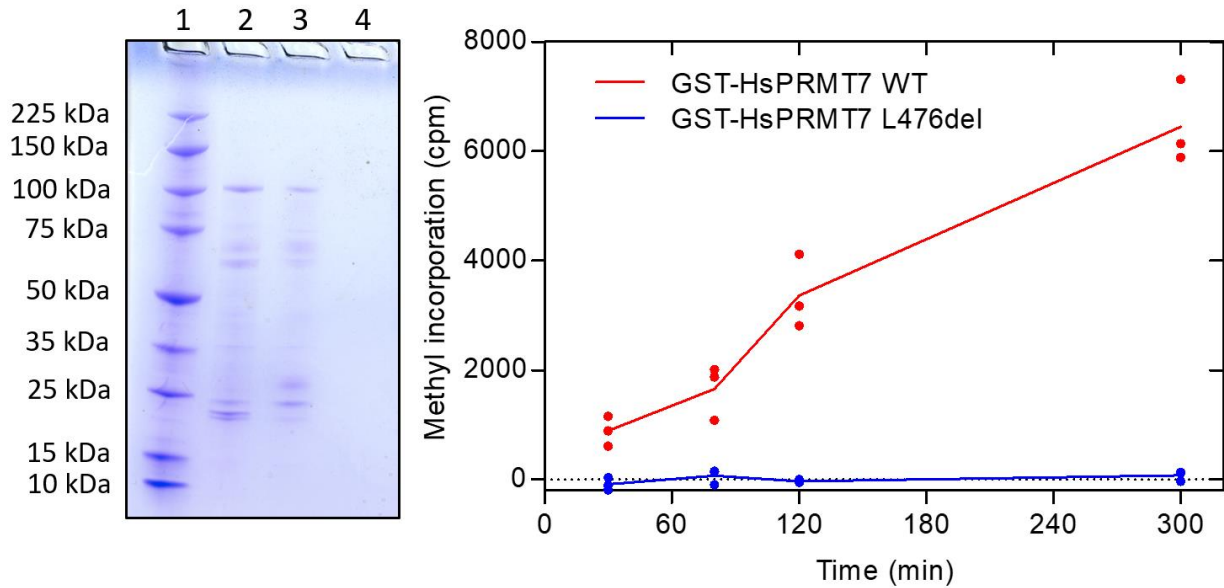
Figure 6: Deletion of the leucine in motif II of PRMT7 abolishes methylation activity. A) Coomassie stained gel of purified 1.5 µg of GST-HsPRMT7 L476del (Lane 2) or GST-HsPRMT7 WT (Lane 3) from e. coli. B) Time course methylation assays of either GST-HsPRMT7 WT or GST-HsPRMT7 L476del with human histone H2B (23-37) as a substrate. 1.43 µg of enzyme was used in each reaction and 10 µM of peptide substrate. Reactions were initiated with 0.35 µM ^{3}H-AdoMet. Buffer conditions consisted of 50 mM HEPES, and 1 mM DTT at a pH of 8.5. Reactions were incubated at 17 °C for the indicated times. Reactions were assayed using our P81 phosphocellulose assay. Points represent individual experiments. Concentrations of enzymes were determined by A280 nanodrop where 1 absorbance unit is equal to 1 mg/mL.